Synthetic Polymers To Address Multiscale Drug Delivery Challenges For Cancer Immunotherapy

Dinh Chuong Nguyen

A dissertation

submitted in partial fulfillment of the

requirements for the degree of

Doctor of Philosophy

University of Washington

2025

Reading Committee:

Suzie H. Pun, Chair

Patrick S. Stayton

Hao Yuan Kueh

Program Authorized to Offer Degree:

Molecular Engineering and Sciences

University of Washington

Abstract

Synthetic Polymers To Address Multiscale Drug Delivery Challenges For Cancer Immunotherapy

Dinh Chuong Nguyen

Chair of the Supervisory Committee:

Suzie H. Pun

Department of Bioengineering

Immunotherapy has revolutionized cancer treatment, yet its clinical impact is limited by toxicity and/or low therapeutic response in many different tumor types. Eliciting optimal spatiotemporal antitumor immune responses is crucial to overcoming this hurdle, but is complicated by multiscale drug delivery challenges to immune activators. This work utilizes targeted, bioresponsive synthetic polymeric drug delivery platforms to address these challenges in engineering next-generation cancer immunotherapies. First, we adapted the Virus-Inspired Polymer for Endosomal Release (VIPER) platform to cytosolically deliver peptide antigens to lymphatic dendritic cells (DCs) for cancer vaccination. Co-polymerized mannose ligands confer lymph node targeting and DC internalization, while the VIPER design selectively lyses maturing endosome to release peptide antigens into the cytosol. This induces superior cytotoxic T-cell activation and tumor suppression compared to simple peptide vaccines and non-endosome releasing designs. Next, we engineered a targeted polymeric prodrug of Stimulator of Interferon Genes (STING) agonist for targeted immune activation in DCs in an intravenous immunotherapy application. A STING agonist is formulated into a monomer with an endosomal cathepsin-labile linker, and co-polymerized with mannose to form a STING 'drugamer' (polySTING) that selectively delivers agonist to DCs. Intravenous polySTING administration results in a DC-driven immune cascade that potently suppresses tumor growth in aggressive murine tumor models. Structural variants of STING drugamers were then co-formulated with VIPER to yield two distinct STING-adjuvanted polymeric vaccines that achieved partial remission through distinct antitumor immunity mechanisms. Finally, a T-cell-targeted cationic brush polymer platform is being developed for T-cell transfection for Chimeric Antigen Receptor (CAR) T-cell production.

DEDICATION

To my grandfather, **Ngoc Quynh Nguyen,** and my good friend **Dang Khoa Nguyen.** Grandpa, you instilled in me my sense of scholarship, curiosity, and unaccented English speech. Khoa, you bestowed me with the gift of friendship and brotherhood during a time when I struggled to understand where I stood in the world. I miss you both dearly and hope to be able to tell you a wonderful story when we are reunited wherever the end of life takes us. This work thus far focused on the very disease that took both of you from this world is dedicated to your memory.

To my friend **Quang Nghi Vu Huynh**, I hope you have found peace where kindred souls come to lay rest. I remember all the joy you brought us with Smash Bros games on the PSP you always had with you, and I wish I had brought you more joy when you were still with us. Your departure instilled in me a deep appreciation of those around me and the joys of whom that has sustained me all this time during my studies.

To my grandmother **Thi Thu Hong Vo.** Your love and care best encapsulated in your delicious springrolls nourished my childhood, and how you would peer into my overseas calls to my parents warms my soul during the cold months of the United States. I wish I had spoken in a way that you could hear my voice better during those calls.

ACKNOWLEDGEMENTS

People often say that a PhD is a marathon. It refers to the grueling long-run nature of the degree, but there is more to that image that should be appreciated. The people cheering you on in the sidelines, the coach (virtual or in-person) who pushes you but also keeps you healthy and focused, and the ones who run before to guide and inspire. They are all integral to the PhD marathon that is coming to an end for me, and it is to them that I dedicate this section.

First and foremost, my PhD advisors **Profs. Suzie H. Pun** and **Patrick S. Stayton.** Suzie, your infinite kindness, patience and encouragement has been invaluable to me. You foster such an amazing environment that has brought out the sense of camaraderie and scientific exploration in me that I know you are fond of. Pat, your constant challenges of my scientific acumen and your stories of the world constantly inspire me to be a better scientist. Yet you spare no words to advocate me to the world and remind me of how far I have come. Being your co-advisees feels like the perfect childhood to me – the freedom of exploration and enjoyment coupled with gentle guidance and a bulletproof safe zone. I can ask for no better.

I would also like to thank my advisory committee, past and present: **Profs. Matthew R. Golder, Hao Yuan Kueh & Chunlong Chen.** Your feedback and guidance have been invaluable to the direction of my work.

Pun Lab

My close collaborator, **Dr. Kefan Song.** I keep no secrets that you are invaluable to all I have been able to do during my PhD, setting up the in vivo and in vitro experiments in a fifth of the time it would have taken me to do so. You have also been my friend through the ups and downs of my PhD studies that I was fortunate enough to share with you. I wish you nothing but the best wherever my life takes you.

The Tea Time crew, **Dr. Lucy F. Yang, Dr. Kefan Song & soon-to-be-Dr. Melissa Ling.** It often is the highlight of my week to be able to enjoy a nice bubble tea with you guys and just talk about everything going on in our lives. Lucy, all the best in your new life in Japan. Melissa, I hope the Attune will be good to you for the rest of your time here, and I hope you and Lawrence will have many more marathons and Spartan races to enjoy in your life.

The MolES 340 crew, **Dr. Alexander Prossnitz, Dr. Trey Pichon, Ethan Mickelson & Trevor Corrigan.** It has been a blast learning, doing chemistry, and just being dudes all around my time with you all in MolES 340. Alex, thank you for guiding me on my first steps into hardcore chemistry. Trey, I deeply enjoyed brainstorming chemistry and talking about life with you. Ethan, your appetite for living life and knowledge has been so fun and inspiring, and thank you for allowing me to trust that our MolES lab will be in good hands. Trevor, your booming laugh makes MolES 340 all the more fun.

The pillars of the Pun Lab, **Dr. Nataly Kacherovsky and Prof. Drew Sellers.** Nataly, thank you for the delicious cakes from Dane, your patient maintenance of the lab, and your fascinating stories of the world. Drew, thank you for your stern yet caring way of showing me how to fix things in Foege as a MolES troublemaker.

My Pun Lab predecessors, **Dr. Shixian Lv, Dr. Meilyn Sylvestre, Dr. Albert Yen, Pacino Wang & Dr. Clinton Heinze.** Thank you for laying the foundations of my science, and for fostering the learning and caring culture that defines our lab.

My labmates, **Kairui Jiang, Abe Wu, Kelly Wang, Omeed Yazdani.** Kairui, your unflappable skills will bring the kidney project to heights unimaginable in my time. Abe, thank you for being my badminton mate, and for trying 20 different aptamer-polymer conjugation ideas that I thought of (that all failed). Kelly, thank you for advancing the bottlebrush project, and for taking over the vaccine project. Omeed, thank you for being with us during all those all-night in vivo studies.

My undergraduates, **Tran Luu, Benjamin Mous & Makenna Carnahan.** Thank you for being such wonderful mentees and scientists to work with, and I have absolute faith that you all will achieve great things in life. Being your mentor has been an honor and a wonderful learning and growing experience.

Stayton Lab

The one and only, **Dr. Simbarashe Jokonya.** Your methodical and unflappable approach to synthetic chemistry inspires me, and your deep insight into the world educates me. All the best to you, Kaitlin, and little Mumu, mate.

My labmates, **Patrick Gerber, Min-Yi You, Kacy Liang, and Jordan Koehler.** You were always there for when I needed to barge onto your doors and talk about what goes into my mind. Patrick, your determination in your work is inspiring and your friendship is steady and warming. Min, thank you for your friendship and patience as I keep mistaking your nationality. Kacy, my trusted fun yap-, complain- and rave-mate. Jordan, I am excited to follow your journey in the Stayton Lab.

My Stayton Lab predecessors, **Dr. Selvi Srinivasan, Dr. Ciana Lopez and Dr. Ayumi Pottenger.** Selvi, I have you to thank for knowing that drugamer synthesis can be conquered with the right method. Ciana, thank you for guiding me through my first in vitro experiments, and for your infectious love of rigorous science. Ayumi, your deep connection with everyone you meet, and the chaos and fun you bring to everywhere you go is a highlight of my doctoral life.

The Stayton Lab scientists and postdocs, **Dr. Sreekanth Kokkonda, Dr. Takuma Yoshikawa, Dr. Sarah Snyder, Dr. Naomi Hamelmann.** Sreekanth, thank you for bringing your wide chemistry knowledge and the CombiFlash to the Stayton Lab. Takuma, thank you for keeping the lab running in one piece and for being an absolute tour-de-force of a scientist. Sarah, happy hours have never been more fun with you. Naomi, thank you for being kind and understanding as I take down the GPC for the 20th time, and for all the fun times you bring to the lab.

Past mentors

My undergraduate mentors, **Dr. John T. Wilson & Dr. Daniel C. Shae.** You were with me during my first steps into science, and your rigorous training and nurturing had given me the footing I need to thrive in this stage of my life. I also want to thank the **SyBBURE-Searle** program for providing me with mentorship and support to tackle undergraduate research that laid the foundations of who I am today. Finally, I thank **Ms. Nguyet Pham** for sparking my interest in the chemical sciences.

Family

My parents, **Ky Phong Nguyen & Thi Kim Cuong Vo.** Thank you for your love, care and support for the entirety of my life. Through thick and thin, ups and downs, you have loved me and supported my decisions with all your heart, and I can only hope that the pride you feel in my achievements and the love I am trying to give back can compare with your love.

My brother, **Vu Phuong Nguyen.** Thank you for instilling in me my sense of adventure and independence, and for buying me all kinds of outdoor gear whenever I find myself back home. Thank you for caring about mom and dad all the time ever since I started living one ocean away.

My dear wife, **Do Thuy Dung (Ellie) Nguyen.** You have always been my biggest supporter, most reliable mental health counselor and adult guiding light in the turbulence that defined my life. Choosing to stay with you in Seattle and getting married to you (twice!) during our time here has been and will be the best decision I have ever made in my life. There is no one I would rather navigate life with, and I love you to the moon and back. I can only hope my love and dedication for you in the coming chapters of my life comes close to what you have given me then and now.

Friends

To the Cuoi Tuan group, **Hung Dang, Hao Dang, Quyen (Liz) Dao.** You have been my closest friends that I feel most comfortable with, and I can always rely on you guys for fun trips that nourished my soul.

My MolES cohort and Beer O'Clock mates, **Evan Pepper, Ryan Cardiff, Dr. Sarah Wait, Andrew Favor, Marc Exposit Goy, Rory Majule, Cassandra Maranas, Janis Shin & Joe Henthorn.** Hanging out with you during the pandemic has been some of the most fun experiences. I know for a fact you all will do great, and I hope we could keep in touch.

My Illenium and rave family of three years, **Phuc To, Phong Pham, Khanh Dinh, Cong Truong, Mai Dao, Thu Nguyen, Anh Nguyen, Nam Tran.** Letting loose and connecting with you guys in the pit has been the highlight of my later years.

My good friends, states and countries away. **Han Le, Huy Nguyen, Thinh Nguyen, Nhiem Ngo, Doan (Donna) Ezell.** Especially you, Han. Thank you for being a great friend, conversationalist, intellectual and gift giver. I cannot wait to see you defend your PhD soon.

My good friends down the hall in Foege, **Dr. Peter Chien & Duru Tasman.** I can always rely on you guys for yapping, having a good time and talking science.

Table of Contents

Chapter 1. Mobilizing the Cancer-Immunity Cycle – A Multiscale Drug Delivery Problem

Dinh Chuong Nguyen, *Patrick S. Stayton, Suzie H. Pun*

Synopsis

Cancer immunotherapy has transformed the cancer treatment landscape, but durable response remains elusive for many indications. Tumors exhibit a milieu of immunosuppressive features underpinning such therapy failures, the collection of which is best problematized by the 'cancer-immunity cycle' (CIC). By representing systemic antitumor responses as a cyclic self-reinforcing multistage process, opportunities for cancer immunotherapy development can be identified in the form of immunostimulatory or disinhibiting factors at each rate-limiting stage. Drug delivery obstacles exist in addressing each step of the CIC, and this work utilizes synthetic polymers to overcome these obstacles towards the goal of developing better cancer immunotherapies. By modulating antigen delivery and systemic immunostimulation, the synthetic polymers described in this work stimulates multiple stages of the CIC, in isolation or in combination, that results in improved antitumor responses.

i. The current state of cancer immunotherapy

Cancer immunotherapy has transformed the landscape of cancer treatment. The discovery of existing endogenous immune responses against malignancies and immunological mechanisms of response to traditional therapies inspired strategies to either stimulate or rescue these responses[1]. Chimeric Antigen Receptor T-cell (CAR-T cell) and Immune Checkpoint Inhibitor (ICI) therapies has yielded unprecedented response rates in hematological and solid cancers, respectively, with multiple advanced clinical trials underway for these therapies in combination with first-line treatments for a wide variety of indications[2,3]. Likewise, therapeutic cancer vaccines have graced the clinical landscape since the 1990s approval of the BCG vaccine for early-stage bladder cancer, with additional approvals for cellular vaccines for melanoma a decade later, and a milieu of vaccine clinical trials of an ever-expanding portfolio of approaches[4]. Yet, response to immunotherapy remains inconsistent at best and non-existent at worst for many cancers, chiefly solid malignancies[5]. While patient stratification and selection has helped improve response rates in clinical trials[6,7], there is still a need to address fundamental weaknesses in cancer immunotherapy.

ii. The 'Cancer-Immunity Cycle' and the development of immunotherapies

A fundamental underpinning of cancer's resistance to immunotherapy is its inherent immunosuppressive features[8]. The discovery of increased predisposition towards malignancies in immunodeficient populations, and transplantation studies highlighting tumor rejection capabilities of immunocompetent animals led to one of the newer Hallmarks of Cancer – evading immune destruction[9]. The immunosuppressive mechanisms of tumors are convoluted and multifactorial, but now extensively studied by a growing and respectable body of literature[10]. The frameworks of understanding established around this work have aided the development and adoption of cancer immunotherapy. One salient example is the stratification of tumors into different immunotypes characterized by immune cell infiltrate[10], which identified likely immunotherapy responders through this indirect measure of 'immunosuppression', and advanced cancer immunotherapy clinical trials throughout. An equally important framework, and more so in the context of this work, is Chen and Mellman's seminal "Cancer-Immunity Cycle" (CIC), first introduced in 2013[11] and later expanded in 2023[12].

The CIC (**Figure 1**, 2023 version) describes what can be considered an 'ideal' antitumor response in a systemic context. Simply put, it describes a sequential, multi-stage, but most importantly cyclical set of immune interactions (e.g. antigen recognition, cell activation, migration, cytolysis…) that overall drives a self-reinforcing antitumor immune response. The CIC can start from many of its different stages, but here we provide a simplified instance to illustrate its self-reinforcing nature. Tumor cell death, either spontaneous or treatment-induced, releases immune-distinguishable tumor antigens into the tumor microenvironment. These antigens are then carried to secondary lymphoid organs (SLOs, e.g. lymph nodes) through either lymphatic trafficking or cellular transport to be presented by antigen-presenting cells (APCs) for cytotoxic T-lymphocyte (CTL, or CD8+ T-cell) activation. CTLs migrate out of SLOs into circulation and towards tumors through chemotactic gradients, where they recognize and lyse tumor cells. These tumor cells in turn release more antigen, identical and/or distinct, that can be delivered to SLOs for the next iteration of the CIC. These subsequent rounds of prime-migrate-effect can reinforce depleted or exhausted immune cells of previous rounds, provide additional antigen recognition capabilities, and overall lead to a durable immune response that is conducive to remission and resistance to recurrence/metastasis[11,12].

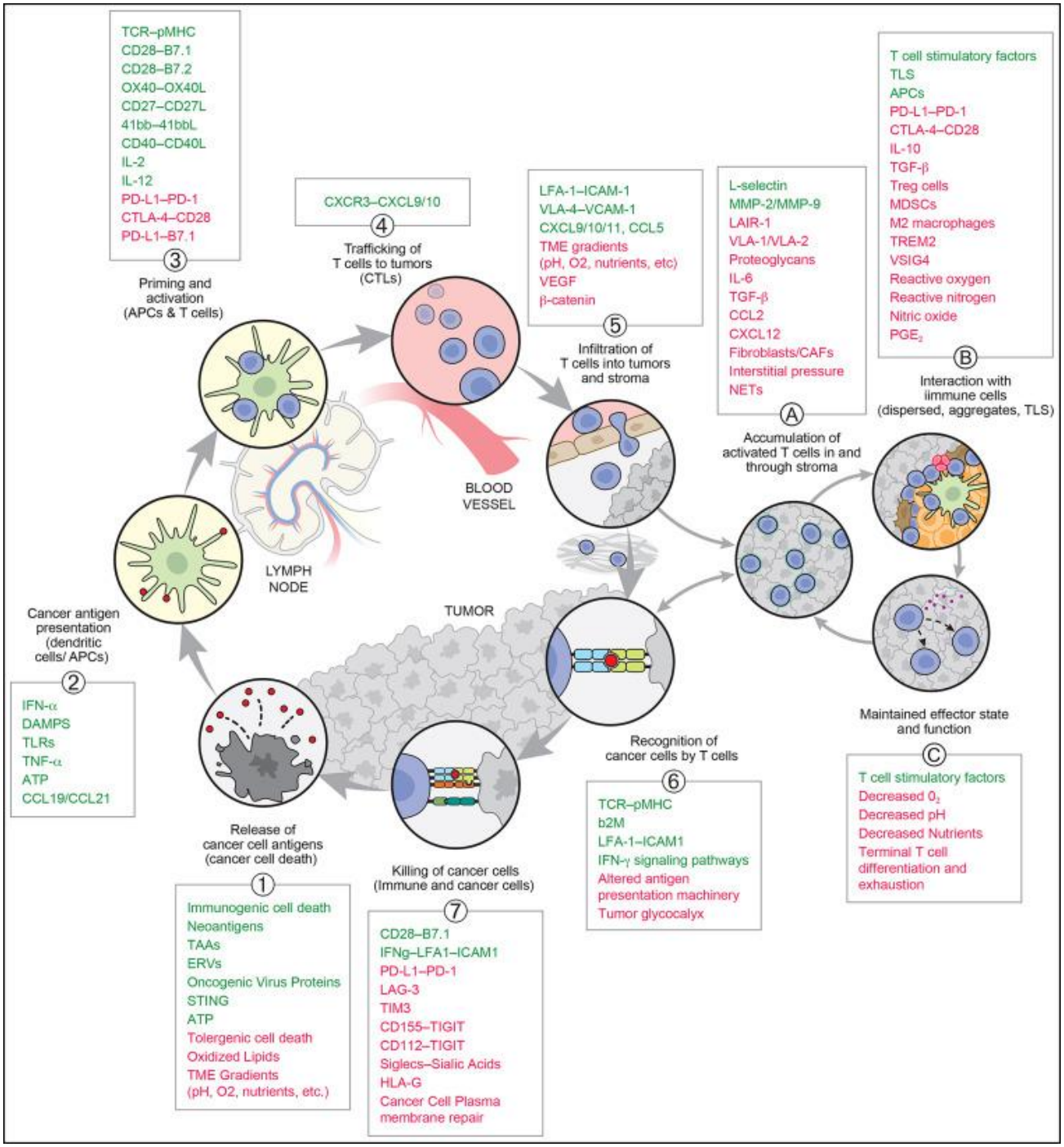

Figure 1. The 'Cancer-Immunity Cycle'[12]

In the development of immunotherapy, the CIC classifies the disparate tumor immunosuppression mechanisms through their relevance to each stage of the cycle (**Figure 1**), and problematizes them in a systemic manner. Describing systemic antitumor immunity as a self-reinforcing multistage process also recognizes each stage as rate-limiting, and draws out the systemic impact of each immunosuppressive mechanism from its limited local-level understanding. This enables more deliberate development of new immunotherapies focusing on stimulating or disinhibiting specific steps of the CIC instead of the pursuit of broad strokes of clinical efficacy[13,14]. This also illustrates the mechanisms behind the shortcomings of previous generations of immunotherapy, which may have been developed without this systems-level understanding of cancer immunity. Thus, the CIC is a valuable guiding principle to the development of new cancer immunotherapies, including that described herein in this work.

iii. Synthetic Polymers for Biomedical Applications, Drug Delivery and Cancer Immunotherapy

Synthetic polymers are attractive materials for biomedical applications. Their synthetic versatility and low-cost petroleum-based feedstock allows for a wide design space to achieve manufacturable formulations with desirable physicochemical properties[15]. Polymeric implants (e.g. silicone implants) have made its way into the clinic since the 1960s[16], while the first two decades of the 21st century have seen FDA approvals of polymeric formulations with advanced properties (e.g. drug-eluting stents[17], biodegradable depots[18], 3D-printed implants[19]). The contribution of polymers to medicine is wide-ranging and extensively covered elsewhere[20] – this work focuses on the application of synthetic polymers to drug delivery and cancer immunotherapy.

Synthetic polymers as drug delivery systems offer one major additional benefit to synthetic versatility. The macromolecular nature of polymers allows wider access to an important design axis not normally explored by medicinal chemistry – molecular size[21]. Molecular weight (MW) is an important factor in the pharmacokinetics and biodistribution of macromolecules[22], but the range of molecular weights for a particular ADME profile can be too large to be effectively modulated by small-molecule chemistry on the mili-Dalton (mDa) scale (assuming similar non-MW physicochemical characteristics)[23]. In contrast, the tractable control over the degrees of polymerization (DP) of synthetic polymers can modulate MW on the kilo-Dalton (kDa), sometimes even the mega-Dalton (MDa) scale. This is only one design parameter of its kind accessible through polymer chemistry, giving synthetic polymers access to a wide range of ADME profiles useful for the drug delivery of a wide variety of cargos. These design parameters are in addition to more traditional design parameters such as charge or hydropathy[24], whose access is also enhanced in synthetic polymers through comonomer choice and polymer backbone design. The application of synthetic polymers to drug delivery on multiple scales has been widely reported and summarized elsewhere[25].

Drug delivery challenges are pervasive and multi-scale in cancer immunotherapy. Each step of the CIC poses different drug delivery obstacles unique to the compartment it takes place in. For instance, release of cancer cell antigens requires cell death, which should be specific to tumors and tumor cells to avoid toxicity or even immune dysregulation[26]. Cancer antigen presentation, CTL priming and activation requires APC uptake and intracellular trafficking, and/or proper lymphatic drainage[27–29]. T-cell migration towards tumors requires chemotactic gradients, whose induction is possible but needs to be localized to tumors and cell subsets capable of generating such chemokines[30]. CTL recognition and killing of cancer cells can be aided by ICIs or adjuvant therapy, but again needs to be tumor-specific to avoid toxicity[31]. Within tumors, repolarizing tolerogenic APCs can facilitate productive immune-immune interactions, but requires navigation of the complex local tumor microenvironment and targeting specific receptors on these APCs[32]. Drug delivery strategies targeting one of these steps is feasible and can be productive, but the ability to modulate multiple stages of the CIC is also ideal. The illustrated advantages of synthetic polymers as drug delivery systems position them as ideal candidates for the development of cancer immunotherapies.

iv. Single-stage stimulation – Synthetic Polymers for Vaccine Delivery

Cancer vaccines are among the oldest cancer immunotherapy in clinical use. In contrast to the prophylactic (disease-preventing) manner often associated with ‘vaccines’, cancer vaccines are often used in a therapeutic (disease-treating) setting. This still shares the fundamentals with prophylactic vaccines – antigens are introduced and presented to the adaptive immune system for priming and activation, ultimately leading to durable adaptive immunity effective against disease[33].

Vaccines can be developed for humoral (i.e. antibody-mediated) or cellular (e.g. T-cell) immunity; the former is suitable for extracellular pathogens, while the latter is apt for intracellular pathogens[34]. Cancer is not a pathogen in the virulent sense of the word, and as the mechanistic origins of carcinogenesis is intracellular, cancer vaccines are best developed to elicit cellular immunity[35].

There exist many sources of antigen for cancer vaccination. Two of the earliest FDA-approved 'cancer vaccines'[4], the BCG vaccine for bladder cancer and talimogene laherparepvec (T-VEC) for unresectable melanoma, utilizes an approach often described as an "*in situ* vaccine". In the CIC, both treatments start at cancer cell death and antigen release – BCG infects cancer cells and induce immunogenic cell death[36], while T-VEC stimulates peripheral immune cells to induce inflammatory cell death[37]. Semantics of 'vaccination' aside, both BCG and T-VEC resulted in high instances of adverse events and low response rate in other indications[37,38]. The identification and artificial introduction of immune-recognizable tumor-specific antigens, so-called 'neoantigens', promises higher efficacy at lower toxicity from a more 'specific' immune response. The FDA-approved Sipuleucel-T (Provenge) for prostate cancer introduces the antigen prostatic acid phosphatase through autologous, artificially matured dendritic cells[39]. While having a more manageable toxicity profile, Provenge is costly and difficult to manufacture while offering only modest improvement over standard-of-care[39]. Subunit vaccines, such as peptide neoantigen vaccines, are more cost-effective and manufacturable, but are considerably less immunogenic and efficacious[40].

The CIC (**Figure 1**) highlights T-cell Receptor-Major Histocompatibility Complex (TCR-pMHC) interactions as a driver of both priming and activation in the SLOs, and killing of cancer cells in the tumor. This is traceable to antigen presentation to CTLs in SLOs – effective MHC-I presentation of tumor antigens in lymphoid APCs is a requisite for activation and expansion of tumoricidal CTLs expressing tumor-specific TCRs. Peptide neoantigen vaccines face a multi-scale drug delivery challenge in this context – lymphatic drainage, APC uptake, and intracellular trafficking to the MHC-I antigen presentation machinery[27–29]. Chapter 2 introduces Mannosylated Virus-Inspired Polymer for Endosomal Release (Man-VIPER, **Figure 2**), a self-assembling polymeric peptide delivery platform featuring a mannose outer corona and an endosome-lysing polymer-melittin conjugate[41]. Man-VIPER assembles into 40-50 nm micelles capable of efficient SLO drainage through subcutaneous administration, where its mannose corona facilitates APC uptake, and its melittin moiety enables endosomal escape of co-delivered peptides for processing into the MHC-I pathway. We show that Man-VIPER better mediates effective MHC-I presentation of delivered peptide antigens compared to non-endosomolytic formulations, which leads to superior antigen-specific CTL induction and antitumor activity. By directly facilitating TCR-pMHC interactions in the SLO, and indirectly enabling TCR-pMHC interactions in the tumor, Man-VIPER drives the CIC and yields a superior immunotherapy.

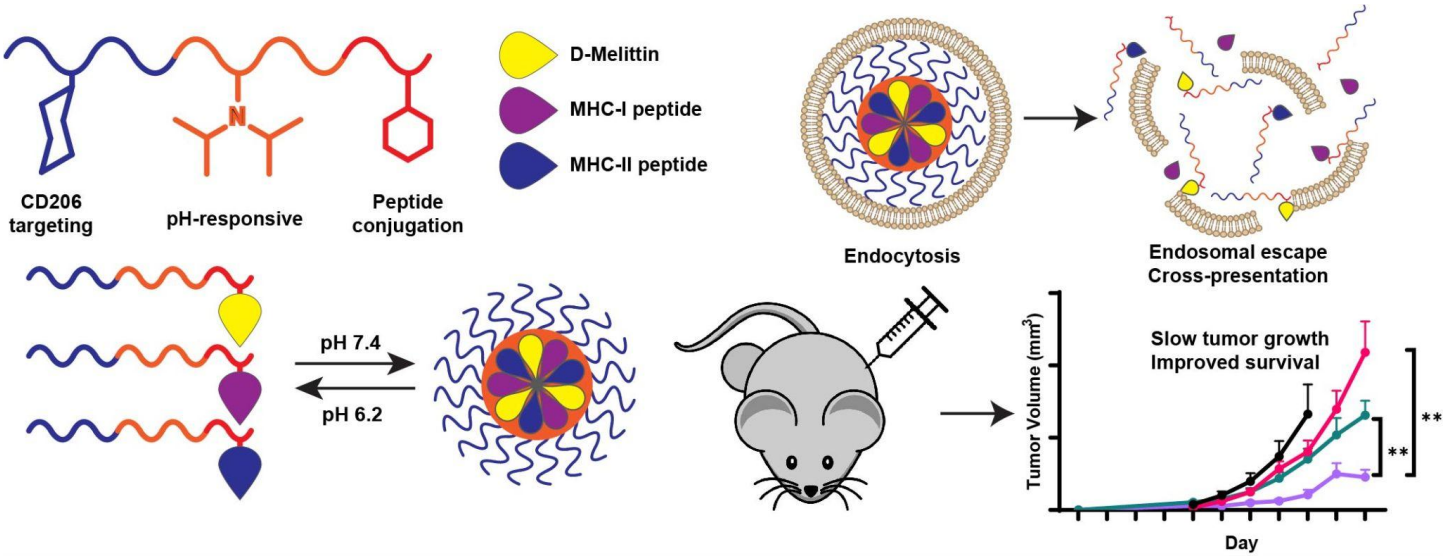

Figure 2 – A Mannosylated Polymer With Endosomal Release Properties for Peptide Vaccine Delivery

v. Specific-stage stimulation – Synthetic Polymers for Targeted Tumor Immune Cell Stimulation

Another attractive mode of cancer immunotherapy is local or systemic administration of immunostimulatory factors, first noted by the tumor-shrinking capabilities of Coley's toxins[42]. In this manner, the CIC offers attractive targets at many different stages of the cycle for therapeutic perturbation – for instance, cytokines such as interferons (IFN) or interleukins (IL), or chemokines such as C-C Chemokine Ligands (CCL) appear as driving factors in almost all stages of the CIC (**Figure 1**). As was the case for cancer vaccines, immune stimulation of this kind can drive the CIC for effective antitumor therapy. This approach was recognized through the FDA's approval of IFN-alpha (Intron A) and IL-2 (Proleukin) in the late 80s-early 90s. Since then, a respectable body of work has been dedicated to the advancement of cytokine therapy and later innate immune agonist therapy (e.g. Toll-Like Receptor or TLR agonists) in the clinic[43]. However, success has proven elusive due to a preponderance of immune-related adverse events (iRAEs)[44].

The pervasiveness of immunostimulatory factors in the CIC highlights therapeutic opportunities, but also belies perilous off-target toxicity. Cytokines and innate immune agonists, as part of the innate immune system, constitute the first line of defense against pathogens. A necessary consequence of this is ubiquitous responsiveness to these immunostimulatory factors to enable effective initial responses at different pathogen entry points[45]. This increases cytokine and innate immune agonist therapy's susceptibility to off-target effects, leading to iRAEs in clinical trials[44]. Drug delivery platforms for these therapeutics have been developed to address these off-target effects, though these challenges can persist in the presence of additional obstacles[46]. For instance, antibody-drug conjugates (ADCs) face issues with manufacturability, functionalization and drug incorporation[47], while severe iRAEs have persisted in clinical trials of ADCs of innate immune agonists (e.g. UP-NEXT, Mersana Therapeutics).

Chapter 3 of this work introduces polySTING, a polymeric targeted prodrug platform of the Stimulator of Interferon Genes (STING) pathway for targeted STING activation in tumoral APCs in intravenous therapy. STING is a ubiquitous cytosolic pathogenic DNA sensor whose activation can mount potent antitumor responses, but whose clinical translation has been affected by iRAEs[48]. PolySTING utilizes our 'drugamer' platform – a STING agonist is formulated into a prodrug monomer labile to endosomal enzymes, and co-polymerized with a mannose monomer for APC targeting and internalization[49]. Upon

intravenous administration, polySTING targets and preferentially deliver a STING agonist to tumoral APCs for specific APC STING activation. This strategy elicits a dendritic cell (DC)-mediated antitumor immune response, restricting perturbation to DC-driven steps in the CIC. Intravenous polySTING cancer immunotherapy is tolerable, but stimulates a potent adaptive immune response that can suppress the growth of aggressive, poorly immunogenic murine tumor models.

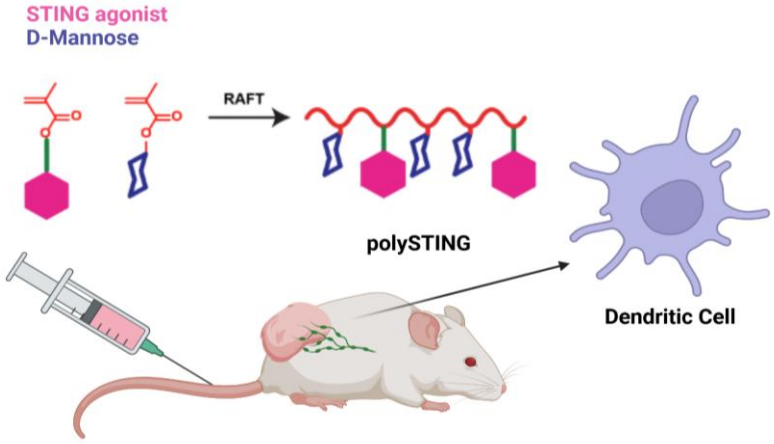

Figure 3 – Mannosylated STING Agonist 'Drugamers' for Dendritic Cell-Mediated Cancer Immunotherapy

vi. Exploring Multi-stage Stimulation – Combinatorial approaches with synthetic polymers

The rate-limiting nature of each stage of the CIC highlights the potential for multi-stage stimulation, which can feed one another and overcome limitations on other steps to improve CIC progression. While the previous section describes the peril of non-specific multi-stage immune activation, a well-executed immune stimulation strategy can result in strong therapeutic effects. Drug delivery strategies can bring about these desired outcomes, exemplified by one applied by the Seder group with their self-assembling peptide-TLR7/8a (SNP-7/8a) neoantigen peptide vaccine platform[50]. A homologous SNP-7/8a intravenous prime-boost (SNP-IV), or heterologous subcutaneous-intravenous prime-boost (SNP-SQ-IV) strategy outperformed homologous subcutaneous prime-boost (SNP-SQ) in a therapeutic cancer vaccine model. While SNP-SQ had been demonstrated to effectively overcome the TCR-pMHC stages of the CIC, SNP-IV and SNP-SQ-IV remodeled the tumor microenvironment and modulated splenic antigen presentation to enhance the tumoral sub-cycle of the CIC[51,52]. Similar results have been reported with different vaccine vectors, such as adenoviral vectors[53], demonstrating the utility of multi-stage CIC stimulation.

Chapter 4 takes a step back compared to the SNP-7/8a work and explores the co-delivery of Man-VIPER and STING agonist drugamers in a homologous prime-boost subcutaneous vaccination context (**Figure 4**). While co-delivery of antigen and adjuvant have been explored elsewhere[54], and that this can be construed as merely stronger stimulation of the same stages, the synthetic versatility of the polymeric STING drugamers enables structure-delivery-activity studies. We explored two STING agonist drugamers – polySTING and a Man-VIPER-analogous self-assembling STING polymer, CP-STING – with distinct physicochemical characteristics that may enable different delivery profiles when formulated with Man-VIPER. We showed distinct immunostimulatory activity between polySTING and CP-STING, where CP-STING exhibited higher dose-dependent potency but also immuno-cytotoxicity. We showed polySTING and CP-STING both enhance vaccine efficacy of Man-VIPER through distinct immunological mechanisms traceable to their distinct pharmacokinetics profile. While free STING treatment resulted in immune stimulation superior to VIPER and sometimes on par with the druagmers, it did not enhance VIPER efficacy. This shows the utility of multi-stage stimulation, but also its perils and technical difficulty.

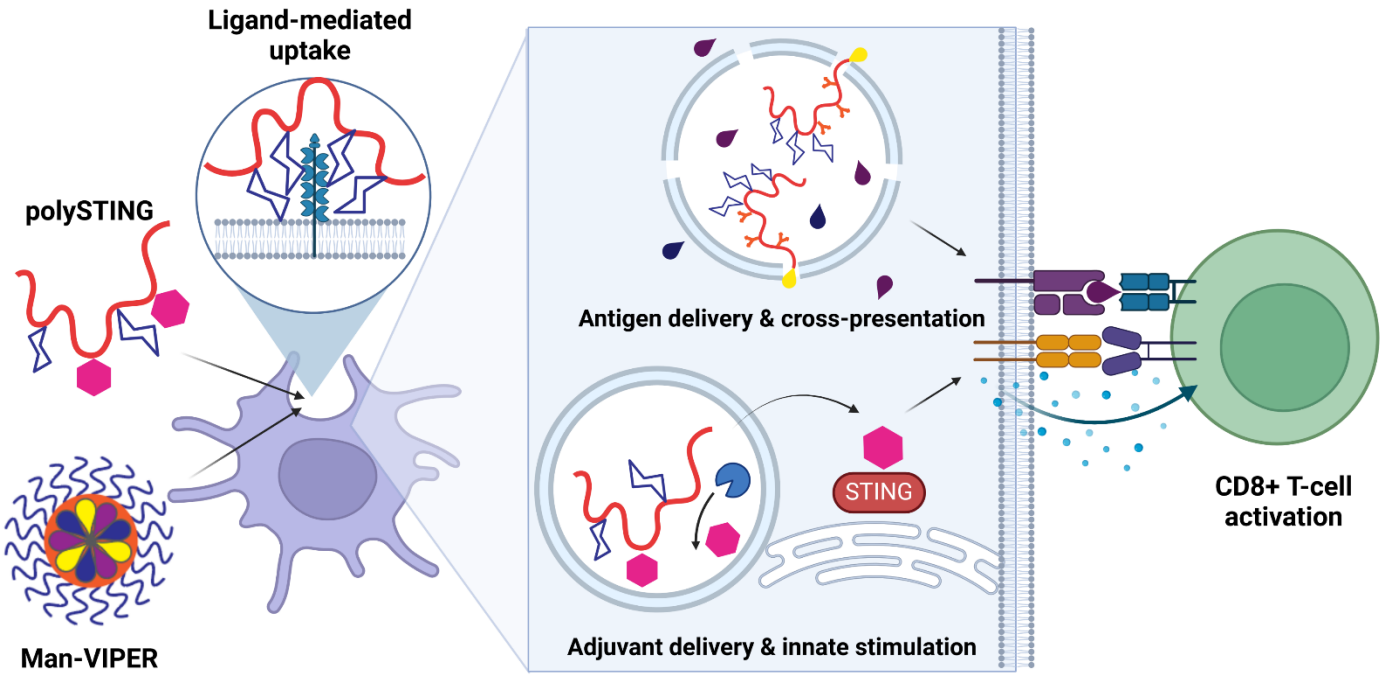

Figure 4 - Peptide Vaccine Formulations with Structurally Distinct STING Agonist Drugamers Induce Discrete, Efficacious Antitumor Responses

vi. Moving past the endogenous cancer-immunity cycle – Facilitating CAR-T cell manufacturing with synthetic polymers

CAR-T cells are among the first revolutionary cancer immunotherapies. However, their complex manufacturing and associated costs hinder their wider clinical impact[55,56]. In a way, this can be construed as an obstacle to effective cancer-immunity cycle mobilization via CAR-T cells. CAR transduction is part of this challenge, requiring lentiviral transfection that necessitates bioprocess complexities and controls[57]. Non-viral methods suffer from low efficiency due to specific complexities with T-cell cargo processing pathways[58,59], posing another drug delivery challenge to the cancer-immunity cycle. In this chapter, we expand upon our previous work developing cationic bottlebrush polymers that were capable of T-cell transfection, but limited by low uptake[60]. Functionalizing these polymers with glycoprotein-interacting phenylboronic acids (PBAs) allows for receptor-mediated endocytosis via sialylations on the T-cell surface[61]. We demonstrated that cationic-PBA bottlebrush polymers mediate superior transfection in the immortalized human T-cell line Jurkat compared to cationic bottlebrush polymers, across a number of different nucleic acid cargoes. We also showed this to be a Jurkat-specific effect in our results thus far. In all, we showcase another albeit indirect approach to mobilize the cancer-immunity cycle by facilitating CAR-T cell manufacturing with synthetic polymers.

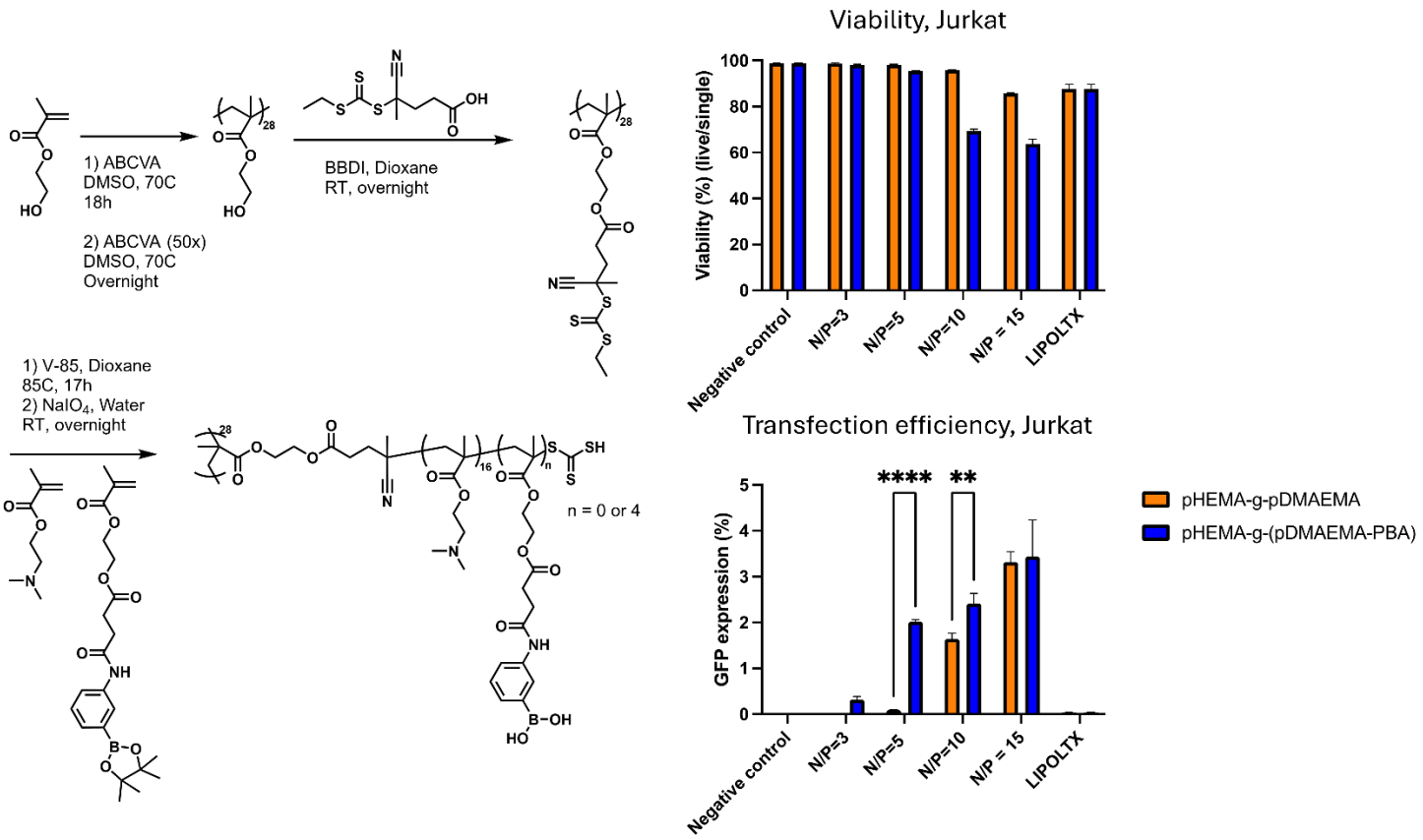

Figure 5 - Cationic Bottlebrush Polymers Functionalized with Phenylboronic Acid for T-Cell Transfection

vii. References

(1) Mellman, I.; Coukos, G.; Dranoff, G. Cancer Immunotherapy Comes of Age. *Nature* **2011**, *480* (7378), 480–489. https://doi.org/10.1038/nature10673.

(2) Zhang, X.; Zhu, L.; Zhang, H.; Chen, S.; Xiao, Y. CAR-T Cell Therapy in Hematological Malignancies: Current Opportunities and Challenges. *Front. Immunol.* **2022**, *13*.

(3) Sun, Q.; Hong, Z.; Zhang, C.; Wang, L.; Han, Z.; Ma, D. Immune Checkpoint Therapy for Solid Tumours: Clinical Dilemmas and Future Trends. *Signal Transduct. Target. Ther.* **2023**, *8* (1), 1–26. https://doi.org/10.1038/s41392-023-01522-4.

(4) Hargrave, A.; Mustafa, A. S.; Hanif, A.; Tunio, J. H.; Hanif, S. N. M. Recent Advances in Cancer Immunotherapy with a Focus on FDA-Approved Vaccines and Neoantigen-Based Vaccines. *Vaccines* **2023**, *11* (11), 1633. https://doi.org/10.3390/vaccines11111633.

(5) Keilson, J. M.; Knochelmann, H. M.; Paulos, C. M.; Kudchadkar, R. R.; Lowe, M. C. The Evolving Landscape of Immunotherapy in Solid Tumors. *J. Surg. Oncol.* **2021**, *123* (3), 798–806. https://doi.org/10.1002/jso.26416.

(6) van der Meel, R.; Sulheim, E.; Shi, Y.; Kiessling, F.; Mulder, W. J. M.; Lammers, T. Smart Cancer Nanomedicine. *Nat. Nanotechnol.* **2019**, *14* (11), 1007–1017. https://doi.org/10.1038/s41565-019-0567-y.

(7) Kossai, M.; Radosevic-Robin, N.; Penault-Llorca, F. Refining Patient Selection for Breast Cancer Immunotherapy: Beyond PD-L1. *ESMO Open* **2021**, *6* (5), 100257. https://doi.org/10.1016/j.esmoop.2021.100257.

(8) Kalathil, S. G.; Thanavala, Y. High Immunosuppressive Burden in Cancer Patients: A Major Hurdle for Cancer Immunotherapy. *Cancer Immunol. Immunother.* **2016**, *65* (7), 813–819. https://doi.org/10.1007/s00262-016-1810-0.

(9) Hanahan, D.; Weinberg, R. A. Hallmarks of Cancer: The Next Generation. *Cell* **2011**, *144* (5), 646–674. https://doi.org/10.1016/j.cell.2011.02.013.

(10) Chen, D. S.; Mellman, I. Elements of Cancer Immunity and the Cancer–Immune Set Point. *Nature* **2017**, *541* (7637), 321–330. https://doi.org/10.1038/nature21349.

(11) Chen, D. S.; Mellman, I. Oncology Meets Immunology: The Cancer-Immunity Cycle. *Immunity* **2013**, *39* (1), 1–10. https://doi.org/10.1016/j.immuni.2013.07.012.

(12) Mellman, I.; Chen, D. S.; Powles, T.; Turley, S. J. The Cancer-Immunity Cycle: Indication, Genotype, and Immunotype. *Immunity* **2023**, *56* (10), 2188–2205. https://doi.org/10.1016/j.immuni.2023.09.011.

(13) Pio, R.; Ajona, D.; Ortiz-Espinosa, S.; Mantovani, A.; Lambris, J. D. Complementing the Cancer-Immunity Cycle. *Front. Immunol.* **2019**, *10*.

(14) Li, Y.; Liu, X.; Zhang, X.; Pan, W.; Li, N.; Tang, B. Immune Cycle-Based Strategies for Cancer Immunotherapy. *Adv. Funct. Mater.* **2021**, *31* (50), 2107540. https://doi.org/10.1002/adfm.202107540.

(15) Tian, H.; Tang, Z.; Zhuang, X.; Chen, X.; Jing, X. Biodegradable Synthetic Polymers: Preparation, Functionalization and Biomedical Application. *Prog. Polym. Sci.* **2012**, *37* (2), 237–280. https://doi.org/10.1016/j.progpolymsci.2011.06.004.

(16) Teo, A. J. T.; Mishra, A.; Park, I.; Kim, Y.-J.; Park, W.-T.; Yoon, Y.-J. Polymeric Biomaterials for Medical Implants and Devices. *ACS Biomater. Sci. Eng.* **2016**, *2* (4), 454–472. https://doi.org/10.1021/acsbiomaterials.5b00429.

(17) Khan, W.; Farah, S.; Domb, A. J. Drug Eluting Stents: Developments and Current Status. *J. Controlled Release* **2012**, *161* (2), 703–712. https://doi.org/10.1016/j.jconrel.2012.02.010.

(18) Park, K.; Skidmore, S.; Hadar, J.; Garner, J.; Park, H.; Otte, A.; Soh, B. K.; Yoon, G.; Yu, D.; Yun, Y.; et al. Injectable, Long-Acting PLGA Formulations: Analyzing PLGA and Understanding Microparticle Formation. *J. Controlled Release* **2019**, *304*, 125–134. https://doi.org/10.1016/j.jconrel.2019.05.003.

(19) Ho, C. M. B.; Ng, S. H.; Yoon, Y.-J. A Review on 3D Printed Bioimplants. *Int. J. Precis. Eng. Manuf.* **2015**, *16* (5), 1035–1046. https://doi.org/10.1007/s12541-015-0134-x.

(20) Maitz, M. F. Applications of Synthetic Polymers in Clinical Medicine. *Biosurface Biotribology* **2015**, *1* (3), 161–176. https://doi.org/10.1016/j.bsbt.2015.08.002.

(21) Hawker, C. J. Molecular Weight Control by a "Living" Free-Radical Polymerization Process. *J. Am. Chem. Soc.* **1994**, *116* (24), 11185–11186. https://doi.org/10.1021/ja00103a055.

(22) Tibbitts, J.; Canter, D.; Graff, R.; Smith, A.; Khawli, L. A. Key Factors Influencing ADME Properties of Therapeutic Proteins: A Need for ADME Characterization in Drug Discovery and Development. *mAbs* **2016**, *8* (2), 229–245. https://doi.org/10.1080/19420862.2015.1115937.

(23) Imran ul-haq, M.; Lai, B. F. L.; Chapanian, R.; Kizhakkedathu, J. N. Influence of Architecture of High Molecular Weight Linear and Branched Polyglycerols on Their Biocompatibility and Biodistribution. *Biomaterials* **2012**, *33* (35), 9135–9147. https://doi.org/10.1016/j.biomaterials.2012.09.007.

(24) Kaminskas, L. M.; Boyd, B. J.; Porter, C. J. Dendrimer Pharmacokinetics: The Effect of Size, Structure and Surface Characteristics on ADME Properties. *Nanomed.* **2011**, *6* (6), 1063–1084. https://doi.org/10.2217/nnm.11.67.

(25) Englert, C.; Brendel, J. C.; Majdanski, T. C.; Yildirim, T.; Schubert, S.; Gottschaldt, M.; Windhab, N.; Schubert, U. S. Pharmapolymers in the 21st Century: Synthetic Polymers in Drug Delivery Applications. *Prog. Polym. Sci.* **2018**, *87*, 107–164. https://doi.org/10.1016/j.progpolymsci.2018.07.005.

(26) Printezi, M. I.; Kilgallen, A. B.; Bond, M. J. G.; Štibler, U.; Putker, M.; Teske, A. J.; Cramer, M. J.; Punt, C. J. A.; Sluijter, J. P. G.; Huitema, A. D. R.; et al. Toxicity and Efficacy of Chronomodulated Chemotherapy: A Systematic Review. *Lancet Oncol.* **2022**, *23* (3), e129–e143. https://doi.org/10.1016/S1470-2045(21)00639-2.

(27) Mempel, T. R.; Henrickson, S. E.; von Andrian, U. H. T-Cell Priming by Dendritic Cells in Lymph Nodes Occurs in Three Distinct Phases. *Nature* **2004**, *427* (6970), 154–159. https://doi.org/10.1038/nature02238.

(28) Acar, H.; M. Ting, J.; Srivastava, S.; L. LaBelle, J.; V. Tirrell, M. Molecular Engineering Solutions for Therapeutic Peptide Delivery. *Chem. Soc. Rev.* **2017**, *46* (21), 6553–6569. https://doi.org/10.1039/C7CS00536A.

(29) Joffre, O. P.; Segura, E.; Savina, A.; Amigorena, S. Cross-Presentation by Dendritic Cells. *Nat. Rev. Immunol.* **2012**, *12* (8), 557–569. https://doi.org/10.1038/nri3254.

(30) Raza, S.; Rajak, S.; Tewari, A.; Gupta, P.; Chattopadhyay, N.; Sinha, R. A.; Chakravarti, B. Multifaceted Role of Chemokines in Solid Tumors: From Biology to Therapy. *Semin. Cancer Biol.* **2022**, *86*, 1105–1121. https://doi.org/10.1016/j.semcancer.2021.12.011.

(31) Walsh, M. J.; Dougan, M. Checkpoint Blockade Toxicities: Insights into Autoimmunity and Treatment. *Semin. Immunol.* **2021**, *52*, 101473. https://doi.org/10.1016/j.smim.2021.101473.

(32) Andón, F. T.; Digifico, E.; Maeda, A.; Erreni, M.; Mantovani, A.; Alonso, M. J.; Allavena, P. Targeting Tumor Associated Macrophages: The New Challenge for Nanomedicine. *Semin. Immunol.* **2017**, *34*, 103–113. https://doi.org/10.1016/j.smim.2017.09.004.

(33) Tran, T.; Blanc, C.; Granier, C.; Saldmann, A.; Tanchot, C.; Tartour, E. Therapeutic Cancer Vaccine: Building the Future from Lessons of the Past. *Semin. Immunopathol.* **2019**, *41* (1), 69–85. https://doi.org/10.1007/s00281-018-0691-z.

(34) Amanna, I. J.; Slifka, M. K. Contributions of Humoral and Cellular Immunity to Vaccine-Induced Protection in Humans. *Virology* **2011**, *411* (2), 206–215. https://doi.org/10.1016/j.virol.2010.12.016.

(35) Nagorsen, D.; Scheibenbogen, C.; Marincola, F. M.; Letsch, A.; Keilholz, U. Natural T Cell Immunity against Cancer. *Clin. Cancer Res.* **2003**, *9* (12), 4296–4303.

(36) Hakim, A. A.; Grand, N. G. Mechanism of Action of BCG Vaccine on Neoplastic Proliferation and Host Immune Responses. *J. Pharm. Sci.* **1976**, *65* (3), 339–343. https://doi.org/10.1002/jps.2600650306.

(37) Rehman, H.; Silk, A. W.; Kane, M. P.; Kaufman, H. L. Into the Clinic: Talimogene Laherparepvec (T-VEC), a First-in-Class Intratumoral Oncolytic Viral Therapy. *J. Immunother. Cancer* **2016**, *4* (1), 53. https://doi.org/10.1186/s40425-016-0158-5.

(38) Orihuela, E.; Herr, H. W.; Pinsky, C. M.; Whitmore Jr., W. F. Toxicity of Intravesical BCG and Its Management in Patients with Superficial Bladder Tumors. *Cancer* **1987**, *60* (3), 326–333. https://doi.org/10.1002/1097-0142(19870801)60:3<326::AID-CNCR2820600309>3.0.CO;2-5.

(39) Schwaab, T.; Pili, R. Provenge: Combating Prostate Cancer with a Vengeance? *Expert Rev. Vaccines* **2011**, *10* (8), 1113–1114. https://doi.org/10.1586/erv.11.85.

(40) Tsoras, A. N.; Champion, J. A. Protein and Peptide Biomaterials for Engineered Subunit Vaccines and Immunotherapeutic Applications. *Annu. Rev. Chem. Biomol. Eng.* **2019**, *10* (1), 337–359. https://doi.org/10.1146/annurev-chembioeng-060718-030347.

(41) Song, K.; Nguyen, D. C.; Luu, T.; Yazdani, O.; Roy, D.; Stayton, P. S.; Pun, S. H. A Mannosylated Polymer with Endosomal Release Properties for Peptide Antigen Delivery. *J. Controlled Release* **2023**, *356*, 232–241. https://doi.org/10.1016/j.jconrel.2023.03.004.

(42) Wiemann, B.; Starnes, C. O. Coley's Toxins, Tumor Necrosis Factor and Cancer Research: A Historical Perspective. *Pharmacol. Ther.* **1994**, *64* (3), 529–564. https://doi.org/10.1016/0163-7258(94)90023-X.

(43) Propper, D. J.; Balkwill, F. R. Harnessing Cytokines and Chemokines for Cancer Therapy. *Nat. Rev. Clin. Oncol.* **2022**, *19* (4), 237–253. https://doi.org/10.1038/s41571-021-00588-9.

(44) Olsen, T. A.; Zhuang, T. Z.; Caulfield, S.; Martini, D. J.; Brown, J. T.; Carthon, B. C.; Kucuk, O.; Harris, W.; Bilen, M. A.; Nazha, B. Advances in Knowledge and Management of Immune-Related Adverse Events in Cancer Immunotherapy. *Front. Endocrinol.* **2022**, *13*.

(45) Uthaisangsook, S.; Day, N. K.; Bahna, S. L.; Good, R. A.; Haraguchi, S. Innate Immunity and Its Role against Infections. *Ann. Allergy. Asthma. Immunol.* **2002**, *88* (3), 253–265. https://doi.org/10.1016/S1081-1206(10)62005-4.

(46) Riley, R. S.; June, C. H.; Langer, R.; Mitchell, M. J. Delivery Technologies for Cancer Immunotherapy. *Nat. Rev. Drug Discov.* **2019**, *18* (3), 175–196. https://doi.org/10.1038/s41573-018-0006-z.

(47) Abdollahpour-Alitappeh, M.; Lotfinia, M.; Gharibi, T.; Mardaneh, J.; Farhadihosseinabadi, B.; Larki, P.; Faghfourian, B.; Sepehr, K. S.; Abbaszadeh-Goudarzi, K.; Abbaszadeh-Goudarzi, G.; et al. Antibody–Drug Conjugates (ADCs) for Cancer Therapy: Strategies, Challenges, and Successes. *J. Cell. Physiol.* **2019**, *234* (5), 5628–5642. https://doi.org/10.1002/jcp.27419.

(48) Garland, K. M.; Sheehy, T. L.; Wilson, J. T. Chemical and Biomolecular Strategies for STING Pathway Activation in Cancer Immunotherapy. *Chem. Rev.* **2022**, *122* (6), 5977–6039. https://doi.org/10.1021/acs.chemrev.1c00750.

(49) Su, F.-Y.; Srinivasan, S.; Lee, B.; Chen, J.; Convertine, A. J.; West, T. E.; Ratner, D. M.; Skerrett, S. J.; Stayton, P. S. Macrophage-Targeted Drugamers with Enzyme-Cleavable Linkers Deliver High Intracellular Drug Dosing and Sustained Drug Pharmacokinetics against Alveolar Pulmonary Infections. *J. Controlled Release* **2018**, *287*, 1–11. https://doi.org/10.1016/j.jconrel.2018.08.014.

(50) Lynn, G. M.; Sedlik, C.; Baharom, F.; Zhu, Y.; Ramirez-Valdez, R. A.; Coble, V. L.; Tobin, K.; Nichols, S. R.; Itzkowitz, Y.; Zaidi, N.; et al. Peptide–TLR-7/8a Conjugate Vaccines Chemically Programmed for Nanoparticle Self-Assembly Enhance CD8 T-Cell Immunity to Tumor Antigens. *Nat. Biotechnol.* **2020**, *38* (3), 320–332. https://doi.org/10.1038/s41587-019-0390-x.

(51) Baharom, F.; Ramirez-Valdez, R. A.; Tobin, K. K. S.; Yamane, H.; Dutertre, C.-A.; Khalilnezhad, A.; Reynoso, G. V.; Coble, V. L.; Lynn, G. M.; Mulè, M. P.; et al. Intravenous Nanoparticle Vaccination Generates Stem-like TCF1+ Neoantigen-Specific CD8+ T Cells. *Nat. Immunol.* **2021**, *22* (1), 41–52. https://doi.org/10.1038/s41590-020-00810-3.

(52) Baharom, F.; Ramirez-Valdez, R. A.; Khalilnezhad, A.; Khalilnezhad, S.; Dillon, M.; Hermans, D.; Fussell, S.; Tobin, K. K. S.; Dutertre, C.-A.; Lynn, G. M.; et al. Systemic Vaccination Induces CD8+ T Cells and Remodels the Tumor Microenvironment. *Cell* **2022**, *185* (23), 4317-4332.e15. https://doi.org/10.1016/j.cell.2022.10.006.

(53) Ramirez-Valdez, R. A.; Baharom, F.; Khalilnezhad, A.; Fussell, S. C.; Hermans, D. J.; Schrager, A. M.; Tobin, K. K. S.; Lynn, G. M.; Khalilnezhad, S.; Ginhoux, F.; et al. Intravenous Heterologous Prime-Boost Vaccination Activates Innate and Adaptive Immunity to Promote Tumor Regression. *Cell Rep.* **2023**, *42* (6), 112599. https://doi.org/10.1016/j.celrep.2023.112599.

(54) Shae, D.; Baljon, J. J.; Wehbe, M.; Christov, P. P.; Becker, K. W.; Kumar, A.; Suryadevara, N.; Carson, C. S.; Palmer, C. R.; Knight, F. C.; et al. Co-Delivery of Peptide Neoantigens and Stimulator of Interferon Genes Agonists Enhances Response to Cancer Vaccines. *ACS Nano* **2020**, *14* (8), 9904–9916. https://doi.org/10.1021/acsnano.0c02765.

(55) Hao, Y.; Hsu, W.-C.; Parzynski, C. S.; Degtyarev, E.; Hampson, L. V.; Masood, A.; Wu, W.-H. Effectiveness of Tisagenlecleucel versus Real-World Standard of Care in Relapsed/Refractory Follicular Lymphoma. *J. Comp. Eff. Res.* **2023**, *12* (7), e220173. https://doi.org/10.57264/cer-2022-0173.

(56) Vormittag, P.; Gunn, R.; Ghorashian, S.; Veraitch, F. S. A Guide to Manufacturing CAR T Cell Therapies. *Curr. Opin. Biotechnol.* **2018**, *53*, 164–181. https://doi.org/10.1016/j.copbio.2018.01.025.

(57) Okuma, A. Generation of CAR-T Cells by Lentiviral Transduction. In *Mammalian Cell Engineering*; Humana, New York, NY, 2021; pp 3–14. https://doi.org/10.1007/978-1-0716-1441-9_1.

(58) Raes, L.; De Smedt, S. C.; Raemdonck, K.; Braeckmans, K. Non-Viral Transfection Technologies for next-Generation Therapeutic T Cell Engineering. *Biotechnol. Adv.* **2021**, *49*, 107760. https://doi.org/10.1016/j.biotechadv.2021.107760.

(59) Charpentier, J. C.; King, P. D. Mechanisms and Functions of Endocytosis in T Cells. *Cell Commun. Signal.* **2021**, *19* (1), 92. https://doi.org/10.1186/s12964-021-00766-3.

(60) Olden, B. R.; Cheng, Y.; Yu, J. L.; Pun, S. H. Cationic Polymers for Non-Viral Gene Delivery to Human T Cells. *J. Controlled Release* **2018**, *282*, 140–147. https://doi.org/10.1016/j.jconrel.2018.02.043.

(61) Ji, M.; Li, P.; Sheng, N.; Liu, L.; Pan, H.; Wang, C.; Cai, L.; Ma, Y. Sialic Acid-Targeted Nanovectors with Phenylboronic Acid-Grafted Polyethylenimine Robustly Enhance siRNA-Based Cancer Therapy. *ACS Appl. Mater. Interfaces* **2016**, *8* (15), 9565–9576. https://doi.org/10.1021/acsami.5b11866.

Chapter 2 – A Mannosylated Polymer With Endosomal Release Properties For Peptide Antigen Delivery

*Kefan Song, **Dinh Chuong Nguyen**, Tran Luu, Omeed Yazdani, Debashish Roy, Patrick S. Stayton, Suzie H. Pun*

Synopsis

Peptide cancer vaccines have had limited clinical success despite their safety, characterization and production advantages. We hypothesize that the poor immunogenicity of peptides can be surmounted by delivery vehicles that overcome the systemic, cellular and intracellular drug delivery barriers faced by peptides. Here, we introduce Man-VIPER, a self-assembling (40-50nm micelles), pH-sensitive, mannosylated polymeric peptide delivery platform that targets dendritic cells in the lymph nodes, encapsulates peptide antigens at physiological pH, and facilitates endosomal release of antigens at acidic endosomal pH through a conjugated membranolytic peptide melittin. We used D-melittin to improve the safety profile of the formulation without compromising the lytic properties. We evaluated polymers with both releasable (Man-VIPER-R) or non-releasable (Man-VIPER-NR) D-melittin. Both Man-VIPER polymers exhibited superior endosomolysis and antigen cross-presentation compared to non-membranolytic D-melittin-free analogues (Man-AP) *in vitro*. *In vivo*, Man-VIPER polymers demonstrated an adjuvanting effect, induced the proliferation of antigen-specific cytotoxic T cells and helper T cells compared to free peptides and Man-AP. Remarkably, antigen delivery with Man-VIPER-NR generated significantly more antigen-specific cytotoxic T cells than Man-VIPER-R *in vivo*. As our candidate for a therapeutic vaccine, Man-VIPER-NR exerted superior efficacy in a B16F10-OVA tumor model. These results highlight Man-VIPER-NR as a safe and powerful peptide cancer vaccine platform for cancer immunotherapy.

i. Introduction

Cancer subunit vaccines utilize neoantigens to train the immune system to recognize and attack tumor cells[1]. Among multiple tumor antigen sources, peptide antigens have garnered significant attention for multiple reasons: improved safety compared to whole antigens, facile incorporation of multiple epitopes, low cost, manufacturing ease, shelf stability and well-defined structures[1]. Peptide antigen sequences can be identified empirically by mass spectrometry and sequencing or computationally designed and validated[2]. Despite these salient features, peptide antigen vaccines have only met moderate clinical success, and even less so in the context of cancer vaccines due to peptides' poor immunogenicity[3].

Cytotoxic T-cells ($CD8^+$) T-cells are most prominently credited for tumor-killing responses. As $CD8^+$ T cell priming requires antigen presentation through the MHC class I (MHC-I) pathway (called "cross-presentation"), providing access to the MHC-I presentation is important to cancer peptide vaccines' ability to induce tumor clearance[4]. There are three major barriers to MHC-I presentation for peptide subunit vaccine formulations – systemic, cellular and intracellular. Systemically, peptides need to preferentially localize into lymph nodes (LNs) where T-cell priming takes place[5], while facing risk of degradation due to peptidases in circulation[6]. Cellularly, peptides need to be internalized by antigen-presenting cells (APCs) in order to be properly processed for antigen presentation. Intracellularly, peptides need to access the cytosolic compartment in order to access the MHC-I presentation pathway[7]. All of these pose significant barriers to generating efficient antitumor responses that peptide formulations alone cannot surmount.

Various drug delivery platforms have been proposed to surmount these barriers with impressive results. Antigens can either be conjugated to targeting moieties or formulated into sub-50 nm nanoparticles that can traffic to LNs from the interstitium[8–10]. For instance, soluble antigen-mannose conjugates[11] and self-assembling antigen micelles[12] or antigen-protein complexes[13] have both been demonstrated to preferentially accumulate in the LNs. Interestingly, the same technology could be leveraged to overcome the cellular barrier – APC-targeting moieties and nanoparticle formulation have both been shown to promote endocytosis[14,15]. These can be in turn incorporated into controlled-release platforms such as hydrogels to impart additional benefits[16]. To surmount the intracellular barriers, strategies such as 'proton-sponge' cationic materials[17], pH-responsive solubility-switching anionic polymers and combinations thereof[18,19], amphiphilic polymers[20,21] or membrane-perforating biomolecules[22] have been employed to facilitate endosomal release. Successful integration of technologies to overcome these three barriers have resulted in preclinically efficacious formulations[23].

We previously reported two formulations for cancer peptide subunit vaccine applications. Our first report utilizes our well-developed Virus-Inspired Polymers for Endosomal Release (VIPER) platform[24]. The VIPER platform is a self-assembling pH-responsive cationic amphiphilic polymer conjugated to the membranolytic peptide melittin[25]. Melittin is sequestered in the self-assembled structure at physiological conditions, but is bioavailable in the acidic endosome where it can lyse the endosomal membrane to release disulfide-conjugated peptide cargo into the cytosol for MHC-I presentation. We co-formulated a cationic VIPER conjugated to antigen peptide with the nucleic acid adjuvant poly(I:C) to form polyplexes[26]. This formulation relied on non-specific, charge-mediated uptake to local dendritic cells after subcutaneous injection. The VIPER formulation improved antigen cross-presentation when tested *in vitro* and increased generation of antigen-specific cytotoxic T cells, but had modest effects on tumor growth rate and overall survival, possibly due to poor LN localization. In our second report, we focused on targeting dendritic cells (DCs) in the draining LN and synthesized a diblock copolymer that self-assembles into ~30 nm micelles with a poly(mannose) corona for targeting mannose receptor (CD206) expressed on DCs[27]. We demonstrated that the targeted micelles were effective in LN localization and induction of DC maturation. In summary, our first formulation surmounted the intracellular and cellular barriers, but not the systemic barrier while our second surmounted the systemic and cellular barrier, but leaves the intracellular barrier unchallenged.

In this work, we addressed the aforementioned shortcomings with a mannosylated VIPER platform that self-assembles into sub-60nm micelles that allows for efficient LN draining and DC targeting. Upon endocytosis and acidification, the VIPER design with the pH-responsive, melittin-conjugated inner block induces endosomal rupture and antigen release into the cytosol and thus the MHC-I antigen presentation pathway in addition to MHC-II presentation from intact matured endosomes (**Figure 1**). We also used D-amino acids instead of L-amino acids to synthesize the melittin peptide (D-Melittin) to prevent antibody generation against the VIPER carrier[28]. In addition, we explored stable conjugation of melittin to the polymeric backbone using a pentafluorobenzyl-thiol reaction to form a thioether bond to improve the endosomal release properties of VIPER[29] compared to our previously-employed disulfide conjugation strategy. Our previous work established that polymer-conjugated melittin is considerably more membranolytic[25], which can translate to improved endosomal release of antigen and MHC-I antigen presentation. Therefore, in this work, we evaluated a form of VIPER that retains melittin as a polymer-bound species within the endosome (VIPER-NR) as well as a form of VIPER for which melittin can be reduced and released in as a monomeric peptide (VIPER-R). The mannosylated VIPER formulation induced efficient endosomal release and MHC-I antigen presentation *in vitro*, and potent T-cell responses against a model antigen *in vivo*. Ultimately, this platform significantly slowed tumor growth and prolonged survival in an aggressive melanoma model, demonstrating the utility of our platform as a cancer peptide subunit vaccine formulation.

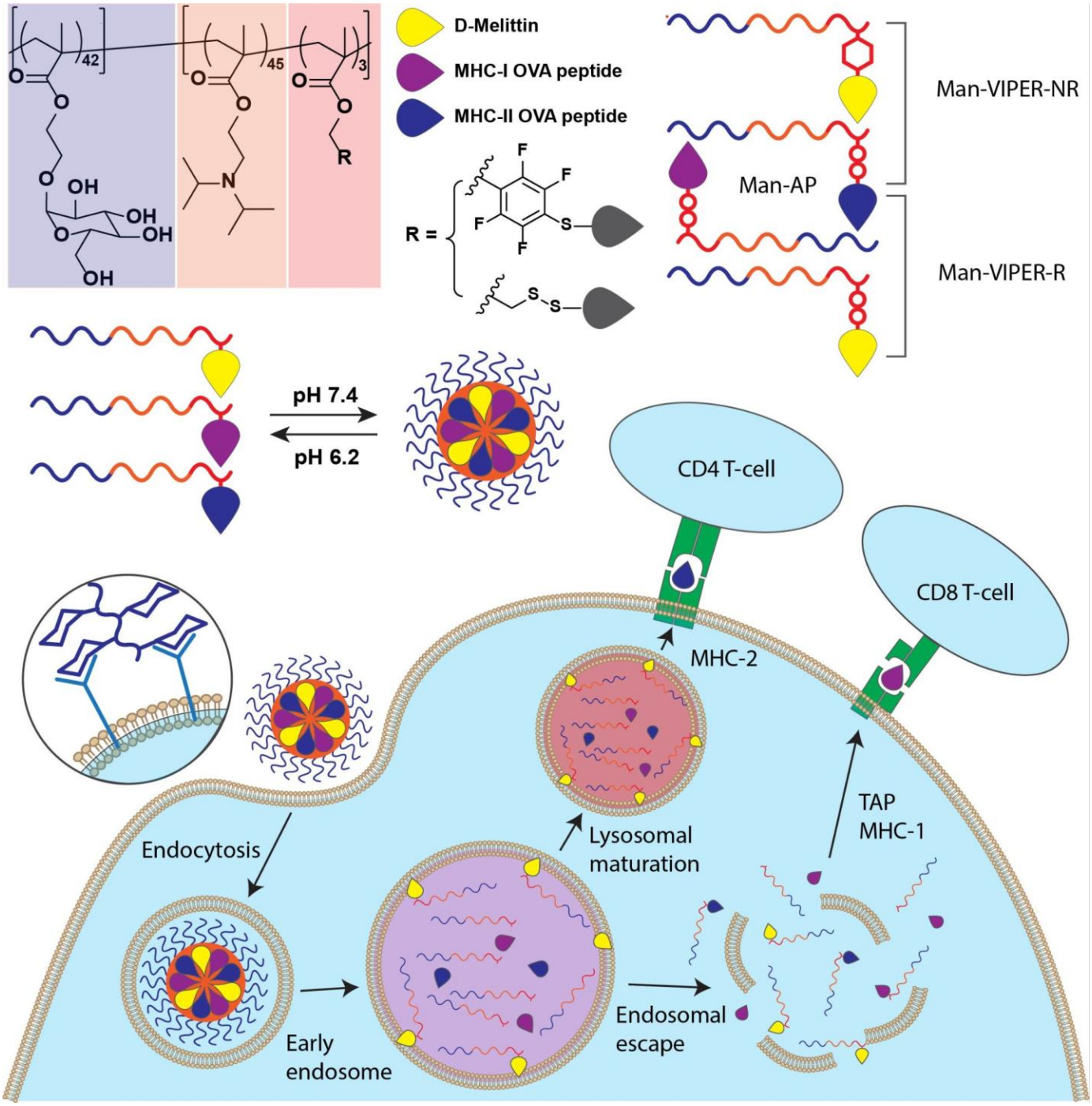

Figure 1. Schematic illustration of Man-VIPER delivery systems. The Man-VIPER formulations consist of releasable disulfide conjugated OVA antigens, and either releasable disulfide conjugated membranolytic melittin (Man-VIPER-R) or non-releasable pentafluorobenzyl conjugated melittin (Man-VIPER-NR). The formulations self-assemble into well-defined micelles, which are preferentially endocytosed via the mannosylated hydrophilic segment. The micelles disassemble upon endosomal maturation, and either results in endosomal disruption and cross-presentation of MHC-1 epitopes, or lysosomal maturation and presentation of MHC-2 epitopes, to their own respective T-cell subsets.

ii. Materials and methods

Materials

RAFT chain transfer agent 4-((((2-Carboxyethyl)thio)carbonothioyl)thio)-4-cyanopentanoic acid (CCC) was purchased from Boron Molecular. Azobisisobutyronitrile (AIBN), 4,4'-azobis(4-cyanovaleric acid) (ABCVA), cysteamine hydrochloride, piperidine, triisopropylsilane (TIPS) and ethanedithiol (EDT) were purchased from Sigma-Aldrich. Mannose ethyl methacrylate (ManEMA) was purchased from Omm Scientific. Diisopropylcarbodiimide (DIC) and ethyl cyanohydroxyiminoacetate (Oxyma) were purchased from Chem-Impex. Dimethoxybenzene (DMB), trifluoroacetic acid (TFA), acetic acid (AcOH), acetonitrile (ACN) and Ellman's reagent were purchased from Fisher Scientific. Dithiothreitol (DTT) was purchased from Enzo Life Sciences. All were used as received. Diisopropyl ethyl methacrylate (DIPAMA) was purchased from Sigma-Aldrich. Pyridyl disulfide ethyl methacrylate (PDSEMA, also known as 2-(2-pyridinyldithio)ethyl methacrylate) and pentafluorobenzyl methacrylate (PFBzMA) was purchased from Tokyo Chemical Industries Ltd. These aforementioned monomers were purified by passing through a basic alumina column to remove any existing inhibitor prior to polymerization. Anhydrous N-methyl-2-pyrrolidone (NMP, 99.5%), and dimethylsulfoxide (DMSO, > 99%) were purchased from Sigma-Aldrich and stored with activated molecular sieves. Protected amino acids were purchased from Novabiochem and used as received. Buffers were prepared in-house using endotoxin-free water and salts purchased from Fisher Scientific.

Polymer synthesis

All polymers were synthesized by RAFT polymerization. Briefly, the mannose hydrophilic block (ManCTA) was synthesized by RAFT polymerization of ManEMA. ManEMA was combined with CCC, ABCVA (CCC:ManEMA = 1:44.4, CCC:ABCVA = 1:20) in dry DMSO (2.5 wt% monomer), purged with argon for 30 minutes, and reacted at 70°C for 3h with vigorous stirring. ManCTA was purified by 3x precipitation in 1:1 (v/v) acetone and diethyl ether, dissolving in DMF in-between, and dried *in vacuo* for 2 days. To synthesize CP-R and CP-NR, ManCTA was combined with AIBN (ManCTA:AIBN = 10:1), DIPAMA and either PDSEMA for CP-R (ManCTA:DIPAMA:PDSEMA = 1:45:8) or PFBzMA for CP-NR (ManCTA:DIPAMA:PFBzMA = 1:45:5) in NMP (20 wt% monomer), purged with argon for 30 minutes, and reacted at 70°C in NMP solvent (20 wt% monomer) for 18h with vigorous stirring. CP-R was purified through serial dialysis in NMP for 1 day and deionized (DI) water for 3 days. CP-NR was dialyzed in NMP for 1 day, and 30x AIBN used in polymerization was added directly to the solution and reacted at 70°C overnight to remove CTA head-groups[30], which can interfere with the conjugation reaction from aminolyzed thiols on the head-groups (data not shown). CP-NR is then purified in a similar manner to CP-R. All polymers were lyophilized post-dialysis and stored at -20°C until used.

Polymer Characterization

All ^{1}H NMR spectra were recorded on a Bruker AV 300 (Bruker Corporation, Billerica, MA) nuclear magnetic resonance (NMR) instrument in deuterated DMSO (DMSO-d6). Polymer molecular weights (Mw, Mn) and polydispersity index (Đ = Mw/Mn) were determined by gel permeation chromatography (GPC). The system consisted of an Agilent 1260 HPLC stack running heated LiBr-supplemented (0.1% w/v) DMF mobile phase at a flow rate of 1 mL min^{-1} through a semi-prep three-column setup (Phenogel-TSKgel). Samples (5 mg/mL) were filtered through a 0.2 μm PTFE filter before analysis. We observed a difference between the theoretical Mn calculated by NMR and the Mn calculated by GPC, as well as a lower-than-expected shift in retention time for the block copolymers. This may be caused the presence of bimolecular termination products in the mannose macro-CTA owing to high conversion masking the retention time shift, as well as differences in

the molecular weight-hydrodynamic radii relationship between mannose-CTA and CP polymers. The size distribution profiles of micelles were recorded on a dynamic light scattering (DLS) system (DynaPro NanoStar, Wyatt technology) at a micelle concentration of 1 mg/mL.

Peptide synthesis and conjugation

MHC-1 OVA epitope peptide (CSSSIINFEKL, or OVA-1), MHC-2 OVA epitope peptide (CSSISQAVHAAHAEINEAG, or OVA-2) and D-Melittin (GIGAVLKVLTTGLPALISWIKRKRQQC, or D-Mel) were synthesized using a Liberty Blue (CEM) microwave peptide synthesizer on Rink Amide resin (Millipore) using Fmoc-piperidine deprotection and DIC-Oxyma activation chemistry before cleavage and deprotection (5% DMB, 2.5% TIPS, 2.5% EDT, 0.5% H2O in TFA), and purification with reverse-phase HPLC (TFA-supplemented H2O:ACN).

AP-1, AP-2 and VIPER-R were synthesized by conjugating OVA-1, OVA-2 and D-Melittin to CP-R using disulfide exchange chemistry. Briefly, CP-R and peptides were dissolved in separate solutions of 2% (v/v) AcOH in DMSO at a CP-R concentration equivalent to 12.5 mM PDSEMA and 14-19 mM peptide. The two solutions were combined in equal volumes and allowed to react overnight at room temperature. The reaction solution was then dialyzed against DMSO (SpectraPor 6-8 kDa MWCO) for 2 days, against MilliQ water for 3 days to remove free peptides, and lyophilized over the weekend. Peptide loading was assessed by reacting conjugated polymers with DTT for 30 minutes at 37°C and comparing 2-mercaptopyridine release (Abs_{max} = 347 nm) compared to unconjugated polymers as previously reported by our group[25].

VIPER-NR was synthesized by conjugating D-Melittin to CP-NR using a recently-described pentafluorobenzyl-thiol (PFB-thiol) reaction[29]. Briefly, D-Melittin was dissolved with CP-NR at a CP-NR concentration equivalent to 30 mM PFB and 10 mM peptide. The concentrations were adjusted to achieve a theoretical peptide loading of 19% by weight of the final conjugate. DBU (2 mmol) was added in excess to counteract acidic counterions present in D-Melittin and the reaction allowed to proceed overnight at room temperature. The reaction was quenched by addition of TFA, and dialyzed as above to remove free peptides. Peptide loading was assessed by reacting conjugated and unconjugated polymers with a 2-fold excess of cysteamine hydrochloride (50 mM in dry DMSO) in a similar manner to conjugation, and comparing cysteamine depletion using Ellman's reagent to determine extent of PFB conjugation. ^{19}F-NMR was also used to determine PFB substitution extent, but was disfavored due to low solubility of polymers in NMR solvents coupled with low mass sensitivity of ^{19}F-NMR.

Micelle formulation

We utilized our previously-described pH-switch method to formulate our micelles with slight modifications[27]. Briefly, individual polymer conjugates were dissolved in endotoxin-free water. The polymer solutions were combined at equal volumes. HCl (0.6% to 2.5% of 1 N solution) was added to the mixture until a clear solution was obtained. The solution was probe-sonicated for 30 seconds to ensure complete dissolution. A solution of 0.2 M pH 5.0 monobasic sodium phosphate was added, followed by 0.2 M pH 9.0 dibasic sodium phosphate to obtain the final pH in the range of 6.6-7.4. The formulations were prepared at ambient conditions. The critical micellar concentration (CMC) and transition point of the micelles were determined using the Nile Red assay[31]. Briefly, micelles with different concentrations or pH were mixed with 1μM Nile Red. Fluorescence intensity was measured using a plate reader (ex. 556 nm, em. 625 nm).

Hemolysis assay for endosomal rupture quantification

The polymers' ability to disrupt endosomal membranes in a pH-dependent manner was evaluated using a hemolysis assay as previously described[32]. Briefly, red blood cells (RBCs) isolated from de-identified human whole blood samples (Bloodworks Northeast) were pelleted at 500g and washed three times with 150 mM NaCl and once with pH 7.4 PBS. The washed RBCs were resuspended in PBS of various pHs (pH 7.4, 6.2, and 5.6). RBCs were then treated with polymers at various concentrations of melittin or equivalent melittin-free polymer concentrations (polymer:RBC 10:190 v/v) in V-bottom well-plates and incubated at 37°C for 1 h. Cells were then pelleted and the supernatant was transferred to flat-bottom well-plates. The amount of hemoglobin leakage into the supernatant was quantified via absorbance spectroscopy (Tecan, λ = 575 nm) and normalized to 100% hemolysis with 20% Triton X-100 and 0% hemolysis with PBS at its respective pHs.

Cell lines and animals

The B16F10-OVA cell line (gift of Prof. Amanda Lund) was cultured in DMEM supplemented with 10% FBS and 1% P/S. The DC2.4-Gal8-GFP and Hela-Gal8-GFP cell lines were generated as previously described[26]. DC2.4-Gal8-GFP cells were cultured in RPMI supplemented with 10% heat-inactivated FBS, 1% P/S, 1x nonessential amino acids, 10 mM HEPES buffer and 55 μM β-mercaptoethanol. Hela-Gal8-GFP cells were cultured in DMEM supplemented with 10% FBS and 1% P/S. The B3Z cell line (gift of Prof. Nilabh Shastri) was cultured in RPMI supplemented with 10% heat-inactivated FBS, 1% P/S, 1 mM sodium pyruvate and 50 μM β-mercaptoethanol. Cells were incubated at 37°C and 5% CO_2. Female C57BL/6 mice aged 6 to 8 weeks were purchased from Charles River Laboratories. All animal studies were approved by the University of Washington Institutional Animal Care and Use Committee (IACUC).

Gal8 endosomal disruption assay

DC2.4-Gal8-GFP and Hela-Gal8-GFP cells were cultured in TC-treated 96-well imaging plates overnight. Cells were incubated with polymers containing 2 μg/ml CSSSIINFEKL, 2 μg/ml CSSISQAVHAAHAEINEAGR, 38 μg/ml D-Melittin peptide for 18 hr. Media was replaced with Fluorobrite DMEM supplemented with 10% FBS, 25 mM HEPES. Hoechst 33342 was used to stain the nucleus and propidium iodide was used to stain the dead cells. Images were obtained using a Leica SP8X confocal microscope using a 20x objective.

DC2.4 Cross-Presentation and Viability Assays

The DC2.4 cell line was seeded into U-bottom TC-treated 96 well plates at 20,000 cells per well and incubated at 37°C and 5% CO2 overnight. To assess cross-presentation, cells were treated with the ovalbumin protein or polymers containing 2 μg/ml CSSSIINFEKL and 2 μg/ml CSSISQAVHAAHAEINEAGR with different amounts of D-Melittin peptide. After 4 hours, cells were washed twice with PBS and co-cultured with 100,000 B3Z cells for an additional 18-20 hours in the incubator. After co-culture, cells were pelleted by centrifugation and resuspended in 150 μL CPRG lysis buffer (0.15 mM chlorophenol red-β-D-galactopyranoside + 0.1% Triton-X100 + 9 mM MgCl2 + 100 μM β-mercaptoethanol + PBS). Cells were incubated at 37°C in the dark for 90 minutes. The supernatant was transferred to a flat-bottom 96-well plate and the absorbance was measured at 570 nm (reference 650 nm) using a plate reader. Cell viability was analyzed using the MTS/PMS assay 24 hours post-treatment (Promega).

In vivo dendritic cell activation

Female C57BL/6 mice were injected subcutaneously at the tail base with PBS or with 15 μg CSSSIINFEKL and 15 μg CSSISQAVHAAHAEINEAGR antigen peptides either in free peptide form or in Man-VIPER-R or Man-VIPER-NR formulations. Polymer formulations also contained 286 μg D-Melittin peptide (1:5 molar ratio of antigen and melittin). Twenty-four hours-post immunization, inguinal lymph nodes were harvested and digested in 50 U/mL type IV collagenase + 100 U/mL DNase I. Single-cell suspension was obtained by mashing the tissue through a 70 μm cell strainer. Cells were stained for viability with Zombie NIR viability kit, blocked with anti-CD16/32, and then stained with anti-CD86-BV510, anti-CD40-FITC, anti-CD11c-APC and anti-SIINFEKL-PE. An Attune NxT flow cytometer was used to analyze the data.

In vivo T cell responses

Female C57BL/6 mice were immunized with PBS, free peptides, AP, Man-VIPER-R and Man-VIPER-NR on day 0 and day 14. Spleens were harvested on day 21. Tissues were passed through 70 μm cell strainers and treated with ACK lysis buffer. Splenocytes were resuspended in IMDM and plated in separate 96-well plates for tetramer staining and intracellular cytokine staining (ICCS). For the tetramer staining, splenocytes were stained with Zombie NIR for viability and then stained with PE-labeled H-2Kb/SIINFEKL tetramer (NIH Tetramer Core). Cells were blocked with anti-CD16/32 and stained with anti-CD3-eFluor450 and anti-CD8-FITC. For ICCS, splenocytes were either restimulated with 5 μg/ml SIINFEKL peptide or 5 mg/ml OVA protein. 3 hr later, Protein Transport Inhibitor Cocktail (PTIC) was added and cells were incubated for another 3 hr. After incubation, cells were stained with Zombie NIR for viability, blocked with anti-CD16/32 and stained with either anti-CD3-eFluor450 + anti-CD8-FITC for $CD8^+$ T cells or anti-CD3-eFluor450 + anti-CD4-FITC for $CD4^+$ T cells. Cells were then treated with the BD Cytofix/Cytoperm Fixation/Permeabilization Kit and stained with either anti-TNFα-PE and anti-IFNγ-APC for $CD8^+$ T cells and anti-IL-2-PE and anti-IFNγ-APC for $CD4^+$ T cells. Data was collected using the Attune NxT flow cytometer and analyzed using Flowjo.

Tumor studies

Female C57BL/6 mice (N=8) were inoculated with 1.5×10^5 B16F10-OVA cells in the right-hind flank on day 0. On days 3, 10, and 19, mice were immunized with PBS, free peptides containing 15 μg CSSSIINFEKL and 15 μg CSSISQAVHAAHAEINEAGR, AP or MAN-VIPER-NR containing the same amount of peptides. On days 4, 11, and 20, mice were injected with 100 μg of anti PD-1 ICB (Clone 29F.1A12, BioXCell) via intraperitoneal injection. Tumor length and width were then measured every other day using a vernier caliper, and volume was subsequently calculated using the formula: Volume = $(\text{Width}^2 \times \text{Length}) \div 2$. Weight was also measured every other day. Mice were euthanized if total tumor volume exceeded 1500 mm^3, visible discharge was observed on ulcers of the tumors, or the body weight loss exceeded 20%.

Statistical analysis

Statistical analysis was performed using the Graphpad Prism software. One-way ANOVA with post-hoc Tukey HSD test was used to compare more than two groups. Log-rank test was used for survival analysis.

iii. Results and discussion

Polymer synthesis and characterization

Polymers were synthesized by RAFT polymerization in a two-step process. Mannose ethyl methacrylate (ManEMA) was polymerized first to make a macro-RAFT chain transfer agent (ManCTA), followed by copolymerization of diisopropylamino ethyl methacrylate (DIPAMA) with either pyridyl disulfide ethyl methacrylate (PDSEMA) or pentafluorobenzyl methacrylate (PFBzMA), to form well-defined diblock copolymers with low dispersity (**Table S1, Figure S1-S2**). The polymers without any conjugated peptides are denoted as CP, or control polymer, in accordance with previous nomenclature. To differentiate between polymers synthesized with the PDSEMA and PFBzMA monomers, which result in a labile disulfide or a nonlabile thioether bond upon peptide conjugation respectively, we denote polymers as CP-R (CP-Releasable) and CP-NR (CP-Non-Releasable).

We selected the model antigen OVA and the lytic peptide D-Melittin for conjugation. OVA is highly immunogenic and its MHC-I and MHC-II epitope sequences are well-defined, so we chose these peptide sequences with an N-terminal Cys-Ser-Ser sequence for conjugation (CSSIINFEKL and CSSISQAVHAAHAEINEAG, respectively). Melittin was chosen for its effective membrane-lytic capability and used in its D-amino acid form, which retains lytic activity without the adverse immunogenicity of L-melittin. [28]. Both antigens were conjugated through disulfide exchange with PDSEMA on CP-R, while D-melittin was conjugated through either PDSEMA on CP-R or a base-catalyzed thiol-PFBzMA substitution reaction on CP-NR[29]. We decided to explore different conjugation strategies solely for D-Melittin because of its direct role in endosomal escape induction in VIPER, as well as the need to retain releasability for conjugated antigen. All peptides were conjugated with >50% efficiency as measured by the amount of conjugated peptides. The antigen-functionalized polymers without D-Melittin are denoted AP-1 and AP-2 for "Antigen Polymer", demarcated by the MHC epitope identity. The melittin-functionalized polymers are denoted MP-R and MP-NR for "Melittin Polymer" in accordance with the CP-R and CP-NR nomenclature. The peptide conjugation results are displayed in **Table 1**. ^{19}F-NMR was also performed to confirm conjugation for MP-NR (**Figure S3**).

Table 1. Characterization of peptide conjugation in constituents of Man-VIPER formulations

Polymer name	Conjugated peptide	Approx. peptide/polymer[a]	Peptide wt%[a]
Man-AP-1	OVA MHC-I epitope	2.9	14.1
Man-AP-2	OVA MHC-II epitope	3.0	22.7
Man-MP-R	D-melittin	2.2	22.3
Man-MP-NR	D-melittin	1.8	19.4

a - Calculated by determining residual conjugating groups - quantifying PDS release with DTT reduction (AP-1, AP-2, MP-R) or cysteamine depletion with Ellman's assay (MP-NR)

The full formulation (visualized in **Figure 1**) of AP-1 coformulated with AP-2 and either MP-R (Man-VIPER-R) or MP-NR (Man-VIPER-NR) self-assembles into micelles with narrowly-distributed sizes at physiological pH (**Figure 2a**). Melittin-containing formulations (i.e. Man-VIPER-R and Man-VIPER-NR) had larger micelle sizes (51.6 nm and 40 nm in diameter, respectively) compared to non-melittin (i.e. Man-AP, 27.6 nm), likely due to additional peptide in the micelle core. The size difference is consistent with our previous work showing that formulations with higher peptide loading exhibit larger micelle sizes[27]. Man-VIPER-NR formed smaller micelle sizes than Man-VIPER-R, possibly due to pi-pi stacking

interactions from the pentafluorobenzyl linkers within the micelle core, which has been observed with other polymeric micellar systems in the literature[33]. All formulations exhibited pH-dependent micelle disassembly with a transition point around pH 6.2 as determined by a Nile Red assay (**Figure 2b**). Interestingly, Man-VIPER-NR exhibits disassembly over a broader pH range compared to Man-VIPER-NR or Man-AP, also possibly due to pi-pi stacking interactions within the reversibly hydrophobic polymer blocks. To determine whether or not Man-VIPER-NR might have a lower critical micelle concentration (CMC) than Man-VIPER-R due to aforementioned additional pi-pi interactions within the core, we measured CMC by evaluating micellization at various polymer concentrations using the Nile Red Assay but observed no difference between the two formulations (**Figure S4**). These results demonstrate that Man-VIPER-R and Man-VIPER-NR exhibit desired self-assembly and pH-responsive properties for antigen delivery.

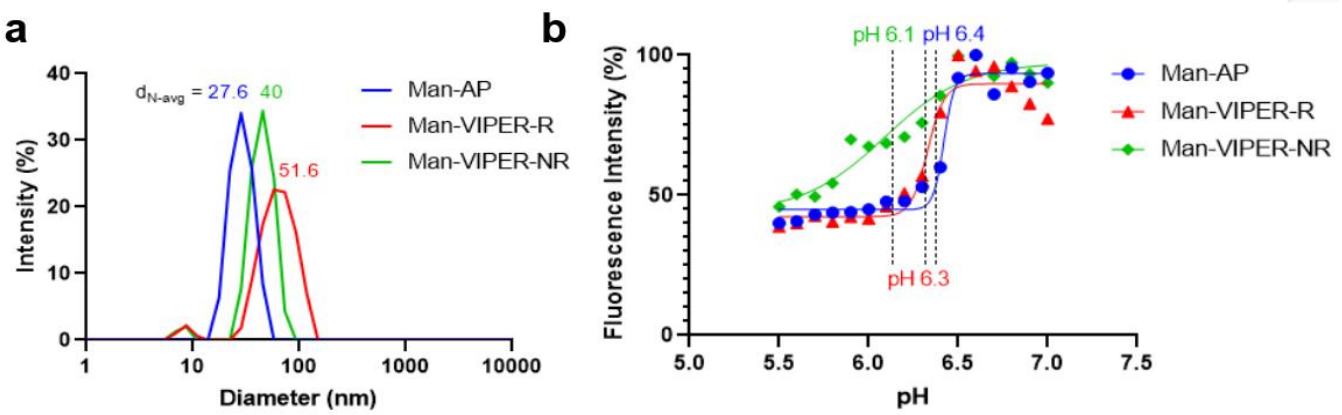

Figure 2. Polymer characterization. (a) Size distribution of Man-AP, Man-VIPER-R and Man-VIPER-NR characterized by dynamic light scattering (d_{mean} = 27.6nm, 51.6nm, 40nm respectively). (b) pH-dependent micellization of Man-AP, Man-VIPER-R and Man-VIPER-NR (transition pH = 6.4, 6.3, 6.1, respectively).

Man-VIPER-R and Man-VIPER-NR enhances antigen cross-presentation through endosomolytic activity

The lytic properties of Man-VIPER-R and Man-VIPER-NR were examined using a hemolysis assay. The polymers were incubated with human red blood cells (RBCs) at various concentrations at pH 7.4, 6.2, and 5.6, representing the pH of the extracellular environment, early endosomes, and late endosomes/lysosomes (**Figure 3a**). Both Man-VIPER-R and Man-VIPER-NR showed no lytic activity pH 7.4, confirming full encapsulation and inactivation of D-melittin at physiological pH[24–26]. Man-VIPER-R showed pH-dependent lytic activity at acidic endosomal pHs (HC_{50} = 0.090 μg/ml at pH 6.2, 0.068 μg/ml at pH 5.6), while Man-VIPER-NR showed similar lytic activity at pH 5.6 and pH 6.2 (HC_{50} = 0.045 μg/ml at pH 6.2, HC_{50} = 0.043 μg/ml at pH 5.6). Man-AP showed negligible hemolysis compared to Man-VIPER-R and Man-VIPER-NR at pH 5.6, emphasizing the role of D-melittin in hemolysis induction.

Next, we directly evaluated the endosomal disruption ability of Man-VIPER-R and Man-VIPER-NR using a Gal8-GFP assay developed by the Duvall group[34]. Gal8 is a protein that is dispersed in the cytoplasm but redistributes to the inner membrane of the endosomes upon its disruption, resulting in visualizable "punctaes" of redistributed Gal8-GFP. We used the dendritic cell DC2.4 cell line that stably expresses the Gal8-GFP fusion protein (DC 2.4 Gal8-GFP) and treated the cells for 18 hours with the nanoparticles before imaging Gal8 punctae by confocal microscopy. Man-VIPER-R-treated cells exhibit more punctae (~10% of cells) compared to Man-AP and Man-VIPER-NR (**Figure 3b-d**). All formulations showed no cytotoxicity at the tested concentrations. We observed a similar but more striking trend with the same experiment using a HeLa-Gal8-GFP cell line (**Figure 3e**). Most cells (>90%) treated with Man-VIPER-R had multiple disrupted endosomes. These results suggest that Man-VIPER-R is more capable of inducing endosomal disruption than Man-VIPER-NR, which is contrary to our initial expectations given previous data showing higher hemolysis with polymer-conjugated melittin[25].

As antigen cross-presentation towards MHC-1 is desired, we evaluated *in vitro* cross-presentation using a DC2.4 and B3Z cell co-culture assay. B3Z is a T cell hybridoma that specifically recognizes the MHC I-SIINFEKL complex and produces measurable β-galactosidase upon binding[35]. We tested Man-VIPER-R and Man-VIPER-NR with different antigen to melittin molar ratios to optimize for our *in vivo* studies (1:1, 1:3 and 1:5). Both Man-VIPER-R and Man-VIPER-NR demonstrated higher cross-presentation compared to Man-AP in a melittin dose-dependent manner (**Figure 3f**). Interestingly, no significant differences in the cross-presentation of Man-VIPER-R and Man-VIPER-NR was observed despite their different endosomal disruption properties. There are several possible explanations for this difference. For example, the Gal8 assay evaluated endosomal disruption at 18 hours post-incubation, and the two formulations may have different kinetics of peptide display and endosomal release unresolvable through the single timepoint. The cross-presentation assay evaluates display of antigen peptide on MHC-I complexes which is downstream of uptake and endosomal disruption and thus less susceptible to kinetic differences in endosomal release. The discrepancy in these two assays observed may also reflect differences in other steps in the cross-presentation process. We chose the 1:5 molar ratio of antigen to melittin for the *in vivo* studies due to the higher cross-presentation at this ratio.

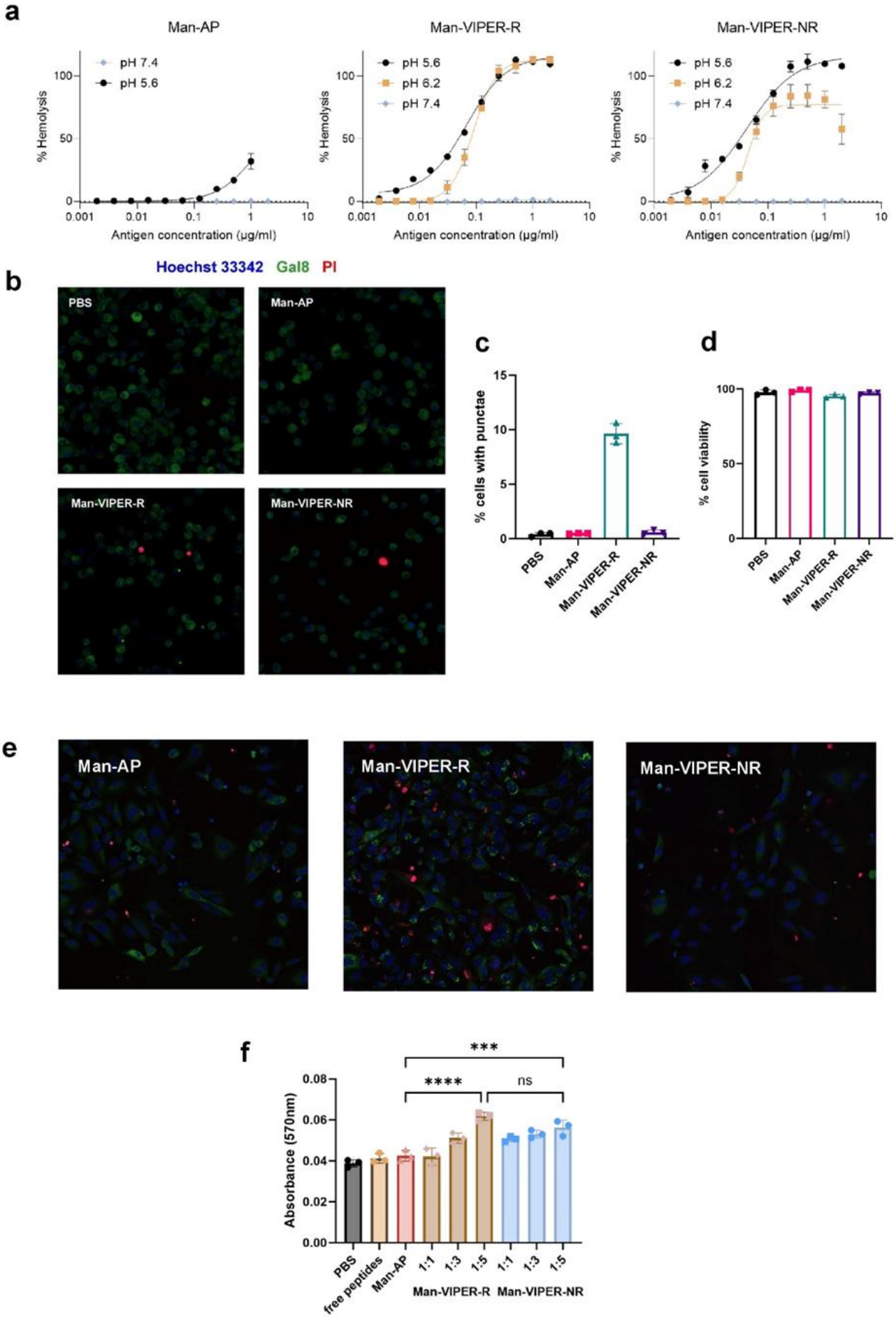
a
Man-AP
Man-VIPER-R
Man-VIPER-NR
pH 7.4
pH 5.6
pH 6.2
% Hemolysis
Antigen concentration (μg/ml)
b
Hoechst 33342 Gal8 PI
PBS
Man-AP
Man-VIPER-R
Man-VIPER-NR
c
% cells with punctae
d
% cell viability
e
Man-AP
Man-VIPER-R
Man-VIPER-NR
f
Absorbance (570nm)
***
****
ns
PBS
free peptides
Man-AP
1:1
1:3
1:5
Man-VIPER-R
Man-VIPER-NR

Figure 3. *In vitro* characterization of Man-AP and Man-VIPER. (a) Hemolytic activity of the micelles against human RBCs at pH 5.6, pH 6.2 and pH 7.4. (b-d) Endosomal disruption in DC2.4-Gal8-GFP cells. (b) Representative images of DC2.4-Gal8 cells. Hoechst 33342 was used to stain the nucleus in blue. Gal8-GFP in green was dispersed in the cytosol and localized to the disrupted endosomes. Propidium iodide in red stained dead cells. (c) Percentage of cells with disrupted endosomes. (d) Percentage cell viability (e) Endosomal disruption in Hela-Gal8-GFP cells. (f) Cross-presentation of Man-AP and Man-VIPER at different antigen to melittin ratios. DC2.4 cells were treated with vaccine formulations and co-cultured with B3Z cells. Production of β-galactosidase was quantified using a CPRG assay kit by measuring the absorbance at 570 nm. Data are represented as mean ± SD. N = 3 biological replicates. Statistical analysis was performed using one-way ANOVA with post-hoc Tukey HSD test (***$p \leq 0.001$, **** $p \leq 0.0001$).

Man-VIPER enhances DC maturation in vivo

DC activation is a fundamental step in mounting a T-cell-based immune response. We therefore assessed the effect of Man-VIPER formulations on dendritic cell (DC) activation *in vivo* by measuring expression of co-stimulatory molecules CD86 and CD40 in lymph node DCs[36]. Mice were injected subcutaneously at the tail base with vaccine formulations (free peptides, Man-AP, Man-VIPER-R and Man-VIPER-NR), followed by cell isolation from the inguinal lymph nodes (ILNs) 24 hours later and analysis with flow cytometry. Both Man-VIPER-R and Man-VIPER-NR significantly increased CD86 and CD40 expression in $CD11c^+$ DCs compared to Man-AP and free peptides (**Figure 4, Figure S5**), suggesting that Man-VIPER formulations exhibit adjuvant activity. Melittin has been shown to activate the NLRP3 inflammasome,[37]. which in DCs triggers the secretion of interleukin-1β (IL-1β) and helps in priming $CD8^+$ T cells[38]. Our previous studies have shown that D-Melittin also exhibits similar activity[39], corroborating these results. DCs from animals treated with free peptides or Man-AP showed no difference in CD86 and CD40 expression compared to PBS. This is contrary to our previous study in which Man-AP increased the expression of CD86[27]. The lower expression of the costimulatory molecules reported here might be due to the reduced antigen dosage employed in this study. We decreased the antigen dosage from 25 µg to 15 µg per mouse due to co-formulation with melittin-containing polymers for endosomal release.

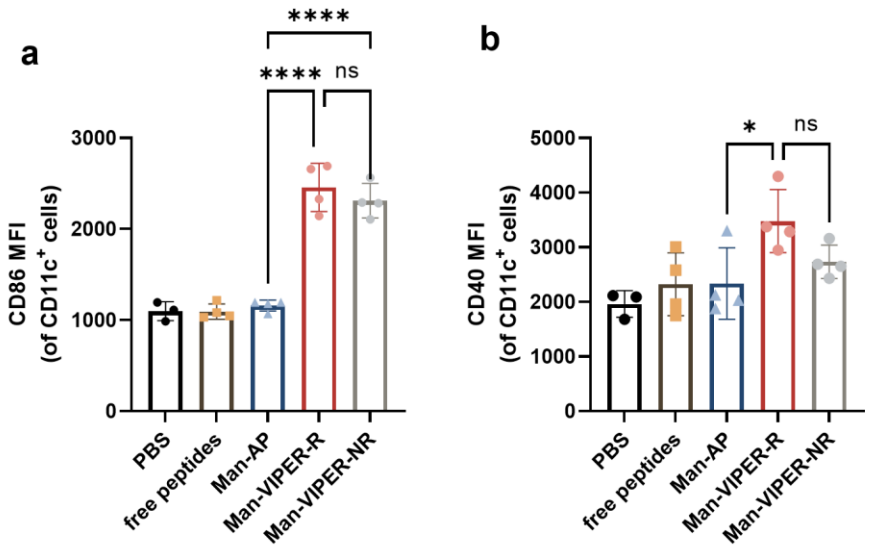

Figure 4. Evaluation of the expression of the co-stimulatory molecules in DCs *in vivo*. (a) Median fluorescence intensity of CD86 in $CD11c^+$ DCs characterized by flow cytometry 24 h post immunization (b) Median fluorescence intensity of CD40 in $CD11c^+$ DCs. Data are represented as mean ± SD. N = 4 biological replicates. Statistical analysis was performed using one-way ANOVA with post-hoc Tukey HSD test (*$p \leq 0.05$, **** $p \leq 0.0001$)

Encouraged by these results, we then assessed immunogenicity in a vaccination context. Mice were immunized twice with all formulations on days 0 and 14, and splenocytes were collected, isolated and analyzed on day 21 for antigen-specific T cell responses. The amount of antigen-specific cytotoxic T cells was assessed with SIINFEKL tetramer staining, while the cellular response to antigen was evaluated using intracellular cytokine staining upon restimulation with the antigens. All three polymeric nanoparticles, Man-AP, Man-VIPER-R and Man-VIPER-NR generated more antigen-specific $CD8^+$ T cells compared to free peptides, suggesting that the mannosylated polymeric delivery vehicle enhances antigen delivery to DCs and promotes antigen-specific T cell proliferation (**Figure 5**). Notably, immunization with Man-VIPER-NR generated 2.7-fold more SIINFEKL-specific $CD8^+$ T cells compared to Man-AP and Man-VIPER-R, which may indicate more robust $CD8^+$ T-cell activation (**Figure 5a**). Particles with sizes around 40 nm enter the lymphatic system most efficiently in some reports[9]. Man-VIPER-NR has a diameter of 40 nm, while Man-VIPER-R has a slightly larger size of 51.6 nm, which might explain the higher number of antigen-specific $CD8^+$ T generated by Man-VIPER-NR. As mentioned previously, we attribute the small diameter in Man-VIPER-NR nanoparticles to the presence of the pentafluorobenzyl linker. Animals treated with Man-VIPER-R or Man-VIPER-NR had significantly higher numbers of antigen-specific cytokine-producing $CD8^+$ and $CD4^+$ T cells compared to animals treated with Man-AP, although similar numbers of antigen-specific $CD8^+$ T cells were observed in animals treated with Man-AP and Man-VIPER-R (**Figure 5b, Figure S6**). Man-AP generated an average of 6-fold more cytokine-producing T cells compared to free peptides, while Man-VIPER-R and Man-VIPER-NR generated 41- and 42- fold more compared to free peptides. This phenomenon can be attributed to the higher expression of co-stimulatory molecules CD86 and CD40 in DCs generated by Man-VIPER compared to Man-AP in the DC maturation study (**Figure 4**). It has been reported that CD28, the T-cell cognate receptor for CD80/CD86, can amplify early TCR signaling[40]. Therefore, it is possible that T cells in Man-VIPER treated mice require less antigens to be activated. Both Man-VIPER-R and Man-VIPER-NR generated similar levels of IFNγ-, TNFα-producing $CD8^+$ T cells and IFNγ-producing $CD4^+$ T cells upon antigen restimulation (**Figure 5c**). Man-VIPER-R generated more IL-2-producing $CD4^+$ T cells than Man-VIPER-NR, indicating that Man-VIPER-R generates a more robust $CD4^+$ T cell response. The higher $CD4^+$ T cell activation induced by Man-VIPER-R could be attributed to the slightly higher expression of CD40 on DCs (**Figure 4b**), which is critical for activation of $CD4^+$ T cells[41]. However, as $CD8^+$ T cells are directly associated with tumor cell elimination, we used Man-VIPER-NR in the tumor reduction study as it induced a higher antigen-specific $CD8^+$ T cell proliferation compared to Man-VIPER-R.

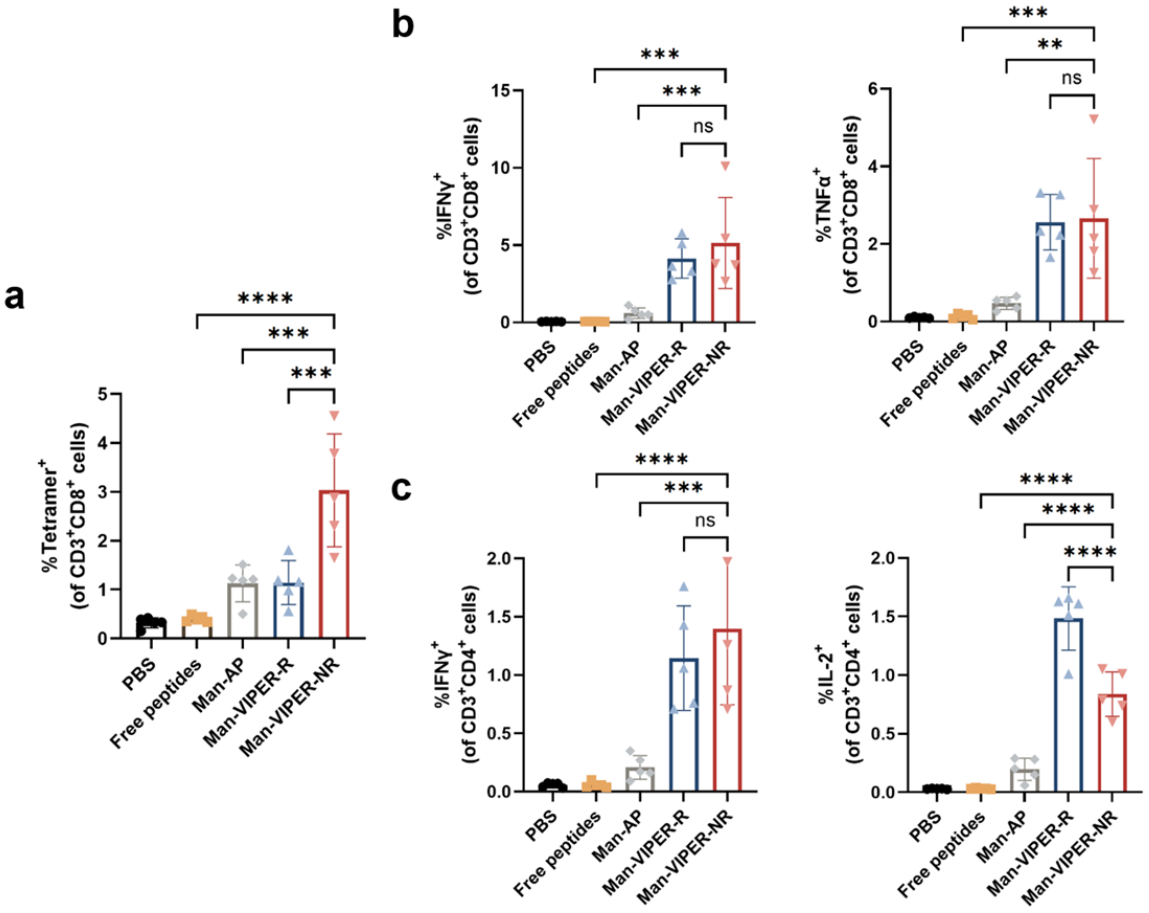

Figure 5. Evaluation of the antigen-specific T cell responses *in vivo*. (a) Percentage of SIINFEKL-tetramer$^+$ CD8$^+$ T cells in spleens after immunization. (b-c) Intracellular cytokine staining of the splenocytes. (b) Splenocytes were restimulated with SIINFEKL peptide and percentage of IFNγ$^+$ and TNFα$^+$ CD8$^+$ T cells were characterized by flow cytometry (c) Splenocytes were restimulated with OVA protein and percentage of IFNγ$^+$ and IL-2$^+$ CD4$^+$ T cells were characterized by flow cytometry. Data are represented as mean ± SD. N = 5 biological replicates. Statistical analysis was performed using one-way ANOVA with post-hoc Tukey HSD test (**p ≤ 0.01, ***p ≤ 0.001, **** p ≤ 0.0001).

Man-VIPER-NR slowed tumor growth and improved survival in an antigen-expressing melanoma model

We evaluated the utility of Man-VIPER-NR as a therapeutic vaccine against an aggressive, poorly immunogenic B16F10 murine melanoma model. Mice were subcutaneously injected with B16F10 cells engineered to express the OVA antigen (B16F10-OVA) on day 0. On days 3, 10 and 19, mice were immunized subcutaneously at the tail base with either PBS, free peptides, Man-AP or Man-VIPER-NR. Anti PD-1 immune checkpoint blockade (ICB) was given to some of the mice one day after each immunization through intraperitoneal injection (**Figure 6a**). ICB had no effect on tumor growth compared to PBS, likely because the B16F10-OVA tumor model is poorly immunogenic and inefficient in activating antigen-specific cytotoxic T cells[42]. Man-VIPER-NR significantly delayed tumor growth and improved survival compared to free peptides and Man-AP, while Man-AP exhibited modest tumor growth delay and survival benefits consistent with our previous data[27] (**Figure 6b,c, Figure S7**). Co-treatment with ICB interestingly did not result in increased therapeutic efficacy (**Figure S8**). The immunosuppressive tumor microenvironment, T cell exhaustion and other inhibitory signaling can all lead to the resistance in the ICB therapy[43]. The tumor response to immunization might be further improved by administration of TGF-β blockade[44], blocking other inhibitory pathways by combining with anti-CTLA-4[45], and increasing T cell infiltration[46]. We also noticed 5%-10% weight loss in mice treated with Man-VIPER-NR two days after vaccination, but the mice recovered weight later and demonstrated no other side effects (**Figure S9**). These results establish Man-VIPER-NR as a promising

therapeutic cancer peptide vaccine platform. There exists avenues to improve this Man-VIPER-NR, which includes co-formulation with known adjuvants such as STING, TLR or NLR agonists.

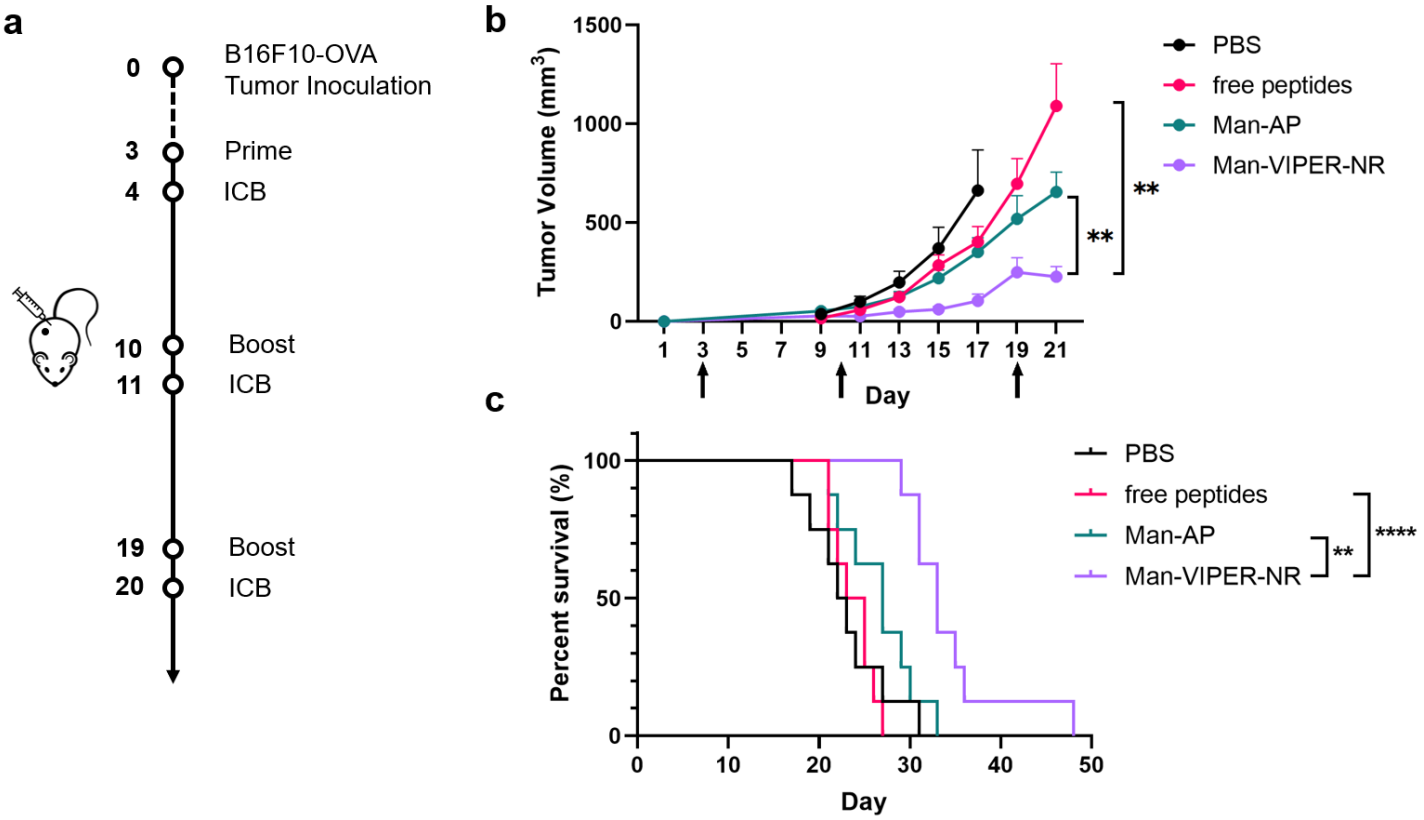

Figure 6. Evaluation of the antitumor effect in a B16F10-OVA tumor model. (a) Study timeline. Mice were inoculated with B16F10-OVA cells on day 0, vaccinated on days 3, 10, 19, and treated with ICB on days 4, 11, 20. (b) Tumor growth curve. Tumor was measured every other day. Data are represented as mean ± SEM. N = 8 biological replicates. Statistical analysis was performed using unpaired t test on day 21 (**$p \leq 0.01$). (c) Kaplan-Meier survival curve. Survival analysis was performed using the log-rank test (**$p \leq 0.01$, **** $p \leq 0.0001$).

iv. Conclusions

In this work, we developed a mannosylated endosomolytic cancer peptide vaccine platform building from our previous mannosylated peptide delivery work and our established Virus-Inspired Polymers for Endosomal Release (VIPER) system. Man-VIPER-NR self-assembles into micelles suitable for lymph node trafficking and efficiently delivers peptide antigens to the cytosol through endosomal lysis induction, resulting in superior antigen cross-presentation, cytotoxic T-cell priming and potent antitumor response. This culminates into superior efficacy as a therapeutic vaccine compared to non-endosomolytic formulations in an aggressive, poorly immunogenic murine melanoma model.

v. Acknowledgements

K.S. and D.C.N. contributed equally to this work. This work was supported by the U.S. National Institutes of Health, National Cancer Institute Grant R01CA257563. Confocal microscopy was completed at the UW Keck Microscopy Center; the Leica SP8X microscope and software was funded by NIH S10 OD016240 and the UW Student Technology Fee

(UWSTF). We thank the Institute for Protein Design (IPD) at the University of Washington for the use of Dynamic Light Scattering, as well as the Mass Spectrometry Core at the University of Washington for the use of MALDI. We thank Prof. Amanda Lund for providing the B16F10-OVA cell line, Prof. Nilabh Shastri (Johns Hopkins University) for providing the B3Z cells, and the NIH Tetramer Core Facility for providing the PE-labeled H-2Kb/SIINFEKL tetramer. We thank Prof. Jordan Green (Johns Hopkins University) for the Gal8-GFP and PiggyBac transposon plasmids and Prof. Craig Duvall (Vanderbilt University) for the MATLAB code for Gal8 quantification.

vi. References

1. Hu, Z., Ott, P. A. & Wu, C. J. Towards personalized, tumour-specific, therapeutic vaccines for cancer. *Nat. Rev. Immunol.* **18**, 168–182 (2018).
2. Parvizpour, S., Pourseif, M. M., Razmara, J., Rafi, M. A. & Omidi, Y. Epitope-based vaccine design: a comprehensive overview of bioinformatics approaches. *Drug Discov. Today* **25**, 1034–1042 (2020).
3. Liu, W. *et al.* Peptide-based therapeutic cancer vaccine: Current trends in clinical application. *Cell Prolif.* **54**, e13025 (2021).
4. Durgeau, A., Virk, Y., Corgnac, S. & Mami-Chouaib, F. Recent Advances in Targeting CD8 T-Cell Immunity for More Effective Cancer Immunotherapy. *Front. Immunol.* **9**, 14 (2018).
5. Mempel, T. R., Henrickson, S. E. & von Andrian, U. H. T-cell priming by dendritic cells in lymph nodes occurs in three distinct phases. *Nature* **427**, 154–159 (2004).
6. Acar, H., M. Ting, J., Srivastava, S., L. LaBelle, J. & V. Tirrell, M. Molecular engineering solutions for therapeutic peptide delivery. *Chem. Soc. Rev.* **46**, 6553–6569 (2017).
7. Joffre, O. P., Segura, E., Savina, A. & Amigorena, S. Cross-presentation by dendritic cells. *Nat. Rev. Immunol.* **12**, 557–569 (2012).
8. Reddy, S. T., Rehor, A., Schmoekel, H. G., Hubbell, J. A. & Swartz, M. A. In vivo targeting of dendritic cells in lymph nodes with poly(propylene sulfide) nanoparticles. *J. Controlled Release* **112**, 26–34 (2006).
9. Bachmann, M. F. & Jennings, G. T. Vaccine delivery: a matter of size, geometry, kinetics and molecular patterns. *Nat. Rev. Immunol.* **10**, 787–796 (2010).
10. Oussoren, C., Zuidema, J., Crommelin, D. J. A. & Storm, G. Lymphatic uptake and biodistribution of liposomes after subcutaneous injection.: II. Influence of liposomal size, lipid composition and lipid dose. *Biochim. Biophys. Acta BBA - Biomembr.* **1328**, 261–272 (1997).

11. Wilson, D. S. *et al.* Antigens reversibly conjugated to a polymeric glyco-adjuvant induce protective humoral and cellular immunity. *Nat. Mater.* **18**, 175–185 (2019).

12. Lynn, G. M. *et al.* Peptide–TLR-7/8a conjugate vaccines chemically programmed for nanoparticle self-assembly enhance CD8 T-cell immunity to tumor antigens. *Nat. Biotechnol.* **38**, 320–332 (2020).

13. He, Y. *et al.* Peptide-Based Cancer Vaccine Delivery via the STINGΔTM-cGAMP Complex. *Adv. Healthc. Mater.* **11**, 2200905 (2022).

14. Akinc, A. & Battaglia, G. Exploiting Endocytosis for Nanomedicines. *Cold Spring Harb. Perspect. Biol.* **5**, a016980 (2013).

15. Liang, W., Shi, X., Deshpande, D., Malanga, C. J. & Rojanasakul, Y. Oligonucleotide targeting to alveolar macrophages by mannose receptor-mediated endocytosis. *Biochim. Biophys. Acta BBA - Biomembr.* **1279**, 227–234 (1996).

16. Liu, X. *et al.* Co-localized delivery of nanomedicine and nanovaccine augments the postoperative cancer immunotherapy by amplifying T-cell responses. *Biomaterials* **230**, 119649 (2020).

17. Shen, C. *et al.* Polyethylenimine-based micro/nanoparticles as vaccine adjuvants. *Int. J. Nanomedicine* **12**, 5443–5460 (2017).

18. Flanary, S., Hoffman, A. S. & Stayton, P. S. Antigen Delivery with Poly(Propylacrylic Acid) Conjugation Enhances MHC-1 Presentation and T-Cell Activation. *Bioconjug. Chem.* **20**, 241–248 (2009).

19. Foster, S., Duvall, C. L., Crownover, E. F., Hoffman, A. S. & Stayton, P. S. Intracellular Delivery of a Protein Antigen with an Endosomal-Releasing Polymer Enhances CD8 T-Cell Production and Prophylactic Vaccine Efficacy. *Bioconjug. Chem.* **21**, 2205–2212 (2010).

20. Wilson, J. T. *et al.* pH-Responsive Nanoparticle Vaccines for Dual-Delivery of Antigens and Immunostimulatory Oligonucleotides. *ACS Nano* **7**, 3912–3925 (2013).

21. Lin, W. *et al.* Co-Delivery of Imiquimod and Plasmid DNA via an Amphiphilic pH-Responsive Star Polymer that Forms Unimolecular Micelles in Water. *Polymers* **8**, 397 (2016).

22. Derouazi, M. *et al.* Novel Cell-Penetrating Peptide-Based Vaccine Induces Robust CD4+ and CD8+ T Cell–Mediated Antitumor Immunity. *Cancer Res.* **75**, 3020–3031 (2015).

23. Shae, D. *et al.* Co-delivery of Peptide Neoantigens and Stimulator of Interferon Genes Agonists Enhances Response to Cancer Vaccines. *ACS Nano* **14**, 9904–9916 (2020).

24. Cheng, Y., Yumul, R. C. & Pun, S. H. Virus-Inspired Polymer for Efficient In Vitro and In Vivo Gene Delivery. *Angew. Chem. Int. Ed.* **55**, 12013–12017 (2016).

25. Peeler, D. J. *et al.* pH-sensitive polymer micelles provide selective and potentiated lytic capacity to venom peptides for effective intracellular delivery. *Biomaterials* **192**, 235–244 (2019).

26. Peeler, D. J., Yen, A., Luera, N., Stayton, P. S. & Pun, S. H. Lytic Polyplex Vaccines Enhance Antigen-Specific Cytotoxic T Cell Response through Induction of Local Cell Death. *Adv. Ther.* **n/a**, 2100005.

27. Lv, S. *et al.* Well-Defined Mannosylated Polymer for Peptide Vaccine Delivery with Enhanced Antitumor Immunity. *Adv. Healthc. Mater.* **11**, 2101651 (2022).

28. Sylvestre, M. *et al.* Replacement of L-amino acid peptides with D-amino acid peptides mitigates anti-PEG antibody generation against polymer-peptide conjugates in mice. *J. Controlled Release* **331**, 142–153 (2021).

29. Noy, J.-M. *et al.* Para-Fluoro Postpolymerization Chemistry of Poly(pentafluorobenzyl methacrylate): Modification with Amines, Thiols, and Carbonylthiolates. *Macromolecules* **50**, 7028–7040 (2017).

30. Perrier, S., Takolpuckdee, P. & Mars, C. A. Reversible Addition−Fragmentation Chain Transfer Polymerization: End Group Modification for Functionalized Polymers and Chain Transfer Agent Recovery. *Macromolecules* **38**, 2033–2036 (2005).

31. Prossnitz, A. N. & Pun, S. H. Modulating Boronic Ester Stability in Block Copolymer Micelles via the Neighbor Effect of Copolymerized Tertiary Amines for Controlled Release of Polyphenolic Drugs. *ACS Macro Lett.* **11**, 276–283 (2022).

32. Evans, B. C. *et al.* Ex Vivo Red Blood Cell Hemolysis Assay for the Evaluation of pH-responsive Endosomolytic Agents for Cytosolic Delivery of Biomacromolecular Drugs. *JoVE J. Vis. Exp.* e50166 (2013) doi:10.3791/50166.

33. Li, S. *et al.* Pi-Stacking Enhances Stability, Scalability of Formation, Control over Flexibility, and Circulation Time of Polymeric Filamentous Nanocarriers. *Adv. NanoBiomed Res.* **1**, 2100063 (2021).

34. Kilchrist, K. V. *et al.* Gal8 Visualization of Endosome Disruption Predicts Carrier-Mediated Biologic Drug Intracellular Bioavailability. *ACS Nano* **13**, 1136–1152 (2019).

35. Karttunen, J. & Shastri, N. Measurement of ligand-induced activation in single viable T cells using the lacZ reporter gene. *Proc. Natl. Acad. Sci.* **88**, 3972–3976 (1991).

36. Tai, Y., Wang, Q., Korner, H., Zhang, L. & Wei, W. Molecular Mechanisms of T Cells Activation by Dendritic Cells in Autoimmune Diseases. *Front. Pharmacol.* **9**, 642 (2018).

37. Martín-Sánchez, F. *et al.* Lytic cell death induced by melittin bypasses pyroptosis but induces NLRP3 inflammasome activation and IL-1β release. *Cell Death Dis.* **8**, e2984–e2984 (2017).

38. Ghiringhelli, F. *et al.* Activation of the NLRP3 inflammasome in dendritic cells induces IL-1β–dependent adaptive immunity against tumors. *Nat. Med.* **15**, 1170–1178 (2009).

39. Lv, S., Sylvestre, M., Song, K. & Pun, S. H. Development of D-melittin polymeric nanoparticles for anti-cancer treatment. *Biomaterials* **277**, 121076 (2021).

40. Zumerle, S., Molon, B. & Viola, A. Membrane Rafts in T Cell Activation: A Spotlight on CD28 Costimulation. *Front. Immunol.* **8**, 1467 (2017).

41. Grewal, I. S. & Flavell, R. A. The Role of CD40 Ligand in Costimulation and T-Cell Activation. *Immunological Reviews* **153**, 85–106 (1996).

42. Chen, S. *et al.* Combination of 4-1BB agonist and PD-1 antagonist promotes antitumor effector/memory CD8 T cells in a poorly immunogenic tumor model. *Cancer Immunol. Res.* **3**, 149–160 (2015).

43. Lei, Q., Wang, D., Sun, K., Wang, L. & Zhang, Y. Resistance Mechanisms of Anti-PD1/PDL1 Therapy in Solid Tumors. *Front. Cell Dev. Biol.* **8**, 672 (2020).

44. Martin, C. J. *et al.* Selective inhibition of TGFβ1 activation overcomes primary resistance to checkpoint blockade therapy by altering tumor immune landscape. *Sci. Transl. Med.* **12**, eaay8456 (2020).

45. Curran, M. A., Montalvo, W., Yagita, H. & Allison, J. P. PD-1 and CTLA-4 combination blockade expands infiltrating T cells and reduces regulatory T and myeloid cells within B16 melanoma tumors. *Proc. Natl. Acad. Sci.* **107**, 4275–4280 (2010).

46. Tang, H. *et al.* Facilitating T cell infiltration in tumor microenvironment overcomes resistance to PD-L1 blockade. *Cancer Cell* **29**, 285–296 (2016).

vi. Supplemental Information

Table S1. Characterization of Man-VIPER polymeric backbones

Polymer name	Conversion by NMR (%)[a]	DP (NMR)[b]	NMR Mn (kDa)[c]	GPC Mw (kDa)[d]	GPC Mn (kDa)[d]	GPC Dispersity (Đ = Mw/Mn)[d]
ManCTA	96	43 Man	12.4	14.5	13.8	1.12

CP-R	87	44 DIPAMA, 4 PDSEMA	23.0	45.2	44.8	1.14
CP-NR	84	44 DIPAMA, 4 PFBzMA	23.1	31.1	30.2	1.15

a - Calculated by vinyl peak depletion (5.5-6 ppm) in NMR spectroscopy. b - Calculated by a combination of conversion NMR and either downfield PDSEMA peaks (7-9ppm) for CP-R or F-NMR for CP-NR. c - Calculated from DP. d - Calculated from GPC using light scattering

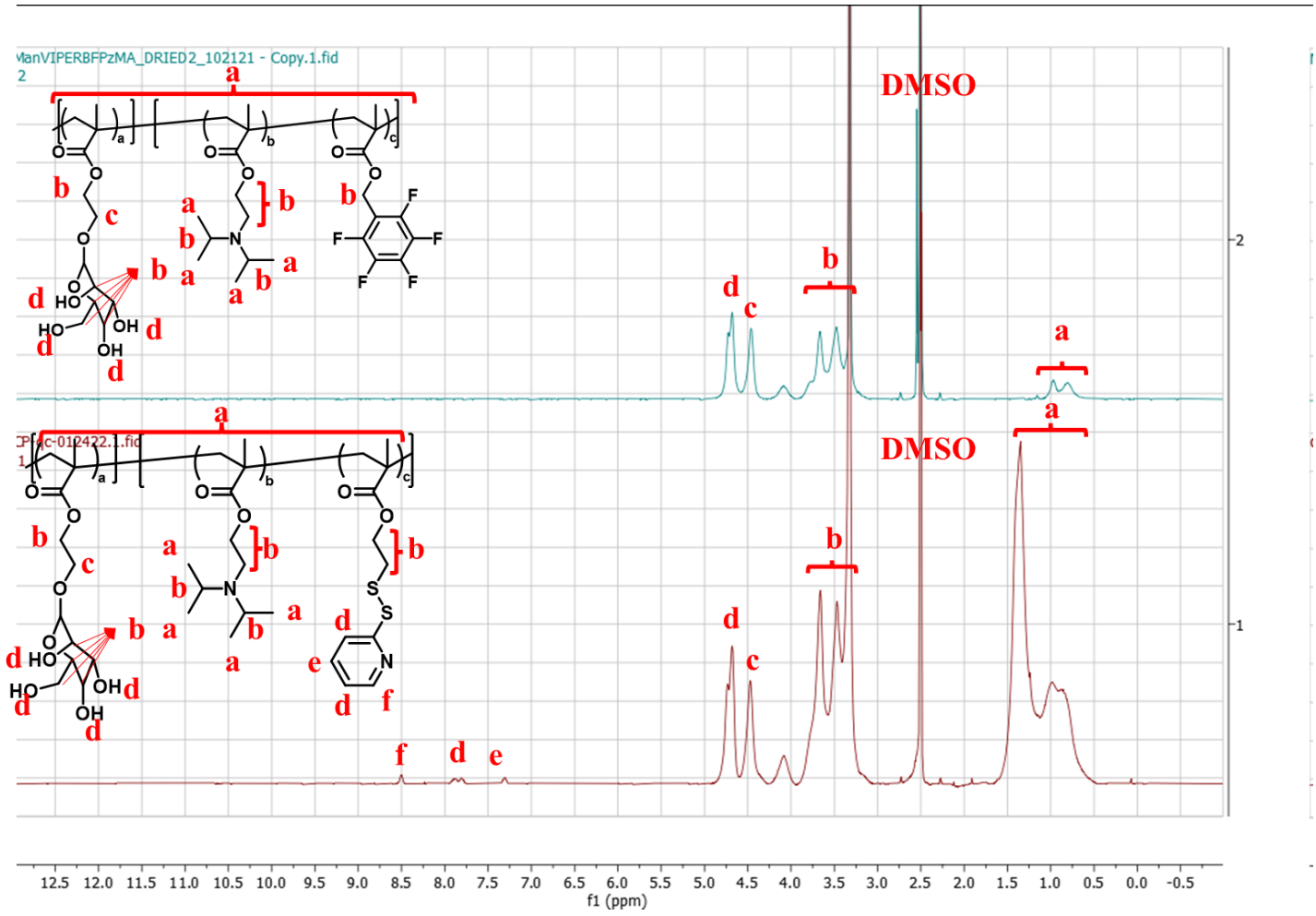

Figure S1. [1]H-NMR of CP-NR (top) and CP-R (bottom) in DMSO-d6

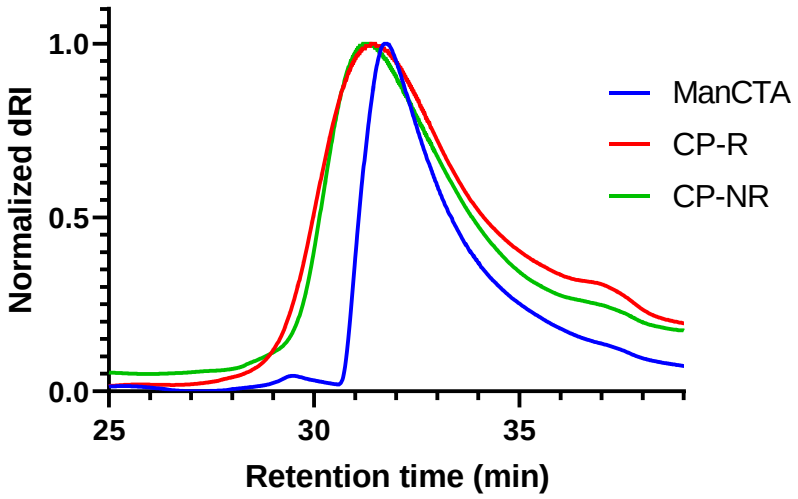

Figure S2. GPC traces of CP polymers, as well as the Mannose CTA from which it was chain-extended. Obtained from an Agilent 1260 HPLC stack running heated LiBr-supplemented (0.1% w/v) DMF mobile phase at a flow rate of 1 mL min^{-1} through a semi-prep three-column setup (Phenogel-TSKgel) with filtered 5 mg/mL samples

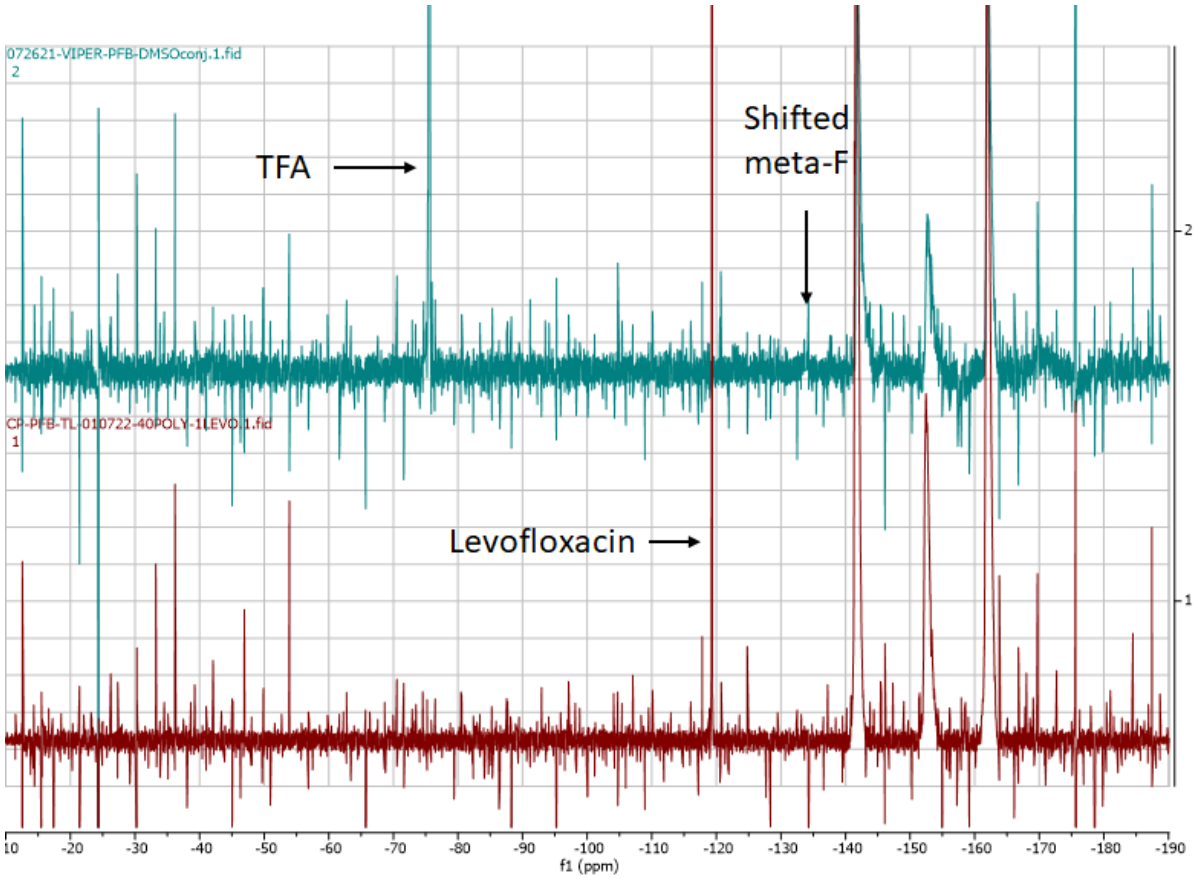

Figure S3. ^{19}F-NMR of MP-NR (top) and CP-NR (bottom) in DMSO-d6. TFA in MP-NR represents TFA counterions in synthesized peptides. Levofloxacin in CP-NR is an internal standard used to determine PFB wt%

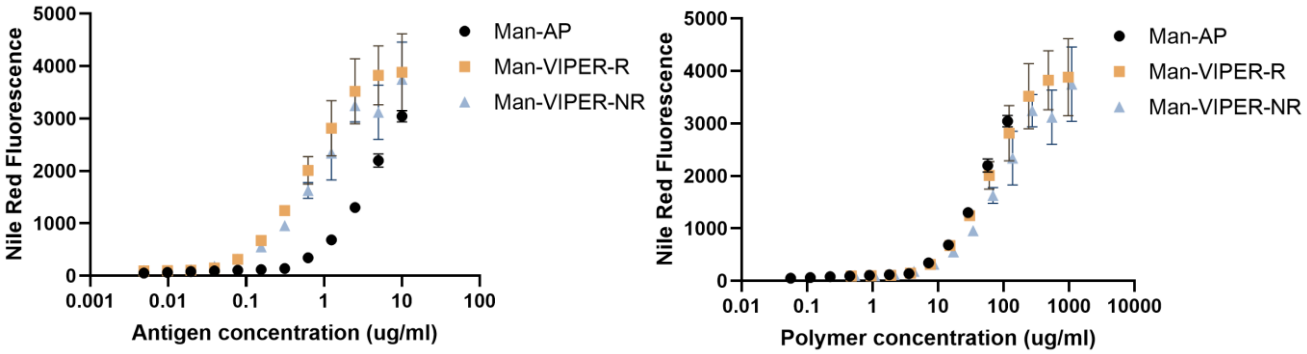

Figure S4. Critical micelle concentration (CMC) was determined by the Nile Red fluorescence assay. The left panel shows the concentration of the peptide antigens and the right panel shows the concentration of the polymers.

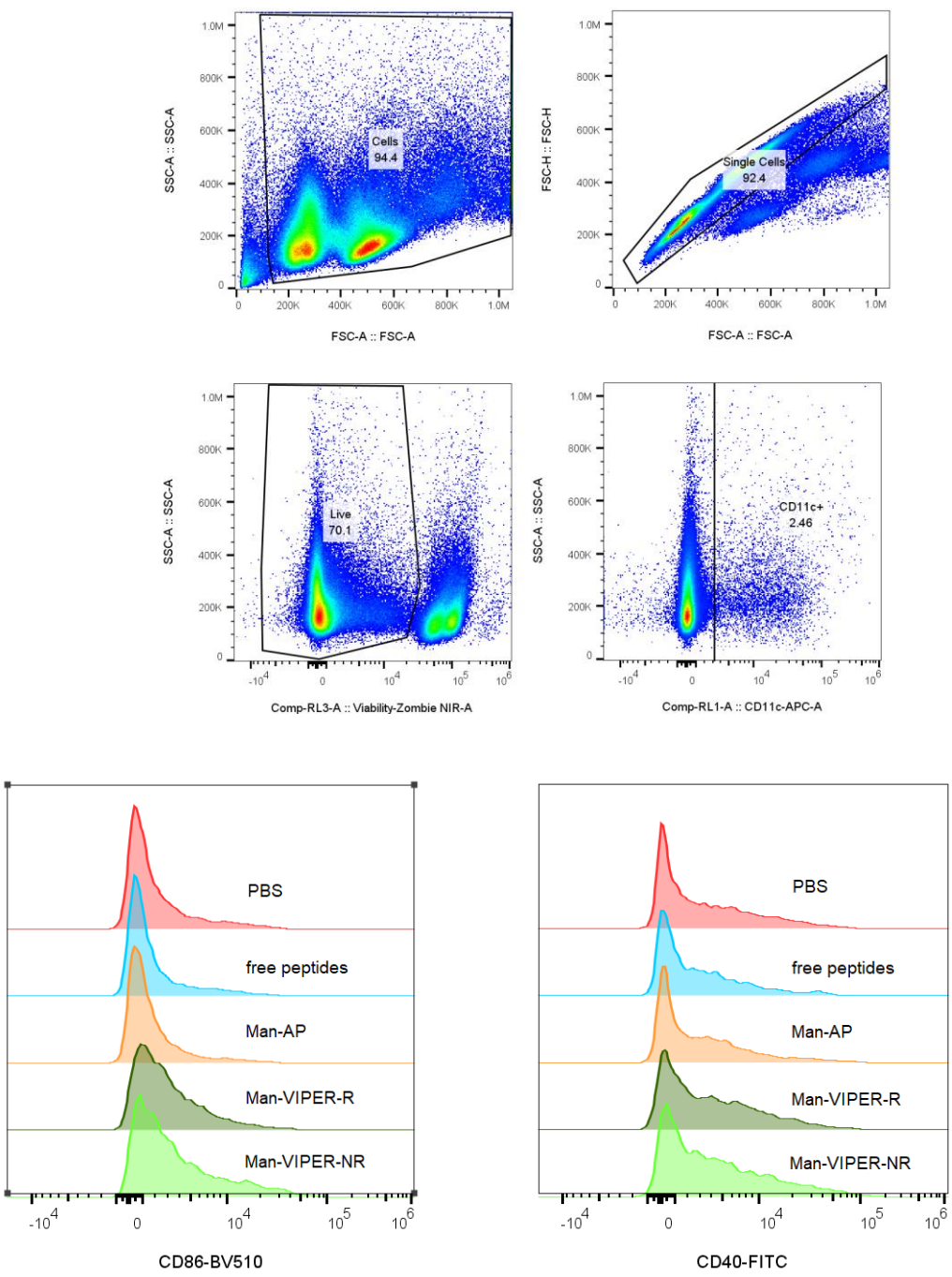

Figure S5. (a) Gating for CD11c$^+$ DCs in the ILNs. (b) Representative histograms of CD86-BV510 and CD40-FITC in CD11c$^+$ cells.

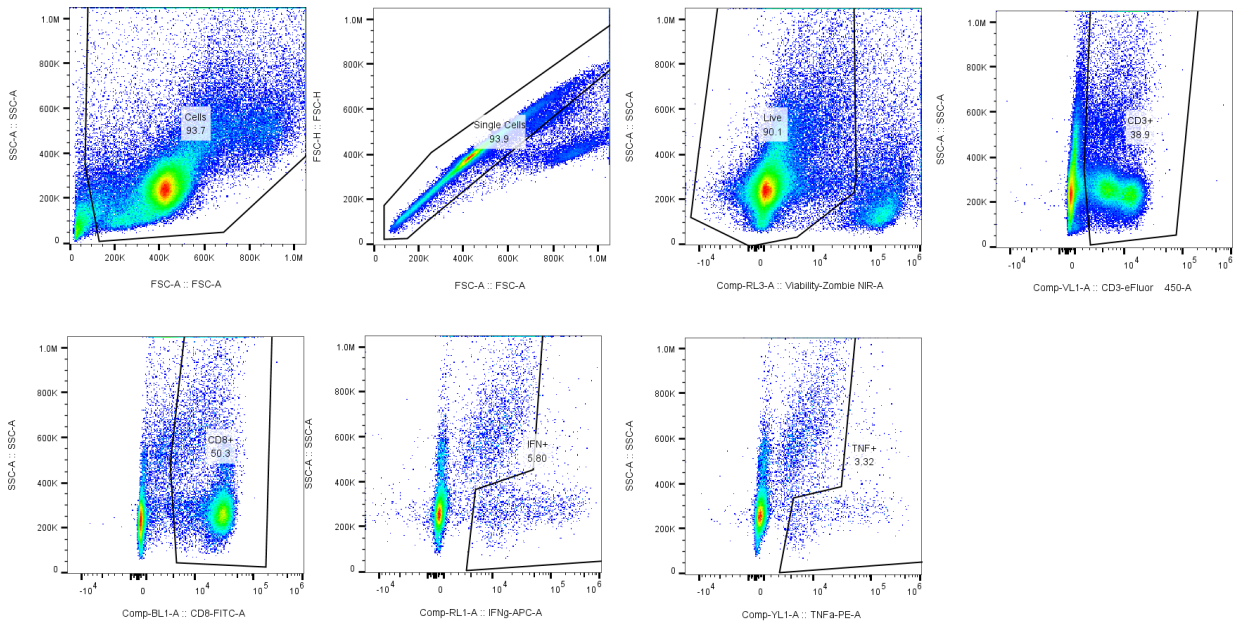

Figure S6. Gating for IFNγ^+ and TNFα^+ CD8$^+$ T in the splenocytes.

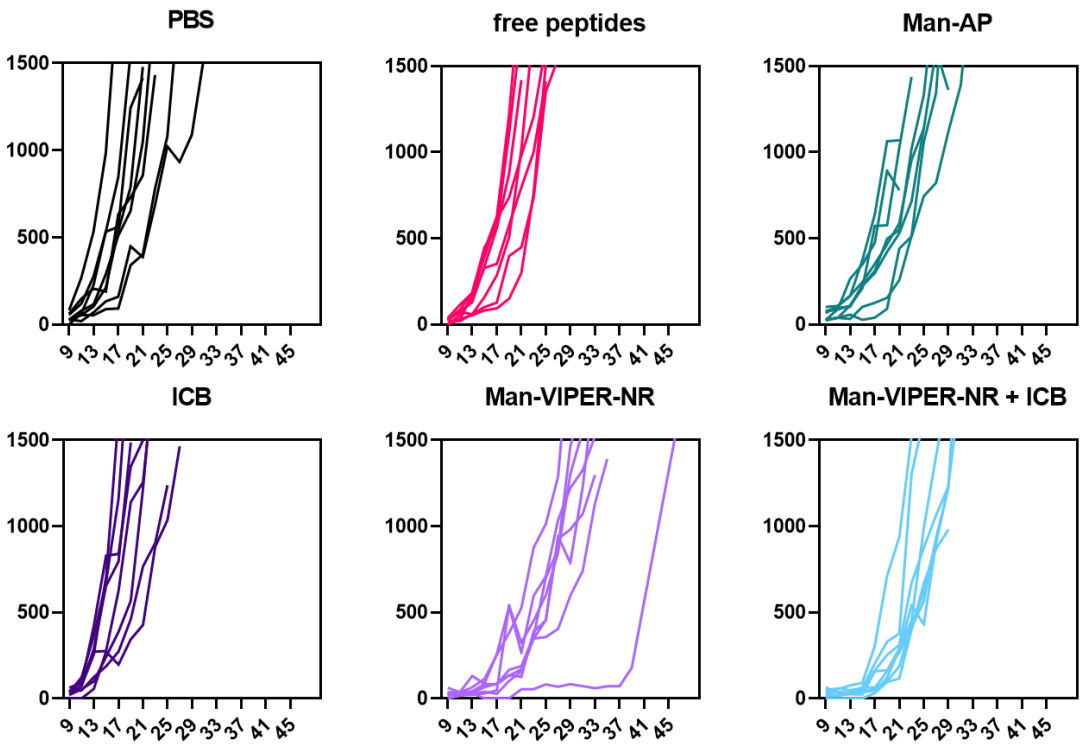

Figure S7. Individual tumor growth curves (N=8). Y-axis: tumor volume mm^3, x-axis: days post tumor inoculation.

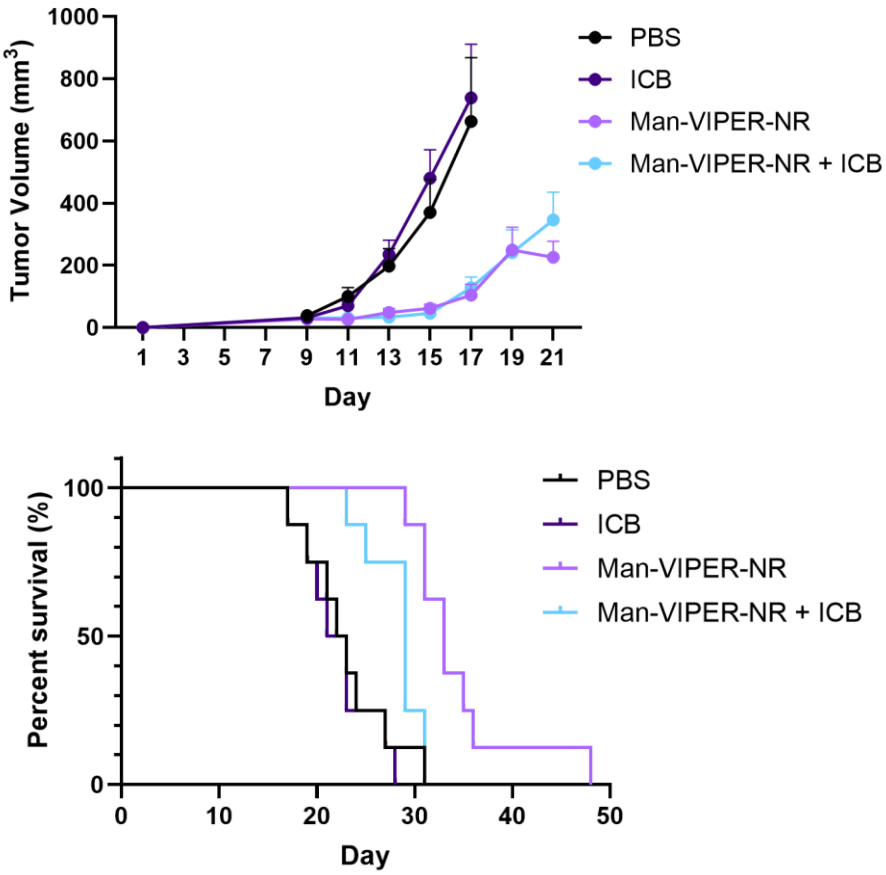

Figure S8. Tumor growth curve and Kaplan-Meier survival curve of mice treated with anti-PD-1 ICB and Man-VIPER-NR. Data are represented as mean ± SEM. N = 8 biological replicates.

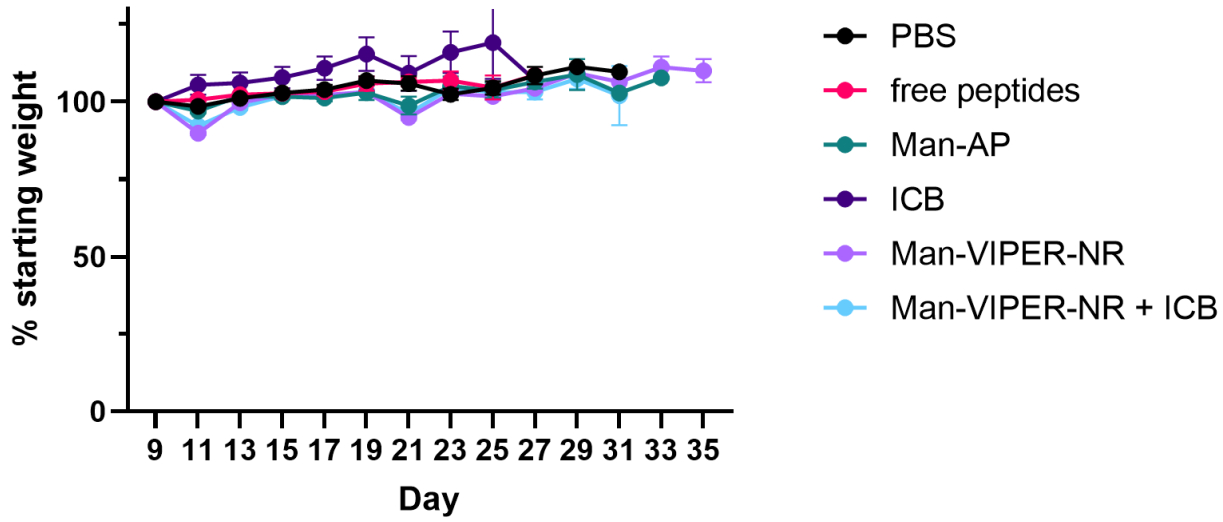

Figure S9. Weight change in the tumor reduction study (N=8). Mice were treated with PBS, free peptides, Man-AP and Man-VIPER-NR on days 3, 10 and 19. Mice were treated with ICB on days 4, 11, and 20.

Chapter 3. Mannosylated STING Agonist 'Drugamers' For Dendritic Cell-Mediated Cancer Immunotherapy

Dinh Chuong Nguyen*, Kefan Song, Simbarashe Jokonya, Omeed Yazdani, Yonghui Wang, ABM Zakaria, Drew L. Sellers, Suzie H. Pun, Patrick S. Stayton*

Synopsis

The Stimulator of Interferon Genes (STING) pathway is a promising target for cancer immunotherapy. Despite recent advances, therapies targeting the STING pathway are often limited by routes of administration, sub-optimal STING activation or off-target toxicity. Here, we report a dendritic cell (DC)-targeted polymeric prodrug platform (polySTING) that is designed to optimize intracellular delivery of a diamidobenzimidazole (diABZI) small molecule STING agonist, while minimizing off-target toxicity after parenteral administration. PolySTING incorporates mannose targeting ligands as a comonomer, which facilitates its uptake in $CD206^+$/mannose $receptor^+$ professional antigen-presenting cells (APCs) in the tumor microenvironment (TME). The STING agonist is conjugated through a cathepsin B-cleavable Valine-Alanine (VA) linker for selective intracellular drug release after receptor-mediated endocytosis. When administered intravenously in tumor-bearing mice, polySTING selectively targeted $CD206^+$/mannose $receptor^+$ APCs in the TME, resulting in increased cross-presenting $CD8^+$ DCs, infiltrating $CD8^+$ T cells in the TME, as well as maturation across multiple DC subtypes in the tumor-draining lymph node (TDLN). Systemic administration of polySTING slowed tumor growth in a B16-F10 murine melanoma model, as well as a 4T1 murine breast cancer model with an acceptable safety profile. Thus, we demonstrate that polySTING delivers STING agonists to professional APCs after systemic administration, generating an efficacious DC-driven anti-tumor immunity with minimal side effects. This new polymeric prodrug platform may offer new opportunities for combining efficient targeted STING agonist delivery with other selective tumor therapeutic strategies.

i. Introduction

Immune therapies that enlist patients' endogenous immune systems are an effective and expanding strategy in treating cancer[1]. While many of the recent innovations such as checkpoint inhibitors[2] and CAR T cell therapies[3] have focused on directly stimulating the adaptive immune system, therapeutics that engage the innate immune system provide an alternative approach to activating both adaptive and innate arms of immunity against cancer[4]. The Stimulator of Interferon Genes (STING) pathway has emerged as a leading target. STING activation elicits a Type-1 interferon-driven response which induces a potent multifaceted innate and adaptive immune response[5]. Systemic administration of STING agonists can initiate the cancer-immunity cycle[6]. In a tumor-targeted context, initial STING activation in the tumor microenvironment (TME) provides an initial wave of immunogenic ablation through either direct, cell- or cytokine-mediated cytotoxicity. Resultant tumor antigens drain to secondary lymphoid organs, where they are presented by professional antigen-presenting cells (APCs) such as dendritic cells (DCs) to activate adaptive immunity with the help of STING-derived immunogenic cues (e.g. cytokines and co-stimulatory molecules). Activated adaptive immune cells mobilize towards tumors where they further induce immunogenic tumor cell killing to perpetuate the cycle[7]. Indeed, successful STING activation can result in potent tumor suppression, eradication, or even long-term immunity to rechallenge/relapse[8].

The potential in activating STING in cancer immunotherapy is clear, but drug delivery challenges have limited clinical translation of STING agonists. Canonical STING agonists such as 2'3'-cyclic GMP-AMP (2'3'-cGAMP) face significant systemic, cellular and intracellular barriers in reaching the STING protein[9], necessitating either toxic high doses or the impractical intratumoral administration route[10]. In addition to the development of alternative small-molecule STING agonists[11–13], multiple drug delivery platforms have been developed to address STING delivery challenges[14]. Lipid micelles[15], polymersomes[16,17], liposomes[18,19], inorganic nanoparticles[20], or drug-conjugated polymeric particles[21] have all been employed as systemic STING agonist carriers with potent responses.

Tumor-targeted STING delivery vehicles hold great promise. A reported tumor-targeted STING agonist antibody-drug conjugate (ADC) platform demonstrated an impressive safety profile and good efficacy[22]. However, this platform encounters inherent issues with target availability and scale-up manufacturability[23]. In addition, low-level STING activation in tumors can induce immunosuppressive factors such as indoleamine-2,3-deoxygenase (IDO) causing pathogenesis[24]. As tumor cells can downregulate STING[25], agonist delivery to tumor cells can either be ineffective or counterproductive through this mechanism. Conversely, overactivation of STING can result in unproductive non-immunogenic cell ablation[26,27], rendering patients vulnerable to relapse or metastasis. In light of this, targeted STING delivery to intratumoral APCs such as dendritic cells (DCs) may induce antitumor immunity without the aforementioned shortcomings. In tumor rejection models with or without immunotherapy, DC subsets such as type-1 conventional DCs (cDC1) play indispensable roles in antigen transport, cross-priming, and lymphocyte recruitment and maintenance in the TME[28–32]. STING activation in DCs strongly induces DC maturation[33], and activation in cDC1 was crucial to the function of a intratumoral viral vector STING delivery platform[27]. We hypothesize that a STING delivery platform targeting tumoral APCs can induce potent antitumor responses with minimal toxicity. A Clec9a$^+$ DC-targeted STING delivery platform showcased this possibility.[34]

Here, we report a DC-targeted STING polymeric prodrug platform that elicits a robust DC-driven antitumor response after systemic intravenous administration. We synthesized a polymerizable STING agonist prodrug monomer by conjugating a diamidobenzimidazole (diABZI) type agonist[11] "STING Agonist-3" to a polymerizable methacrylate via an intracellular cathepsin-cleavable Valine-Alanine (VA) linker. The monomer was co-polymerized with a targeting mannose methacrylate monomer[35] to produce the targeted macromolecular STING agonist prodrug 'drugamer', termed polySTING. We showed that polySTING targets CD206$^+$/mannose receptor$^+$ professional APCs in the TME, activates STING *in vivo*, and is well-tolerated. We confirmed polySTING's efficacy in an aggressive 'cold' B16-F10 murine melanoma model. We examined polySTING's mechanism in the same model and found a strong DC-driven antitumor immune response. Specifically,

polySTING strongly enhanced $CD8^+$ cDC1 responses along with TME T-lymphocyte infiltration and $CD8^+$ T cell activation while promoting DC maturation in the tumor-draining lymph nodes (TDLN). PolySTING also reduced tumor growth kinetics in the aggressive 4T1 breast cancer model of a different murine strain, demonstrating the utility of polySTING as a standalone systemic cancer immunotherapy or especially as a candidate for combination immune-therapy strategies.

ii. Materials and methods

Safety Statement

No unexpected or unusually high safety hazards were encountered in this work.

Materials

SMA N-hydroxysuccinimide ester (SMA-NHS, compound 2, **Scheme S1**) was synthesized as previously described[36]. 2-(methylsulfinyl)ethyl methacrylate (MSEMA) was synthesized as previously described[37]. The STING agonist "STING Agonist-3" (CAS 2138299-29-1) was purchased from MedChemExpress. L-Valyl-L-Alanine (H-Val-Ala-OH) was purchased from Combi-Blocks. RAFT chain transfer agent 4-(((ethylthio)carbonothioyl)thio)-4-cyanopentanoic acid (ECT) and the monomer mannose ethyl methacrylate (ManEMA) were purchased from Omm Scientific. The rhodamine monomer, methacryloylethyl thiocarbamoyl rhodamine B (RhMA) was purchased from PolySciences Inc. The initiator 2,2'-azobis(4-methoxy-2,4-dimethylvaleronitrile) (also known as V70) was purchased from Wako Fujifilm. N-Ethoxycarbonyl-2-ethoxy-1,2-dihydroquinoline (EEDQ) and 4-nitrophenol chloroformate (PNP-Cl) was purchased from Chem-Impex International Inc.. 4-aminobenzyl alcohol (PABA) was purchased from Tokyo Chemical Industries. Diisopropylethylamine (DIPEA), triethylamine (TEA) and dimethylaminopyridine (DMAP) were purchased from Sigma-Aldrich. Dimethylformamide (DMF), tetrahydrofuran (THF), dichloromethane (DCM) and chloroform were purchased from Fisher. Argon gas was purchased from Linde Gas & Equipment Inc. All reagents mentioned above were used as received.

Anhydrous deuterated dimethyl sulfoxide (DMSO-d6, > 99%) was purchased from Sigma-Aldrich and stored with activated molecular sieves. Buffers were prepared in-house using endotoxin-free water and salts purchased from Fisher Scientific. All antibodies were purchased from BioLegend, with the exception of anti-TCF1-PE and anti-PD1-eFluor450.

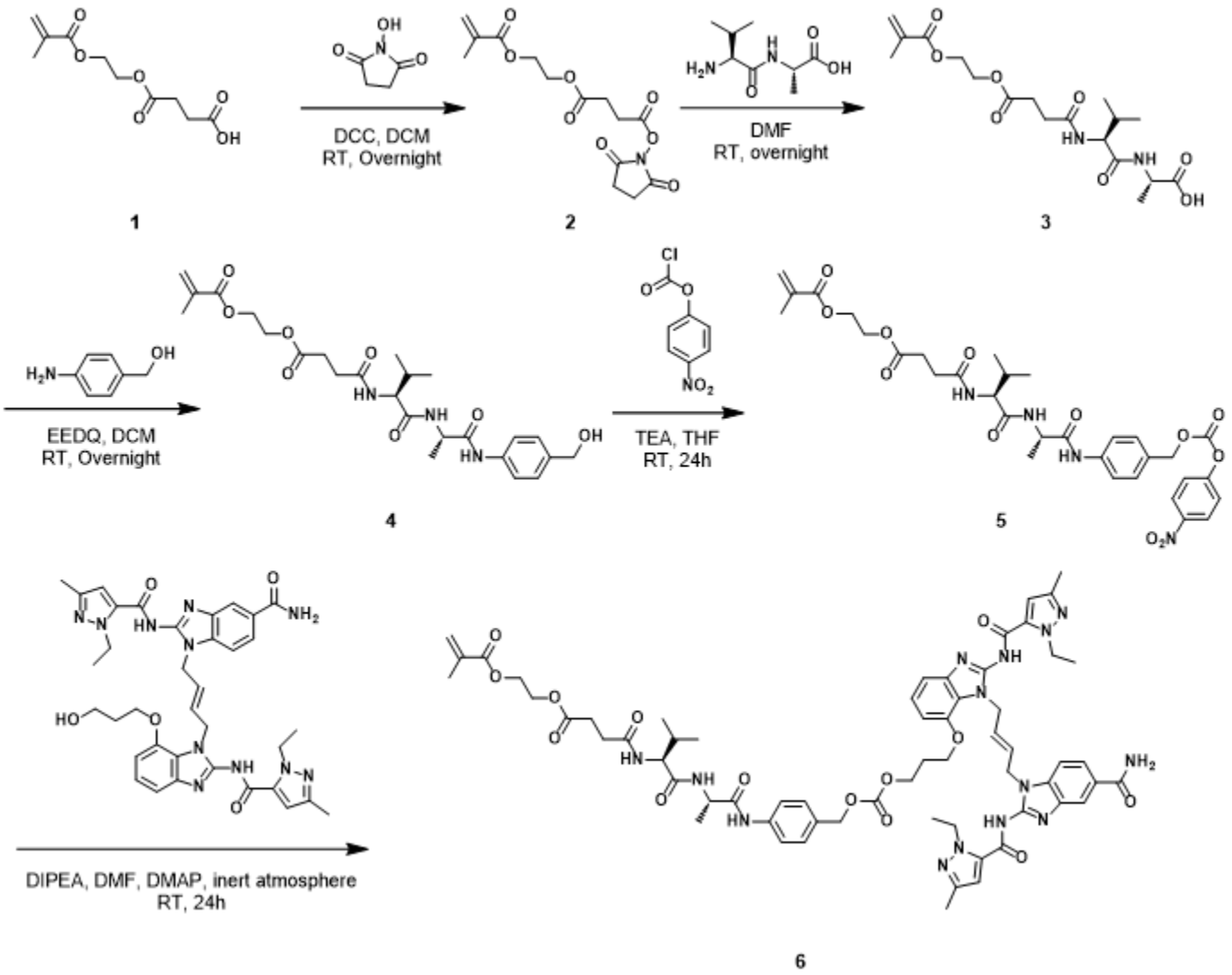

Scheme S1 - Synthesis of STING agonist prodrug monomer

Synthesis of SVA (Compound 3)

H-Val-Ala-OH (1.81 g, 9.63 mmol, 1 eq) was dissolved in DMF (22 mL). SMA-NHS/compound 2 (3.27 g, 10.0 mmol, 1.04 eq) was introduced to the stirring solution of VA. The reaction mixture was stirred overnight at room temperature and subsequently diluted with chloroform (300 mL), washed with ice-cold water (200 mL) and brine (15 mL), twice. The aqueous layer was back-extracted with 30 mL of chloroform and the combined organic layers were washed with 100 mL of water and 10 mL of brine. The organic layer was evaporated under reduced pressure to ca. 15 mL and precipitated into 1:1 (v/v) diethyl ether/pentane, and vortexed and centrifuged. SVA was obtained as a white pellet which was dried under in-house vacuum for 24 h to yield 2.81 g of SVA (73.1 % yield).

Synthesis of SVA-PAB-OH (Compound 4)

SVA (2.48g, 6.0 mmol, 1 eq) and PABA (0.88g, 7.2 mmol, 1.2 eq) were added into a round bottom flask and stirred in 50 mL DCM/MeOH (4:1) for 10 minutes. To the stirring solution, EEDQ (2.97g, 12.0 mmol, 2 eq) was slowly added over 5

minutes. The reaction mixture was allowed to stir overnight at room temperature. The reaction mixture was diluted with chloroform (100 mL) and extracted with water (70 mL) and brine (10 mL), twice. The aqueous layers were back-extracted with chloroform (30 mL). The combined organic layers were subsequently extracted with water and brine. The organic layer was concentrated, and the resultant viscous liquid was purified by silica gel column chromatography running 95:5 (v/v) chloroform:methanol. The SVA-PABA fractions (Rf = 0.6) were collected and precipitated into 1:1 (v/v) diethyl ether/pentane. The precipitate was vortexed and centrifuged and the pellet was dried under in-house vacuum overnight.

Synthesis of SVA-PAB-PNP (Compound 5)

SVA-PAB-OH (1.82 g, 3.6 mmol, 1 eq) and PNP-Cl (1.524 g, 7.56 mmol, 2.1 eq) were dissolved in 80 mL of THF. The solution was cooled in an ice bath before the addition of TEA (801.4 mg, 7.92 mmol, 2.2 eq). The mixture was stirred on ice for 30 minutes, and allowed to warm up to room temperature on its own accord for a total reaction time of 24 hours. The resultant reaction mixture was filtered to remove the TEA salt. The filtrate was concentrated to a thick yellow oil via rotary evaporation, precipitated into diethyl ether, vortexed and centrifuged. The pellet was collected by decanting the ether layer, taken up in 150 mL chloroform and washed with 100 mL water and 15 mL brine, respectively. The organic phase was dried over anhydrous sodium sulfate, before concentration and final precipitation in 1:1 (v/v) diethyl ether/pentane. Following centrifugation, the pellet was dried under in-house vacuum to yield 1.74 g of SVA-PAB-PNP (72.5% yield).

Synthesis of STING monomer (SVA-PAB-STING) (Compound 6)

To synthesize the final STING agonist prodrug monomer, STING Agonist-3 (280.8 g, 0.375 mmol, 1 eq) and SVA-PAB-PNP (301.8 mg, 0.45 mmol, 1.5 eq) were dissolved in 8.3 mL of anhydrous DMF (stored under inert atmosphere). The solution was sparged with argon, and cooled on an ice bath before the addition of DIPEA (242.3 mg, 1.875 mmol, 5 eq) and DMAP (45.8 mg, 0.46 mmol, 1.22 eq). The mixture was stirred on ice for 30 minutes, and then at room temperature for 24 hours. Thereafter, the mixture was diluted with 3:1 (v/v) CHCl3:iPrOH (35 mL) and washed three times with cold 2:1 (v/v) saturated NH4Cl:water (19 mL each time). The aqueous wash was back-extracted with 3:1 (v/v) CHCl3:iPrOH (10 mL). The combined organic layers were dried with anhydrous sodium sulfate. The organic phase was concentrated to a thick oil with high-vacuum rotary evaporation with a dry ice cold finger, and combined with 60A silica gel for dry column loading. The monomer was purified using a CombiFlash NextGen 300 flash chromatography system running a binary dichloromethane and 10:1 (v/v) MeOH:NH4OH mobile phase (0-15% MeOH:NH4OH gradient over 15-20 minutes), collecting the second peak (Rf = 0.5 with 18% MeOH:NH4OH in DCM). The fractions were combined and subject to rotary evaporation to near-dryness (a thick gel) and completely evaporated with in-house vacuum for 2-3 days to yield 150-200 mg (30-40% yield) of SVA-PAB-STING. It is noted that manual gradient column chromatography can also be employed (5-12% MeOH:NH4OH gradient with 2% increments every 100 mL mobile phase) with some co-eluted fractions. Running the reaction for extended amounts of time (72 h) decreased yield (around 50 mg, 10% yield).

For characterization, mass spectra were recorded on a Bruker EsquireLC Ion Trap (Bruker Corporation, Billerica, MA) Electrospray Ionization Mass Spectrometer instrument with direct injection in methanol (20 µg/mL) in negative ion mode. ^{1}H NMR spectra were recorded on a Bruker NEO 500 (Bruker Corporation, Billerica, MA) autosampler nuclear magnetic resonance (NMR) instrument in deuterated DMSO (DMSO-d6).

^{1}H NMR (500 MHz, DMSO-d6) δ 12.81 (s, 2H), 9.90 (s, 1H), 8.15 (d, *J* = 7.0 Hz, 1H), 8.01 – 7.90 (m, 3H), 7.71 (dd, *J* = 8.4, 1.7 Hz, 1H), 7.66 (s, 1H), 7.62 – 7.56 (m, 2H), 7.41 (d, *J* = 8.4 Hz, 1H), 7.34 – 7.27 (m, 4H), 6.53 (d, *J* = 10.3 Hz, 2H), 6.03 (s, 1H), 5.98 (dd, *J* = 13.3, 7.8 Hz, 1H), 5.76 – 5.66 (m, 2H), 5.01 (s, 2H), 4.94 (d, *J* = 5.3 Hz, 2H), 4.81 (d, *J* = 5.7 Hz, 2H), 4.52 (d, *J* = 6.9 Hz, 4H), 4.38 (p, *J* = 7.1 Hz, 1H), 4.26 (dt, *J* = 8.0, 4.1 Hz, 4H), 4.20 – 4.13 (m, 3H), 4.09 (t, *J* = 6.2 Hz, 2H), 3.78 (p, *J* = 6.1 Hz, 1H), 2.11 (d, *J* = 6.1 Hz, 5H), 1.97 (dt, *J* = 12.1, 6.4 Hz, 3H), 1.87 (d, *J* = 1.3 Hz, 3H), 1.33 – 1.23 (m, 9H), 1.05 (d, *J* = 6.1 Hz, 5H), 0.85 (dd, *J* = 17.6, 6.8 Hz, 6H), -0.06 (s, 1H).

Polymer synthesis

ManEMA (200 mg, 0.68 mmol, 35.7 eq), SVA-PAB-STING (55.9 mg, 0.044 mmol, 2.2 eq), were all dissolved in DMSO-d6 (0.34 mL) in a 5 mL oven-dried pear-shaped flask. Trioxane (15 mg) was added as an internal standard for monomer conversion calculations. Next, a stock solution (20.2 mg/mL in DMSO-d6) of the RAFT chain transfer agent ECT (0.25 mL, 5.05 mg, 0.019 mmol, 1 eq) was added. Thereafter, a stock solution of V70 (17.7 mg/mL in anhydrous DMF) was prepared and quickly added to the solution (0.05 mL, 0.88 mg, 0.0029 mmol, 0.15 eq). After taking a small aliquot (0.02 mL) for NMR conversion analysis, the reaction vessel was sealed with a septa and purged with argon gas for 30 minutes. The flask was then placed into an oil bath set to 42 C, and allowed to react for 22 hours. Upon completion, the reaction mixture was dialyzed against DMSO (500 mL) for 3 days using a SnakeSkin 3.5 kDa MWCO regenerated cellulose membrane, changing the DMSO twice daily. The reaction mixture was then dialyzed against ice-cold water (4C, 4000 mL) in a cold room for 2 days to remove DMSO, changing water twice daily. The dialysate was then lyophilized for 3 days to yield 188 mg (85% gravimetric conversion) of polySTING.

For the synthesis of rhodamine-labelled polySTING (polySTING-Rh), 3.8 mg of RhMA (0.0055 mmol, 0.38 eq) was added to the following: 0.48 mL DMSO-d6, 150 mg of ManEMA (0.51 mmol, 35.3 eq), 42.4 mg of SVA-PAB-STING (0.038 mmol, 2.3 eq), 3.82 mg of ECT (0.015 mmol, 1 eq) and 0.67 mg of V70 (0.0022 mmol, 0.15 eq). Following the addition of RhMA, the above protocol was exactly repeated.

For the synthesis of rhodamine-labeled non-glycan STING drugamer control (MSEMA-STING), 5.7 mg of RhMA (0.0084 mmol) was added to the following: 0.48 mL DMSO-d6, 140 mg of MSEMA (0.79 mmol, 42.3 eq), 54.1 mg of SVA-PAB-STING (0.042 mmol, 2.3 eq), 4.9 mg ECT (0.018 mmol, 1 eq) and 0.87 mg of V70 (0.0028 mmol, 0.15 eq). Following the addition of RhMA, the above protocol was exactly repeated.

Polymer Characterization

All ^{1}H NMR spectra were recorded on a Bruker NEO 500 (Bruker Corporation, Billerica, MA) autosampler nuclear magnetic resonance (NMR) instrument in deuterated DMSO (DMSO-d6). Drug incorporation into polymers was assessed by ^{1}H NMR analysis of a known polymer mass (typically >10mg in 600 uL solvent) and the internal standard levofloxacin (typically 1 mg/mL in solvent) (Levofloxacin δ 8.9 (s, 1H), STING δ 6.45 (d, 2H)). Polymer molecular weights (Mw, Mn) and polydispersity index (Đ = Mw/Mn) were determined by gel permeation chromatography (GPC). The system consisted of an Agilent 1260 HPLC stack running heated LiBr-supplemented (0.1% w/v) DMF mobile phase at a flow rate of 1 mL min^{-1} through a semi-prep three-column setup (Tosoh TSKGel alpha-4000 to Tosoh TSKGel alpha-300 to Phenomenex Phenogel 10^{3} A). Samples (10 mg/mL) were filtered through a 0.2 µm hydrophilic PTFE filter before analysis. The unimeric form of the polymer in solution was verified by Dynamic Light Scattering (DLS) on a DynaPro NanoStar (Wyatt Technology, Santa Barbara, CA) through different polymer concentrations (200-1.25 mg/mL) in PBS.

Formulation of STING treatments

For the free drug STING-3, the received powder was dissolved into sterile DMSO at 4 mg/mL with sonication, and stored at -20C until use, where it is diluted to *in vivo* concentrations with 1X DPBS. For the polymeric STING prodrug polySTING, the lyophilized powder was reconstituted in 1X DPBS at *in vivo* concentrations. All formulations were sterile-filtered through a 0.2 µm PVDF membrane before use.

Cell lines and animals

The B16F10 cell line was cultured in DMEM supplemented with 10% FBS and 1% P/S. The 4T1 cell line was cultured in RPMI supplemented with 10% FBS and 1% P/S. Cells were incubated at 37°C and 5% CO_2. Female C57BL/6 mice and female BALB/c mice aged 6 to 8 weeks were purchased from Charles River Laboratories and The Jackson Laboratories. All animal studies were approved by the University of Washington Institutional Animal Care and Use Committee (IACUC).

Bone marrow-derived macrophage polarization

Bone marrow cells were extracted from murine femurs and tibias. Cells were seeded in 10 cm non-TC plates with plating media: DMEM + 10% FBS + 1% P/S + 20 ng/ml M-CSF. On day 4, 10 more ml of plating media was added per plate. On day 7, cells were polarized to either M1 using 100 ng/ml LPS + 20 ng/ml IFNγ, or M2 using 20 ng/ml IL-4. After a 48 hour incubation, M1 cells were treated with PBS and M2 cells were treated with either PBS, free STING, or polySTING at a concentration of 20 μg/ml. After a 24 hour incubation, cells were stained for viability with Zombie NIR, blocked with anti-CD16/32, and finally stained with anti-CD206-PerCP-eFluor710, anti-CD11b-FITC, anti-CD163-PE, and anti-CD86-BV510. An Attune NxT flow cytometer was used to analyze the data. M2 BMDMs were treated with PBS, free STING, or polySTING at a concentration of 20 μg/ml for 48 hours. RNA was extracted using RNeasy mini kit (Qiagen). cDNA was synthesized using the high capacity cDNA reverse transcription kit (Applied Biosystems). qPCR was performed to analyze the amount of cDNA. Arg1 and Nos2 expressions were normalized to the GAPDH housekeeping gene. The DNA primers were used as follows: GAPDH: AATGGATTTGGACGCATTGGT; TTTGCACTGGTACGTGTTGAT. ARG1: CAAGACAGGGCTCCTTTCAG; TGGCTTATGGTTACCCTCCC. NOS2: GATGTTGAACTATGTCCTATCTCC; GAACACCACTTTCACCAAGAC.

Toxicity study

Female BALB/c mice were injected with free STING at 30 μg and polySTING at 10, 20 and 30 μg (STING equivalent) on days 0 and 4, and were observed for signs of decrease in activity, hunched posture and weight loss. Liver toxicity was analyzed by injecting PBS, free STING and polySTING at 10 μg through the tail vein twice, with 3 days apart to C57BL/6 mice and collecting serum 24 h post 2nd injection. Serum alanine aminotransferase (ALT) level was measured using an ALT activity assay (Sigma). Aspartate Aminotransferase (AST) level was taken from frozen serum using an AST activity assay kit (Abcam). A Tecan Infinite plate reader was used to take the colorimetric readouts.

ELISA for cytokine quantification

Female C57BL/6 mice were injected with 30 μg free drug STING agonist-3 or polySTING containing 10, 20 or 30 μg of STING agonist-3 through the tail vein. Blood was collected through tail vein 4 h post injection in EDTA-treated tubes. Blood was spun down for 10 min at 1000 g and upper layer plasma was collected for ELISA to measure IFNβ expression level (Invivogen).

Interferon-stimulated gene expression

Female BALB/c mice with 4T1 tumors around 100-200 mm^3 were injected with PBS or 30 μg free STING agonist-3 or 30 μg (STING equivalent) polySTING through the tail vein. Tumors were collected 24 hr post injection. Female C57BL/6 mice with B16F10 tumors around 100-200 mm^3 were injected with PBS or 10 μg free STING agonist-3 or 10 μg polySTING through the tail vein, twice, 4 days apart. Tumors and TDLNs were collected 24 hr post 2nd injection. RNA was extracted from tumor tissues or TDLN cells using Trizol or RNeasy mini kit (Qiagen). cDNA was synthesized using the high capacity cDNA reverse transcription kit (Applied Biosystems). qPCR was performed to analyze the amount of cDNA. Ifnb1 and cxcl10 expressions were normalized to the GAPDH housekeeping gene. The DNA primers were used as follows: GAPDH: AATGGATTTGGACGCATTGGT; TTTGCACTGGTACGTGTTGAT. Ifnb1: AGCTCCAAGAAAGGACGAACA; GCCCTGTAGGTGAGGTTGAT. Cxcl10: CCAAGTGCTGCCGTCATTTTC; GGCTCGCAGGGATGATTTCAA.

Tissue processing

Tumors were cut into small pieces, treated with 20 U/mL type IV collagenase + 125 U/mL DNase I, and dissociated with the GentleMACS Dissociator. Tumors were then incubated on a rotating platform at 37 °C for 30 min. Single-cell suspensions were obtained by passing homogenate through a 70 μm cell strainer. Cells were treated with the ACK lysing buffer to remove red blood cells. Inguinal lymph nodes were dissociated with pipette tips and digested with 50 U/mL type IV collagenase + 100 U/mL DNase I. Cells were incubated at 37 °C for 30 min with gentle agitation. Single-cell suspensions were obtained by passing homogenate through a 70 μm cell strainer.

Pharmacokinetic characterization

Female C57BL/6 mice were inoculated with 2×10^5 B16F10 cells in the right-hind flank on day -8. On day 0 (tumor volume approx. 100-200 mm3), they were treated with polySTING (10 μg STING equivalent) through tail-vein injection. 30 minutes post-administration, mice were sacrificed and whole blood collected through cardiac puncture, followed by tumor isolation. Tumor and plasma were snap frozen in dry ice and stored at -80ºC until analysis. Samples were processed and analyzed with tandem LC/MS-MS (Xevo TQ-S, Waters Corporation, Milford, MA) according to previously-published procedures[36]. The MS instrument was operated on a positive ion multiple-reaction monitoring (MRM) mode monitoring 136 m/z for the STING agonist and 112 m/z for the internal standard gemcitabine (LLOQ-ULOQ 0.57-1248 ng/mL plasma or 2.57-624.0 ng/g tumor).

Tumor cellular uptake studies

Female C57BL/6 mice were inoculated with 2×10^5 B16F10 cells in the right-hind flank on day -8. On day 0 (tumor volume approx. 100-200 mm3), they were treated with either MSEMA-STING-RhPBS or polySTING-Rhod (10 μg STING equivalent) through tail-vein injection. 30 minutes post-administration, tumors were harvested and made into single-cell suspension as described previously. Cells were stained for viability with Zombie Violet viability kit, blocked with Trustain anti-mouse CD16/32, and then stained with anti-CD45-APC/Cy7, anti-CD11c-FITC or anti-F4/80-FITC. An Attune NxT flow cytometer was used to analyze the data.

Organ-level biodistribution studies

Female C57BL/6 mice were inoculated with 2×10^5 B16F10 cells in the right-hind flank on day -8. On day 0 (tumor volume approx. 100-200 mm3), they were treated with polySTING-Rh (10 μg STING equivalent) through tail-vein injection. 30 minutes post-administration, mice were sacrificed and perfused for organ collection. Tissues were homogenized in RIPA buffer with 2500 U/mL DNase-I and supernatant were collected after centrifugation. The fluorescent polySTING-Rh signal of organ homogenates were measured on a Tecan Infinite M21000 pro plate reader (Tecan Life Sciences, Mannedorf, Switzerland, Ex/Em: 530/580 nm). Homogenate protein level was measured using the Pierce BCA protein assay kit. Calibrators were prepared by spiking naive organ homogenates (1:10 v/v) with stock solutions of polySTING-Rh covering a final concentration range of 0.854-6.795 μg/mL homogenate of polySTING-Rh.

Tumor-infiltrating lymphocytes (TIL) and TDLN analysis

Female C57BL/6 mice were inoculated with 2×10^5 B16F10 cells in the right-hind flank on day -8. On days 0 (tumor volume approx. 100-200 mm3) and 4, they were treated with either PBS or polySTING (10 μg STING equivalent) through tail-vein injections. On day 5, tumors and the tumor-draining lymph nodes (TDLNs, inguinal LN in the same flank as tumor) were harvested. Tissues were made into single-cell suspension as previously described.

Tumor cells were stained for viability with Zombie Violet viability kit, blocked with Trustain anti-mouse CD16/32, and then stained in three plates for T cells (anti-CD45-APC/Cy7, anti-CD3-PE/Cy5, anti-CD4-PE, anti-CD8-FITC), macrophages (anti-CD45-APC/Cy7, anti-F4/80-FITC, anti-CD80-PE, anti-CD206-BV605), and DCs (anti-CD45-APC/Cy7, anti-CD11c-FITC, anti-CD80-PE, anti-MHCII-PE/Cy5). In a separate study, tumor cells were stained for viability with Zombie NIR viability kit, blocked with Trustain anti-mouse CD16/32, and then stained in two plates for DCs (anti-CD11c-APC, anti-CD8-FITC, anti-CD103-PE, anti-CD86-BV510) and T cells (anti-CD3-PE/Cy5, anti-CD8-FITC, anti-TCF1-PE, anti-PD1-eFluor450).

TDLN cells were stained for viability with Zombie NIR viability kit, blocked with anti-mouse CD16/32, and then stained in two plates for DCs (anti-CD11c-APC, anti-CD8-FITC, anti-CD103-PE, anti-CD86-BV510) and T cells (anti-CD3-eFluor450, anti-CD4-PE, anti-CD8-FITC). In a separate study with 30 μg STING agonists and a single tail-vein injection, TDLN cells were stained for viability with Zombie NIR viability kit, blocked with anti-mouse CD16/32, and then stained in with anti-CD11c-APC, anti-CD86-BV510, anti-CD40-FITC and anti-CD80-PE. An Attune NxT flow cytometer was used to analyze the data.

Therapeutic studies

For the B16F10 tumor model, female C57BL/6 mice were inoculated with 2×10^5 B16F10 cells in the right-hind flank on day -8. On days 0, 4, and 8, mice were treated intravenously (tail vein on days 0, 4, and retro-orbitally on day 8) with PBS, or either free STING or polySTING with an equivalent STING agonist dose of 10 μg. For the 4T1 tumor model, female BALB/c mice were inoculated with 5×10^5 4T1 cells in the mammary fat pad on day -8. On days 0, 7, and 14, mice were treated intravenously (tail vein on days 0, 7, and retro-orbitally on day 14) with PBS, or either free STING or polySTING with an equivalent STING agonist dose of 10 μg. On days 1, 8, and 15, mice were injected with 100 μg of anti PD-1 ICB via intraperitoneal injection. Tumor length and width were then measured using a vernier caliper, and volume was subsequently calculated using the formula: Volume = $(\text{Width}^2 \times \text{Length}) \div 2$. Weight was measured the same time as tumor measurements. Mice were euthanized if total tumor volume exceeded 2000 mm^3 for B16F10 tumors, and 1500 mm^3 for

4T1 tumors, visible discharge was observed on ulcers of the tumors, signs of mortality such as excessive lethargy, or the body weight loss exceeded 20%.

Statistical analysis

Statistical analysis was performed using the Graphpad Prism software. Unpaired t test was used to compare two groups. One-way ANOVA with post-hoc Tukey HSD test was used to compare more than two groups. Log-rank test was used for survival analysis. Mixed-effects analysis of two-way ANOVA with Tukey's multiple comparison was used to analyze tumor growth curves.

iii. Results and discussion

Synthesis and characterization of polySTING

"STING Agonist-3" was selected for our studies because it shows excellent activity[11], and it has a single hydroxyl group amenable to synthesis of the polymerizable prodrug monomer. The synthetic scheme for the STING Agonist-3 prodrug monomer is summarized in **Figure 1a** (more detail in **Scheme S1**). Using the polymerizable mono-2-(methacryloyloxy)ethyl succinate (SMA) moiety, the prodrug monomer was synthesized by incorporating the cathepsin B-cleavable Val-Ala linker with a self-immolative para-aminobenzyl alcohol (PABA) moiety that has been validated in the human antibody-conjugate field[38], to yield SMA-Val-Ala-PABA-STING Agonist-3 (SVA-PAB-STING). The prodrug monomer product was validated using ^{1}H-NMR and mass spectrometry (**Figure S1-S2**). We then synthesized the targeted polymer prodrug "drugamer" polySTING by co-polymerizing SVA-PAB-STING with mannose ethyl methacrylate (ManEMA) (**Figure 1b,** characterization in **Figure S3-S5**). PolySTING has an average Mw of 12 kDa, with an average degree of polymerization (DP) of 35 for ManEMA and 2 for SVA-PAB-STING. We confirmed by dynamic light scattering that polySTING is highly soluble in aqueous solutions as unimers up to 200 mg/mL in PBS (**Figure S6)**. PolySTING is thus designed for internalization by receptor-mediated endocytosis in $CD206^{+}$ APCs, followed by endosomal cathepsin cleavage and release of the membrane-permeable diABZI-type "STING Agonist-3" that can activate the cytosolic STING protein in these APCs (**Figure 1c**).

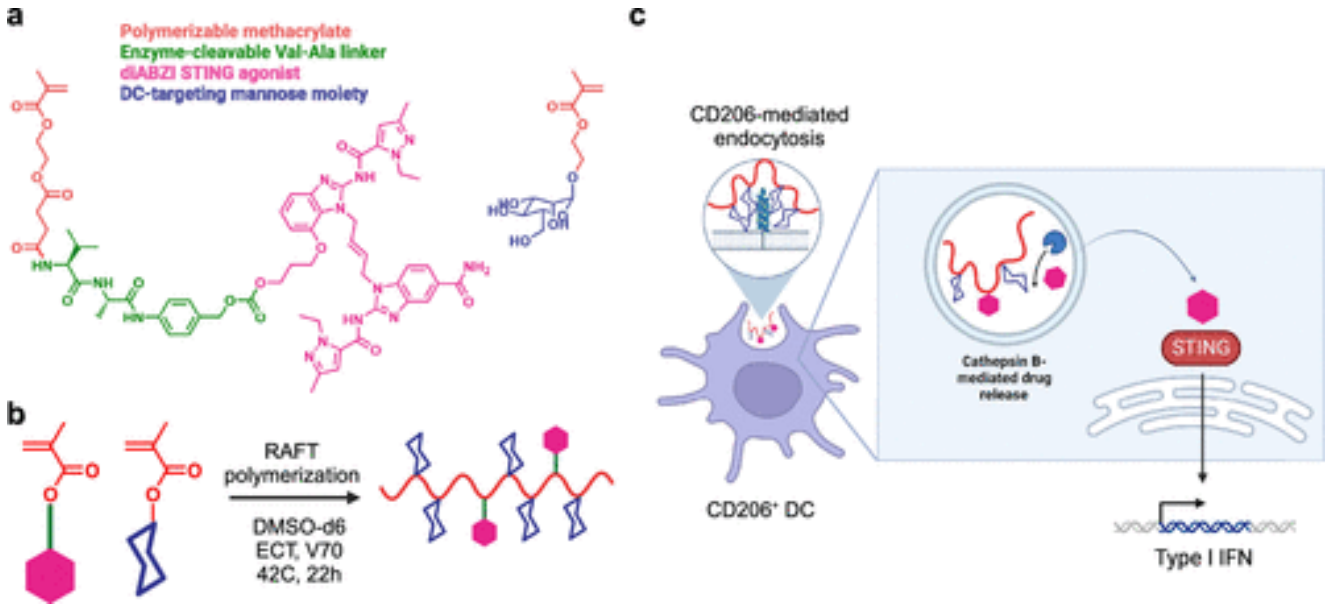

Figure 1. Design of polySTING polymeric prodrug. (a) Structure of the enzyme-cleavable methacrylate-based STING agonist prodrug monomer and mannose ethyl methacrylate monomer. (b) Schematic of polySTING synthesis by RAFT polymerization. (c) Schematic of polySTING uptake by $CD206^+$ DCs, endosomal prodrug cleavage and agonist release, and STING activation in DCs. Created with BioRender.com

PolySTING targets APCs in the TME and activates STING

In our preliminary pharmacokinetic characterization in B16-F10 tumor-bearing mice, we observed that intravenous administration of polySTING resulted in higher plasma and tumor STING agonist concentrations compared to free STING agonist 30 minutes after administration (**Table S1**). These results motivated us to investigate the professional APC targeting selectivity of polySTING in the tumor after intravenous administration, as these cells play pivotal roles in antitumor responses[39,40] and may be targeted by mannose through the CD206 receptor. To this end, a fluorescent rhodamine-labelled polySTING (polySTING-Rh) was synthesized alongside a non-targeted control substituting ManEMA with the hydrophilic non-glycan 2-methylsulfinyl ethyl methacrylate (MSEMA-STING-Rh, NMR characterization in **Figure S7**). PolySTING-Rh and MSEMA-STING-Rh were administered to B16-F10-bearing C57BL/6 mice and rhodamine-positive cell subsets in the tumor were characterized. PolySTING-Rh was shown to selectively target immune cells ($CD45^+$) including DCs ($CD11c^+$) and macrophages ($F4/80^+$), which all have a significant fraction of polySTING-Rh-positive cells, unlike non-immune $CD45^-$ cells (**Figure 2a, b**). MSEMA-STING-Rh exhibited much less uptake in both immune cell subsets compared to polySTING (**Figure 2a**). We still observed preferential uptake of MSEMA-STING in macrophages and DCs, but the difference compared to $CD45^-$ cells is less pronounced and explainable through inherent phagocytic activity. We observed similar results 4 hours after treatment (**Figure S8)**. PolySTING therefore has a unique TME distribution profile compared to prior non-targeted STING agonist formulations, which all have significant uptake in $CD45^-$ cells[15,16,21]. Thus, by transforming the STING agonist to a mannosylated macromolecular prodrug, we successfully restricted STING agonist delivery to immune cells in the TME.

STING activation was also assessed via the expression of STING-related genes Ifnb1 and Cxcl10 in the tumor and the tumor-draining lymph nodes (TDLNs). Tumor and TDLN STING gene expression was sampled 4 hours after a single treatment. PolySTING elicited a significant increase in both Ifnb1 and Cxcl10 expression in the tumor compared to free STING agonist and untreated mice (**Figure 2c**). PolySTING generated a 9.3 fold increase in Ifnb1 expression and a 13 fold

increase in Cxcl10 expression compared to free STING agonist. In the TDLN, polySTING induced a 111 fold increase in Ifnb1 expression and a 383 fold increase in Cxcl10 expression(**Figure 2d**)[41,42]. These results establish that polySTING preferentially targets APCs, resulting in STING pathway activation in the TME and in the TDLNs.

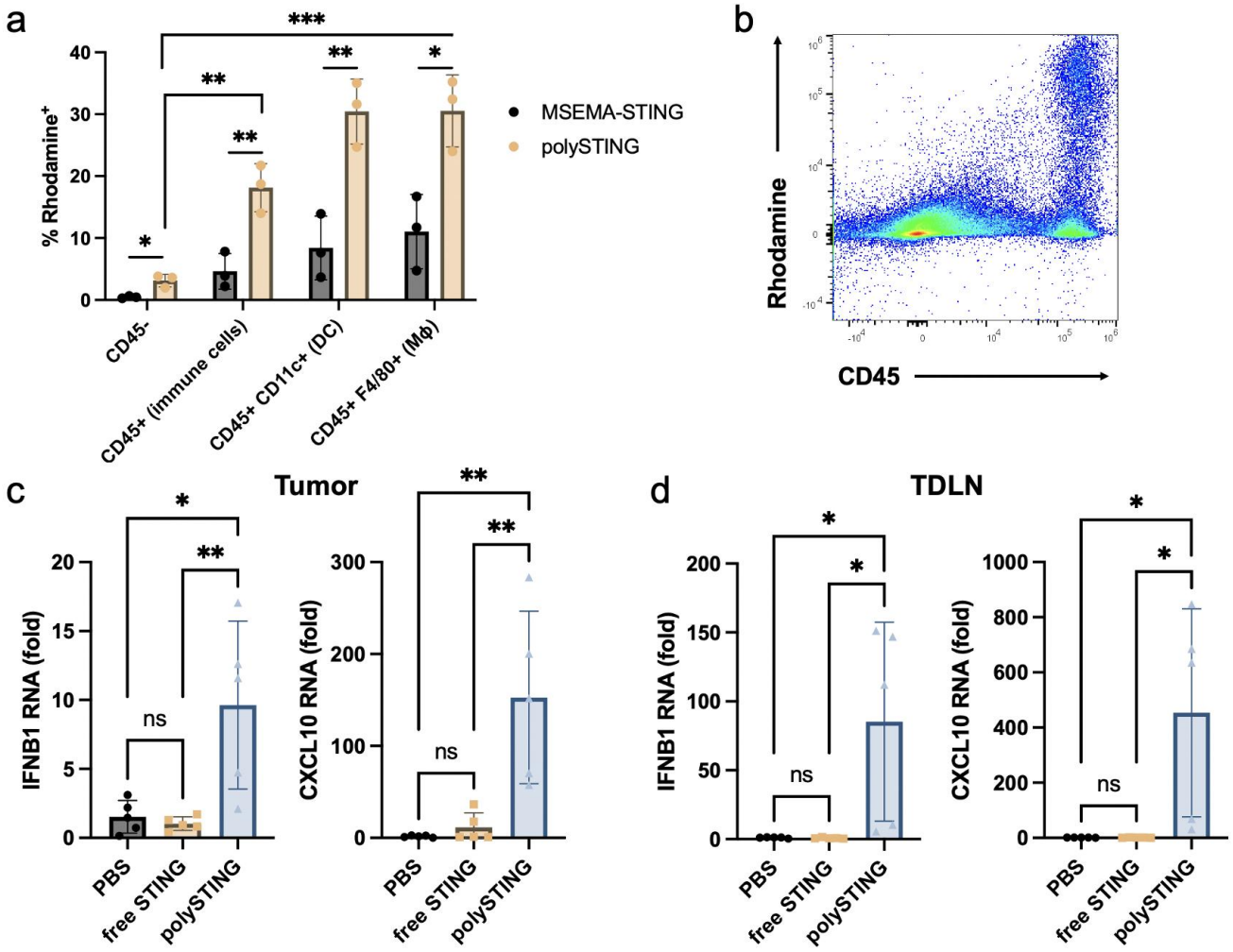

Figure 2. PolySTING targets immune cells and activates the STING pathway. (a) B16F10 tumor-bearing C57BL/6 mice were treated with polySTING-Rh or MSEMA-STING-Rh intravenously and tumors (100-200 mm^3) were harvested 30 min post injection. Percentage of rhodamine-positive cells in different cell subsets were quantified by flow cytometry (N=3). (b) Representative flow dot plot of rhodamine and CD45 expression in tumor. (c, d) Expression levels of interferon-stimulated genes IFNB1 and CXCL10 in the tumor and TDLN 4 h post treatment by RT-qPCR (N=5). Gene expression was normalized to the GAPDH housekeeping gene. Data are represented as mean ± SD. (a) Unpaired t-test was used to compare polySTING and MSEMA-STING under different cell subsets. One-way ANOVA with post-hoc Tukey HSD test was used to compare polymer uptake in different cell subsets after polySTING treatment. (*$p \leq 0.05$, **$p \leq 0.01$, ***$p \leq 0.001$). (c, d) Statistical analysis was performed using one-way ANOVA with post-hoc Tukey HSD test (*$p \leq 0.05$, **$p \leq 0.01$).

Because polySTING was shown to localize to both macrophages and DCs in the TME, downstream activation markers were investigated in each cell type. In macrophages, STING activation has been reported to drive polarization towards the pro-inflammatory M1 phenotype over the tolerogenic, tumorigenic M2 phenotype[43]. Surprisingly, polySTING slightly increased M1 marker CD80 expression in tumor-associated macrophages (TAMs) compared to free STING agonist and untreated

mice, but had no effect on M2 marker CD206 expression **(Figure S9)**. We investigated this trend *in vitro* with bone marrow-derived macrophages (BMDM) incubated with STING agonists and formulations. Similarly, STING treatments increased the expression of M1 marker CD86 in M2 macrophages, but didn't change the expression level of the M2 markers CD206 and CD163 (**Figure S10**). RT-qPCR showed increased NOS2 (M1-related) expression and decreased ARG1 (M2-related) expression in polySTING-treated cells but only ARG1 downregulation for free agonist (**Figure S11**). These results suggest polySTING could drive macrophage polarization towards the pro-inflammatory M1 type. In addition, polySTING induced significant DC maturation across all markers (CD86, CD80 and CD40) in the DC-enriched TDLN (**Figure S12).** The potent DC response suggests the potential for a strong DC-mediated adaptive antitumor immune response. We therefore moved to therapeutic evaluation *in vivo*.

Systemic therapy of polySTING is tolerable and results in potent suppression of melanoma growth

We next investigated the organ-level biodistribution of polySTING using polySTING-Rh in the same B16-F10 model. At 30 minutes post-intravenous injection, we observed the most polySTING-Rh signal in the liver, followed by the tumor and spleen **(Figure S13)**. As aberrantly activated liver macrophages/Kupffer cells can cause liver damage, we next investigated liver toxicity. We intravenously administered polySTING or free STING agonist into C57BL/6 mice twice, 3 days apart, and sampled serum levels of alanine aminotransferase (ALT) and aspartate aminotransferase (AST) as markers of hepatotoxicity. Neither intravenous administration of polySTING nor the free drug elevated ALT or AST levels above saline treatment **(Figure S14)**. In addition, neither treatment resulted in significant weight loss, while polySTING exhibited dose-dependent IFNβ stimulation **(Figure S15-S16).**

These indications of tolerability permitted the subsequent evaluation of polySTING's anti-cancer efficacy in the aggressive, poorly immunogenic murine melanoma model B16-F10[45]. polySTING significantly inhibited B16-F10 tumor growth and prolonged survival compared to vehicle control (**Figure 3a, b.** Individual curves in **Figure S17)**. Free-form STING Agonist-3 did not yield any therapeutic effect over control. The diABZI family from which "STING Agonist-3" was derived already has an efficacy track record in the CT-26 colon cancer model[11]; these striking results reflect the aggressiveness of B16-F10 model and highlights the therapeutic utility of polySTING. In the same study, a stronger IFNβ response and higher weight loss upon either polySTING or free drug treatment was observed compared to healthy mice, likely due to inflammation in the tumor causing weight loss from ablation (**Figure 3c, d**, compared with **Figure S15-S16**). Weight loss increased with subsequent administrations; however, it remained below 10% loss up to the 3rd injection, a treatment regime comparable with many other reported systemic STING delivery platforms[16,18,21].

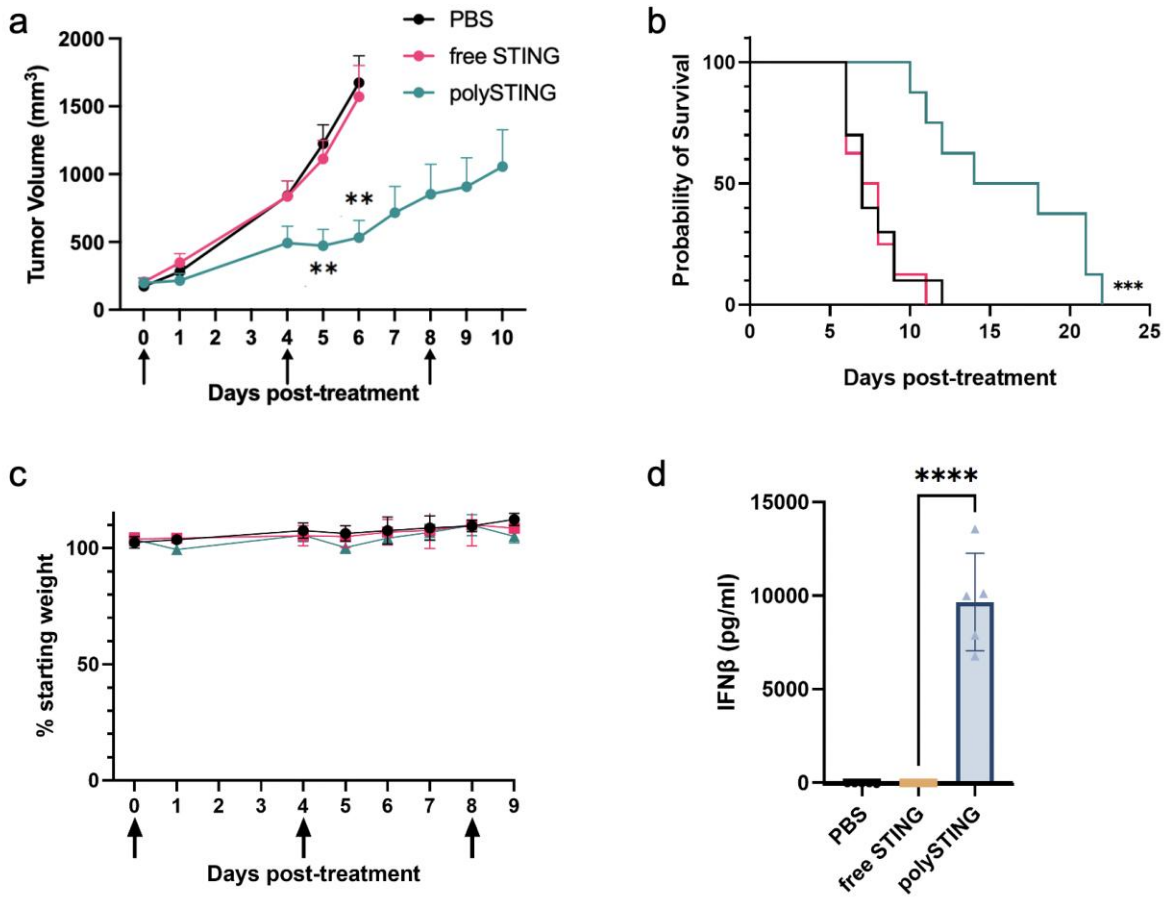

Figure 3. PolySTING inhibits tumor growth and prolongs survival in tumor-bearing mice. (a) Tumor growth curve in B16F10 tumor-bearing C57BL/6 mice. B16F10 cells were inoculated on day -8, and STING treatments were given on days 0, 4 and 8 through tail vein injections. Data are represented as mean ± SEM (N = 8-10). Statistical analysis was performed using mixed-effects of analysis of two-way ANOVA with Tukey's multiple comparisons test(**$p \leq 0.01$, between free STING and polySTING). (b) Kaplan-Meier survival curve (N=8-10). Survival analysis was performed using the log-rank test (*** $p \leq 0.001$). (c) Weight change in B16F10 tumor-bearing C57BL/6 mice. Data are represented as mean ± SD (N = 8-10). (d) Plasma IFNβ level in 4T1 tumor-bearing BALB/c mice 4 h post treatment with free STING and polySTING (N=5). Data are represented as mean ± SD. Statistical analysis was performed using one-way ANOVA with post-hoc Tukey HSD test (****$p \leq 0.0001$).

Examination of polySTING-treated B16-F10-bearing mice reveals a T-cell-inflamed TME maintained by $CD8^+$ DCs

To better understand the mechanism behind polySTING's efficacy, the immune cell population in the B16-F10 TME was examined after the 2nd injection (**Figure 4a**). PolySTING induced more $CD45^+$ immune cell infiltration into the tumor compared to the free drug (**Figure 4b**). As T cells are key contributors in antitumor immunity[46], we first looked at the T cell infiltration (gating scheme in **Figure S18**). In line with the tumor suppression results, polySTING treatment, but not free STING agonist, induced significantly more T cell infiltration (2.3-fold) in the TME compared to untreated mice (**Figure 4c**). More importantly, polySTING treatment increased the percentage of $CD8^+$ T cells in the TME by 4.8-fold, and could partially explain the antitumor effect of polySTING.

As tumor-infiltrating T cells could still be subject to immunosuppression and therapy failure[47], DC subset composition was next examined (gating scheme in **Figure S19**). cDC1s are critical mediators of antigen transport to TDLNs[48], chemoattractant producers in the TME (i.e. $CD103^+$ DCs)[30], as well as antigen cross-presentation to T cells both for priming and maintenance (i.e. $CD8^+$ DCs)[29]. PolySTING increased $CD8^+$ DCs in the TME compared to untreated or free drug groups, but not overall DC population relative to all cells (**Figure 4d**). To our knowledge, this $CD8^+$ DC response without usage of checkpoint blockade therapy has not been reported elsewhere and may represent a novel mechanism for targeted STING immunotherapy. Tumoral DCs have been recognized as crucial in maintaining T-cell activity in the TME through antigen presentation and co-stimulation[32]. Given $CD8^+$ DCs capability for cross-presentation to cytotoxic lymphocytes[49], their population increase in polySTING-treated groups compared to free drug could better maintain tumoral $CD8^+$ T-cell activity. The increased $CD8^+$ DC population in the TME without change in the overall $CD11c^+$ DC population may represent either polarization of $CD11c^+$ cells towards $CD8^+$ phenotypes or a migratory equilibrium between $CD8^+$ DCs and other subsets. This is consistent with reports that STING activation and/or its resultant IFN response stimulates $CD8^+$ DC responses[27,50,51]. There were no differences in $CD103^+$ DC populations between treatment groups (**Figure S20**).

The quality of infiltrating T-cells was also examined through analysis of PD-1 and TCF-1 expression (gating scheme in **Figure S21**). PD-1 is a marker for tumor-reactive $CD8^+$ T cells in melanoma[52]. TCF-1 is a marker indicative of stem-like constitutively-activated T-cells (i.e. exhausted T-cells in the antigen-rich TME) capable of functional rescue[53], and is mechanistically associated with positive response checkpoint blockade therapy[54]. PolySTING increased the fraction of "tumor-reactive" $PD\text{-}1^+$ $CD8^+$ T cells while the free-form STING agonist did not (**Figure 4e**). The increase in $PD\text{-}1^+$ $CD8^+$ T cells may be a consequence of increased T cell infiltration into the tumor, and the heightened persistent antigen exposure associated with it[55]. There was no difference in TCF-1 expression amongst all treatment groups, though the response trended upwards for polySTING (**Figure 4e**).

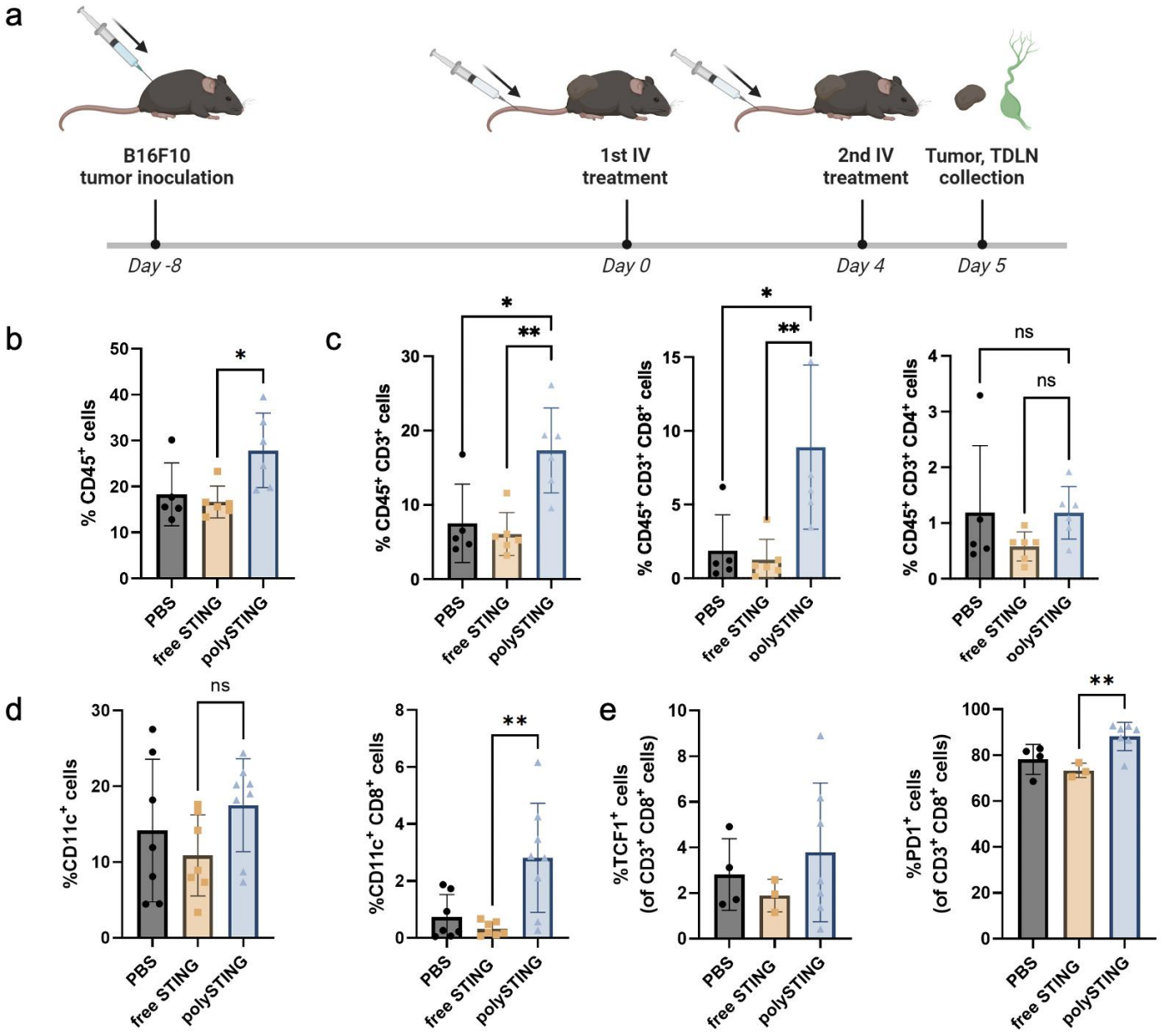

Figure 4. PolySTING induces immune cell infiltration into the tumor. (a) Schematic of polySTING treatment schedule. C57BL/6 mice were inoculated with B16F10 cells on day -8. Treatment was given on day 0 and day 4 intravenously. Tumor and TDLN were harvested 24 h post 2nd injection. (b) Percentage of $CD45^+$ immune cells in the tumor by flow cytometry (N=5-6). (c) Percentage of total T cells, $CD8^+$ T cells and $CD4^+$ T cells in the tumor by flow cytometry (N=5-6). (d) Percentage of total DCs and $CD8^+$ DCs in the tumor by flow cytometry (N=7-8). (e) Percentage of $TCF1^+$ $CD8^+$ T cells and $PD1^+$ $CD8^+$ T cells in the tumor by flow cytometry. Data are represented as mean ± SD. Statistical analysis was performed using one-way ANOVA with post-hoc Tukey HSD test (*$p \leq 0.05$, **$p \leq 0.01$, ns: not significant). Figure 4a created with BioRender.com.

Having demonstrated potent downstream effects of polySTING, we next looked upstream at the TDLNs where T cell priming takes place (gating scheme in **Figure S22**). In contrast to the TME, there is a noticeable increase CD11c$^+$ DCs in polySTING-treated TDLNs, as well as the cDC1 subsets CD8$^+$ and CD103$^+$ DCs (**Figure 5a**). In addition, all DC subsets had a substantial increase in the CD86 maturation marker (**Figure 5b**). Consistent with previous data, free-form STING agonist did not induce any appreciable change. The increased maturation marker expression could be due to a combination of type I IFN production due to STING activation and exposure to tumor antigen[56,57]. The indispensable role of secondary lymphoid organ (SLO)-resident CD8$^+$ DCs in priming cytotoxic T-lymphocytes (CTLs) and subsequent cellular responses to both tumors and pathogens is well-established[29]; thus, their expansion brought about by polySTING indicates stronger CD8$^+$ T cell priming. The increase in CD103$^+$ DCs in the TDLN of polySTING-treated animals compared to control animals is in line with a report showing CD103$^+$ DCs passing tumor antigen to CTL-priming CD8$^+$ DCs via synaptic transfer after migration to TDLNs[58]. CD103$^+$ DCs are also potent activators of naive CD8$^+$ T-cells through cross-presentation, complementing this effect[59]. Thus, a more complete image of polySTING's proposed mechanism of action emerges (**Figure 5c**): DC-targeted polySTING activates the STING pathway in DCs and results in type I IFN production[6]. Type I IFNs activate DCs and induce the survival and proliferation of CD8$^+$ DCs[56]. Tumor antigens travel to the TDLNs either by themselves or transported by migratory DCs[60]. Migratory CD103$^+$ DCs uptake and transport tumor antigen to the TDLNs for cross-presentation through either self or antigen transfer to CD8$^+$ DCs, both resulting in effective T cell priming. Activated T cells travel to the tumor through the vasculature and type I IFNs promote T cell infiltration in the TME[61]. The strong cytotoxic CD8$^+$ T cell response results in a strong anti-tumor effect. More antigens are generated and transported to the TDLNs to further activate DCs and T cells, perpetuating the cancer-immunity cycle[7].

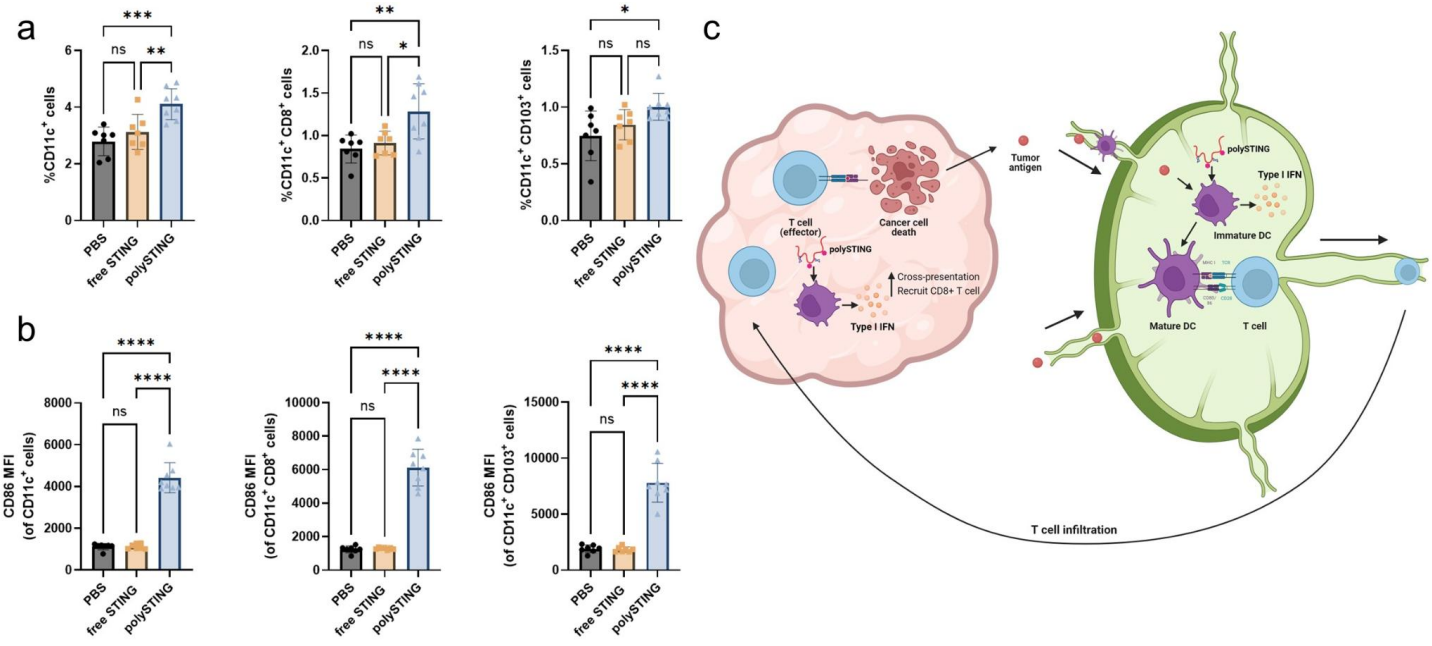

Figure 5. PolySTING induces DC proliferation and maturation in the TDLN. (a) Percentage of total DCs, CD8$^+$ DCs and CD103$^+$ DCs in the TDLN by flow cytometry (N=7-8). (b) CD86 expression on total DCs, CD8$^+$ DCs and CD103$^+$ DCs in the TDLN by flow cytometry (N=7-8). (c) Schematic of polySTING mechanisms in tumor and TDLN. Data are represented as mean ± SD. Statistical analysis was performed using one-way ANOVA with post-hoc Tukey HSD test (*p ≤ 0.05, **p ≤ 0.01, ***p ≤ 0.001, ****p ≤ 0.0001, ns: not significant). Figure 5c generated with BioRender.com.

To further demonstrate the utility of polySTING, we evaluated efficacy in another solid tumor type in a different mouse strain. We chose the 4T1 orthotopic breast cancer model in BALB/c mice also for its low immunogenicity and late-stage aggressiveness[45]. In addition, 4T1's resistance to checkpoint blockade therapy in our experience and polySTING's strong induction of PD-1^{+} CD8^{+} T cells makes it a good candidate to test for synergy with anti-PD-1. We also observed tumor growth inhibition and survival benefits with systemic polySTING treatment in this model, with similar weight loss (**Figure S23**) albeit to a more modest therapeutic effect (**Figure 6**). Consistent with our previous data, the free-form STING agonist did not exert any measurable therapeutic effect. Interestingly, co-therapy with anti-PD-1 did not further inhibit tumor growth nor improve survival.. Activated DCs are known to express PD-L1 that affects response to checkpoint blockade therapy[62,63]. As tumor-activated DCs have been shown to accumulate in solid tumors[64], it is possible that polySTING's DC-centric therapeutic modality generated a tumoral reservoir of DC-associated PD-L1 that outlasts anti-PD-1 antibodies[65] and PD-1-blocked T-cells[32,66]. Conversely, as 4T1 tumors have been reported to express only low levels of PD-L1[67]t, it is possible the tumor model inherently does not benefit from PD-1/PD-L1 immunotherapy. This is consistent with other reports of systemic STING delivery therapy in the 4T1 model showing little to no benefit with anti-PD-1 therapy[21]. Further mechanistic studies in the 4T1 model, as well as therapeutic studies in different tumor models will be necessary to delineate this phenomenon. Regardless, polySTING's efficacy in two different aggressive, non-immunogenic tumor models across two different mouse strains demonstrate its strong utility as a systemic immunotherapy.

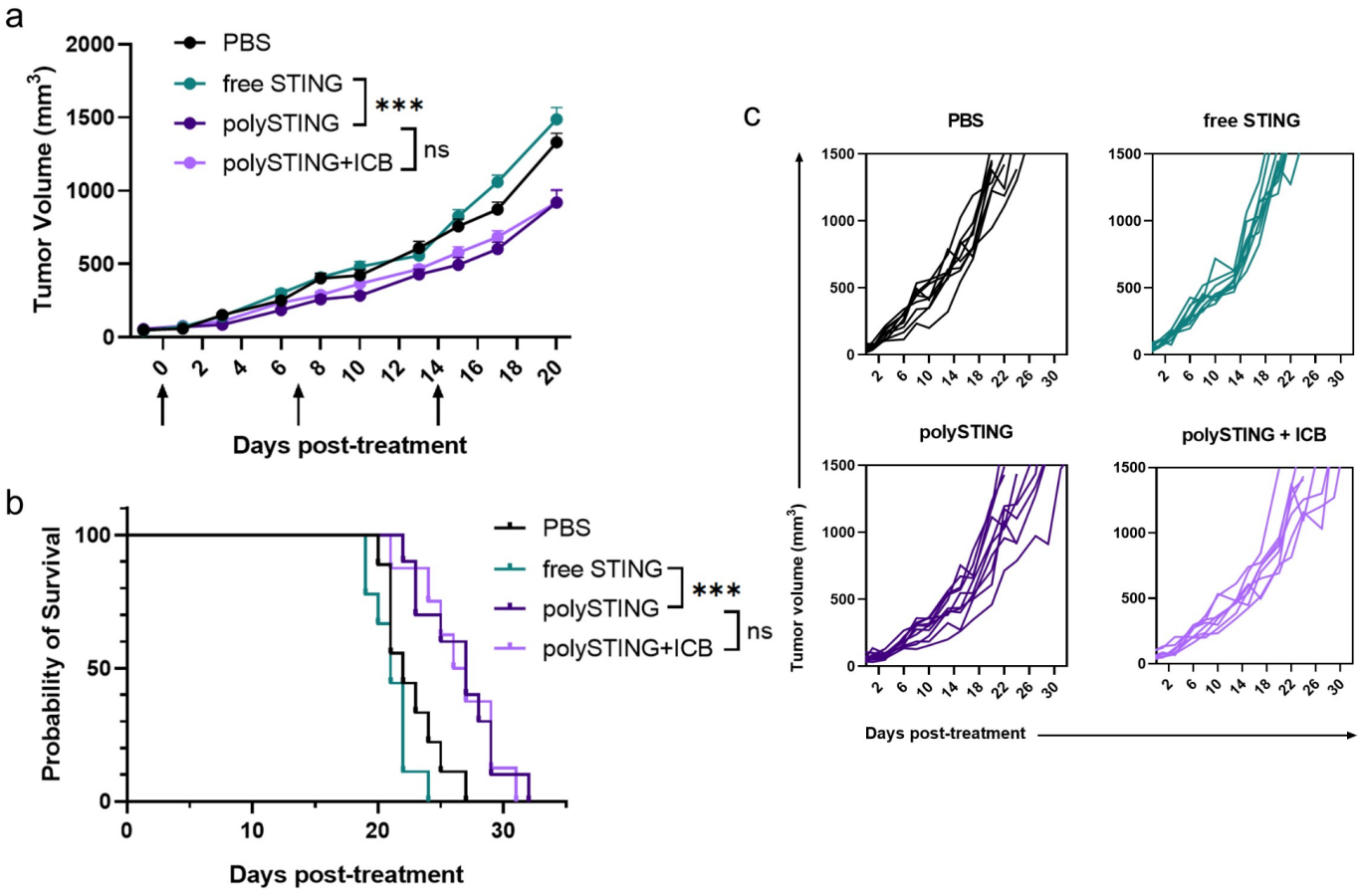

Figure 6. PolySTING shows antitumor efficacy in the 4T1 model. (a) Tumor growth curve in 4T1 tumor-bearing BALB/c mice. 4T1 cells were inoculated on day -8, and STING treatments were given on days 0, 7 and 14. ICB was given on days 1, 8 and 15. Data are represented as mean ± SEM (N = 8-10). Statistical analysis was performed using mixed-effects analysis of two-way ANOVA with Tukey's multiple comparisons test (*** $p \leq 0.001$, ns: no significance, on day 20). (b)

Kaplan-Meier survival curve (N=8-10). Survival analysis was performed using the log-rank test (*** $p \leq 0.001$, ns: no significance). (c) Individual growth curves.

iv. Conclusions

We have developed a novel polymeric platform, polySTING, to deliver STING agonists to DCs through systemic administration. PolySTING was primarily taken up by professional APCs, including DCs, in the TME and resulted in systemic STING activity. PolySTING drove a strong DC-directed immune response through DC activation in the TDLN and induction of cross-presenting $CD8^+$ DCs in both the TDLN and TME. We observed significant therapeutic efficacy in two distinct aggressive non-immunogenic tumor models with a good safety profile as an intravenous immunotherapy. PolySTING is a novel platform for cancer immunotherapy and highlights the potential of targeted STING delivery to DCs.

v. Acknowledgements

K.S. and D.C.N. contributed equally to this work. This work was supported by the U.S. National Institutes of Health, National Cancer Institute Grant R01CA257563 (S.H.P. and P.S.S.), and the U.S. National Institutes of Health National Institute of Allergy & Infectious Diseases Grant R01AI134729 (P.S.S.). NMR data from this work was also supported by the U.S. National Institutes of Health Grant S10 OD030224-01A1, which funded the NEO 500 instrument used. We thank Prof. Hao Yuan Kueh for providing anti-TCF-1 and anti-PD-1 antibodies.

vi. References

(1) Mellman, I.; Coukos, G.; Dranoff, G. Cancer Immunotherapy Comes of Age. *Nature* **2011**, *480* (7378), 480–489. https://doi.org/10.1038/nature10673.
(2) Robert, C. A Decade of Immune-Checkpoint Inhibitors in Cancer Therapy. *Nat. Commun.* **2020**, *11* (1), 3801. https://doi.org/10.1038/s41467-020-17670-y.
(3) Hong, M.; Clubb, J. D.; Chen, Y. Y. Engineering CAR-T Cells for Next-Generation Cancer Therapy. *Cancer Cell* **2020**, *38* (4), 473–488. https://doi.org/10.1016/j.ccell.2020.07.005.
(4) Demaria, O.; Cornen, S.; Daëron, M.; Morel, Y.; Medzhitov, R.; Vivier, E. Harnessing Innate Immunity in Cancer Therapy. *Nature* **2019**, *574* (7776), 45–56. https://doi.org/10.1038/s41586-019-1593-5.
(5) Chen, Q.; Sun, L.; Chen, Z. J. Regulation and Function of the cGAS–STING Pathway of Cytosolic DNA Sensing. *Nat. Immunol.* **2016**, *17* (10), 1142–1149. https://doi.org/10.1038/ni.3558.
(6) Zhu, Y.; An, X.; Zhang, X.; Qiao, Y.; Zheng, T.; Li, X. STING: A Master Regulator in the Cancer-Immunity Cycle. *Mol. Cancer* **2019**, *18* (1), 1–15. https://doi.org/10.1186/s12943-019-1087-y.
(7) Chen, D. S.; Mellman, I. Oncology Meets Immunology: The Cancer-Immunity Cycle. *Immunity* **2013**, *39* (1), 1–10. https://doi.org/10.1016/j.immuni.2013.07.012.
(8) Hines, J. B.; Kacew, A. J.; Sweis, R. F. The Development of STING Agonists and Emerging Results as a Cancer Immunotherapy. *Curr. Oncol. Rep.* **2023**, *25* (3), 189–199. https://doi.org/10.1007/s11912-023-01361-0.
(9) Petrovic, M.; Borchard, G.; Jordan, O. Considerations for the Delivery of STING Ligands in Cancer Immunotherapy. *J. Controlled Release* **2021**, *339*, 235–247. https://doi.org/10.1016/j.jconrel.2021.09.033.
(10) Meric-Bernstam, F.; Sweis, R. F.; Hodi, F. S.; Messersmith, W. A.; Andtbacka, R. H. I.; Ingham, M.; Lewis, N.; Chen, X.; Pelletier, M.; Chen, X.; et al. Phase I Dose-Escalation Trial of MIW815 (ADU-S100), an Intratumoral STING Agonist, in Patients with Advanced/Metastatic Solid Tumors or Lymphomas. *Clin. Cancer Res.* **2022**, *28* (4),

677–688. https://doi.org/10.1158/1078-0432.CCR-21-1963.
(11) Ramanjulu, J. M.; Pesiridis, G. S.; Yang, J.; Concha, N.; Singhaus, R.; Zhang, S.-Y.; Tran, J.-L.; Moore, P.; Lehmann, S.; Eberl, H. C.; et al. Design of Amidobenzimidazole STING Receptor Agonists with Systemic Activity. *Nature* **2018**, *564* (7736), 439–443. https://doi.org/10.1038/s41586-018-0705-y.
(12) Pan, B.-S.; Perera, S. A.; Piesvaux, J. A.; Presland, J. P.; Schroeder, G. K.; Cumming, J. N.; Trotter, B. W.; Altman, M. D.; Buevich, A. V.; Cash, B.; et al. An Orally Available Non-Nucleotide STING Agonist with Antitumor Activity. *Science* **2020**, *369* (6506). https://doi.org/10.1126/science.aba6098.
(13) Chin, E. N.; Yu, C.; Vartabedian, V. F.; Jia, Y.; Kumar, M.; Gamo, A. M.; Vernier, W.; Ali, S. H.; Kissai, M.; Lazar, D. C.; et al. Antitumor Activity of a Systemic STING-Activating Non-Nucleotide cGAMP Mimetic. *Science* **2020**, *369* (6506), 993–999. https://doi.org/10.1126/science.abb4255.
(14) Garland, K. M.; Sheehy, T. L.; Wilson, J. T. Chemical and Biomolecular Strategies for STING Pathway Activation in Cancer Immunotherapy. *Chem. Rev.* **2022**, *122* (6), 5977–6039. https://doi.org/10.1021/acs.chemrev.1c00750.
(15) Dane, E. L.; Belessiotis-Richards, A.; Backlund, C.; Wang, J.; Hidaka, K.; Milling, L. E.; Bhagchandani, S.; Melo, M. B.; Wu, S.; Li, N.; et al. STING Agonist Delivery by Tumour-Penetrating PEG-Lipid Nanodiscs Primes Robust Anticancer Immunity. *Nat. Mater.* **2022**, *21* (6), 710–720. https://doi.org/10.1038/s41563-022-01251-z.
(16) Wehbe, M.; Wang-Bishop, L.; Becker, K. W.; Shae, D.; Baljon, J. J.; He, X.; Christov, P.; Boyd, K. L.; Balko, J. M.; Wilson, J. T. Nanoparticle Delivery Improves the Pharmacokinetic Properties of Cyclic Dinucleotide STING Agonists to Open a Therapeutic Window for Intravenous Administration. *J. Controlled Release* **2021**, *330*, 1118–1129. https://doi.org/10.1016/j.jconrel.2020.11.017.
(17) Wang-Bishop, L.; Kimmel, B. R.; Ngwa, V. M.; Madden, M. Z.; Baljon, J. J.; Florian, D. C.; Hanna, A.; Pastora, L. E.; Sheehy, T. L.; Kwiatkowski, A. J.; et al. STING-Activating Nanoparticles Normalize the Vascular-Immune Interface to Potentiate Cancer Immunotherapy. *Sci. Immunol.* **2023**, *8* (83), eadd1153. https://doi.org/10.1126/sciimmunol.add1153.
(18) Go, E.-J.; Yang, H.; Park, W.; Lee, S. J.; Han, J.-H.; Kong, S. J.; Lee, W. S.; Han, D. K.; Chon, H. J.; Kim, C. Systemic Delivery of a STING Agonist-Loaded Positively Charged Liposome Selectively Targets Tumor Immune Microenvironment and Suppresses Tumor Angiogenesis. *Small n/a* (n/a), 2300544. https://doi.org/10.1002/smll.202300544.
(19) Chen, X.; Meng, F.; Xu, Y.; Li, T.; Chen, X.; Wang, H. Chemically Programmed STING-Activating Nano-Liposomal Vesicles Improve Anticancer Immunity. *Nat. Commun.* **2023**, *14* (1), 4584. https://doi.org/10.1038/s41467-023-40312-y.
(20) Sun, X.; Zhang, Y.; Li, J.; Park, K. S.; Han, K.; Zhou, X.; Xu, Y.; Nam, J.; Xu, J.; Shi, X.; et al. Amplifying STING Activation by Cyclic Dinucleotide–Manganese Particles for Local and Systemic Cancer Metalloimmunotherapy. *Nat. Nanotechnol.* **2021**, 1–11. https://doi.org/10.1038/s41565-021-00962-9.
(21) Dosta, P.; Cryer, A. M.; Dion, M. Z.; Shiraishi, T.; Langston, S. P.; Lok, D.; Wang, J.; Harrison, S.; Hatten, T.; Ganno, M. L.; et al. Investigation of the Enhanced Antitumour Potency of STING Agonist after Conjugation to Polymer Nanoparticles. *Nat. Nanotechnol.* **2023**, 1–13. https://doi.org/10.1038/s41565-023-01447-7.
(22) Wu, Y.; Fang, Y.; Wei, Q.; Shi, H.; Tan, H.; Deng, Y.; Zeng, Z.; Qiu, J.; Chen, C.; Sun, L.; et al. Tumor-Targeted Delivery of a STING Agonist Improves Cancer Immunotherapy. *Proc. Natl. Acad. Sci.* **2022**, *119* (49), e2214278119. https://doi.org/10.1073/pnas.2214278119.
(23) Gordon, M. R.; Canakci, M.; Li, L.; Zhuang, J.; Osborne, B.; Thayumanavan, S. Field Guide to Challenges and Opportunities in Antibody–Drug Conjugates for Chemists. *Bioconjug. Chem.* **2015**, *26* (11), 2198–2215. https://doi.org/10.1021/acs.bioconjchem.5b00399.
(24) Lemos, H.; Mohamed, E.; Huang, L.; Ou, R.; Pacholczyk, G.; Arbab, A. S.; Munn, D.; Mellor, A. L. STING Promotes the Growth of Tumors Characterized by Low Antigenicity via IDO Activation. *Cancer Res.* **2016**, *76* (8), 2076–2081. https://doi.org/10.1158/0008-5472.CAN-15-1456.
(25) Sokolowska, O.; Nowis, D. STING Signaling in Cancer Cells: Important or Not? *Arch. Immunol. Ther. Exp. (Warsz.)* **2018**, *66* (2), 125–132. https://doi.org/10.1007/s00005-017-0481-7.
(26) Sivick, K. E.; Desbien, A. L.; Glickman, L. H.; Reiner, G. L.; Corrales, L.; Surh, N. H.; Hudson, T. E.; Vu, U. T.; Francica, B. J.; Banda, T.; et al. Magnitude of Therapeutic STING Activation Determines CD8+ T Cell-Mediated Anti-Tumor Immunity. *Cell Rep.* **2018**, *25* (11), 3074-3085.e5. https://doi.org/10.1016/j.celrep.2018.11.047.
(27) Jneid, B.; Bochnakian, A.; Hoffmann, C.; Delisle, F.; Djacoto, E.; Sirven, P.; Denizeau, J.; Sedlik, C.; Gerber-Ferder, Y.; Fiore, F.; et al. Selective STING Stimulation in Dendritic Cells Primes Antitumor T Cell Responses. *Sci. Immunol.* **2023**, *8* (79), eabn6612. https://doi.org/10.1126/sciimmunol.abn6612.
(28) Theisen, D. J.; Ferris, S. T.; Briseño, C. G.; Kretzer, N.; Iwata, A.; Murphy, K. M.; Murphy, T. L. Batf3-Dependent Genes Control Tumor Rejection Induced by Dendritic Cells Independently of Cross-Presentation. *Cancer Immunol. Res.* **2019**, *7* (1), 29–39. https://doi.org/10.1158/2326-6066.CIR-18-0138.

(29) Hildner, K.; Edelson, B. T.; Purtha, W. E.; Diamond, M.; Matsushita, H.; Kohyama, M.; Calderon, B.; Schraml, B. U.; Unanue, E. R.; Diamond, M. S.; et al. Batf3 Deficiency Reveals a Critical Role for CD8α+ Dendritic Cells in Cytotoxic T Cell Immunity. *Science* **2008**, *322* (5904), 1097–1100. https://doi.org/10.1126/science.1164206.
(30) Spranger, S.; Dai, D.; Horton, B.; Gajewski, T. F. Tumor-Residing Batf3 Dendritic Cells Are Required for Effector T Cell Trafficking and Adoptive T Cell Therapy. *Cancer Cell* **2017**, *31* (5), 711-723.e4. https://doi.org/10.1016/j.ccell.2017.04.003.
(31) Sánchez-Paulete, A. R.; Cueto, F. J.; Martínez-López, M.; Labiano, S.; Morales-Kastresana, A.; Rodríguez-Ruiz, M. E.; Jure-Kunkel, M.; Azpilikueta, A.; Aznar, M. A.; Quetglas, J. I.; et al. Cancer Immunotherapy with Immunomodulatory Anti-CD137 and Anti–PD-1 Monoclonal Antibodies Requires BATF3-Dependent Dendritic Cells. *Cancer Discov.* **2016**, *6* (1), 71–79. https://doi.org/10.1158/2159-8290.CD-15-0510.
(32) Mellman, I.; Chen, D. S.; Powles, T.; Turley, S. J. The Cancer-Immunity Cycle: Indication, Genotype, and Immunotype. *Immunity* **2023**, *56* (10), 2188–2205. https://doi.org/10.1016/j.immuni.2023.09.011.
(33) Thim-Uam, A.; Prabakaran, T.; Tansakul, M.; Makjaroen, J.; Wongkongkathep, P.; Chantaravisoot, N.; Saethang, T.; Leelahavanichkul, A.; Benjachat, T.; Paludan, S.; et al. STING Mediates Lupus via the Activation of Conventional Dendritic Cell Maturation and Plasmacytoid Dendritic Cell Differentiation. *iScience* **2020**, *23* (9), 101530. https://doi.org/10.1016/j.isci.2020.101530.
(34) Doshi, A. S.; Cantin, S.; Prickett, L. B.; Mele, D. A.; Amiji, M. Systemic Nano-Delivery of Low-Dose STING Agonist Targeted to CD103+ Dendritic Cells for Cancer Immunotherapy. *J. Controlled Release* **2022**, *345*, 721–733. https://doi.org/10.1016/j.jconrel.2022.03.054.
(35) Lv, S.; Song, K.; Yen, A.; Peeler, D. J.; Nguyen, D. C.; Olshefsky, A.; Sylvestre, M.; Srinivasan, S.; Stayton, P. S.; Pun, S. H. Well-Defined Mannosylated Polymer for Peptide Vaccine Delivery with Enhanced Antitumor Immunity. *Adv. Healthc. Mater.* **2022**, *11* (9), 2101651. https://doi.org/10.1002/adhm.202101651.
(36) Su, F.-Y.; Srinivasan, S.; Lee, B.; Chen, J.; Convertine, A. J.; West, T. E.; Ratner, D. M.; Skerrett, S. J.; Stayton, P. S. Macrophage-Targeted Drugamers with Enzyme-Cleavable Linkers Deliver High Intracellular Drug Dosing and Sustained Drug Pharmacokinetics against Alveolar Pulmonary Infections. *J. Controlled Release* **2018**, *287*, 1–11. https://doi.org/10.1016/j.jconrel.2018.08.014.
(37) Li, S.; Omi, M.; Cartieri, F.; Konkolewicz, D.; Mao, G.; Gao, H.; Averick, S. E.; Mishina, Y.; Matyjaszewski, K. Cationic Hyperbranched Polymers with Biocompatible Shells for siRNA Delivery. *Biomacromolecules* **2018**, *19* (9), 3754–3765. https://doi.org/10.1021/acs.biomac.8b00902.
(38) Tiberghien, A. C.; Levy, J.-N.; Masterson, L. A.; Patel, N. V.; Adams, L. R.; Corbett, S.; Williams, D. G.; Hartley, J. A.; Howard, P. W. Design and Synthesis of Tesirine, a Clinical Antibody–Drug Conjugate Pyrrolobenzodiazepine Dimer Payload. *ACS Med. Chem. Lett.* **2016**, *7* (11), 983–987. https://doi.org/10.1021/acsmedchemlett.6b00062.
(39) Christofides, A.; Strauss, L.; Yeo, A.; Cao, C.; Charest, A.; Boussiotis, V. A. The Complex Role of Tumor-Infiltrating Macrophages. *Nat. Immunol.* **2022**, *23* (8), 1148–1156. https://doi.org/10.1038/s41590-022-01267-2.
(40) Marciscano, A. E.; Anandasabapathy, N. The Role of Dendritic Cells in Cancer and Anti-Tumor Immunity. *Semin. Immunol.* **2021**, *52*, 101481. https://doi.org/10.1016/j.smim.2021.101481.
(41) Pokatayev, V.; Yang, K.; Tu, X.; Dobbs, N.; Wu, J.; Kalb, R. G.; Yan, N. Homeostatic Regulation of STING Protein at the Resting State by Stabilizer TOLLIP. *Nat. Immunol.* **2020**, *21* (2), 158–167. https://doi.org/10.1038/s41590-019-0569-9.
(42) Wang-Bishop, L.; Wehbe, M.; Shae, D.; James, J.; Hacker, B. C.; Garland, K.; Chistov, P. P.; Rafat, M.; Balko, J. M.; Wilson, J. T. Potent STING Activation Stimulates Immunogenic Cell Death to Enhance Antitumor Immunity in Neuroblastoma. *J. Immunother. Cancer* **2020**, *8* (1), e000282. https://doi.org/10.1136/jitc-2019-000282.
(43) Ohkuri, T.; Kosaka, A.; Ishibashi, K.; Kumai, T.; Hirata, Y.; Ohara, K.; Nagato, T.; Oikawa, K.; Aoki, N.; Harabuchi, Y.; et al. Intratumoral Administration of cGAMP Transiently Accumulates Potent Macrophages for Anti-Tumor Immunity at a Mouse Tumor Site. *Cancer Immunol. Immunother.* **2017**, *66* (6), 705–716. https://doi.org/10.1007/s00262-017-1975-1.
(44) Downey, C. M.; Aghaei, M.; Schwendener, R. A.; Jirik, F. R. DMXAA Causes Tumor Site-Specific Vascular Disruption in Murine Non-Small Cell Lung Cancer, and like the Endogenous Non-Canonical Cyclic Dinucleotide STING Agonist, 2′3′-cGAMP, Induces M2 Macrophage Repolarization. *PLOS ONE* **2014**, *9* (6), e99988. https://doi.org/10.1371/journal.pone.0099988.
(45) Lechner, M. G.; Karimi, S. S.; Barry-Holson, K.; Angell, T. E.; Murphy, K. A.; Church, C. H.; Ohlfest, J. R.; Hu, P.; Epstein, A. L. Immunogenicity of Murine Solid Tumor Models as a Defining Feature of in Vivo Behavior and Response to Immunotherapy. *J. Immunother. Hagerstown Md 1997* **2013**, *36* (9), 477–489. https://doi.org/10.1097/01.cji.0000436722.46675.4a.
(46) Chen, D. S.; Mellman, I. Elements of Cancer Immunity and the Cancer–Immune Set Point. *Nature* **2017**, *541* (7637), 321–330. https://doi.org/10.1038/nature21349.

(47) Xia, A.; Zhang, Y.; Xu, J.; Yin, T.; Lu, X.-J. T Cell Dysfunction in Cancer Immunity and Immunotherapy. *Front. Immunol.* **2019**, *10*.
(48) Roberts, E. W.; Broz, M. L.; Binnewies, M.; Headley, M. B.; Nelson, A. E.; Wolf, D. M.; Kaisho, T.; Bogunovic, D.; Bhardwaj, N.; Krummel, M. F. Critical Role for CD103+/CD141+ Dendritic Cells Bearing CCR7 for Tumor Antigen Trafficking and Priming of T Cell Immunity in Melanoma. *Cancer Cell* **2016**, *30* (2), 324–336. https://doi.org/10.1016/j.ccell.2016.06.003.
(49) den Haan, J. M. M.; Lehar, S. M.; Bevan, M. J. Cd8+ but Not Cd8− Dendritic Cells Cross-Prime Cytotoxic T Cells in Vivo. *J. Exp. Med.* **2000**, *192* (12), 1685–1696. https://doi.org/10.1084/jem.192.12.1685.
(50) Liang, Y.; Hannan, R.; Fu, Y.-X. Type I IFN Activating Type I Dendritic Cells for Antitumor Immunity. *Clin. Cancer Res.* **2021**, *27* (14), 3818–3824. https://doi.org/10.1158/1078-0432.CCR-20-2564.
(51) Fuertes, M. B.; Kacha, A. K.; Kline, J.; Woo, S.-R.; Kranz, D. M.; Murphy, K. M.; Gajewski, T. F. Host Type I IFN Signals Are Required for Antitumor CD8+ T Cell Responses through CD8α+ Dendritic Cells. *J. Exp. Med.* **2011**, *208* (10), 2005–2016. https://doi.org/10.1084/jem.20101159.
(52) Inozume, T.; Hanada, K.; Wang, Q. J.; Ahmadzadeh, M.; Wunderlich, J. R.; Rosenberg, S. A.; Yang, J. C. Selection of CD8+PD-1+ Lymphocytes in Fresh Human Melanomas Enriches for Tumor-Reactive T-Cells. *J. Immunother. Hagerstown Md 1997* **2010**, *33* (9), 956–964. https://doi.org/10.1097/CJI.0b013e3181fad2b0.
(53) Wen, S.; Lu, H.; Wang, D.; Guo, J.; Dai, W.; Wang, Z. TCF-1 Maintains CD8+ T Cell Stemness in Tumor Microenvironment. *J. Leukoc. Biol.* **2021**, *110* (3), 585–590. https://doi.org/10.1002/JLB.5MR1120-778R.
(54) Im, S. J.; Hashimoto, M.; Gerner, M. Y.; Lee, J.; Kissick, H. T.; Burger, M. C.; Shan, Q.; Hale, J. S.; Lee, J.; Nasti, T. H.; et al. Defining CD8+ T Cells That Provide the Proliferative Burst after PD-1 Therapy. *Nature* **2016**, *537* (7620), 417–421. https://doi.org/10.1038/nature19330.
(55) Jubel, J. M.; Barbati, Z. R.; Burger, C.; Wirtz, D. C.; Schildberg, F. A. The Role of PD-1 in Acute and Chronic Infection. *Front. Immunol.* **2020**, *11*.
(56) Li, A.; Yi, M.; Qin, S.; Song, Y.; Chu, Q.; Wu, K. Activating cGAS-STING Pathway for the Optimal Effect of Cancer Immunotherapy. *J. Hematol. Oncol.J Hematol Oncol* **2019**, *12* (1), 35. https://doi.org/10.1186/s13045-019-0721-x.
(57) Del Prete, A.; Salvi, V.; Soriani, A.; Laffranchi, M.; Sozio, F.; Bosisio, D.; Sozzani, S. Dendritic Cell Subsets in Cancer Immunity and Tumor Antigen Sensing. *Cell. Mol. Immunol.* **2023**, *20* (5), 432–447. https://doi.org/10.1038/s41423-023-00990-6.
(58) Ruhland, M. K.; Roberts, E. W.; Cai, E.; Mujal, A. M.; Marchuk, K.; Beppler, C.; Nam, D.; Serwas, N. K.; Binnewies, M.; Krummel, M. F. Visualizing Synaptic Transfer of Tumor Antigens among Dendritic Cells. *Cancer Cell* **2020**, *37* (6), 786-799.e5. https://doi.org/10.1016/j.ccell.2020.05.002.
(59) Broz, M. L.; Binnewies, M.; Boldajipour, B.; Nelson, A. E.; Pollack, J. L.; Erle, D. J.; Barczak, A.; Rosenblum, M. D.; Daud, A.; Barber, D. L.; et al. Dissecting the Tumor Myeloid Compartment Reveals Rare Activating Antigen-Presenting Cells Critical for T Cell Immunity. *Cancer Cell* **2014**, *26* (5), 638–652. https://doi.org/10.1016/j.ccell.2014.09.007.
(60) du Bois, H.; Heim, T. A.; Lund, A. W. Tumor-Draining Lymph Nodes: At the Crossroads of Metastasis and Immunity. *Sci. Immunol.* **2021**, *6* (63), eabg3551. https://doi.org/10.1126/sciimmunol.abg3551.
(61) Boukhaled, G. M.; Harding, S.; Brooks, D. G. Opposing Roles of Type I Interferons in Cancer Immunity. *Annu. Rev. Pathol. Mech. Dis.* **2021**, *16* (1), 167–198. https://doi.org/10.1146/annurev-pathol-031920-093932.
(62) Peng, Q.; Qiu, X.; Zhang, Z.; Zhang, S.; Zhang, Y.; Liang, Y.; Guo, J.; Peng, H.; Chen, M.; Fu, Y.-X.; et al. PD-L1 on Dendritic Cells Attenuates T Cell Activation and Regulates Response to Immune Checkpoint Blockade. *Nat. Commun.* **2020**, *11* (1), 4835. https://doi.org/10.1038/s41467-020-18570-x.
(63) Oh, S. A.; Wu, D.-C.; Cheung, J.; Navarro, A.; Xiong, H.; Cubas, R.; Totpal, K.; Chiu, H.; Wu, Y.; Comps-Agrar, L.; et al. PD-L1 Expression by Dendritic Cells Is a Key Regulator of T-Cell Immunity in Cancer. *Nat. Cancer* **2020**, *1* (7), 681–691. https://doi.org/10.1038/s43018-020-0075-x.
(64) Krzastek, S. C.; Goliadze, E.; Zhou, S.; Petrossian, A.; Youniss, F.; Sundaresan, G.; Wang, L.; Zweit, J.; Guruli, G. Dendritic Cell Trafficking in Tumor-Bearing Mice. *Cancer Immunol. Immunother.* **2018**, *67* (12), 1939–1947. https://doi.org/10.1007/s00262-018-2187-z.
(65) Lindauer, A.; Valiathan, C.; Mehta, K.; Sriram, V.; de Greef, R.; Elassaiss-Schaap, J.; de Alwis, D. Translational Pharmacokinetic/Pharmacodynamic Modeling of Tumor Growth Inhibition Supports Dose-Range Selection of the Anti–PD-1 Antibody Pembrolizumab. *CPT Pharmacomet. Syst. Pharmacol.* **2017**, *6* (1), 11–20. https://doi.org/10.1002/psp4.12130.
(66) Yost, K. E.; Satpathy, A. T.; Wells, D. K.; Qi, Y.; Wang, C.; Kageyama, R.; McNamara, K. L.; Granja, J. M.; Sarin, K. Y.; Brown, R. A.; et al. Clonal Replacement of Tumor-Specific T Cells Following PD-1 Blockade. *Nat. Med.* **2019**, *25* (8), 1251–1259. https://doi.org/10.1038/s41591-019-0522-3.

(67) Sagiv-Barfi, I.; Kohrt, H. E. K.; Czerwinski, D. K.; Ng, P. P.; Chang, B. Y.; Levy, R. Therapeutic Antitumor Immunity by Checkpoint Blockade Is Enhanced by Ibrutinib, an Inhibitor of Both BTK and ITK. *Proc. Natl. Acad. Sci. U. S. A.* **2015**, *112* (9), E966–E972. https://doi.org/10.1073/pnas.1500712112.

vii. Supporting Information

	Measured Concentration	
Sample Type (unit)	**Free STING/diABZI**	**PolySTING**
Plasma (ng/mL)	**1.57**	**130.41**
Tumor (ng/g)	**103.15**	**2978.72**

Table S1. LC/MS-MS based pharmacokinetic characterization of polySTING and free STING agonist 30 minutes after intravenous administration.

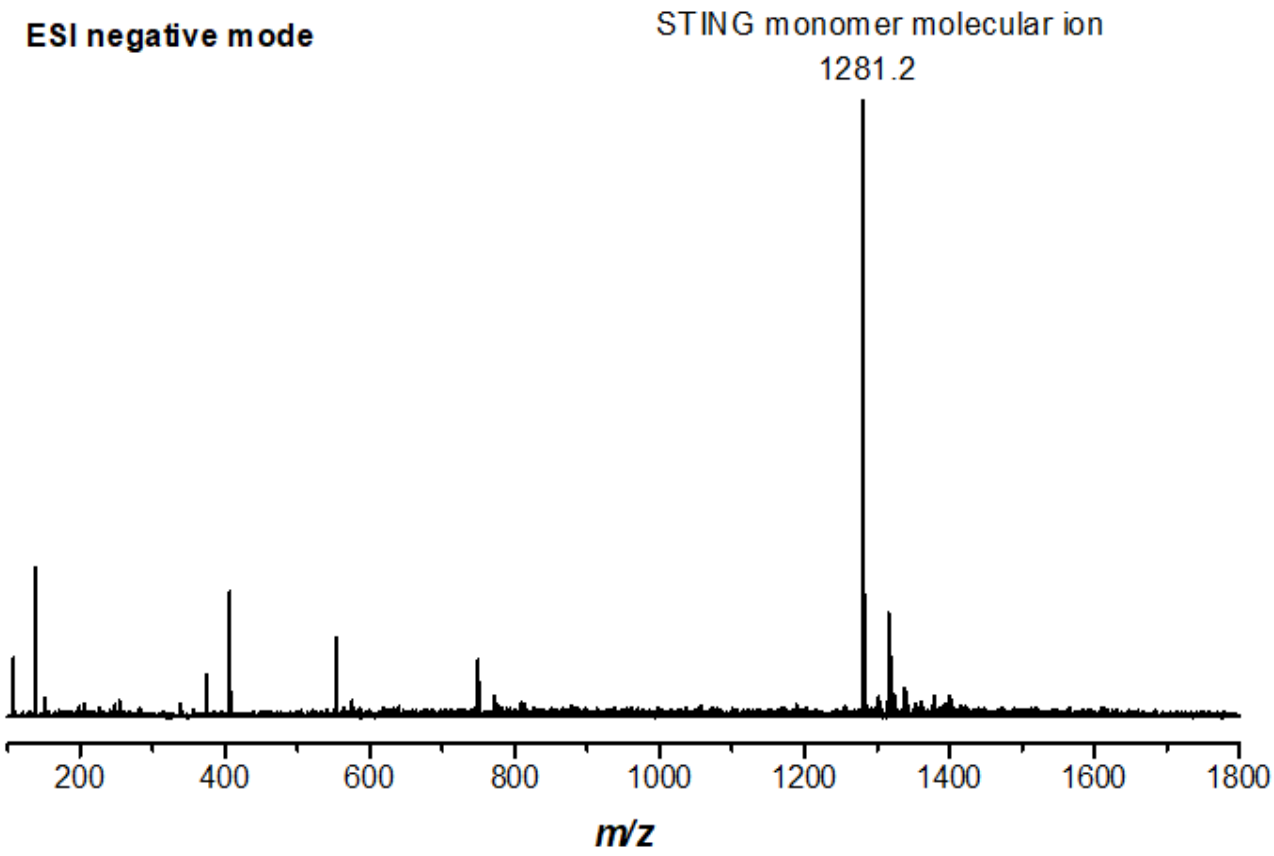

Figure S1. Mass spectrum of SVA-PAB-STING (Compound 6) in methanol.

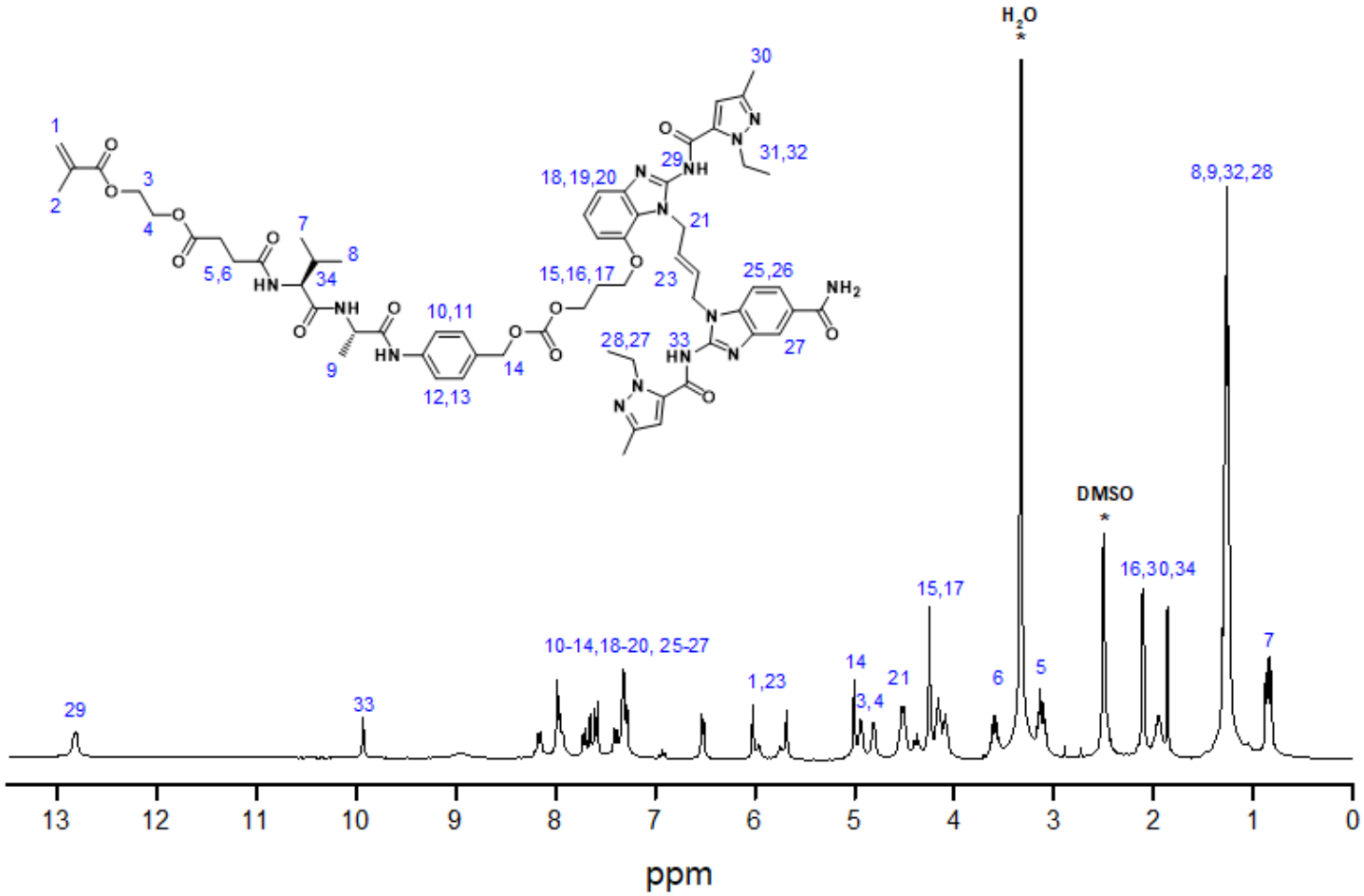

Figure S2. [1]H-NMR spectrum of SVA-PAB-STING (Compound 6) in DMSO-d6.

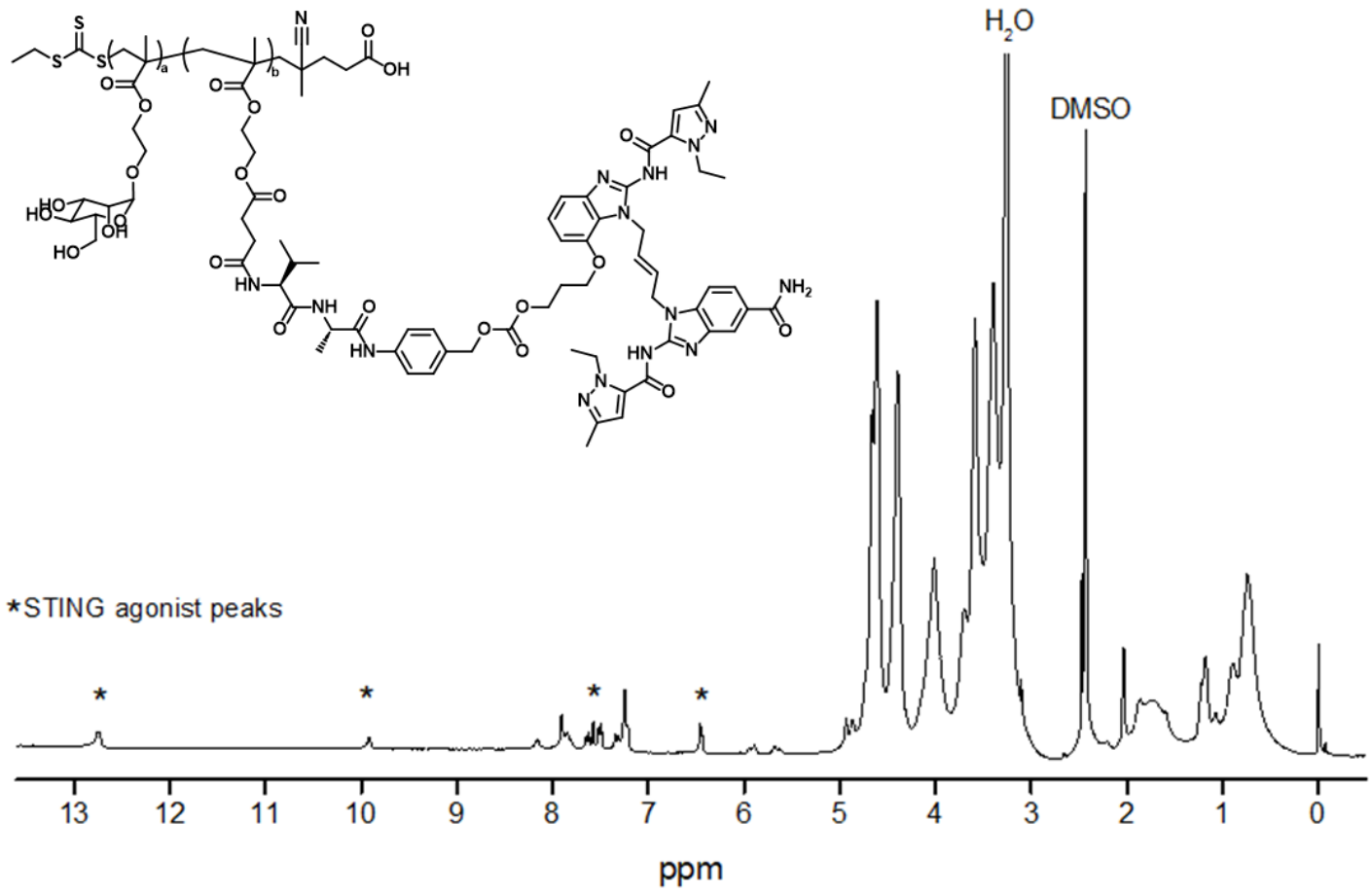

Figure S3. [1]H-NMR spectrum of polySTING in DMSO-d6.

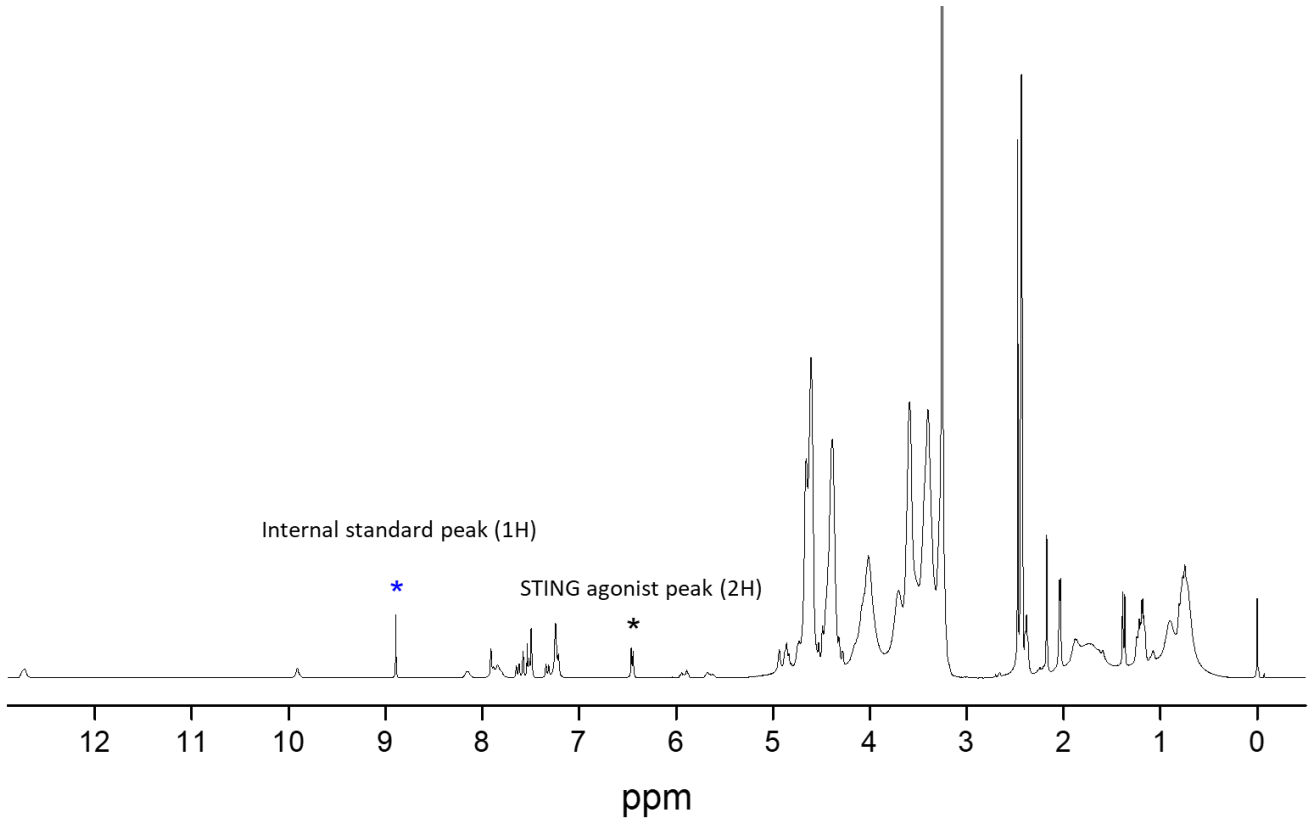

Figure S4. [1]H-NMR spectrum of polySTING and levofloxacin internal standard.

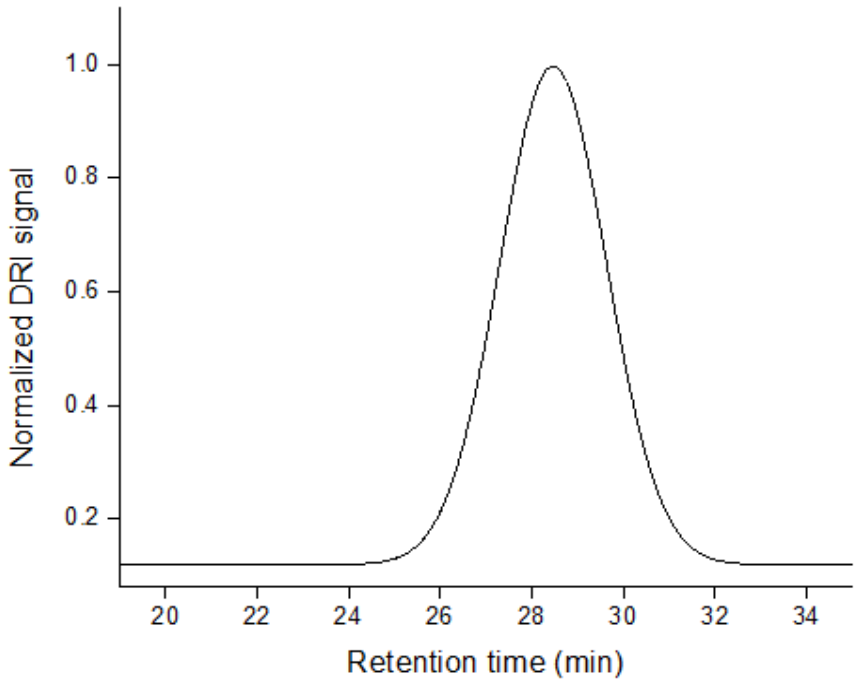

Figure S5. GPC spectrum of polySTING in supplemented DMF (1 g/L LiBr).

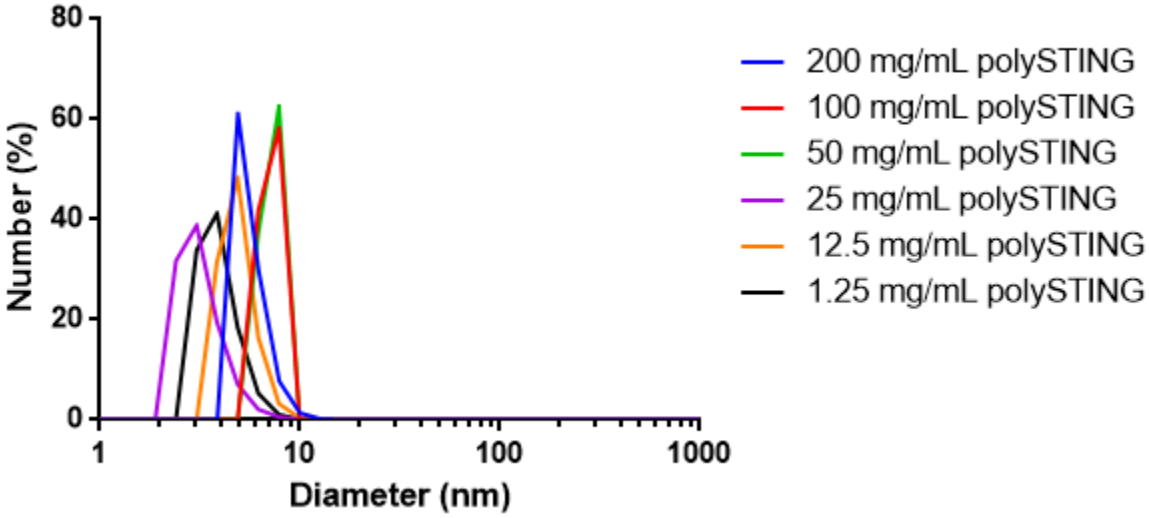

Figure S6. DLS characterization of polySTING in PBS at different concentrations.

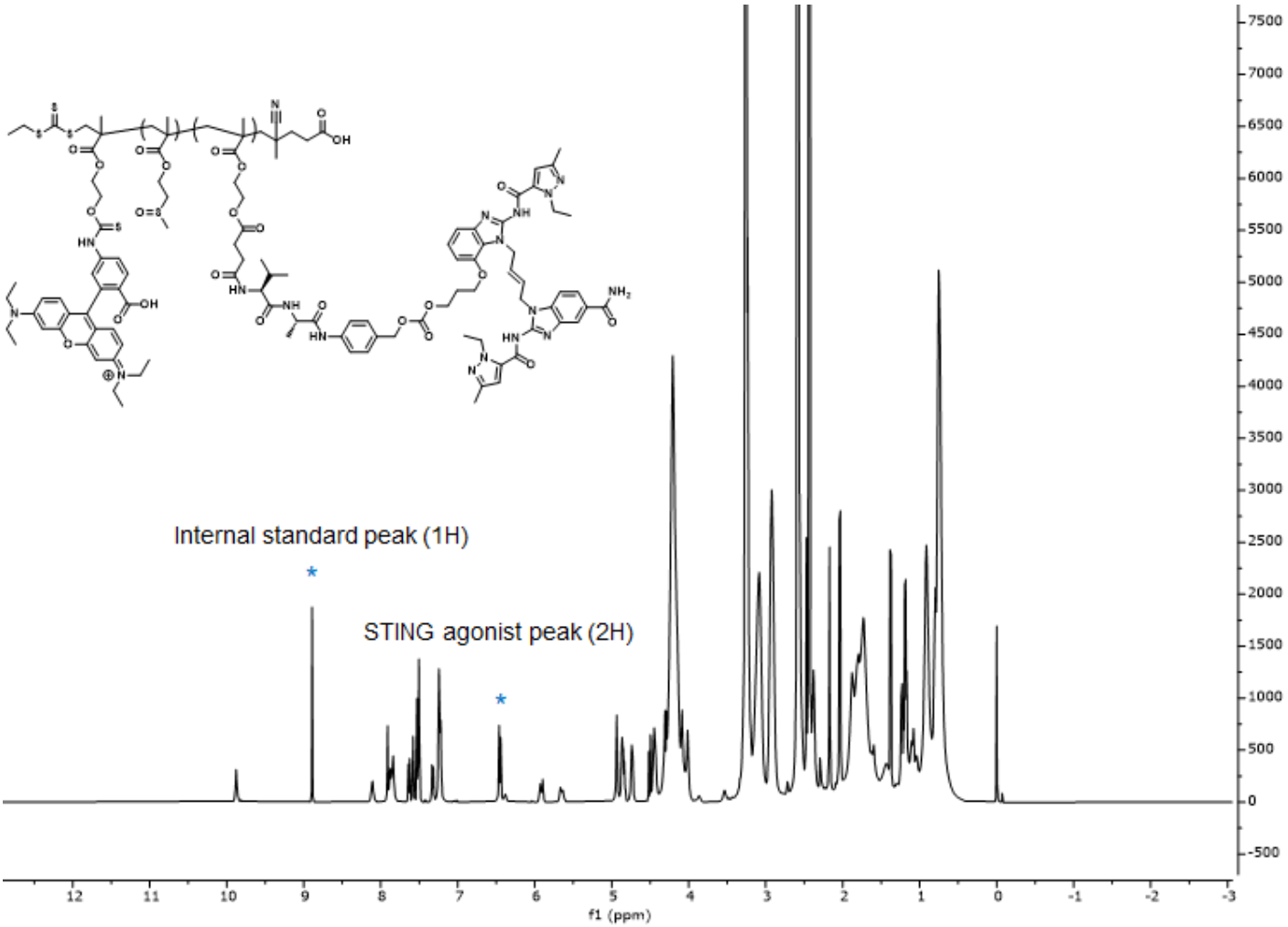

Figure S7. 1H-NMR of MSEMA-STING-Rh in DMSO-d6 with levofloxacin internal standard.

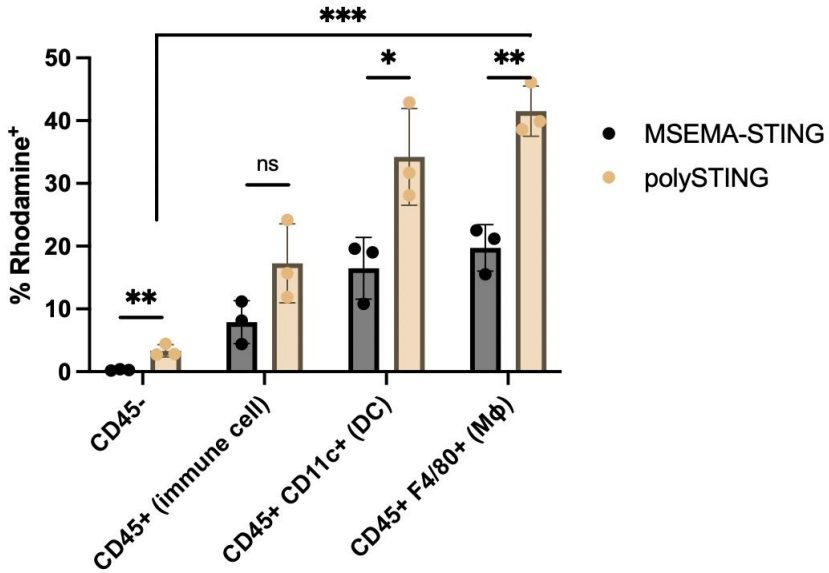

Figure S8. Rhodamine-labeled polySTING and MSEMA-STING uptake in B16F10 tumors 4 h post tail vein injection. Unpaired t-test was used to compare polySTING and MSEMA-STING under different cell subsets. One-way ANOVA

with post-hoc Tukey's test was used to polySTING uptake in different cell types. (*p ≤ 0.05, **p ≤ 0.01, ***p ≤ 0.001, ns: not significant).

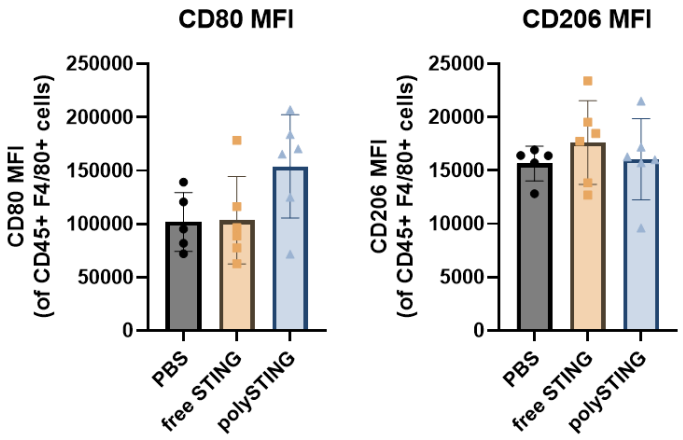

Figure S9. *In vivo* tumor-associated macrophage polarization.

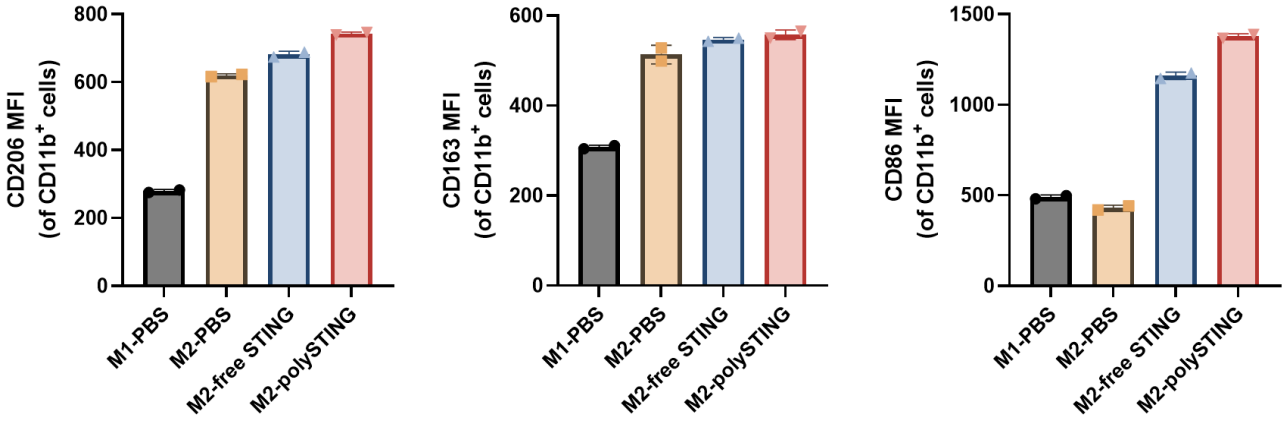

Figure S10. *In vitro* bone marrow-derived macrophage (BMDM) polarization via flow cytometry.

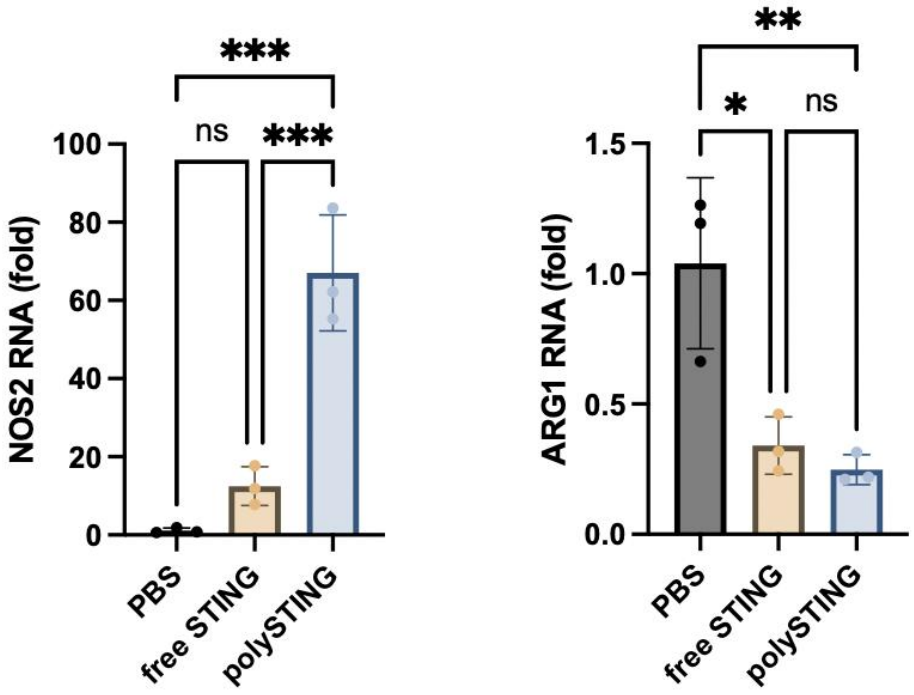

Figure S11. RT-qPCR of BMDM polarization genes in vitro.

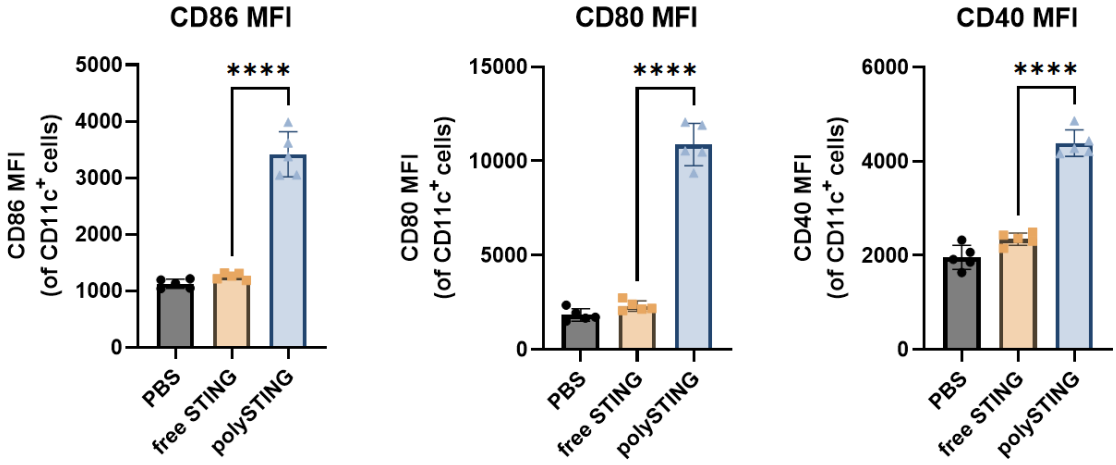

Figure S12. *In vivo* DC maturation in TDLNs

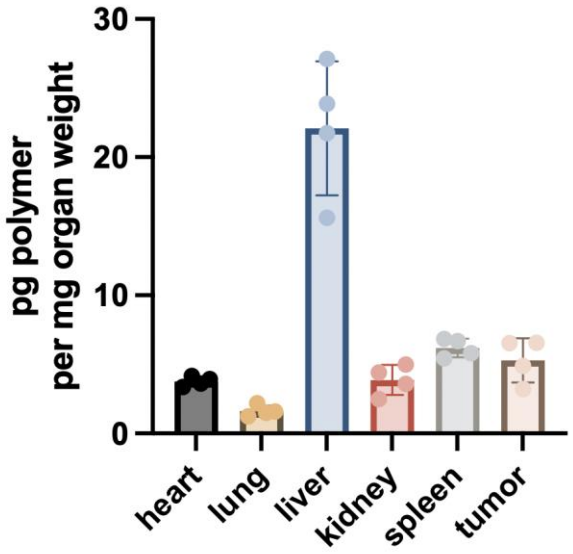

Figure S13. Systemic biodistribution of polySTING-Rh as measured by organ homogenate fluorescence, calibrated against polySTING-Rh-spiked naive homogenate.

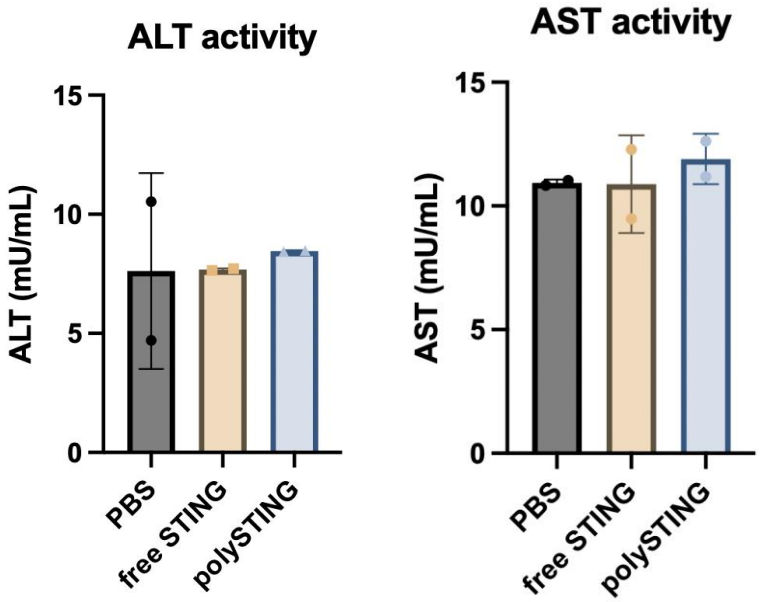

Figure S14. Liver toxicity assay of polySTING, as measured by serum alanine aminotransferase (ALT) and aspartate aminotransferase (AST) levels.

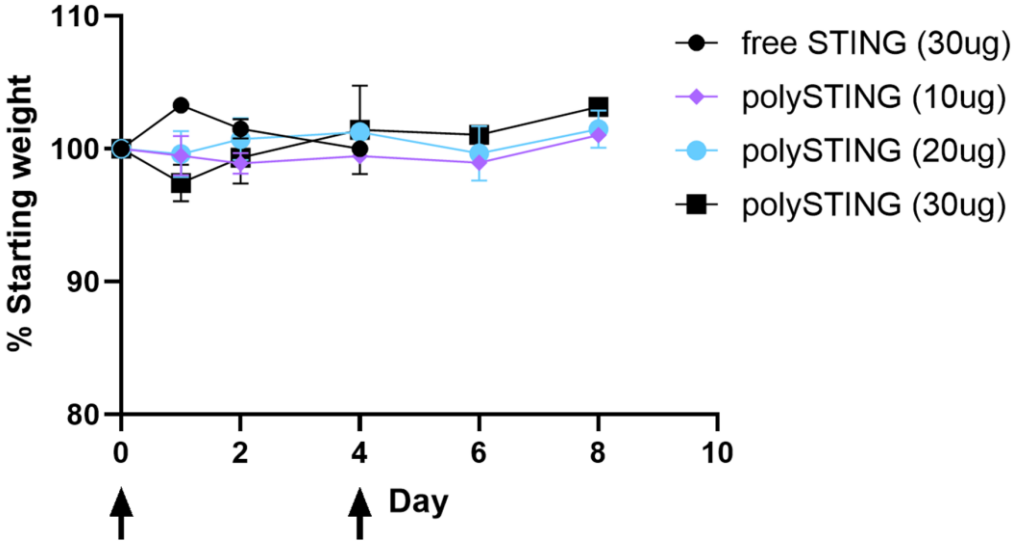

Figure S15. Weight loss in non-tumor bearing mice.

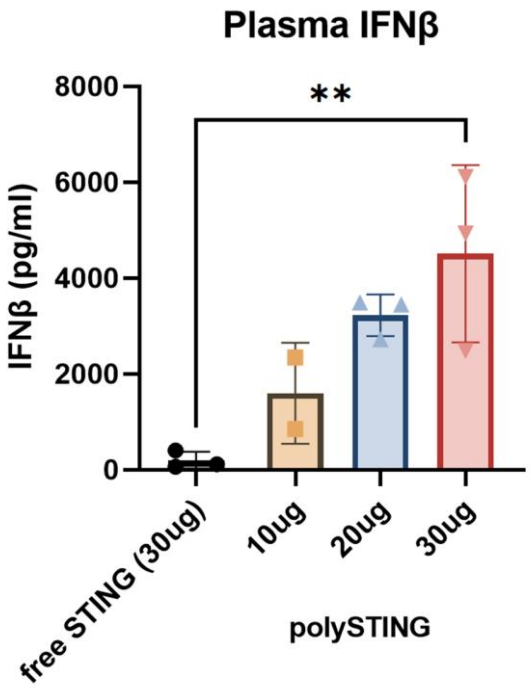

Figure S16. Plasma IFNβ level in healthy C57BL/6 mice 4 h post treatment with free STING and polySTING at different doses (N=3).

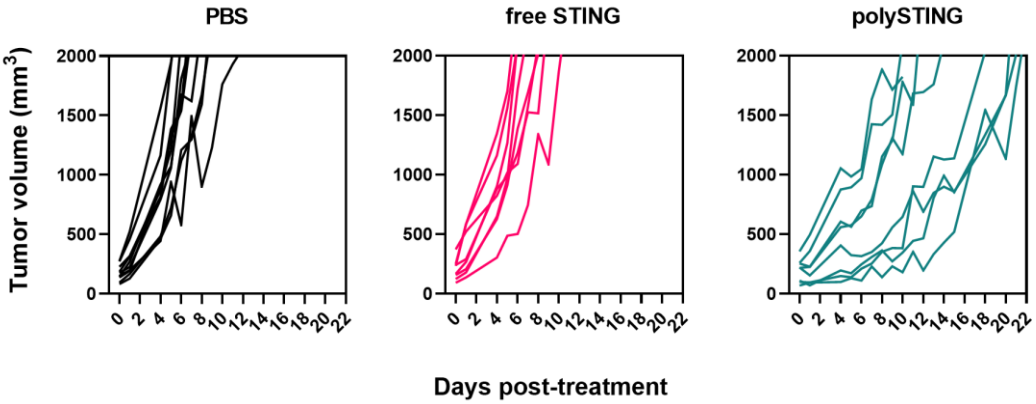

Figure S17. Individual tumor growth curves for B16F10 tumor reduction study.

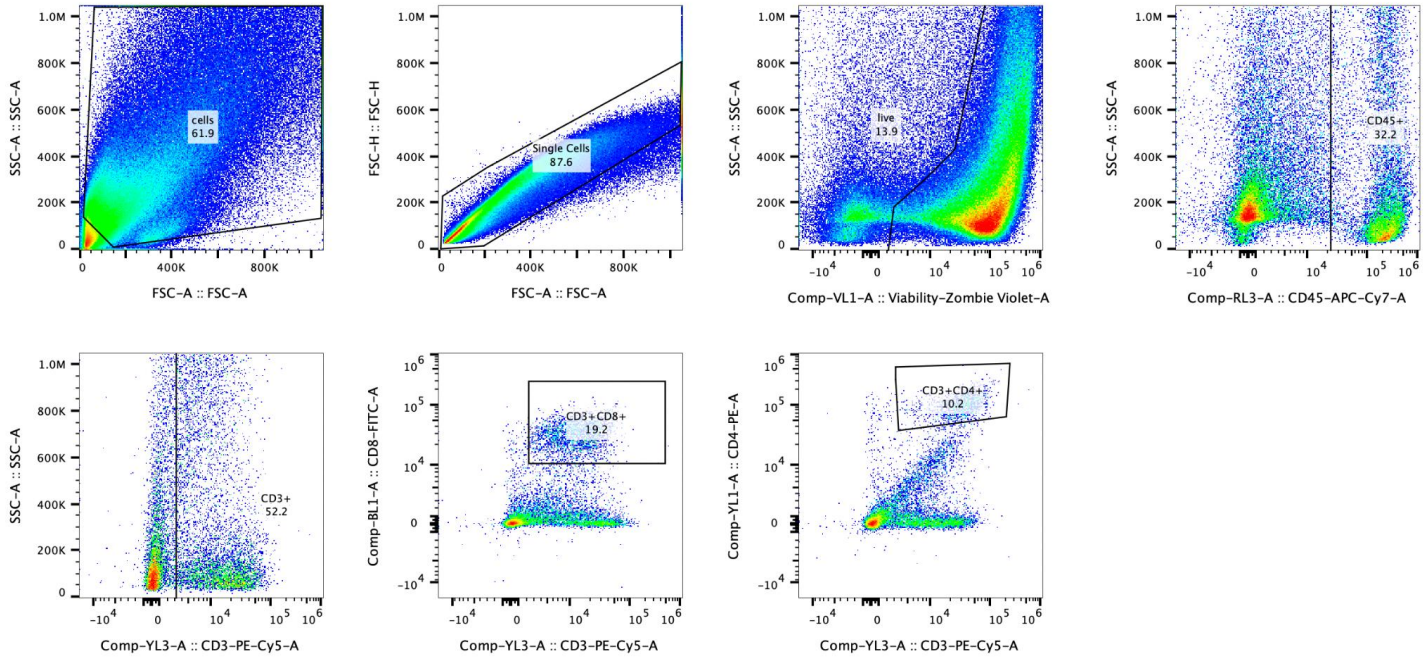

Figure S18. Gating on tumor-infiltrating $CD4^+$ and $CD8^+$ T cells.

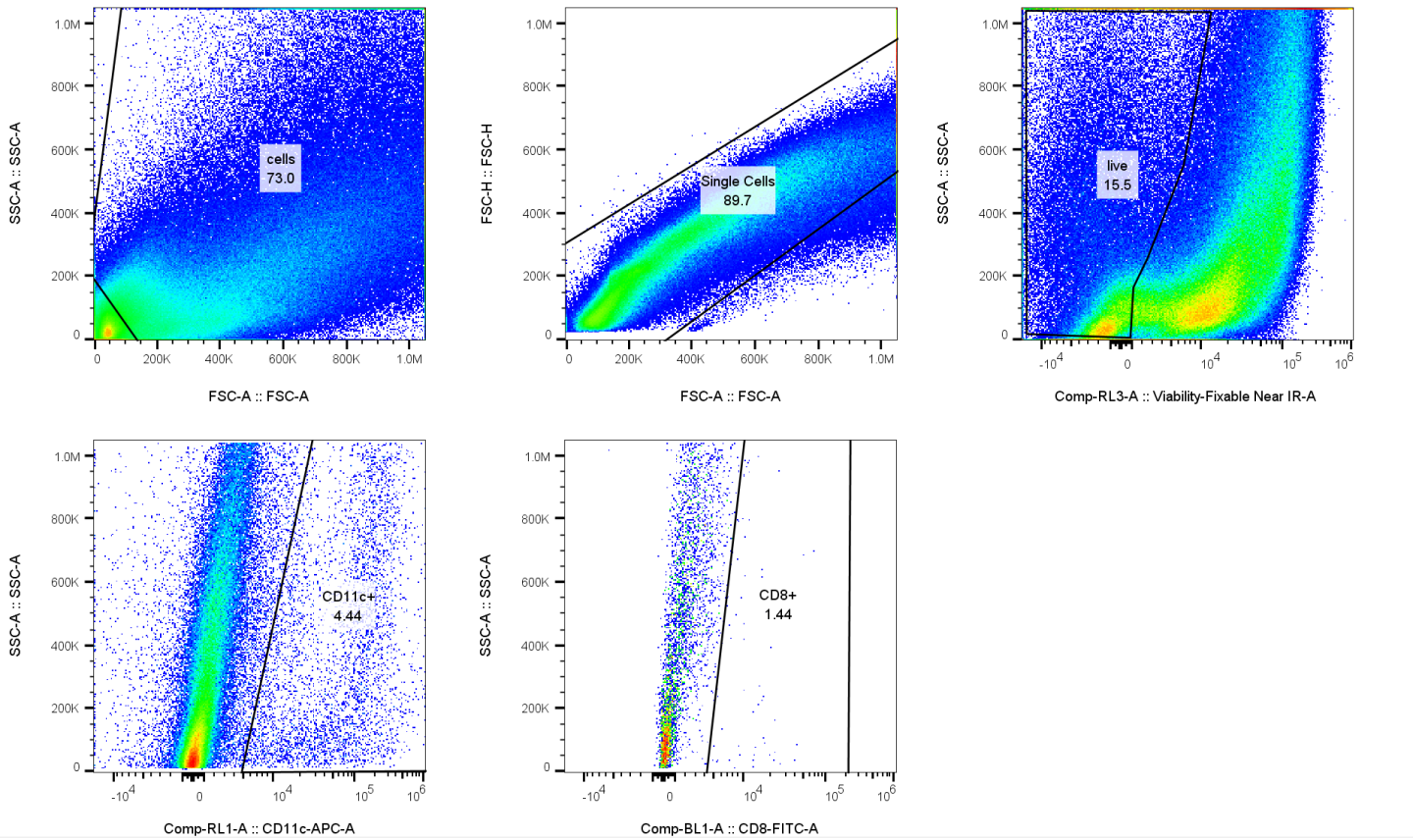

Figure S19. Gating on CD8$^+$ CD11c$^+$ DCs in tumors.

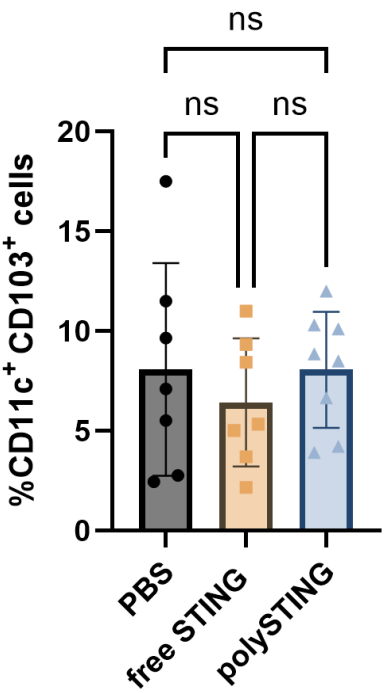

Figure S20. Assessment of CD11c$^+$ CD103$^+$ DCs in the TME

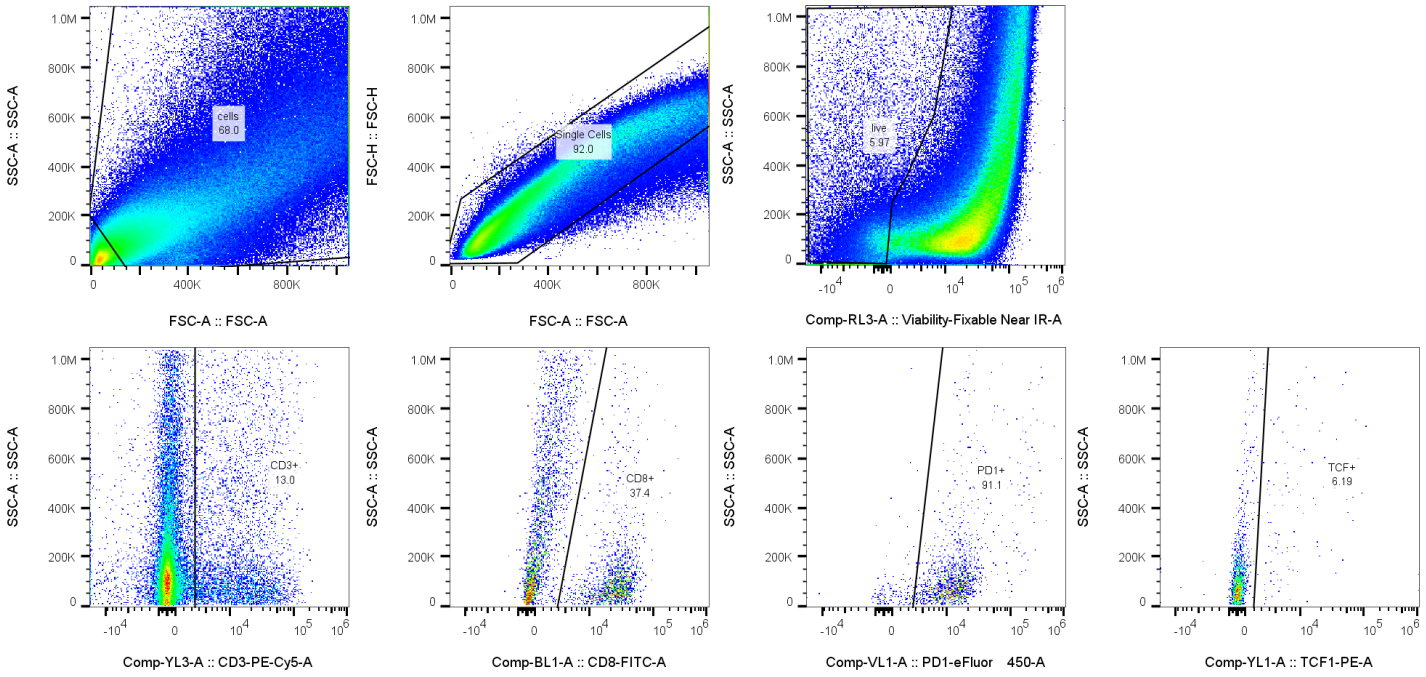

Figure S21. Gating on TCF-1^{+}, PD-1^{+} CD8^{+} T cells in tumors.

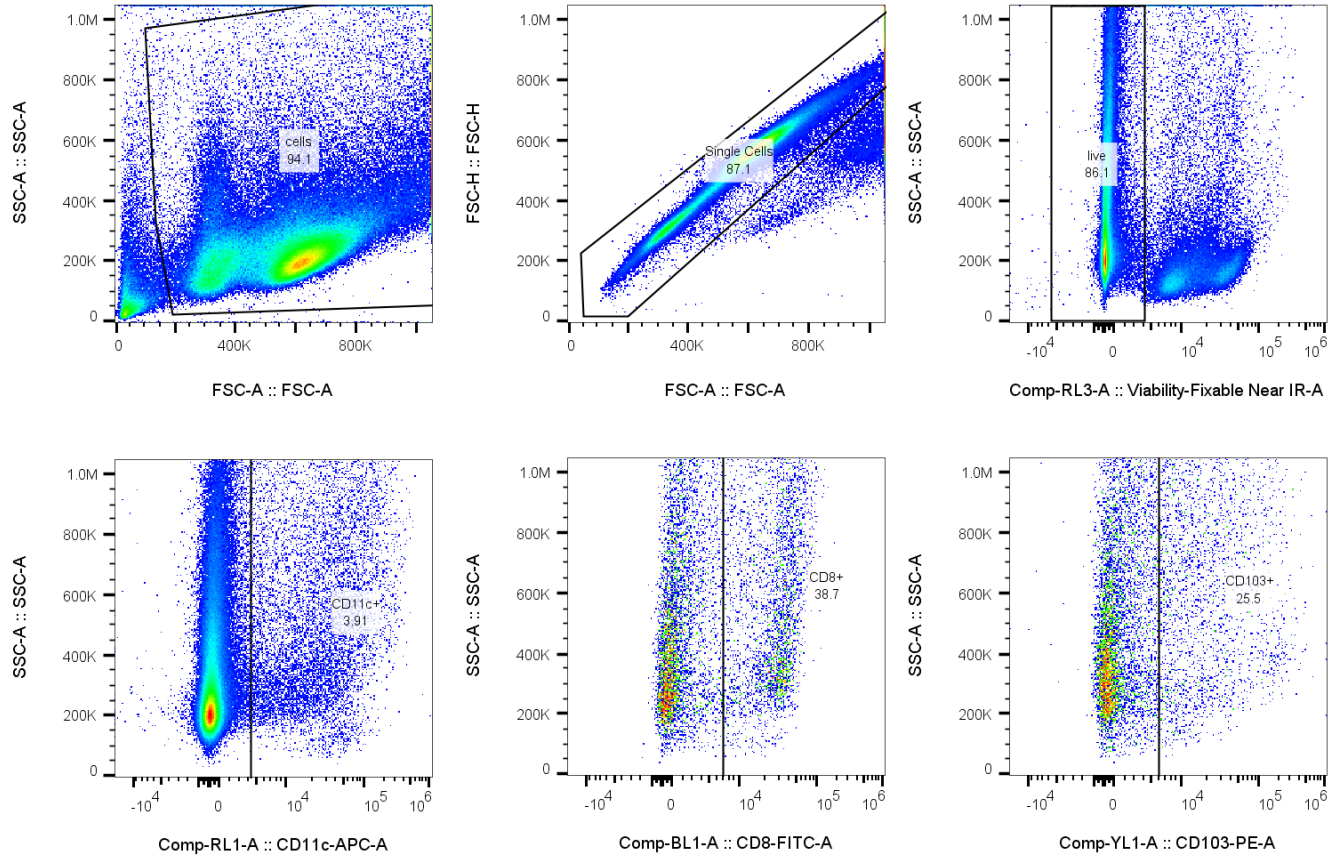

Figure S22. Gating on CD8^{+}, CD103^{+} DCs in TDLN.

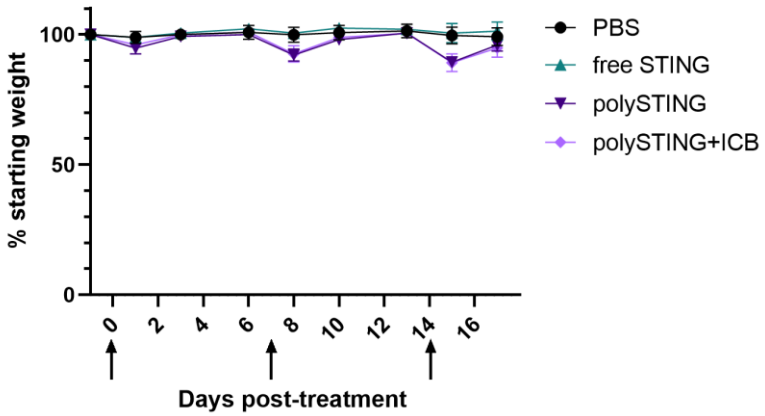

Figure S23. Weight loss in 4T1 study

Chapter 4 – Peptide Vaccine Formulations with Structurally Distinct STING Agonist Drugamers Induce Discrete, Efficacious Antitumor Responses

*Kefan Song, **Dinh Chuong Nguyen**, Yonghui Wang, Simbarashe Jokonya, Omeed Yazdani, Drew L. Sellers, Patrick S. Stayton, and Suzie H. Pun*

Synopsis

Peptide therapeutic cancer vaccines are an attractive treatment modality for their safety and manufacturability, but have been hindered in clinical translation by low immunogenicity and insufficient $CD8^+$ T cell activation. We developed Virus Inspired Polymers for Endosomal Release (VIPER) to address systemic and intracellular delivery obstacles, but durable antitumor immunity remained elusive. Adjuvants stimulating innate immunity, such as Stimulator of Interferon Genes (STING) agonists, can enhance vaccine potency but risks systemic toxicity and improper immune activation. We developed STING "drugamers" with cathepsin-cleavable linkers and dendritic cell (DC)-targeting moieties for intracellular delivery of STING agonists to DCs. We explored two different STING drugamer structures: a hydrophilic statistical polymer "polySTING" and a diblock polymer "NPSTING" that forms into nanoparticles. PolySTING achieved higher systemic STING agonist delivery, whereas NPSTING is more efficient in delivering STING agonists into inguinal lymph nodes (LNs). Both drugamer platforms enhanced STING activation and DC maturation compared to the free drug. When combined with VIPER, NPSTING generated more antigen-presenting DCs in the LNs and more antigen-responsive $CD8^+$ T cells in the spleens, whereas polySTING generated more tumor-infiltrating $CD8^+$ T cells and $CD8^+$ DCs. Both VIPER-STING drugamer platforms demonstrated efficacy in a B16-OVA melanoma model and a MC38 colon cancer model. Combination treatment with anti-PD-1 immune checkpoint inhibitor results in tumor remission and tumor immunity in a subset of mice. This study highlights how an endosomolytic peptide vaccine platform combined with two structurally different drugamers induce superior antitumor responses through distinctive mechanisms.

i. Introduction

Personalized therapeutic cancer vaccines hold great promise in cancer immunotherapy. Tumor cells can have somatic mutations that result in tumor-specific antigens called neoantigens that are not subject to central tolerance.[1] With recent advancements in bioinformatics and computational algorithms, neoantigens can be identified in a patient-specific manner to generate personalized cancer vaccines. Neoantigen vaccines have demonstrated promising results in clinical trials in patients with glioblastoma, melanoma and non-small cell lung cancer.[2–4] On their own, neoantigens generate suboptimal responses and need to be combined with adjuvants such as poly-ICLC[5] that boost the vaccine response. Clinically, these vaccines are compatible with and can benefit from combination therapy with immune checkpoint inhibitors,[6] chemotherapy,[7] and radiation therapy.[8]

Peptide-based cancer vaccines are attractive for their manufacturability and tolerability[9], but generate modest T cell responses[10]. Their low immunogenicity comes partly from multiscale drug delivery challenges: rapid systemic clearance or degradation, insufficient lymph node (LN) drainage, low dendritic cell (DC) uptake and inadequate intracellular access to the major histocompatibility class I (MHC-I) pathway for cross-presentation.[11–13] Altogether, these obstacles lead to poor $CD8^+$ T cell induction and suboptimal antitumor responses. We previously reported a mannosylated polymer-peptide conjugate that form 30-40 nm micelles that efficiently drain to LNs after vaccination and deliver peptide antigens to DCs through their mannose receptors.[14] We incorporated a membrane-lytic peptide D-melittin to make Virus-Inspired Polymers for Endosomal Release (VIPER). VIPER forms micelles at physiological pH but disassembles in the acidic endosomal environment to expose the lytic peptide D-melittin, which disrupts the endosomal membrane to facilitate cytosolic antigen release, cross-presentation, and $CD8^+$ T cell activation.[15] VIPER generated more antigen-specific T cells than antigen-only polymers and showed moderate therapeutic efficacy in the B16-OVA melanoma model. As innate immune adjuvants can improve activity of vaccine formulations,[16,17] we hypothesize that the therapeutic efficacy of VIPER can be further improved by including a rising class of cancer vaccine adjuvant: Stimulator of Interferon Genes (STING) agonists[18].

STING agonism in dendritic cells provides the three signals for effective $CD8^+$ T cell activation: antigen cross-presentation, co-stimulatory molecule expression and inflammatory context in the form of type I interferons (IFNs).[19] STING promotes cross-presentation to facilitate antigen presentation by MHC Class I molecules.[20] In addition, STING activation induces DC maturation. The expression of higher levels of co-stimulatory molecules on mature DCs prevent T cell anergy upon antigen presentation.[21,22] Furthermore, STING activation leads to the production of proinflammatory cytokines like type I IFNs that are essential for the survival, memory and effector function of $CD8^+$ T cells.[19] However, outcomes from clinical testing of STING agonists in oncology have been disappointing, likely due to the poor pharmacokinetics properties and intracellular delivery barriers.[23] Uncontrolled and/or off-target STING activation also leads to toxicity.[24] STING activation in T cells induces ER stress and leads to T cell death.[25] While drug delivery platforms have previously been developed for STING-antigen dual-delivery in cancer vaccines to notable success,[26–30] differences in agonist selection, formulation method, administration route and dosing across heterogeneous vector designs complicates the derivation of general design principles for future cancer vaccine formulation development.

In this work, we adjuvant VIPER with two polymeric prodrugs of a synthetic STING agonist that provide both dendritic cell-targeted STING delivery and enzyme-triggered STING release, but differ in their structure and physicochemical properties to probe adjuvant structure effects on STING pharmacokinetics, immunological outcome and vaccine efficacy. We utilized a commercial synthetic diamidobenzimidazole (diABZI) STING agonist that had both proven potent STING activation[31] and a hydroxyl group amenable to chemical conjugation. The diABZI STING agonist (hereafter referred simply as the STING agonist) is formulated into an enzyme-cleavable monomer through conjugation to a polymerizable methacrylate via a Cathepsin B-labile Val-Ala-PAB (VA) linker[32]. Analogous to its use in clinically-approved and efficacious antibody-drug conjugates (ADCs)[33,34], the VA-STING prodrug is relatively stable in circulation even under elevated protease conditions[35]. It is only labile upon receptor-mediated endocytosis through a co-polymerized internalizing ligand, as we have

previously demonstrated[36]. We previously synthesized polySTING, a hydrophilic, water-soluble statistical copolymer with mannosylated monomers for targeting dendritic cells copolymerized with the STING prodrug monomer. PolySTING showed activity as an intravenous STING agonist cancer immunotherapy.[37] To evaluate the importance of STING-antigen co-delivery, we also synthesized a diblock polymer containing STING agonists in a pH-tunable hydrophobic block that self-assembles into nanoparticles at physiological pH. The drugamer 'NPSTING', named for its nanoparticle-assembling properties, can co-assemble with VIPER polymers to package antigen and STING within single particles. Both STING drugamers contain mannose to target mannose receptors expressed on DCs for optimal DC activation and T cell priming while minimizing off-target toxicity. The drugamers improved the pharmacokinetic properties of the STING agonist: both polySTING and NPSTING increased STING delivery to the lymph nodes, though polySTING also delivered STING to systemic circulation. STING drugamers also improved the level of STING activation compared to the free drug. Both STING drugamers demonstrated enhanced VIPER's DC maturation, while all VIPER-STING formulations enhanced T cell activation and tumoral T cell infiltration. NPSTING's enhanced STING LN delivery compared to polySTING and free STING induced superior DC cross-presentation, while polySTING's systemic activity resulted in increased tumor infiltration of antigen-specific $CD8^+$ T cells and cross-presenting type 1 conventional DC (cDC1s) over all STING formulations. The VIPER-STING drugamer formulations slowed tumor progression and prolonged survival in the B16F10-OVA melanoma model in contrast to VIPER adjuvanted with free STING agonist. VIPER-STING drugamer is also efficacious in the MC38 colon cancer model as a neoantigen vaccine, and works in combination with the immune checkpoint inhibitor anti-PD-1 to induce partial tumor remission.

ii. Materials and Methods

Materials

Azobisisobutyronitrile (AIBN), 4,4'-azobis(4-cyanovaleric acid) (ABCVA), 2'-Azobis(4-methoxy-2,4-dimethylvaleronitrile) (V70) , cysteamine hydrochloride, piperidine, triisopropylsilane (TIPS) and ethanedithiol (EDT) were purchased from Sigma-Aldrich. Mannose ethyl methacrylate (ManEMA) and RAFT chain transfer agent 4-Cyano-4-[[(ethylthio)thioxomethyl]thio]pentanoic Acid (ECT) were purchased from Omm Scientific. Diisopropylcarbodiimide (DIC) and ethyl cyanohydroxyiminoacetate (Oxyma) were purchased from Chem-Impex. Dimethoxybenzene (DMB), trifluoroacetic acid (TFA), acetic acid (AcOH), acetonitrile (ACN) and Ellman's reagent were purchased from Fisher Scientific. Dithiothreitol (DTT) was purchased from Enzo Life Sciences. All were used as received. Diisopropyl ethyl methacrylate (DIPAMA) was purchased from Sigma-Aldrich. Pyridyl disulfide ethyl methacrylate (PDSEMA, also known as 2-(2-pyridinyldithio)ethyl methacrylate) and pentafluorobenzyl methacrylate (PFBzMA) was purchased from Tokyo Chemical Industries Ltd. These aforementioned monomers were purified by passing through a basic alumina column to remove any existing inhibitor prior to polymerization. Anhydrous N-methyl-2-pyrrolidone (NMP, 99.5%), and dimethylsulfoxide (DMSO, > 99%) were purchased from Sigma-Aldrich and stored with activated molecular sieves. Protected amino acids were purchased from Novabiochem and used as received. Buffers were prepared in-house using endotoxin-free water and salts purchased from Fisher Scientific. The STING monomer (SMA-VA-STING) was synthesized as previously described[37].

Polymer synthesis

Polymer synthesis of Man-VIPER and polySTING, and peptide synthesis and conjugation of Man-VIPER was performed as previously described.[15,37]

For the synthesis of NPSTING, a modified synthesis protocol from the polymerization of Man-VIPER was used. ManEMA was combined with ECT, ABCVA (ECT:ManEMA = 1:44.4, ECT:ABCVA = 1:20) in dry DMSO (2.5 wt% monomer), purged with argon for 30 minutes, and reacted at 70°C for 4h with vigorous stirring. The mannose CTA (ManCTA) was purified by 3x precipitation in 1:1 (v/v) acetone and diethyl ether, dissolving in DMF in-between, and dried *in vacuo* for 2 days. To a 5 mL round-bottom flask with a stir bar was added ManCTA, SMA-VA-STING, DIPAMA and V70 (ManCTA:SVA-VA-STING:DIPAMA:V70 = 1:5:33:0.25) and anhydrous NMP as solvent (20 wt% monomer). The solution was stirred until all solids were fully dissolved. 8 µl of DMF was added (~1% v/v NMP) as an internal standard. A 20 µl aliquot of the reaction mixture was taken as a reference for conversion NMR. The flask was sealed with a septum and sparged with argon gas for 30 minutes. The mixture was then allowed to react with stirring at 40°C for 20 hours, before being quenched by introduction of air and chilling via an ice bath. The polymer was purified via dialysis in DMSO for 3 days (2 solvent changes each day), and in cold water for 4 days (2-3 solvent changes each day) before lyophilization to yield a fluffy white powder (150 mg, 90% conversion, 87% yield from purification).

Polymer and Micelle Characterization

All ^{1}H NMR spectra were recorded on a Bruker AV 300 (Bruker Corporation, Billerica, MA) nuclear magnetic resonance (NMR) instrument in deuterated DMSO (DMSO-d6). The size distribution profiles of micelles were recorded on a dynamic light scattering (DLS) system (DynaPro NanoStar, Wyatt technology) at a micelle concentration of 1 mg/mL diluted in the PBS.

Transmission electron microscopy (TEM)

Formulations were prepared freshly and diluted in Nanopure water to 1 mg/mL. The diluted formulations were adsorbed onto 200-mesh lacey carbon grids for 5 mins with the carbon film side facing down, with excess solution wicked away by filter paper. Afterwards, the grids were stained with NanoW (NanoProbes, Yaphank, NY) for 1 min, and blotted with a filter paper. Finally, the grids were dipped in Nanopure water for 30 s to wash away excess stain solution, and dried in a desiccator overnight. Grids were imaged with a Tecnai G2 F20 Supertwin TEM (FEI, Hillsboro, OR) at the Molecular Analysis Facility at University of Washington.

Vaccine formulation

We utilized our previously-described pH-switch method to formulate our micelles with slight modifications[15]. Briefly, individual VIPER polymer conjugates were dissolved in endotoxin-free water. The polymer solutions were combined at equal volumes. HCl (2.5% of 1 N solution) was added to the mixture until a clear solution was obtained. The solution was probe-sonicated for 30 seconds to ensure complete dissolution. 0.2 M pH 9.0 dibasic sodium phosphate was added to obtain the final pH around 7.0. The formulations were prepared at ambient conditions. All VIPER vaccines contain 15 µg of OVA MHC-I epitope, 15 µg of OVA MHC-II epitope and 143 µg of D-melittin. To form VIPER-STING vaccines, free STING and NPSTING were dissolved at 20x in DMSO, and polySTING was dissolved at 20x in PBS. VIPER was mixed with different STING formulations after micelle formation. For VIPER-co-NPSTING, NPSTING was added after HCl addition, and then dibasic sodium phosphate was added to increase the pH to form micelles. Samples were filtered through a 0.22 µm filter before injections.

Cell lines and animals

The B16F10-OVA cell line (gift of Prof. Amanda Lund) and MC38 cell line (Sigma) were cultured in DMEM supplemented with 10% FBS and 1% P/S. Cells were incubated at 37°C and 5% CO_2. Female C57BL/6 mice aged 6 to 8 weeks were purchased from Charles River Laboratories. All animal studies were approved by the University of Washington Institutional Animal Care and Use Committee (IACUC).

Pharmacokinetics characterization

Female C57BL/6 mice were injected subcutaneously at the tail base with free STING agonist, polySTING or NPSTING at 10 μg/mice. 5 minutes before designated PK timepoints, mice were sacrificed with Avertin overdose (i.p.). The chest cavity was then opened to reveal the heart, and cardiac puncture was performed at the desired PK timepoint. Blood was collected into BP heparin tubes and centrifuged at 3000 RCF for 10 minutes at 4°C to isolate plasma. The inguinal lymph nodes (iLNs) and tail base (i.e. injection site) cutaneous fat were also collected and snap frozen on dry ice. To obtain organ homogenates, organs were mixed with molecular biology grade water (5 mL/g organ for iLNs, 2 mL/g for cutaneous fat, 1 mL/g for liver and spleen) and homogenized with a probe sonicator (iLNs and cutaneous fat) or mechanical disruption (Qiagen TissueLyzer II, Hilden, Germany).

Upon analysis, plasma or tissue homogenate were mixed with a gembitabine internal standard solution (0.5 μg/mL in acetonitrile), 50% acetonitrile/water, and 100% acetonitrile in a 3:1:6:90 volumetric ratio. The solution was vortexed for 5 minutes, and centrifuged twice (removing supernatant in-between) to obtain solutions for LC-MS analysis. Calibrators were prepared with naive plasma/homogenate spiked with known STING agonist concentrations in the 50% acetonitrile/water phase (1 μg/mL STING, 1:2 serial dilutions, representative calibration curves in **Fig. S5**). LC/MS was performed at the Mass Spectrometry Center in the University of Washington School of Pharmacy. For LC/MS (Xevo TQ-S, Waters Corporation, Milford, MA), the MS instrument was operated on a positive ion multiple-reaction monitoring (MRM) mode monitoring 136 m/z for the STING agonist and 112 m/z for the internal standard gemcitabine (LLOQ-ULOQ 8.2-2000 ng/mL plasma, 40-10000 ng/g lymph nodes, or 148-2000 ng/g cutaneous fat). The LC was performed with an InfinityLab Proshell 120 EC-C18 analytical (2.1x150mm) column (Agilent, Santa Clara, CA). The LC solvents were water supplemented with 0.1% (v/v) formic acid (solvent A), and acetonitrile supplemented with 0.1% (v/v) formic acid (solvent B). The linear gradient used was from 95:5 A:B to 0:100 A:B over 8 minutes at a 0.25 mL/min flow rate.

In vivo STING activation

Female C57BL/6 mice were injected subcutaneously at the tail base with free STING agonist, polySTING or NPSTING at 10 μg/mice and inguinal LNs were harvested 24 h post injection. In a separate study, female C57BL/6 mice were injected subcutaneously at the tail base with PBS, VIPER, VIPER + free STING, VIPER + polySTING or VIPER-co-NPSTING, with free STING and polySTING containing 10 μg of STING agonist and NPSTING containing 2 μg of STING agonist. Blood and inguinal LNs were harvested 4 h post injection. RT-qPCR was used to analyze interferon-stimulated gene expression as described previously.[37] Plasma IFNβ was analyzed using ELISA (Invivogen).

In vivo dendritic cell activation

Female C57BL/6 mice were injected subcutaneously at the tail base with indicated vaccine formulations. 24 h post immunization, inguinal lymph nodes were harvested, dissociated with pipette tips and digested in 50 U/mL type IV collagenase + 100 U/mL DNase I. Single-cell suspension was obtained by filtering cells through a 70 μm cell strainer. Cells were stained for viability with Zombie NIR viability kit, blocked with anti-CD16/32, and then stained with anti-CD86-BV510, anti-CD40-FITC, anti-CD11c-APC and anti-CD80-PE. In a separate study, cells were stained with anti-CD86-BV510, anti-CD8-FITC, anti-H-2Kb-SIINFEKL-PE and anti-CD11c-APC. An Attune NxT flow cytometer was used to analyze the data. Gating strategies are shown in **Fig. S7, S10**.

In vivo T cell responses

Female C57BL/6 mice were injected subcutaneously at the tail base with the indicated vaccine formulations on day 0 and day 14. Spleens were harvested on day 21. Tissues were passed through 70 μm cell strainers and treated with ACK lysis buffer. Splenocytes were resuspended in IMDM and plated in separate 96-well plates for tetramer staining and intracellular cytokine staining (ICCS). For the tetramer staining, splenocytes were stained with Zombie NIR for viability and then stained with PE-labeled H-2Kb/SIINFEKL tetramer (NIH Tetramer Core). Cells were blocked with anti-CD16/32 and stained with anti-CD3-eFluor450 and anti-CD8-FITC. For ICCS, splenocytes were either restimulated with 5 μg/ml SIINFEKL peptide or 5 mg/ml OVA protein. 3 hr later, Protein Transport Inhibitor Cocktail (PTIC) was added and cells were incubated for another 3 hr. After incubation, cells were stained with Zombie NIR for viability, blocked with anti-CD16/32 and stained with either anti-CD3-eFluor450 + anti-CD8-FITC for $CD8^+$ T cells or anti-CD3-eFluor450 + anti-CD4-FITC for $CD4^+$ T cells. Cells were then treated with the BD Cytofix/Cytoperm Fixation/Permeabilization Kit and stained with either anti-TNFα-PE and anti-IFNγ-APC for $CD8^+$ T cells and anti-IL-2-PE and anti-IFNγ-APC for $CD4^+$ T cells. Data was collected using the Attune NxT flow cytometer and analyzed using Flowjo. Gating strategies are shown in **Fig. S11**.

Tumor-infiltrating lymphocytes

Female C57BL/6 mice were inoculated with 0.15 million B16-OVA cells on the right hind flank on day 0 and immunized subcutaneously at the tail base on day 5 and day 12. Tumors were collected 24 h post the 2nd injection, and digested with 20 U/mL type IV collagenase + 125 U/mL DNase I, and dissociated with the GentleMACS Dissociator. Tumors were then incubated on a rotating platform at 37 °C for 30 min. Single-cell suspensions were obtained by passing homogenate through a 70 μm cell strainer. Cells were treated with the ACK lysing buffer to remove red blood cells.

Tumor cells were stained for viability with Zombie NIR viability kit, blocked with Trustain anti-mouse CD16/32, and then stained in two plates for T cells (anti-CD3-eFluor450, anti-CD4-APC, anti-CD8-FITC, PE-labeled H-2Kb/SIINFEKL tetramer), and DCs (anti-CD11c-APC, anti-CD8-FITC, anti-CD103-PE, anti-CD86-BV510). Data was collected using the Attune NxT flow cytometer and analyzed using Flowjo. Gating strategies are shown in **Fig. S12**.

Tumor studies

Female C57BL/6 mice (N=6-8) were inoculated with 1.5×10^5 B16F10-OVA cells in the right-hind flank on day 0. On days 4, 11, and 18, mice were immunized with PBS, VIPER containing 15 μg CSSSIINFEKL, 15 μg

CSSISQAVHAAHAEINEAGR antigen peptides and 143 μg D-Melittin peptide, VIPER with 10 μg free STING agonist-3, VIPER with NPSTING containing 2 μg STING agonist-3 in different micelles (VIPER+NPSTING), VIPER with NPSTING containing 2 μg STING agonist-3 in same micelles (VIPER-co-NPSTING) or VIPER with polySTING containing 10 μg STING agonist-3. Female C57BL/6 mice (N=7-9) were inoculated with 5×10^5 MC38 cells in the right-hind flank on day 0. On days 8, 14, and 20, mice were immunized with PBS, VIPER, VIPER + free STING, VIPER + polySTING or VIPER-co-NPSTING, with free STING and polySTING containing 10 μg of STING agonist and NPSTING containing 2 μg of STING agonist via subcutaneous injection at the tail base. On days 8, 11, 14, 18, 21 and 25, mice were injected with 150 μg of anti-PD-1 (Clone RMP1-14, BioXCell) via intraperitoneal injection. Tumor length and width were then measured three times a week using a vernier caliper, and volume was subsequently calculated using the formula: Volume = $(\text{Width}^2 \times \text{Length}) \div 2$. Weight was also measured three times a week. Mice were euthanized if total tumor volume exceeded 1500 mm^3, visible discharge was observed on ulcers of the tumors, or the body weight loss exceeded 20%.

Statistical analysis

Statistical analysis was performed using the Graphpad Prism software. One-way ANOVA with post-hoc Tukey HSD test was used to compare more than two groups. Log-rank test was used for survival analysis.

iii. Results

Synthesis and characterization of VIPER and STING drugamers

Co-delivery of antigen and STING agonists has been reported to be an important criterion for STING-adjuvanted vaccines[26]. Systemic administration of STING agonists can lead to broad STING activation and toxicity from resulting systemic cytokines[23]. The 'drugamer' platform utilizes enzyme-cleavable prodrug monomers for facile polymer functionalization with targeting and intracellular release properties, suitable for incorporating STING agonists into the polymeric VIPER platform[37,38]. We synthesized two STING agonist drugamers as adjuvants for our VIPER vaccine platform to make a DC-targeted adjuvanted vaccine that activates both the innate and adaptive immune response with enhanced $CD8^+$ T cell activation (**Fig. 1A**). We previously reported 'VIPER' (also known as 'Man-VIPER-NR'), a mannosylated DC-targeting intracellular peptide vaccine antigen delivery platform. The VIPER diblock polymer (21 kDa) used in this work consists of 42 mannose methacrylate (ManMA) units in the 1st hydrophilic block, 45 pH-responsive diisopropylamino ethyl methacrylate (DIPAMA) units and 2-3 peptide-conjugating units in the 2nd hydrophobic block that are conjugated to either a lytic D-melittin peptide (1-2/polymer) or antigen peptides (2-3/polymer). VIPER self-assembles into 40-50 nm micelles that are loaded with both endosomal releasing D-melittin and peptide antigen[15]. Upon mannose-mediated internalization, VIPER disassembles in the acidic endosome, allowing D-melittin to lyse the endolysosomal membrane and releasing peptide antigens into the cytosolic MHC-I presentation pathway[15].

The first STING agonist drugamer, 'polySTING', is a linear, hydrophilic, statistical copolymer of ManMA and a cathepsin-cleavable STING prodrug monomer. PolySTING (12 kDa) has 35 ManMA units and 2 STING units (**Fig. 1B**). PolySTING is water-soluble and can be co-administered with VIPER, but is not expected to integrate into VIPER micelles. The second STING agonist drugamer, NPSTING, is a diblock copolymer constitutionally similar to the VIPER backbone that carries the STING prodrug monomer in the hydrophobic block. NPSTING (23 kDa) has 50 ManMA units in the 1st hydrophilic block, 33 pH-responsive DIPAMA units and 2 STING units in the hydrophobic 2nd block (**Fig. 1C**). NPSTING self-assembles into 30-40 nm micelles on its own or co-assembled with VIPER, similar to VIPER itself (**Fig. 1D-E, S2**). The

compositional information of all polymers used are described in **Table S1.** Given the suboptimal response of VIPER, we sought to combine the two platforms to make an adjuvanted vaccine that activates both the innate and adaptive immune response with enhanced $CD8^+$ T cell activation (**Fig. 1A**). The two drugamer systems allow us to experimentally test the difference between simultaneous antigen and adjuvant delivery from the same nanoparticle (VIPER-co-NPSTING) and simple co-administration of the antigen delivery formulation (VIPER) with polymeric STING agonist (polySTING) that share a targeting moiety.

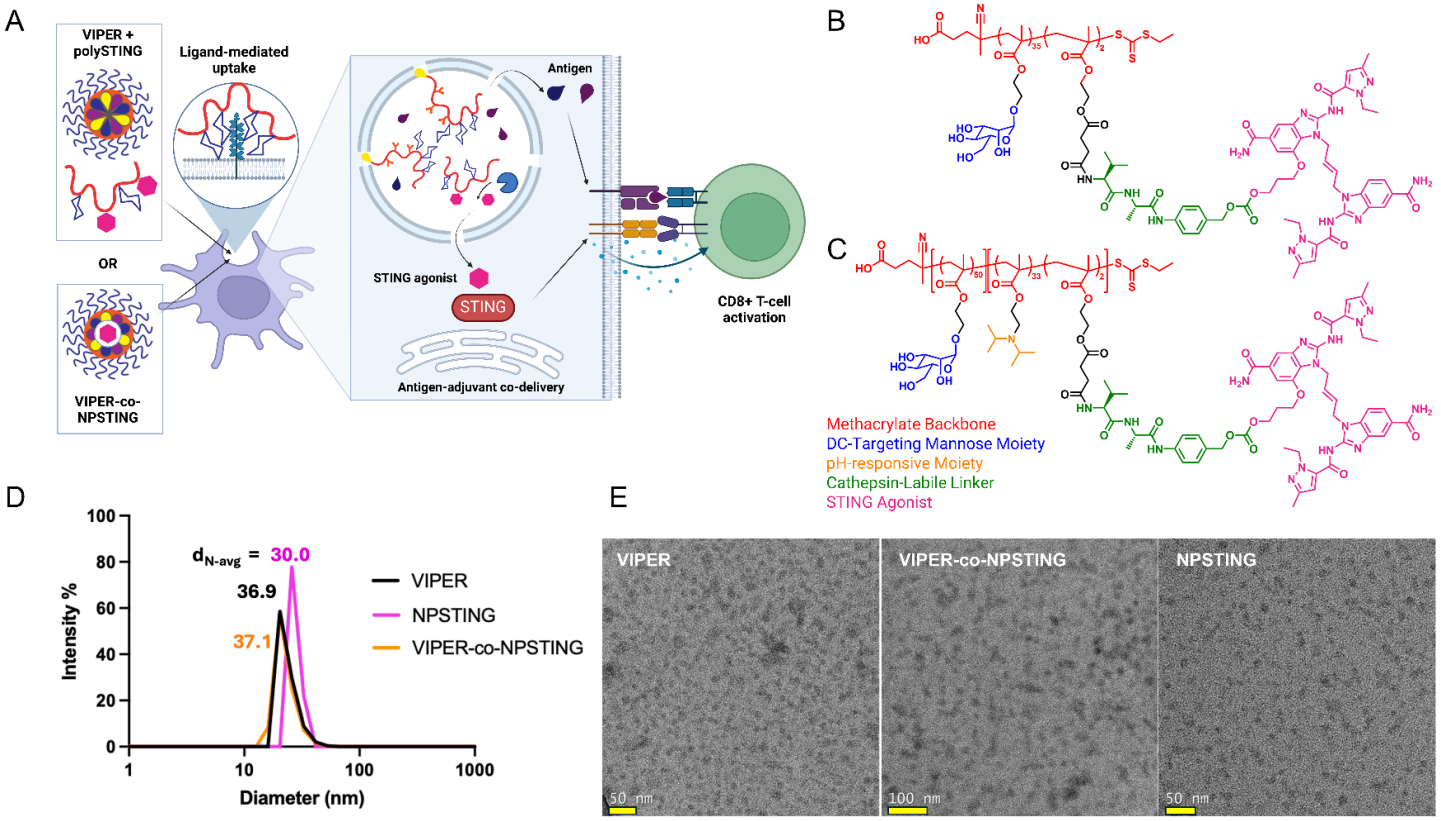

Figure 1. Design and characterization of VIPER and STING polymers. (A) Schematic illustration of VIPER and STING polymers uptake by dendritic cells through receptor-mediated endocytosis, antigen cross-presentation, STING agonist release by cathepsin-cleavage and STING activation, which ultimately leads to enhanced $CD8^+$ T cell activation. (B-C) Chemical structures of polySTING and NPSTING with NMR-determined degree of polymerization indicated, respectively. (D) Size distribution of VIPER,, VIPER-co-NPSTING and NPSTING characterized by dynamic light scattering (d_{mean} = 36.9 nm, 37.1 nm and 30.0 nm respectively). (E) Transmission Electron Microscopy (TEM) of VIPER, VIPER-co-NPSTING and NPSTING micelles.

STING drugamers enhanced drug accumulation in lymph nodes and plasma in a structure-dependent manner

We first investigated how the different drugamer structures impact the pharmacokinetics of the released STING. We injected STING as free agonist, polySTING or NPSTING (10 µg of STING agonist) subcutaneously at the tail base of C57BL/6 mice and analyzed STING agonist concentrations in the plasma and inguinal lymph nodes (iLNs) by liquid chromatography/mass spectrometry (LC/MS). The LC/MS method detects only released, free-agonist STING instead of the prodrug/polymer-bound drugamer form (**Fig. S3, S4**). STING signals were calibrated against naive matrices spiked with known agonist concentrations (**Fig. S5**). Free STING agonist treatment resulted in very low STING agonist concentrations

detected at all timepoints, with only the plasma in two mice in the 1h group showing concentrations above the lower limit of quantification (LLOQ). An additional analysis for free agonist 30 minutes post-administration showed low but detectable STING concentrations in the plasma and spleen, suggesting rapid systemic clearance within minutes (**Table S2**). In contrast, drugamer treatments resulted in significantly higher drug concentrations in both plasma and iLNs. In the iLNs, within the duration of the study, polySTING- and NPSTING-treated mice reached maximal mean STING agonist concentrations of 2300 ng/g and 12000 ng/g respectively, both at 8h post-administration (**Fig. 2A**). Agonist concentration increased between 1h-8h for both drugamers, though NPSTING treatment resulted in a more drastic increase. NPSTING treatments also resulted in significantly higher STING agonist concentrations in the LNs at all timepoints. In the plasma, polySTING-treated mice had the highest systemically available STING agonist (58 ng/mL) at 1h that quickly decreased over time. NPSTING-treated mice had relatively lower systemic STING concentrations that peaked (20 ng/mL) at 4h.

STING drugamers activate STING and induces dendritic cell maturation

We next examined STING pathway activation after STING agonist administrations. Free STING, polySTING and NPSTING were administered subcutaneously at the tail base of C57BL/6 mice at 10 μg equivalent of STING agonist and iLNs were collected 24 h post-injection. The expression of STING-related cytokines (IFNB1) and chemokines (CXCL10) was quantified using RT-qPCR, normalized to the GAPDH housekeeping gene. Free STING, polySTING and NPSTING generated a 2.2-, 4.5-, and 250-fold increase in IFNB1 expression, and a 8.1-, 28-, and 490-fold increase in CXCL10 expression compared to the vehicle control (**Fig. 2C-D**). The robust increases in STING-related gene expression after NPSTING administration are consistent with the PK data, which showed NPSTING has the highest accumulation in the iLNs.

PolySTING and NPSTING activate dendritic cells in a dose-dependent manner (**Fig. S6**). We injected three different dosages of NPSTING (containing 2, 5 or 10 μg of STING agonist) and polySTING (containing 10 μg, 30 μg and 50 μg of STING agonist) subcutaneously at the tail base and analyzed inguinal lymph nodes 24 h post-injection. NPSTING and polySTING both induced higher CD86 and CD80 expression in DCs at higher doses (**Fig. S6A,B**). The difference in CD40 expression was small (**Fig. S6C**). However, at higher dosages, both NPSTING and polySTING induced cell death in the lymph nodes (**Fig. S6D**) and higher dosage of NPSTING decreased the percentage of DCs in the LNs (**Fig. S6E**). This result is in line with STING's possible role in diverse cell death pathways.[39] At the same dosage, NPSTING generated a higher level of IFNB1 expression compared to polySTING (**Fig. S6F**), probably due to higher accumulation of the STING agonist in the LNs as shown in the PK data. We moved forward with using 2 μg of STING agonist as the preferred dose for NPSTING and 10 μg STING agonist as the preferred dosing for polySTING as these dosing levels induced a relatively high level of DC maturation without causing too much toxicity.

We next investigated how the STING drugamers affected DC maturation when combined with VIPER vaccines (gating scheme in **Fig. S7**). VIPER + polySTING and VIPER + NPSTING were formulated by making micellar VIPER containing peptide antigen separately and then admixing with soluble polySTING or NPSTING micelles. VIPER-co-NPSTING was formulated by dissolving both VIPER antigen polymers and NPSTING polymers in acidic solution and increasing pH to induce micelle formulations containing both peptide antigen and STING agonists within the same micelle. As shown in **Fig. 1D-E and S2**, VIPER, NPSTING, VIPER + NPSTING and VIPER-co-NPSTING were all similar in size and morphology, ranging from 30-40 nm in diameter. Given similar physicochemical characteristics, we expect VIPER in all formulations to exhibit similar lymphatic drainage behavior[40]. The addition of polySTING and NPSTING to VIPER induced a much higher DC activation compared to VIPER alone in all three DC maturation markers (**Fig. 2E-G**). VIPER + polySTING induced a 10-, 26-, and 5-fold higher expression in CD86, CD80 and CD40 markers compared to VIPER. VIPER-co-NPSTING induced a 7-, 19-, and 5-fold higher expression in CD86, CD80 and CD40 markers compared to VIPER, whereas VIPER + free STING only induced 1.8-, 2.3- and 1.6-fold increase in the expression of DC maturation markers. The STING drugamers significantly increased DC maturation compared to free STING agonist. The results were in line with the PK

data, which showed that free STING agonist is rapidly eliminated after administration. In addition, VIPER-co-NPSTING demonstrated higher DC activation compared to VIPER + NPSTING (**Fig. S8**), emphasizing the importance of co-delivery of antigens and adjuvants into the same DCs.

PolySTING induces systemic STING activation, while NPSTING increases antigen cross-presentation

When combined with the VIPER vaccine, STING drugamers generated a higher level of STING activation compared to free STING, while VIPER itself does not activate the STING pathway (**Fig. 2H**). VIPER + polySTING generated a higher level of IFNβ in plasma compared to VIPER + free STING and VIPER-co-NPSTING 4 h post injection (**Fig. 2H**), which is consistent with the PK data showing higher STING concentration in plasma after polySTING treatment at earlier time points. STING activation in the iLNs were low for VIPER-co-NPSTING 4 h post injection (**Fig. S9**). This could be due to the fact that NPSTING was administered at a 5-fold lower concentration compared to free STING and polySTING, and the amount of STING agonist is still increasing at the 4 h timepoint for NPSTING (**Fig. 2A**).

STING activation is known to promote cross-presentation through the production of type I IFNs.[22,41] We next examined the level of antigen-presenting DCs in the inguinal LNs 24 h after vaccination (gating scheme in **Fig. S10**). Mice were vaccinated with VIPER containing OVA MHC I (SIINFEKL) and OVA MHC II (ISQAVHAAHAEINEAGR) epitopes and H-2Kb-SIINFEKL antibody was used to detect dendritic cells with SIINFEKL peptide bound to H-2Kb of MHC class I molecules. While STING-adjuvanted treatments trended toward higher numbers of antigen-presenting DCs compared to VIPER immunization alone, only VIPER-co-NPSTING generated a significantly higher level of antigen-presenting CD11c$^+$ DCs compared to VIPER alone (**Fig. 2I**).

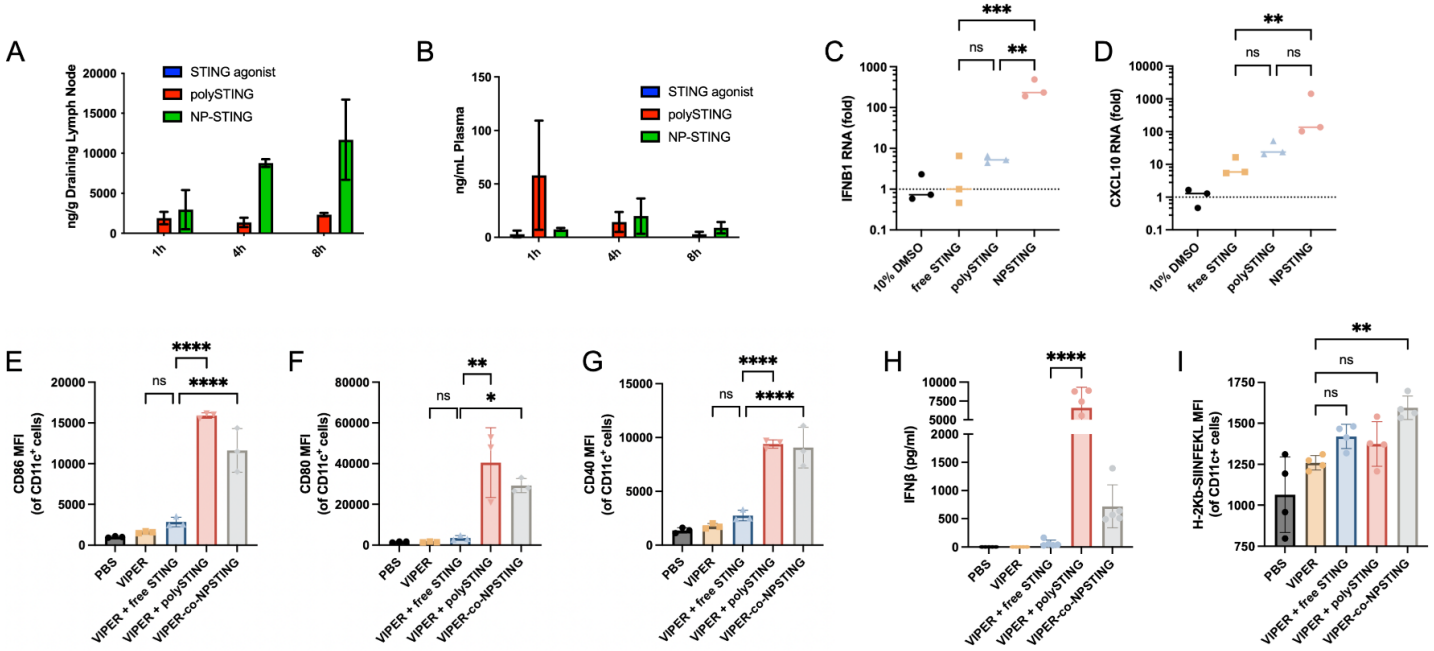

Figure 2. STING drugamers enhance pharmacokinetics and STING activation, promote DC activation and antigen cross-presentation. (A-B) Quantification of STING agonists in iLNs (A) and plasma (B) 1 h, 4 h, and 8 h post injection (N=3). (C-D) IFNB1 and CXCL10 expression in iLNs 24 h post injection, normalized to GAPDH housekeeping gene (N=3). (E-G) Co-stimulatory molecule CD86, CD80 and CD40 expression on CD11c$^+$ cells in iLNs 24 h post injection (N=3). (H) Plasma IFNβ level 4 h post injection (N=5). Values below the detection limit were represented as 0. (I) Median fluorescence intensity (MFI) of H-2Kb-SIINFEKL on CD11c$^+$ cells in iLNs 24 h post injection (N=4). Data are

represented as mean ± SD. Statistical analysis was performed using a one-way ANOVA with posthoc Tukey HSD test (*p ≤ 0.05, **p ≤ 0.01, ***p ≤ 0.001, ****p ≤ 0.0001, ns: not significant).

Co-delivery of STING agonists and antigens enhances T cell activation of VIPER vaccine

We next evaluated the adjuvanted VIPER formulations' capacity for T cell induction, a crucial step towards cytotoxic antitumor immunity (gating scheme in **Fig. S11**).[42] Mice were immunized with PBS, VIPER, or VIPER combined with free STING, polySTING or NPSTING on day 0 and day 14 and spleens were collected 7 days after the 2nd immunization for T cell analysis (**Fig. 3A**). All STING formulations induced more antigen-specific $CD8^+$ T cells in the spleen compared to VIPER (**Fig. 3B**), demonstrating the immunological boost of STING agonist adjuvants, though there were no significant differences between STING-adjuvanted formulations. Only VIPER-co-NPSTING generated a significantly higher amount of cytokine-producing $CD8^+$ T cells compared to VIPER when restimulated with the antigen *ex vivo* (**Fig. 3C**). Similarly, all STING formulations generated a higher amount of antigen-responsive $CD4^+$ T cells compared to VIPER, with VIPER + polySTING and VIPER-co-NPSTING generating slightly higher responses than VIPER + free STING (**Fig. 3D**). Co-stimulatory molecules on DCs lower the T cell activation threshold and make T cells more sensitive to antigen stimulation.[43] Additionally, STING activates the NF-kB pathway and induces the expression of pro-inflammatory cytokines such as TNF-α.[44] polySTING and NPSTING generated higher levels of co-stimulatory molecules expression on DCs and activated the STING pathway to a greater extent, and therefore could generate antigen-specific $CD8^+$ and $CD4^+$ T cells that are more responsive to antigens.

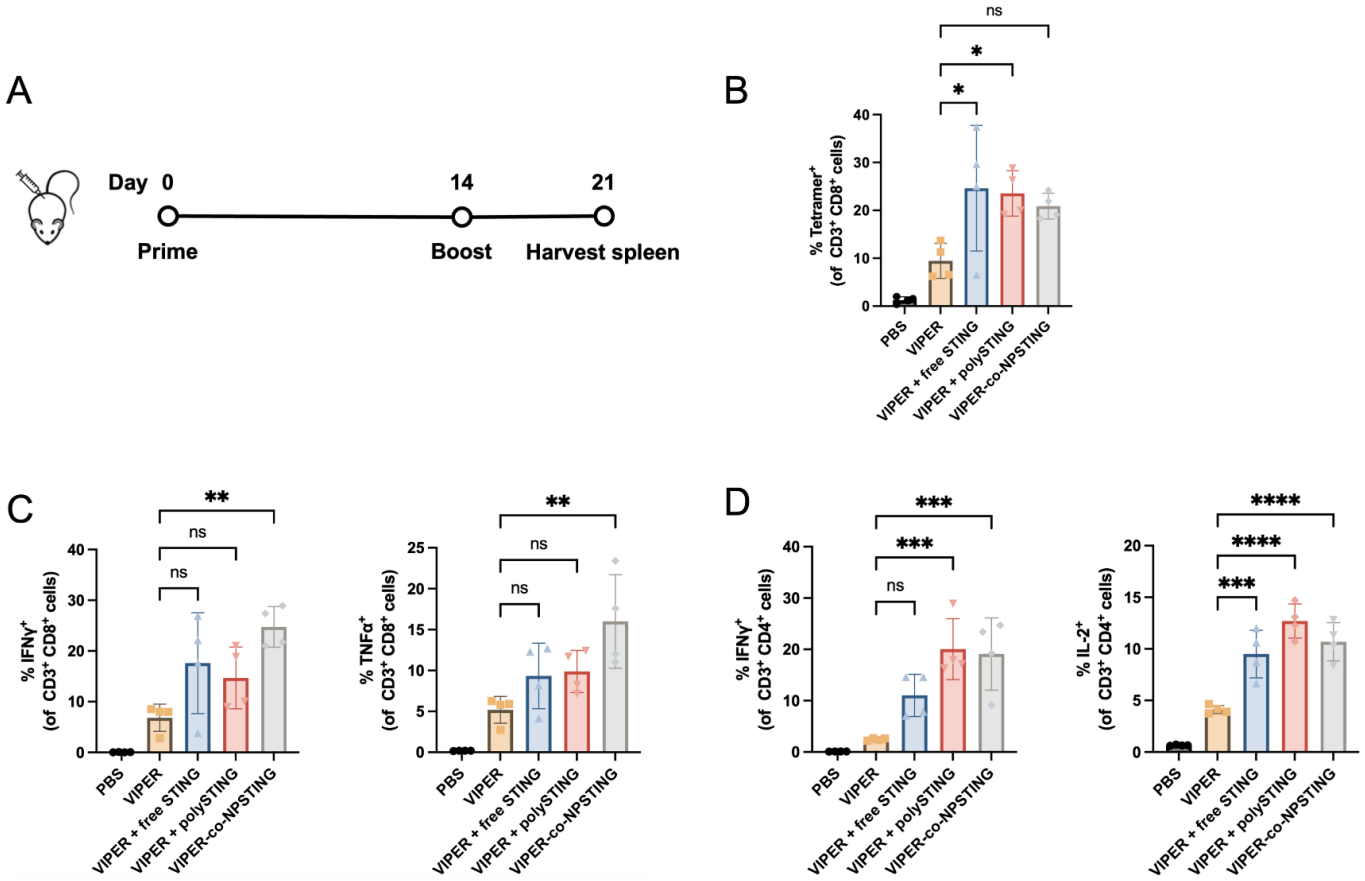

Figure 3. STING agonists improve antigen-specific T cell response *in vivo*. (A) Study timeline. Mice were vaccinated on day 0 and day 14, and spleens were collected on day 21. (B) Percentage of antigen-specific $CD8^+$ T cells in the spleen. (C) Percentage of IFNγ- and TNFα-producing $CD8^+$ T cells in the spleen after restimulation with the antigen *ex vivo*. (D)

Percentage of IFNγ- and IL-2--producing $CD4^+$ T cells in the spleen after restimulation with the antigen *ex vivo* (N=4). Data are represented as mean ± SD. Statistical analysis was performed using a one-way ANOVA with posthoc Tukey HSD test (*$p \leq 0.05$, **$p \leq 0.01$, ***$p \leq 0.001$, ****$p \leq 0.0001$, ns: not significant).

Co-delivery of STING agonists and antigens enhances antigen-specific T cell and cDC1 infiltration into the tumors

To investigate whether the activated immune cells infiltrate into tumors, we immunized B16F10-OVA-bearing mice subcutaneously at the tail base on days 5 and 12, and collected tumors on day 13 (gating scheme in **Fig. S12**). VIPER + polySTING induced significantly higher levels of tumor-infiltrating T cells and antigen-specific $CD8^+$ T cells compared to VIPER (**Fig. 4A-C**). VIPER + free STING and VIPER-co-NPSTING also induced higher levels of antigen-specific $CD8^+$ T cell infiltration compared to VIPER, but were not statistically significant. The higher levels of T cell infiltration after VIPER + polySTING vaccination could be attributed to higher and more prolonged systemic distribution of STING agonist delivered from this formulation and its resultant IFNβ generation (**Fig. 2H**). Type I interferons such as IFNβ promote the production of chemokines like CXCL10,[45] which is critical for T cell infiltration into the tumor microenvironment.[46] We next investigated tumor-infiltrating dendritic cells as they are responsible for immune cell activation and recruitment.[47] All VIPER vaccine groups generated more tumor-infiltrating dendritic cells compared to the vehicle control (**Fig. 4D**). Additionally, VIPER + polySTING generated more tumor-infiltrating $CD8^+$ DCs than VIPER and VIPER-co-NPSTING generated more tumor-infiltrating $CD103^+$ DCs than VIPER (**Fig. 4E, F**). Both $CD8^+$ DCs and $CD103^+$ DCs belong to the conventional type 1 DCs (cDC1s) subset, which contributes to chemokine secretion, antigen cross-presentation and effector $CD8^+$ T cell recruitment in the tumor microenvironment, ultimately leading to antitumor immunity.[48] In summary, all STING-adjuvanted vaccine formulations increased cytotoxic T cell and dendritic cell recruitment into the tumor microenvironment. Of the three formulations, VIPER + polySTING provided the most robust increase in antigen-specific T cells in the tumor, while VIPER-co-NPSTING promoted the largest increase in cDC1s.

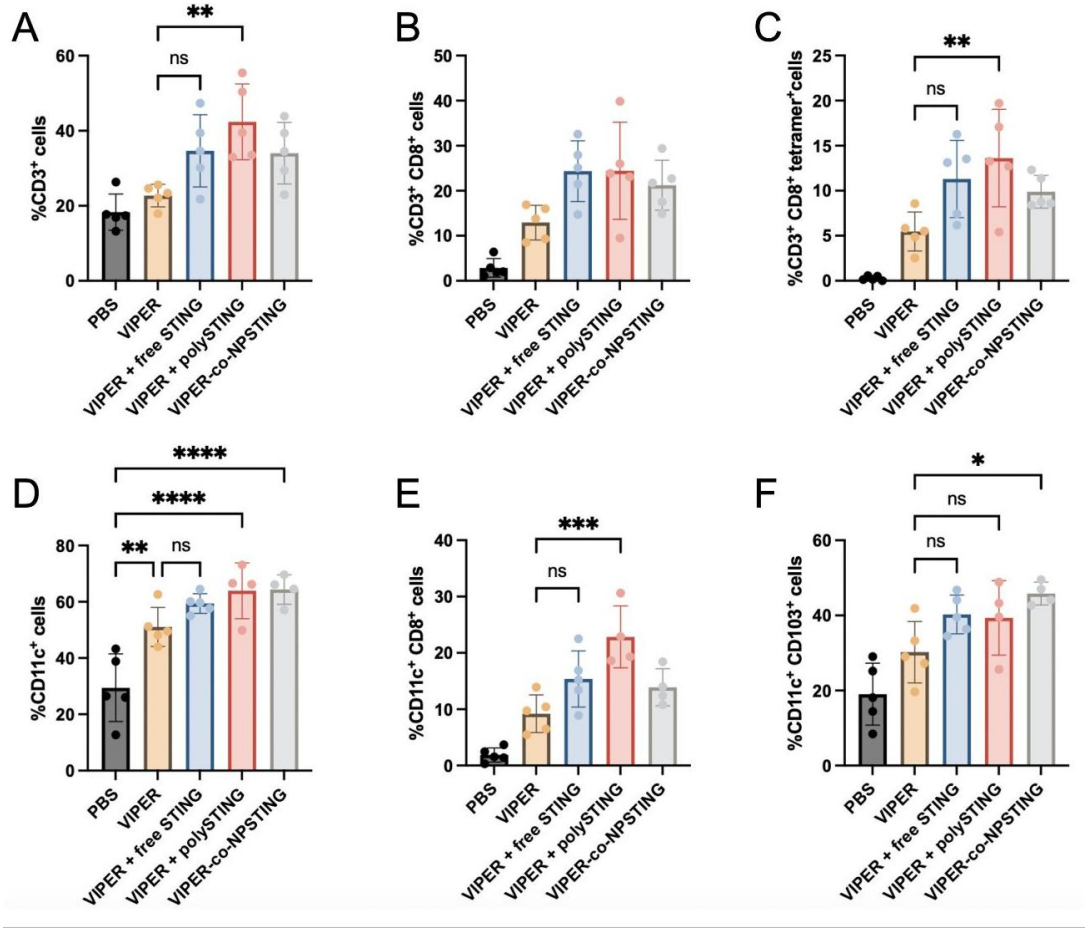

Figure 4. STING agonists induce T cell and cDC1 infiltration into the tumor. (A-F) Frequency of tumor-infiltrating immune cells among all live cells in the tumor. (A) Percentage of T cells in the tumor. (B) Percentage of $CD8^+$ T cells in the tumor. (C) Percentage of antigen-specific $CD8^+$ T cells in the tumor. (D) Percentage of DCs in the tumor. (E) Percentage of $CD8^+$ DCs in the tumor. (F) Percentage of $CD103^+$ DCs in the tumor (N=4-5). Data are represented as mean ± SD. Statistical analysis was performed using a one-way ANOVA with post hoc Tukey HSD test (*$p \leq 0.05$, **$p \leq 0.01$, ***$p \leq 0.001$, ****$p \leq 0.0001$, ns: not significant).

Polymeric co-delivery of peptide antigens and STING agonists demonstrated therapeutic efficacy in murine melanoma and colon cancer models

Finally, we evaluated the efficacy of STING-adjuvanted VIPER formulations in murine tumor models. We first investigated efficacy in the B16-OVA model, an aggressive melanoma model engineered to express the model OVA antigen that we have previously tested with VIPER[15]. C57BL/6 mice were inoculated with B16-OVA cells subcutaneously at the right hind flank on day 0 and were vaccinated three times every 7 days starting on day 4 (**Fig. 5A**). Consistent with our previous results,[15] VIPER suppressed tumor growth and extended survival compared to vehicle-treated groups. This therapeutic effect was enhanced by both polySTING and NPSTING, but was not affected by free STING agonist (**Fig. 5B-C**). Free STING agonists generated a similar level of antigen-specific $CD8^+$ T cells as the STING drugamers (**Fig. 3B**), but the magnitude of antigen-specific T cell response is not the sole predictor of therapeutic cancer vaccine treatment outcome. While there were no differences in tumor growth rate and survival between polySTING and NPSTING, the manner of NPSTING incorporation into VIPER impacted therapeutic efficacy. Specifically, co-micellizing NPSTING with VIPER (VIPER-co-NPSTING) resulted in slightly stronger tumor growth suppression and longer survival than a separate micelle formulation (VIPER + NPSTING) (**Fig. S13**). All these factors highlight the importance of using a polymeric platform to co-deliver antigens and STING agonists to dendritic cells.

We next evaluated the therapeutic outcome of the lead formulations, VIPER + polySTING and VIPER-co-NPSTING, in a neoantigen MC38 colorectal carcinoma model in combination with immune checkpoint inhibitors. VIPER was used to deliver Adpgk, a MHC-I neoantigen peptide discovered previously (polymer composition information in **Table S1**).[49] Mice were vaccinated three times starting on day 8, when tumors were palpable, and anti-PD-1 immune checkpoint inhibitor was given every three to four days via intraperitoneal injections (**Fig. 5D**). Both VIPER + polySTING and VIPER-co-NPSTING suppressed MC38 tumor growth and prolonged survival compared to the vehicle control (**Fig. 5E-F, S14**). Anti-PD-1 alone has minimum tumor growth inhibition, but achieved complete remission in 1/8 mice. Anti-PD-1 treatment further improved outcome after vaccination. Addition of anti-PD-1 slightly slowed tumor growth (**Fig. 5E**) and prolonged survival (**Fig. 5F**), with 2/7 of VIPER + polySTING treated mice and 1/8 of VIPER-co-NPSTING treated mice remaining tumor-free 150 days after tumor inoculation. All tumor-free mice demonstrated tumor rejection when rechallenged with MC38 tumor cells on the left hind flank on day 56, suggesting long-term tumor immunity.

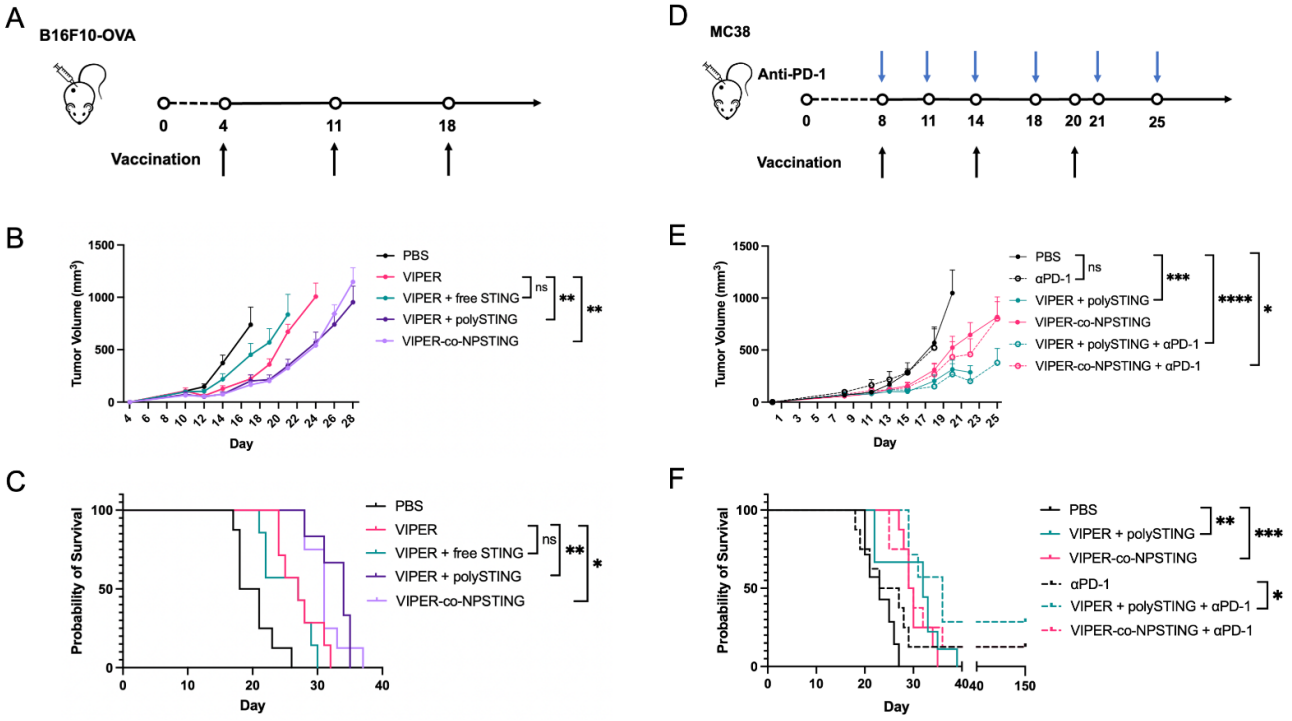

Figure 5. VIPER and the STING drugamer platform show antitumor effects in B16-OVA and MC38 tumor models. (A) Study timeline of the B16-OVA tumor reduction study. Mice were inoculated with B16-OVA cells on day 0 and vaccinated on days 4, 11 and 18. (B) B16-OVA tumor growth curves. Data are represented as the mean ± SEM (N = 6-8). Statistical analysis was performed using two-way ANOVA with Tukey's multiple comparisons test (**p ≤ 0.01, ns: no significance). (C) Kaplan–Meier survival curve (N = 6-8). Survival analysis was performed using the log-rank test (*p ≤ 0.05, **p ≤ 0.01, ns, no significance). (D) Study timeline of the MC38 tumor reduction study. Mice were inoculated with MC38 cells on day 0 and vaccinated on days 8, 14 and 20. Anti-PD-1 was given on days 8, 11, 14, 18, 21 and 25. (E) MC38 tumor growth curves. Data are represented as the mean ± SEM (N = 7-9). Statistical analysis was performed using two-way ANOVA with Tukey's multiple comparisons test (*p ≤ 0.05, ***p ≤ 0.001, ****p ≤ 0.0001, ns: no significance). (F) Kaplan–Meier survival curve (N = 7-9). Survival analysis was performed using the log-rank test (*p ≤ 0.05, **p ≤ 0.01, ***p ≤ 0.001).

iv. Discussion and conclusion

The expanding understanding of vaccinology and the STING pathway, as well as discoveries in novel STING agonists and nanotechnology delivery platforms, have resulted in an impressive number of preclinically efficacious cancer nano-vaccine candidates[26–30]. However, vast differences in agonist choice, route and timing of administration in combination with delivery vector heterogeneity[24] complicates direct comparison between reports, hampering generation of generalizable design rules. In this work, our drugamer platform permitted incorporation of a singular STING prodrug into distinct polymeric architectures that share common targeting and controlled-release properties. By combining these two drugamers with a singular antigen delivery platform, we are able to examine the effects of STING adjuvant structure on the resultant vaccine response.

The pharmacokinetics (PK) of STING agonist delivery to lymph nodes and plasma is improved by both polySTING and NPSTING compared to free STING agonist, resulting in elevated STING activation. Both drugamer treatments resulted in significantly elevated STING concentrations in the draining lymph nodes (LNs), consistent with our previous results utilizing mannnosylated polymers[14,37]. As a ~ 30-40 nm nanoparticle formulation, NPSTING offers the highest passive lymphatic drainage of all formulations[40] and showcases the pharmacological utility of dual active and passive targeting. LN STING concentrations from both drugamer treatments remained elevated during the course of the experiment, indicative of a continuous prodrug cleavage process[38]. Correspondingly, we observed elevated STING-related gene expression at post-acute phases (24h) for both drugamers compared to free drug, whose rapid clearance showed only an acute phase (4h) increase in STING-related gene expression. Prolonged immune activation has been reported with a nanoparticulate imidazoquinoline prodrug platform similar to the utilized drugamers[50]. Jinming Gao's group have reported on the benefits of combining acute and post-acute STING activation utilizing encapsulated canonical STING agonists and polyvalent weak STING binders[51], and here we report similar results with a targeted polymeric prodrug of a strong synthetic STING agonist. This STING activation profile, unique to both drugamers, correlates with their later therapeutic efficacy over the free drug.

The elevated STING concentrations in the LNs resulting from NPSTING treatment posed an early dose-limiting toxicity through cell viability, consistent with STING's ability to induce apoptosis[52]. A reduced NPSTING dosage (5-fold lower) improved VIPER's DC maturation to the same extent as polySTING, which could reflect NPSTING's increased potency in the LNs. PolySTING may have benefited from systemic IFNβ release, as interferons alone can induce DC maturation[53]. NPSTING also increased antigen cross-presenting DCs compared to VIPER alone and other STING adjuvants, which may represent the benefit of antigen-adjuvant co-delivery on a cellular level. While STING agonism improves antigen cross-presentation, it can also induce DC maturation before antigen acquisition, which negatively impacts antigen uptake and presentation downstream[54]. NPSTING co-micellization with antigen polymers can deliver both STING agonist and antigen through every internalization event, minimizing the penalties of STING pre-activation. Free STING adjuvant conferred no meaningful improvement to VIPER's DC response despite some acute-phase STING gene expression in the LNs, likely due to inefficient DC STING delivery as a non-targeted formulation.

NPSTING generated slightly more antigen-responsive $CD8^+$ T cells, while polySTING generated more tumor-infiltrating tumor-specific $CD8^+$ T cells as well as cross-presenting $CD8^+$ DCs. The respective correlation with their therapeutic benefit as adjuvants is notable, but more so is their correlation with pharmacokinetic properties. The superior LN and DC STING delivery of NPSTING likely resulted in superior T cell priming even at a 5-fold lower dose[55]. The systemic entry of polySTING may have allowed polySTING to act upon tumoral APCs, which can generate chemokines that promote tumor lymphocyte infiltration[37,56]. The induction of cross-presenting tumoral DCs, analogous to polySTING's activity as an intravenous immunotherapy, can also maintain intratumoral CTL activity[57–59]. PolySTING's multifactorial mechanism may underlie its arguably superior activity to NPSTING in the MC38 neoantigen model, though its severe systemic cytokine release may hint at potential toxicity mechanisms[60]. NPSTING exhibited comparable efficacy at a 5-fold lower dose (2 μg

vs. 10 μg in other groups), highlighting the utility of enhanced lymphatic targeting but also agreeing with reports on improved potency of nanoparticle-STING conjugates[61]. This improvement in potency can address dose-limiting STING agonist toxicity, a concern in clinical translation[24], but should be considered in conjunction with the earlier-reported localized cytotoxicity. However, the improved potency accompanied the earlier-reported localized cytotoxicity, which should not be discounted. Nevertheless, the unique vaccine responses from both drugamers and their downsides, traceable to the drugamers' PK profiles, highlight the capacity of different polymeric adjuvant structures to induce meaningful therapeutic responses through distinct mechanisms between systemic and localized stimulation. Further PK modulation of STING agonism guided by this work may advance vaccine efficacy of similar platforms beyond the partial responses observed here. Additionally, both drugamer-adjuvanted vaccine formulations resulted in durable antitumor immunity in surviving mice in the MC38 tumor model, achieving a key design goal in cancer vaccines. Future work may either combine different adjuvant structures to achieve an optimal local-systemic STING response, or tailor STING vaccine formulations to be specific to patients' individual immune susceptibility in accordance with cancer nanomedicine paradigms[62]. The former approach is mirrored in a recent report on superior therapeutic efficacy in a subcutaneous prime-intravenous boost (i.e. local prime, systemic boost) vaccination strategy with a TLR7/8a-adjuvanted peptide nanoparticle vaccine platform[63]. Additionally, the MC38 colon tumor cells were implanted subcutaneously for more accessible and reliable tracking of tumor growth, but they are usually less immunosuppressive compared to orthotopic tumor models[64]. Future studies may be conducted in orthotopic models like the 4T1 breast cancer model by introducing cells into the mammary fat pad[65].

It is surprising that free STING adjuvant improved VIPER's T cell response to a similar extent as the drugamers despite the lack of enhanced DC maturation, yet failed to improve VIPER's therapeutic response in orthotopic tumor models. It is more surprising considering that diamidobenzimidazole (diABZI) STING agonists were efficacious as a systemic immunotherapy[31], compared to clinically-tested cyclic dinucleotide (CDN) STING agonists (e.g. 2'3-cGAMP, ADU-S100)[66], at lower doses than synthetic non-CDN agonists (e.g. SR-717, MSA-2…)[67,68]. It is possible that free STING agonist administration did not result in sufficient LN STING concentrations for DC maturation, but can induce sufficient splenic STING concentrations for splenic T cell expansion - consistent with PK data showing detectable splenic STING 30 minutes after free STING administration. STING agonism in T cells can induce strong cytokine signaling, which can also expand existing antigen-specific T cells. However, it also leads to terminal T cell differentiation and apoptosis, which negatively impacts antitumor CTL activity[69]. This may explain free STING's lack of therapeutic efficacy. It is also possible that this is a T cell-independent effect. Immature DCs can be reprogrammed by circulating tumor cells into immunosuppressive TGFβ-generating myeloid cells,[70,71] which is consistent with the relative lack of DC maturation in free STING-adjuvanted groups. Additionally, the lack of therapeutic efficacy of the free STING adjuvant could be attributed to insufficient STING activation and pro-inflammatory cytokine secretion. These results indicate that pharmacological STING activation in LNs, magnitudinally and temporally, and in DCs better correlates with adjuvanted vaccine antitumor responses than T cell responses. Single-dose pharmacological activation and DC maturation studies are less time-consuming than T cell response studies after prime-boost, and our results indicate that they may be better suited for screening adjuvanted vaccine candidates. Nevertheless, considering that diABZI STING agonists have shown efficacy in other tumor models not utilized in this work[31], our results highlight the importance of incorporating STING agonists into drugamers in this context, especially considering the aggressive "immune-desert" B16-OVA model.

In conclusion, we developed and compared two structurally distinct STING drugamers as adjuvants to the VIPER peptide antigen delivery platform. Their unique pharmacokinetics profiles between the lymphatic and systemic compartments induced distinct vaccine response profiles that both resulted in superior antitumor efficacy over VIPER. The direct pharmacological-immunological comparison between the two drugamers provided insight into the benefits and drawbacks of targeted localized and systemic STING stimulation in cancer vaccination.

v. References

1. Xie, N. *et al.* Neoantigens: promising targets for cancer therapy. *Signal Transduct. Target. Ther.* **8**, 1–38 (2023).

2. Keskin, D. B. *et al.* Neoantigen vaccine generates intratumoral T cell responses in phase Ib glioblastoma trial. *Nature* **565**, 234–239 (2019).

3. Ott, P. A. *et al.* A Phase Ib Trial of Personalized Neoantigen Therapy Plus Anti-PD-1 in Patients with Advanced Melanoma, Non-small Cell Lung Cancer, or Bladder Cancer. *Cell* **183**, 347-362.e24 (2020).

4. Hu, Z. *et al.* Personal neoantigen vaccines induce persistent memory T cell responses and epitope spreading in patients with melanoma. *Nat. Med.* **27**, 515–525 (2021).

5. Niemi, J. V. L., Sokolov, A. V. & Schiöth, H. B. Neoantigen Vaccines; Clinical Trials, Classes, Indications, Adjuvants and Combinatorial Treatments. *Cancers* **14**, 5163 (2022).

6. Batista-Duharte, A., Hassouneh, F., Alvarez-Heredia, P., Pera, A. & Solana, R. Immune Checkpoint Inhibitors for Vaccine Improvements: Current Status and New Approaches. *Pharmaceutics* **14**, 1721 (2022).

7. Kerr, M. D., McBride, D. A., Chumber, A. K. & Shah, N. J. Combining therapeutic vaccines with chemo- and immunotherapies in the treatment of cancer. *Expert Opin. Drug Discov.* **16**, 89–99 (2021).

8. Cadena, A. *et al.* Radiation and Anti-Cancer Vaccines: A Winning Combination. *Vaccines* **6**, 9 (2018).

9. Hu, Z., Ott, P. A. & Wu, C. J. Towards personalized, tumour-specific, therapeutic vaccines for cancer. *Nat. Rev. Immunol.* **18**, 168–182 (2018).

10. Liu, W. *et al.* Peptide-based therapeutic cancer vaccine: Current trends in clinical application. *Cell Prolif.* **54**, e13025 (2021).

11. Mempel, T. R., Henrickson, S. E. & von Andrian, U. H. T-cell priming by dendritic cells in lymph nodes occurs in three distinct phases. *Nature* **427**, 154–159 (2004).

12. Acar, H., M. Ting, J., Srivastava, S., L. LaBelle, J. & V. Tirrell, M. Molecular engineering solutions for therapeutic peptide delivery. *Chem. Soc. Rev.* **46**, 6553–6569 (2017).

13. Joffre, O. P., Segura, E., Savina, A. & Amigorena, S. Cross-presentation by dendritic cells. *Nat. Rev. Immunol.* **12**, 557–569 (2012).

14. Lv, S. *et al.* Well-Defined Mannosylated Polymer for Peptide Vaccine Delivery with Enhanced Antitumor Immunity. *Adv. Healthc. Mater.* **11**, 2101651 (2022).

15. Song, K. *et al.* A mannosylated polymer with endosomal release properties for peptide antigen delivery. *J. Controlled Release* **356**, 232–241 (2023).

16. Khong, H. & Overwijk, W. W. Adjuvants for peptide-based cancer vaccines. *J. Immunother. Cancer* **4**, 56 (2016).

17. Lynn, G. M. *et al.* Peptide–TLR-7/8a conjugate vaccines chemically programmed for nanoparticle self-assembly enhance CD8 T-cell immunity to tumor antigens. *Nat. Biotechnol.* **38**, 320–332 (2020).

18. Van Herck, S., Feng, B. & Tang, L. Delivery of STING agonists for adjuvanting subunit vaccines. *Adv. Drug Deliv. Rev.* **179**, 114020 (2021).

19. Curtsinger, J. M. & Mescher, M. F. Inflammatory cytokines as a third signal for T cell activation. *Curr. Opin. Immunol.* **22**, 333–340 (2010).

20. Li, G. *et al.* cGAS-STING pathway mediates activation of dendritic cell sensing of immunogenic tumors. *Cell. Mol. Life Sci.* **81**, 149 (2024).

21. Oh, Y. M. *et al.* Ndrg1 is a T-cell clonal anergy factor negatively regulated by CD28 costimulation and interleukin-2. *Nat. Commun.* **6**, 8698 (2015).

22. Vatner, R. E. & Janssen, E. M. STING, DCs and the link between innate and adaptive tumor immunity. *Mol. Immunol.* **110**, 13–23 (2019).

23. Motedayen Aval, L., Pease, J. E., Sharma, R. & Pinato, D. J. Challenges and Opportunities in the Clinical Development of STING Agonists for Cancer Immunotherapy. *J. Clin. Med.* **9**, 3323 (2020).

24. Garland, K. M., Sheehy, T. L. & Wilson, J. T. Chemical and Biomolecular Strategies for STING Pathway Activation in Cancer Immunotherapy. *Chem. Rev.* **122**, 5977–6039 (2022).

25. Larkin, B. *et al.* Cutting Edge: Activation of STING in T Cells Induces Type I IFN Responses and Cell Death. *J. Immunol.* **199**, 397–402 (2017).

26. Shae, D. *et al.* Co-delivery of Peptide Neoantigens and Stimulator of Interferon Genes Agonists Enhances Response to Cancer Vaccines. *ACS Nano* **14**, 9904–9916 (2020).

27. Luo, M. *et al.* A STING-activating nanovaccine for cancer immunotherapy. *Nat. Nanotechnol.* **12**, 648–654 (2017).

28. Baljon, J. J. *et al.* A Cancer Nanovaccine for Co-Delivery of Peptide Neoantigens and Optimized Combinations of STING and TLR4 Agonists. *ACS Nano* **18**, 6845–6862 (2024).

29. Sun, X. *et al.* Self-Assembled STING-Activating Coordination Nanoparticles for Cancer Immunotherapy and Vaccine Applications. *ACS Nano* **18**, 10439–10453 (2024).

30. Dane, E. L. *et al.* STING agonist delivery by tumour-penetrating PEG-lipid nanodiscs primes robust anticancer immunity. *Nat. Mater.* **21**, 710–720 (2022).

31. Ramanjulu, J. M. *et al.* Design of amidobenzimidazole STING receptor agonists with systemic activity. *Nature* **564**, 439–443 (2018).

32. Jeffrey, S. C. *et al.* Dipeptide-based highly potent doxorubicin antibody conjugates. *Bioorg. Med. Chem. Lett.* **16**, 358–362 (2006).

33. Shen, Y. & Li, X. Cathepsin B as a target in cancer therapy and imaging. *New J. Chem.* **46**, 19593–19611 (2022).

34. Dubowchik, G. M. *et al.* Cathepsin B-Labile Dipeptide Linkers for Lysosomal Release of Doxorubicin from Internalizing Immunoconjugates: Model Studies of Enzymatic Drug Release and Antigen-Specific In Vitro Anticancer Activity. *Bioconjug. Chem.* **13**, 855–869 (2002).

35. Salomon, P. L. *et al.* Optimizing Lysosomal Activation of Antibody–Drug Conjugates (ADCs) by Incorporation of Novel Cleavable Dipeptide Linkers. *Mol. Pharm.* **16**, 4817–4825 (2019).

36. Su, F.-Y. *et al.* Macrophage-targeted drugamers with enzyme-cleavable linkers deliver high intracellular drug dosing and sustained drug pharmacokinetics against alveolar pulmonary infections. *J. Controlled Release* **287**, 1–11 (2018).

37. Nguyen, D. C. *et al.* Mannosylated STING Agonist Drugamers for Dendritic Cell-Mediated Cancer Immunotherapy. *ACS Cent. Sci.* (2024) doi:10.1021/acscentsci.3c01310.

38. Chavas, T. E. J. *et al.* A macrophage-targeted platform for extending drug dosing with polymer prodrugs for pulmonary infection prophylaxis. *J. Controlled Release* **330**, 284–292 (2021).

39. Xu, Y., Chen, C., Liao, Z. & Xu, P. cGAS-STING signaling in cell death: Mechanisms of action and implications in pathologies. *Eur. J. Immunol.* **53**, 2350386 (2023).

40. Bachmann, M. F. & Jennings, G. T. Vaccine delivery: a matter of size, geometry, kinetics and molecular patterns. *Nat. Rev. Immunol.* **10**, 787–796 (2010).

41. Barber, G. N. STING: infection, inflammation and cancer. *Nat. Rev. Immunol.* **15**, 760–770 (2015).

42. Durgeau, A., Virk, Y., Corgnac, S. & Mami-Chouaib, F. Recent Advances in Targeting CD8 T-Cell Immunity for More Effective Cancer Immunotherapy. *Front. Immunol.* **9**, (2018).

43. Zumerle, S., Molon, B. & Viola, A. Membrane Rafts in T Cell Activation: A Spotlight on CD28 Costimulation. *Front. Immunol.* **8**, (2017).

44. Chen, Q., Sun, L. & Chen, Z. J. Regulation and function of the cGAS–STING pathway of cytosolic DNA sensing. *Nat. Immunol.* **17**, 1142–1149 (2016).

45. Makuch, E., Jasyk, I., Kula, A., Lipiński, T. & Siednienko, J. IFNβ-Induced CXCL10 Chemokine Expression Is Regulated by Pellino3 Ligase in Monocytes and Macrophages. *Int. J. Mol. Sci.* **23**, 14915 (2022).

46. Reschke, R. & Gajewski, T. F. CXCL9 and CXCL10 bring the heat to tumors. *Sci. Immunol.* **7**, eabq6509 (2022).

47. Janco, J. M. T., Lamichhane, P., Karyampudi, L. & Knutson, K. L. TUMOR-INFILTRATING DENDRITIC CELLS IN CANCER PATHOGENESIS1. *J. Immunol. Baltim. Md 1950* **194**, 2985–2991 (2015).

48. Böttcher, J. P. & Reis e Sousa, C. The Role of Type 1 Conventional Dendritic Cells in Cancer Immunity. *Trends Cancer* **4**, 784–792 (2018).

49. Yadav, M. *et al.* Predicting immunogenic tumour mutations by combining mass spectrometry and exome sequencing. *Nature* **515**, 572–576 (2014).

50. Wang, B. *et al.* Potent and Prolonged Innate Immune Activation by Enzyme-Responsive Imidazoquinoline TLR7/8 Agonist Prodrug Vesicles. *J. Am. Chem. Soc.* **142**, 12133–12139 (2020).

51. Li, S. *et al.* Prolonged activation of innate immune pathways by a polyvalent STING agonist. *Nat. Biomed. Eng.* **5**, 455–466 (2021).

52. Liu, S. & Guan, W. STING Signaling Promotes Apoptosis, Necrosis, and Cell Death: An Overview and Update. *Mediators Inflamm.* **2018**, 1202797 (2018).

53. Audsley, K. M. *et al.* IFNβ Is a Potent Adjuvant for Cancer Vaccination Strategies. *Front. Immunol.* **12**, (2021).

54. Wilson, N. S. *et al.* Systemic activation of dendritic cells by Toll-like receptor ligands or malaria infection impairs cross-presentation and antiviral immunity. *Nat. Immunol.* **7**, 165–172 (2006).

55. Jneid, B. *et al.* Selective STING stimulation in dendritic cells primes antitumor T cell responses. *Sci. Immunol.* **8**, eabn6612 (2023).

56. Woo, S.-R., Corrales, L. & Gajewski, T. F. The STING pathway and the T cell-inflamed tumor microenvironment. *Trends Immunol.* **36**, 250–256 (2015).

57. Hildner, K. *et al.* Batf3 Deficiency Reveals a Critical Role for CD8α+ Dendritic Cells in Cytotoxic T Cell Immunity. *Science* **322**, 1097–1100 (2008).

58. den Haan, J. M. M., Lehar, S. M. & Bevan, M. J. Cd8+ but Not Cd8− Dendritic Cells Cross-Prime Cytotoxic T Cells in Vivo. *J. Exp. Med.* **192**, 1685–1696 (2000).

59. Mellman, I., Chen, D. S., Powles, T. & Turley, S. J. The cancer-immunity cycle: Indication, genotype, and immunotype. *Immunity* **56**, 2188–2205 (2023).

60. Kitamura, H. *et al.* Long Peptide Vaccination Can Lead to Lethality through CD4+ T Cell-Mediated Cytokine Storm. *J. Immunol.* **185**, 892–901 (2010).

61. Dosta, P. *et al.* Investigation of the enhanced antitumour potency of STING agonist after conjugation to polymer nanoparticles. *Nat. Nanotechnol.* 1–13 (2023) doi:10.1038/s41565-023-01447-7.

62. van der Meel, R. *et al.* Smart cancer nanomedicine. *Nat. Nanotechnol.* **14**, 1007–1017 (2019).

63. Baharom, F. *et al.* Intravenous nanoparticle vaccination generates stem-like TCF1+ neoantigen-specific CD8+ T cells. *Nat. Immunol.* **22**, 41–52 (2021).

64. Guerin, M. V., Finisguerra, V., Van den Eynde, B. J., Bercovici, N. & Trautmann, A. Preclinical murine tumor models: A structural and functional perspective. *eLife* **9**, e50740.

65. Pillar, N., Polsky, A. L., Weissglas-Volkov, D. & Shomron, N. Comparison of breast cancer metastasis models reveals a possible mechanism of tumor aggressiveness. *Cell Death Dis.* **9**, 1–11 (2018).

66. Wehbe, M. *et al.* Nanoparticle delivery improves the pharmacokinetic properties of cyclic dinucleotide STING agonists to open a therapeutic window for intravenous administration. *J. Controlled Release* **330**, 1118–1129 (2021).

67. Chin, E. N. *et al.* Antitumor activity of a systemic STING-activating non-nucleotide cGAMP mimetic. *Science* **369**, 993–999 (2020).

68. Pan, B.-S. *et al.* An orally available non-nucleotide STING agonist with antitumor activity. *Science* **369**, (2020).

69. Larkin, B. *et al.* Cutting Edge: Activation of STING in T Cells Induces Type I IFN Responses and Cell Death. *J. Immunol.* **199**, 397–402 (2017).

70. Ghiringhelli, F. *et al.* Tumor cells convert immature myeloid dendritic cells into TGF-β–secreting cells inducing CD4+CD25+ regulatory T cell proliferation. *J. Exp. Med.* **202**, 919–929 (2005).

71. Kim, R., Emi, M. & Tanabe, K. Functional roles of immature dendritic cells in impaired immunity of solid tumour and their targeted strategies for provoking tumour immunity. *Clin. Exp. Immunol.* **146**, 189–196 (2006).

vi. Supporting Information

Table S1. Compositional information for polymers used.

Name	Description	Mn (kDa)	# Mannose per polymer	# peptides or STING per polymer	Wt% peptide or STING
OVA1	Ovalbumin MHC1 epitope polymer conjugate	24.5	42	1.7 peptides/polymer	8.8%
OVA2	Ovalbumin MHC2 epitope polymer conjugate	29.4	42	3.4 peptides/polymer	23.7%
VIPER-NR	Endosomolytic D-melittin polymer conjugate	25.2	42	1.4 peptides/polymer	12.5%
polySTING	Soluble STING drugamer	12	35	2.4 STING/polymer	9.8%
NP-STING	Self-assembling STING drugamer	24.1	50	1.8 STING/polymer	6.9%
Adgpk	MC38 neoantigen conjugate	28.1	42	4.2 peptides/polymer	20.1%

Table S2. Pharmacokinetics characterization of free STING agonist at 30 minutes post-administration

Mouse	1	2	3
ng/mL plasma	2.38	3.28	< LLOQ
ng/g lymph nodes	<LLOQ	<LLOQ	<LLOQ
ng/g spleen	3.77	2.87	3.34
ng/g liver	5.08	<LLOQ	<LLOQ

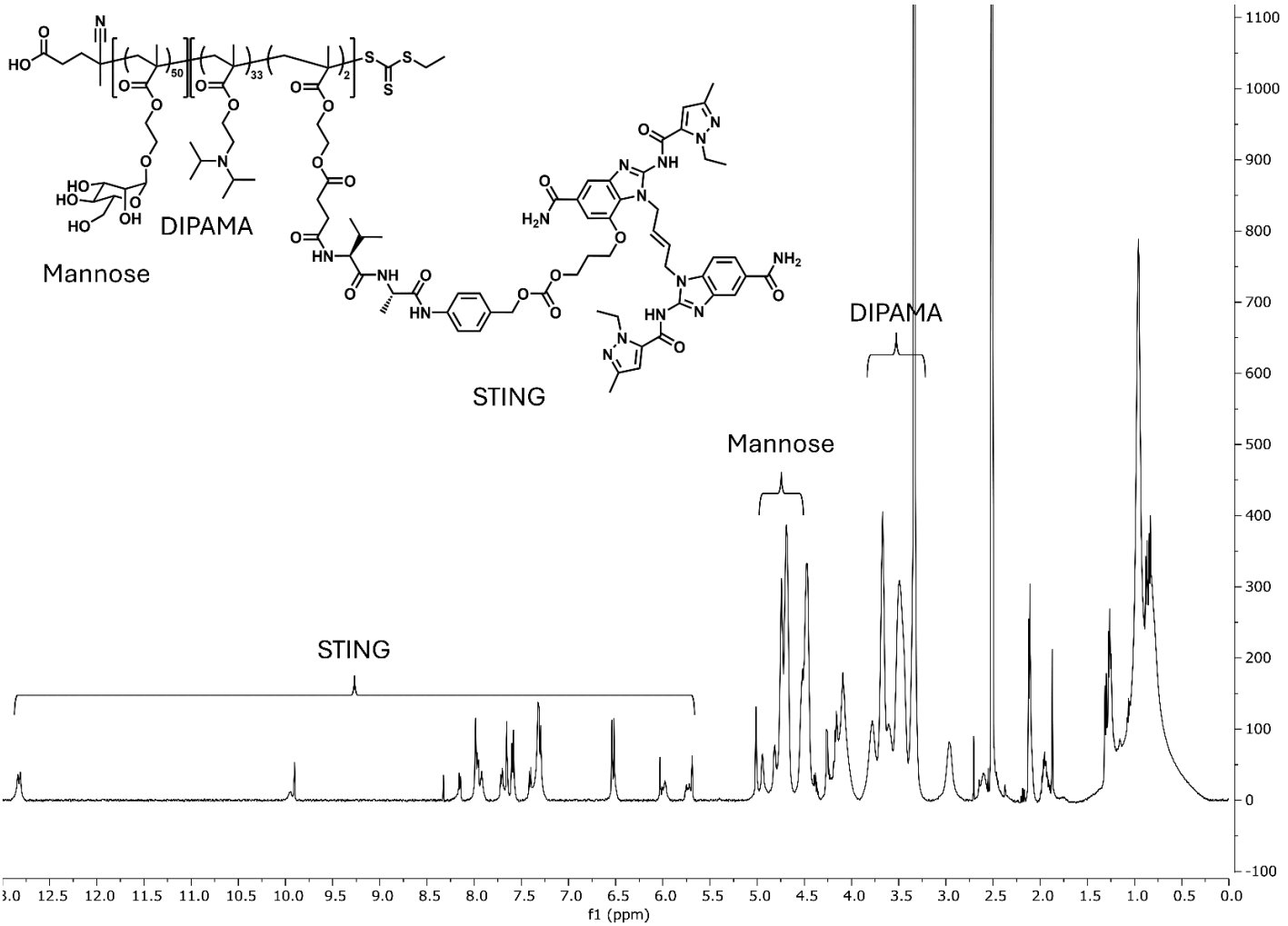

Figure S1. ^{1}H-NMR spectrum of NP-STING.

NMR spectra of VIPER polymers and polySTING have been previously reported[1,2].

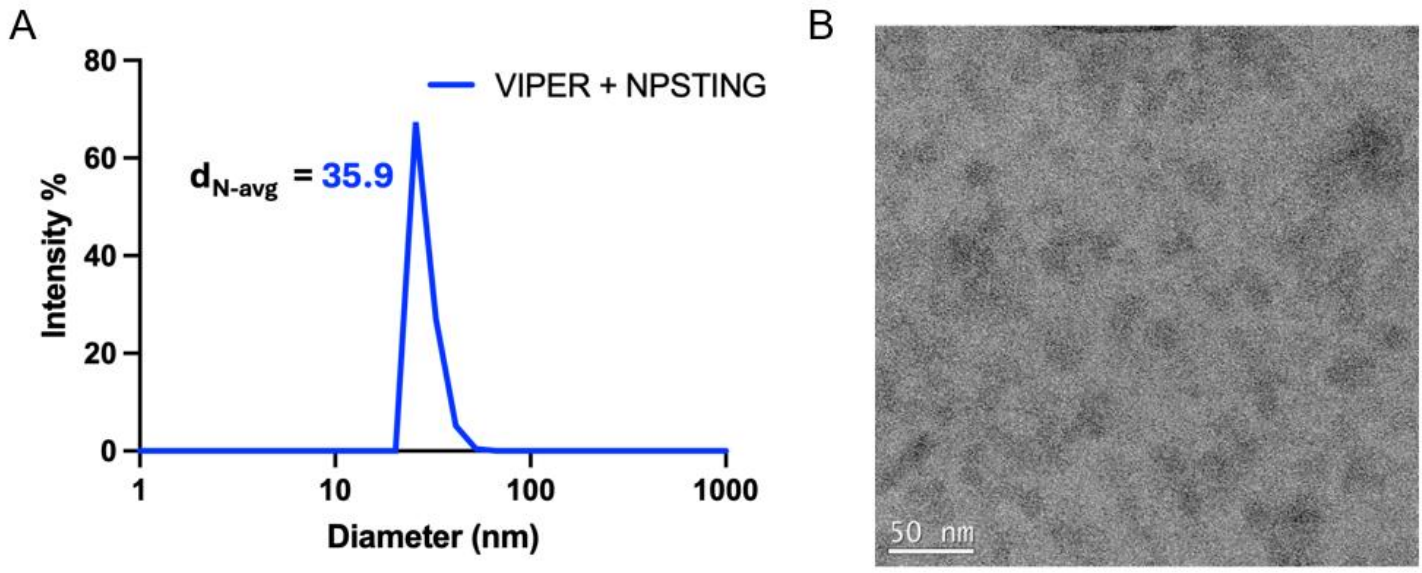

Figure S2. Characterization of VIPER micelles admixed with NPSTING micelles

(A) DLS characterization of VIPER + NPSTING (B) TEM micrograph of VIPER + NPSTING

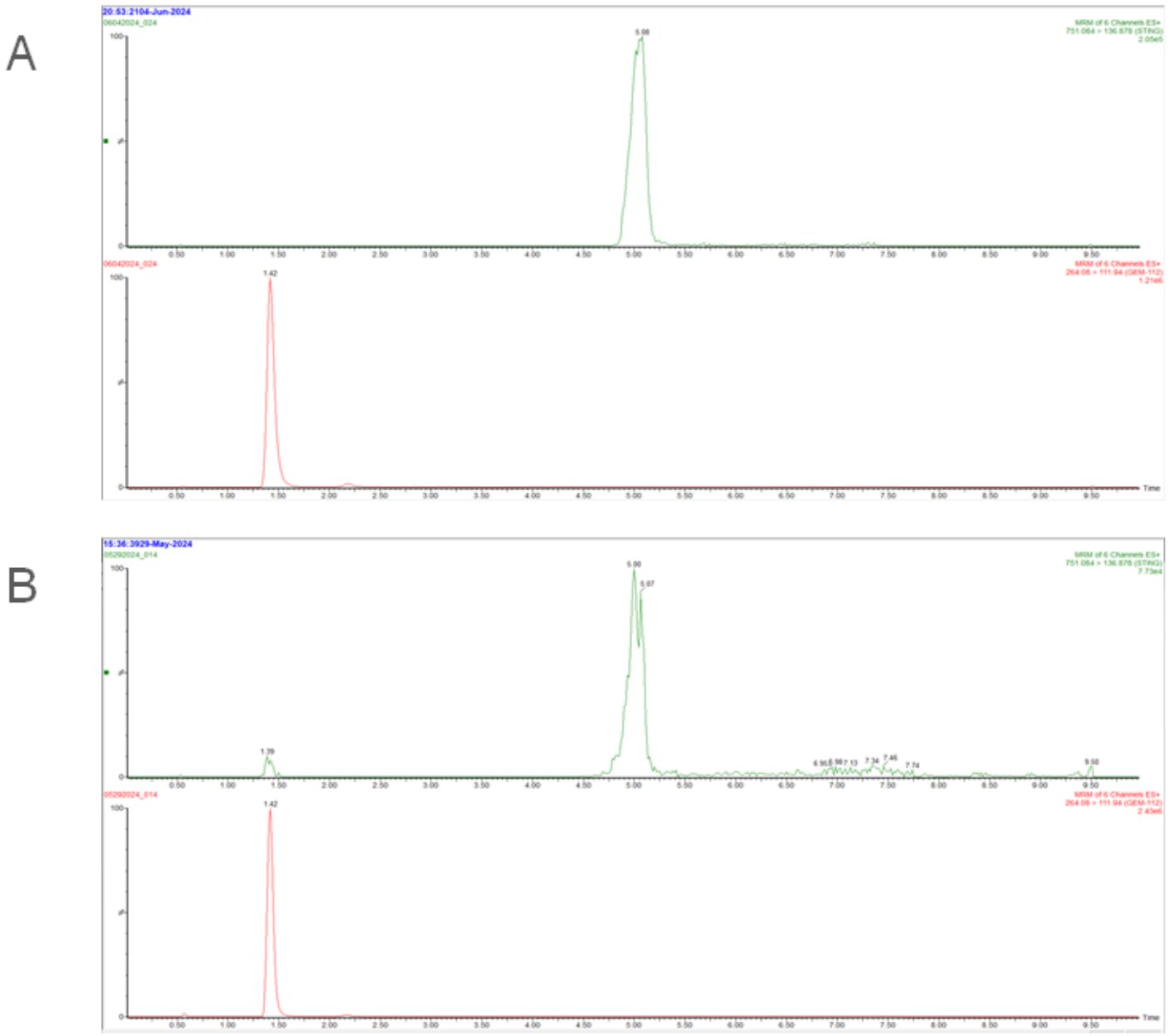

Figure S3. Sample LC/MS chromatograms

Green trace: STING-137 daughter ion for STING quantification. Red trace: Gemcitabine-112 daughter ion for internal standard quantification. (A) Representative LC/MS chromatogram of a calibrator (4000 ng/g lymph node shown). (B) Representative LC/MS chromatogram of a study sample (polySTING lymph node, 1h).

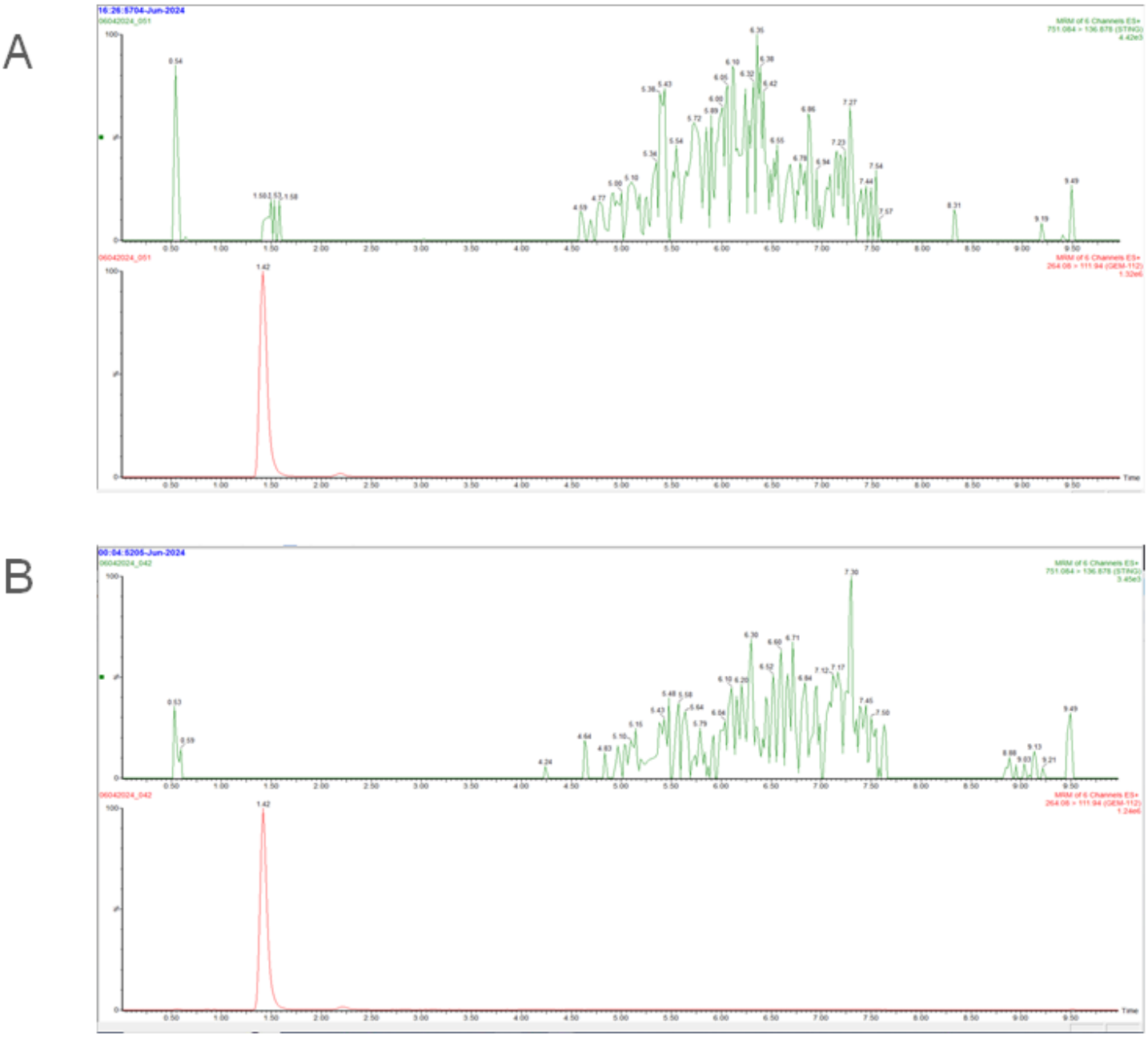

Figure S4. LC/MS method does not detect STING in polymeric prodrug form.

Green trace: STING-137 daughter ion for STING quantification. Red trace: Gemcitabine-112 daughter ion for internal standard quantification. (A) Chromatogram of blank plasma with internal standard. (B) Chromatogram of plasma spiked with polySTING at 1000 ng STING/mL plasma, with internal standard. Identical results were obtained with NPSTING.

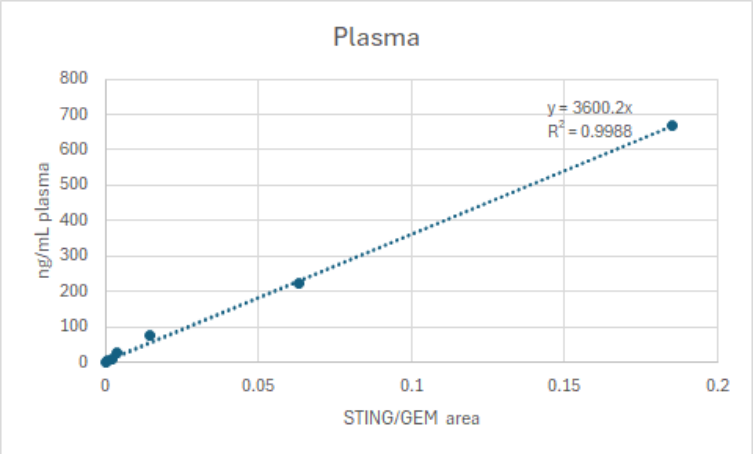

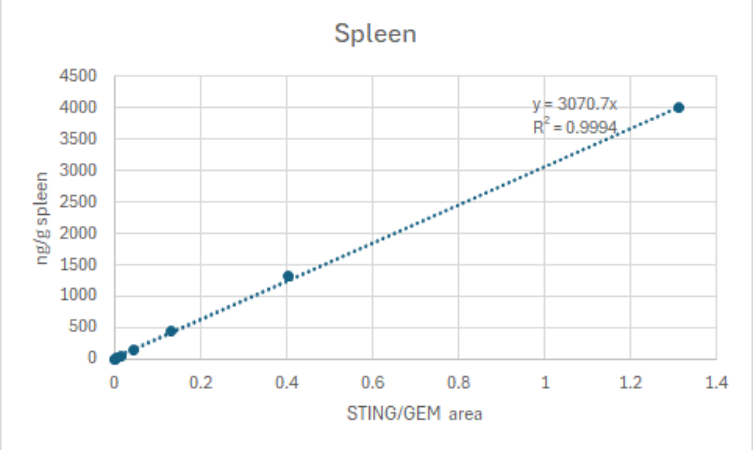

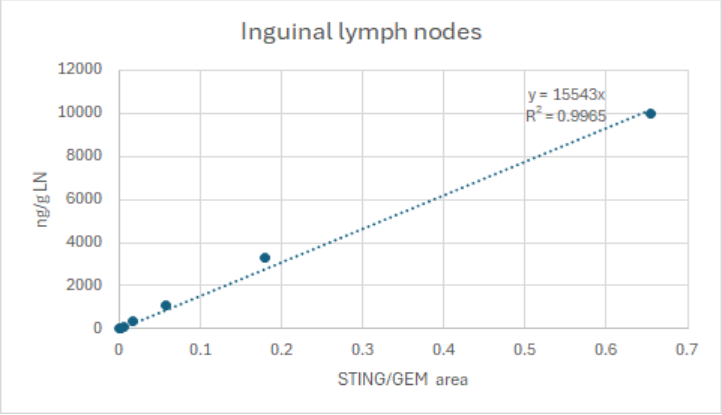

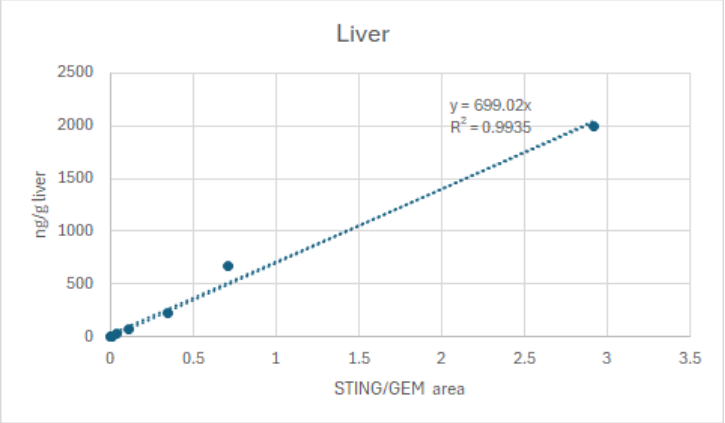

Figure S5. Representative LC/MS calibration curves for the pharmacokinetics study

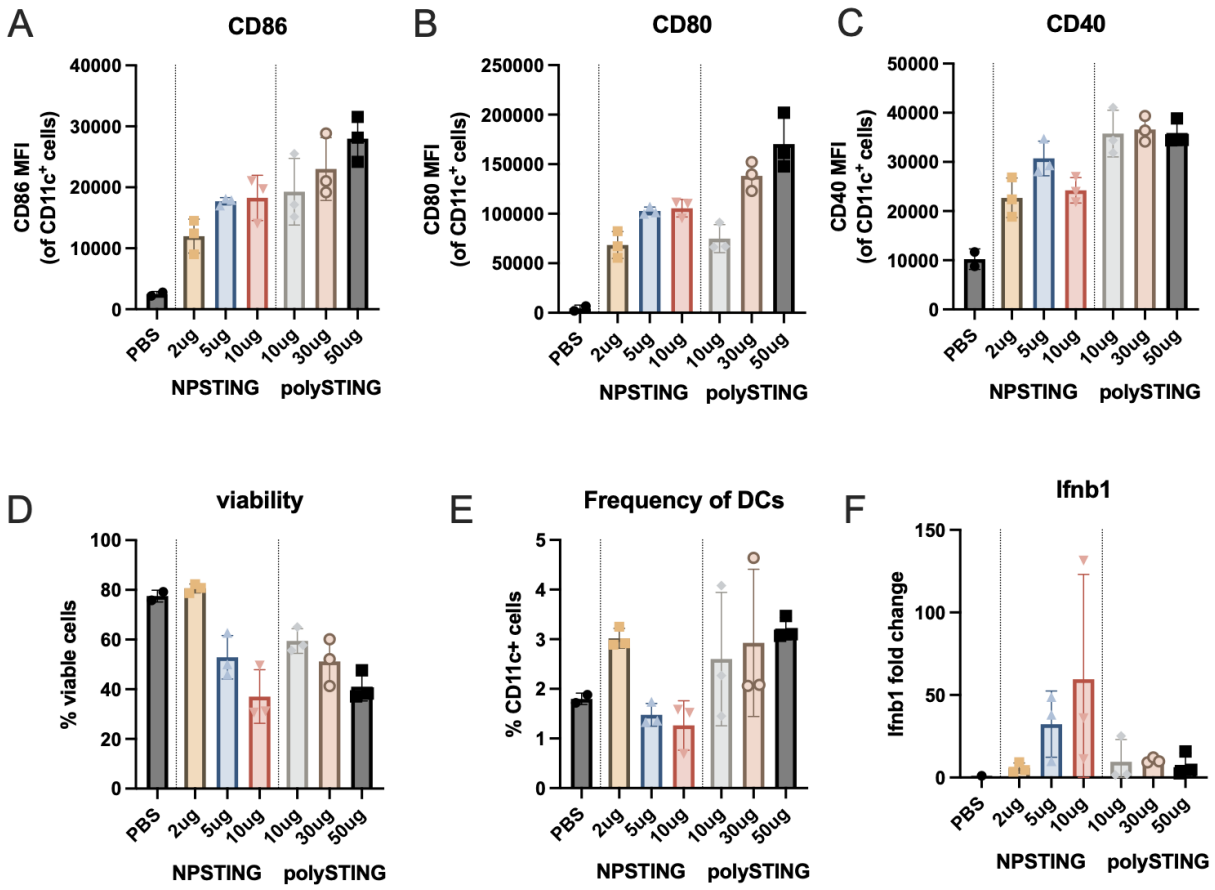

Figure S6. NPSTING and polySTING dose response.

(A-C) Costimulatory molecule CD86, CD80 and CD40 expression in $CD11c^+$ cells in inguinal lymph nodes 24 h after vaccination. (D) Percentage of live cells in the inguinal lymph nodes determined by flow cytometry. (E) Percentage of $CD11c^+$ cells in the inguinal lymph nodes. (F) IFNB1 expression normalized to GAPDH housekeeping gene in inguinal lymph nodes by RT-qPCR. Data are represented as the mean ± SD.

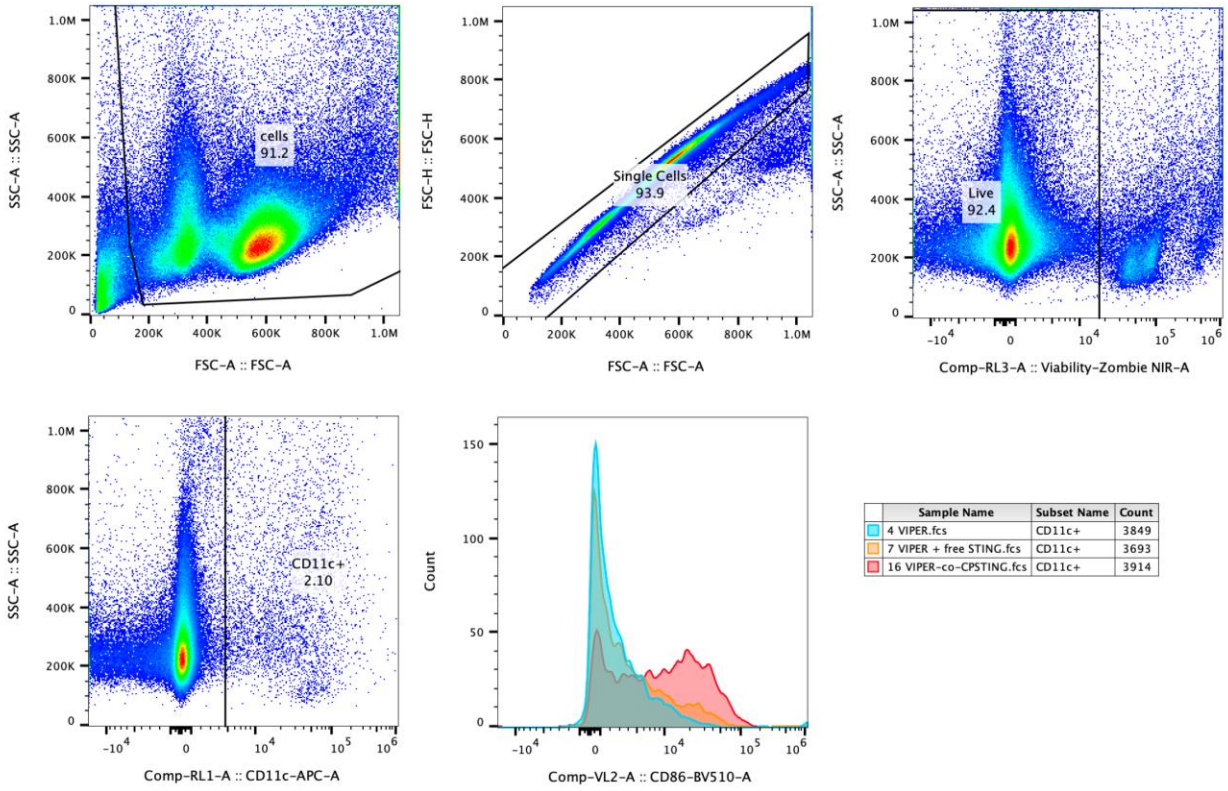

Figure S7. Flow cytometry gating for in vivo dendritic cell maturation study.

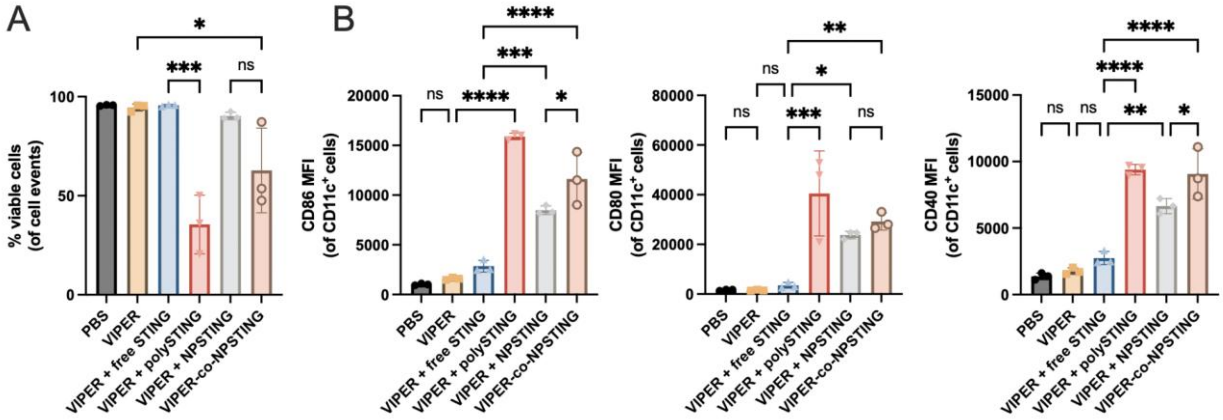

Figure S8. *In vivo* dendritic cell activation

(A) Percentage of live cells in the iLNs 24 h after treatment. (B-D) Costimulatory molecule CD86, CD80 and CD40 expression in $CD11c^+$ cells in iLNs 24 h after vaccination (N=3). Data are represented as mean ± SD. Statistical analysis was performed using a one-way ANOVA with posthoc Tukey HSD test (*$p \leq 0.05$, **$p \leq 0.01$, ***$p \leq 0.001$, ****$p \leq 0.0001$ ns: not significant).

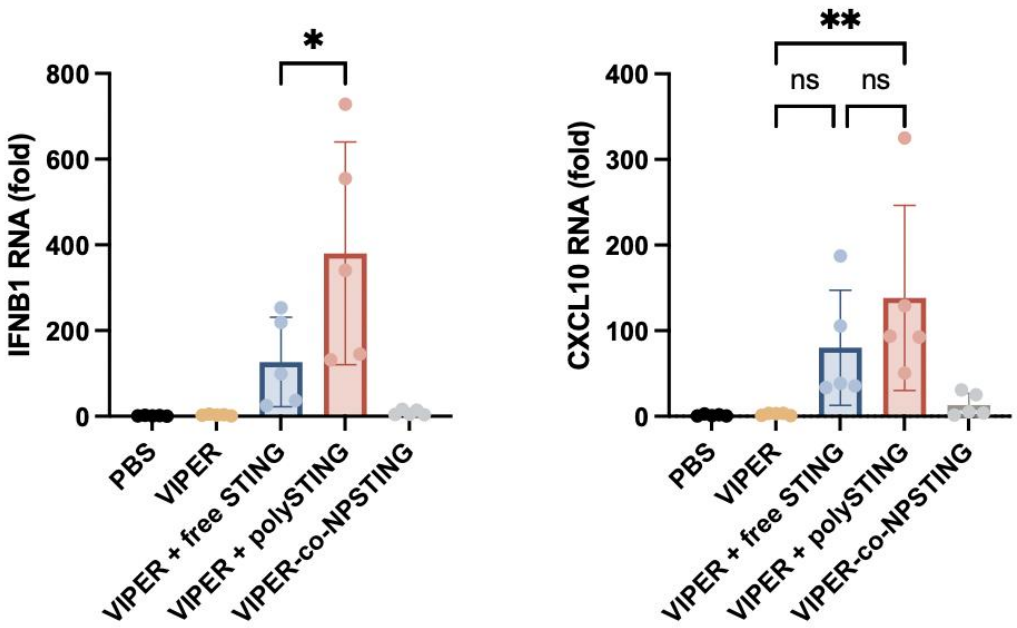

Figure S9. Interferon-stimulated gene expression in iLNs 4 h after vaccination

iLNs were collected 4 h after vaccination. IFNB1 and CXCL10 expression were quantified using RT-qPCR and normalized to the GAPDH housekeeping gene (N=5). Data are represented as mean ± SD. Statistical analysis was performed using a one-way ANOVA with posthoc Tukey HSD test (*$p \leq 0.05$, **$p \leq 0.01$, ns: not significant).

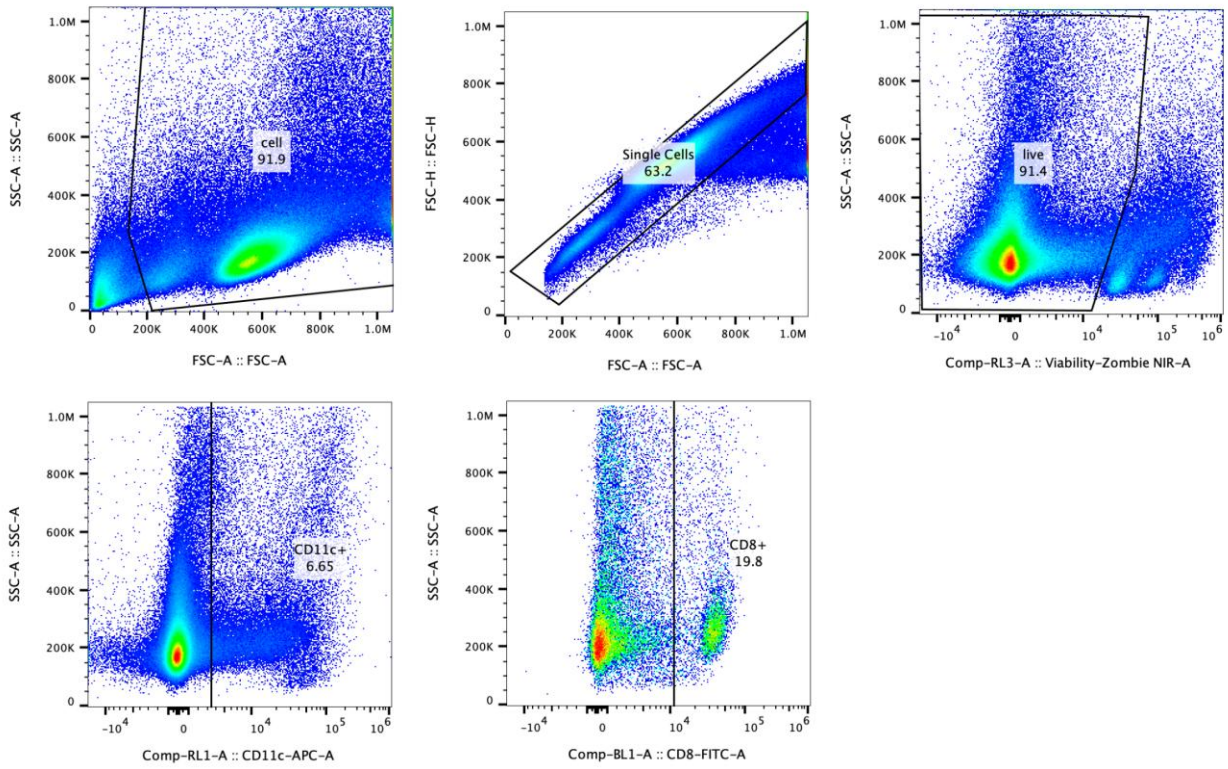

Figure S10. Flow cytometry gating for in vivo cross-presenting dendritic cell study.

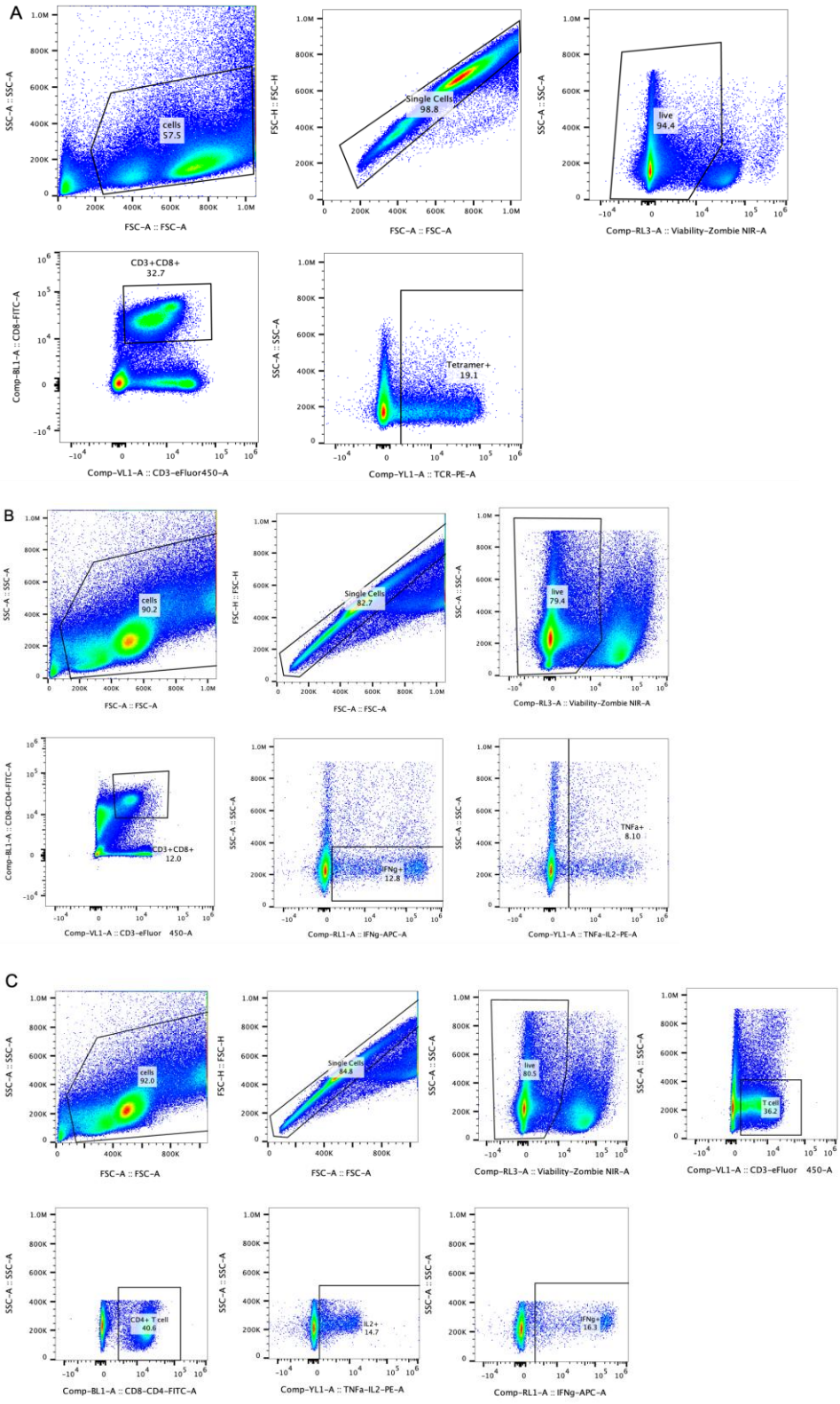

Figure S11. Flow cytometry gating for in vivo T cell activation study.

(A) Flow cytometry gating for antigen-specific $CD8^+$ T cells. (B) Flow cytometry gating for cytokine-producing $CD8^+$ T cells after antigen restimulation analyzed with intracellular cytokine staining. (C) Flow cytometry gating for cytokine-producing $CD4^+$ T cells after antigen restimulation analyzed with intracellular cytokine staining.

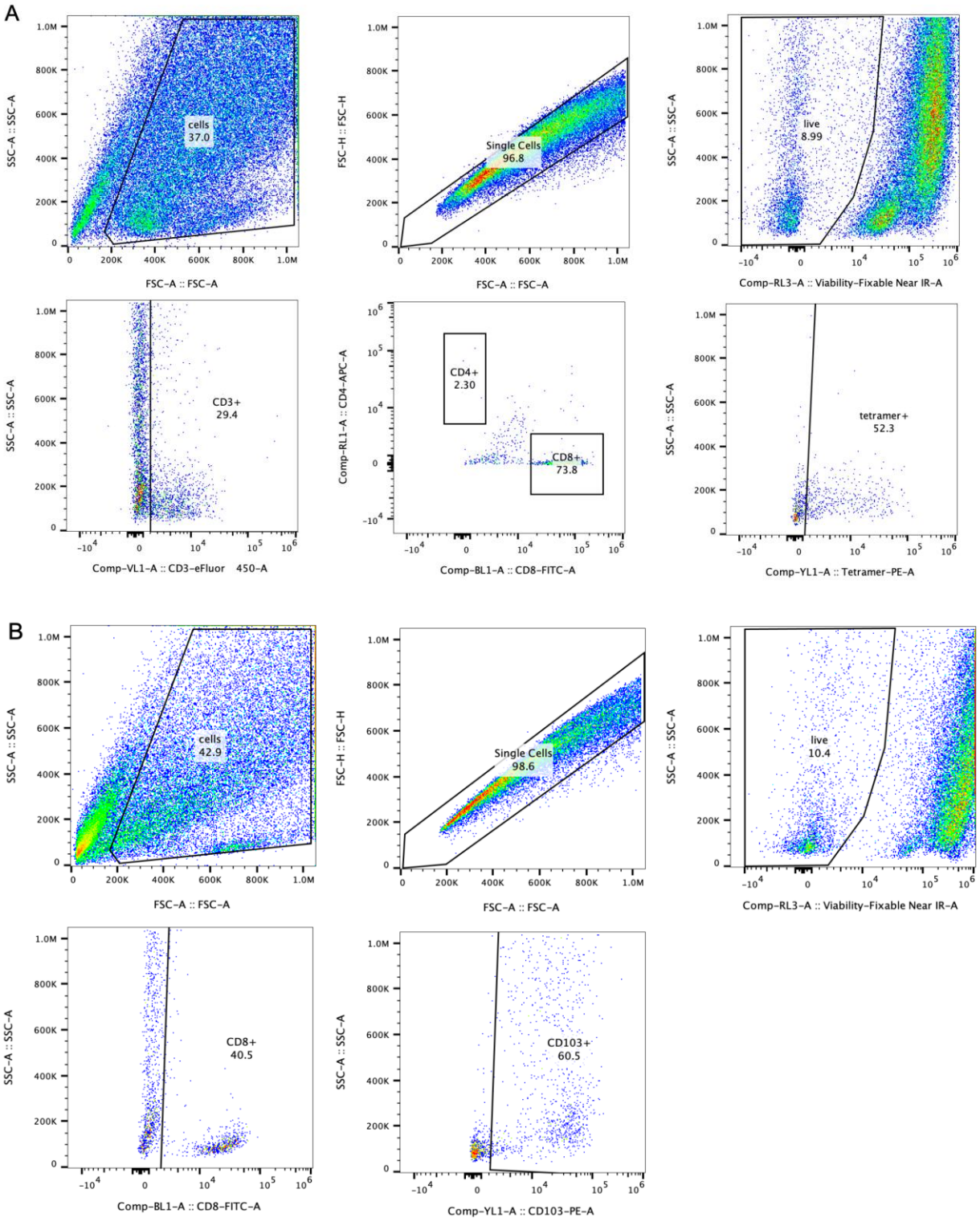

Figure S12. Flow cytometry gating for tumor-infiltrating lymphocytes.

(A) Flow cytometry gating for antigen-specific $CD8^+$ T cells. (B) Flow cytometry gating for $CD8^+$ DCs and $CD103^+$ DCs.

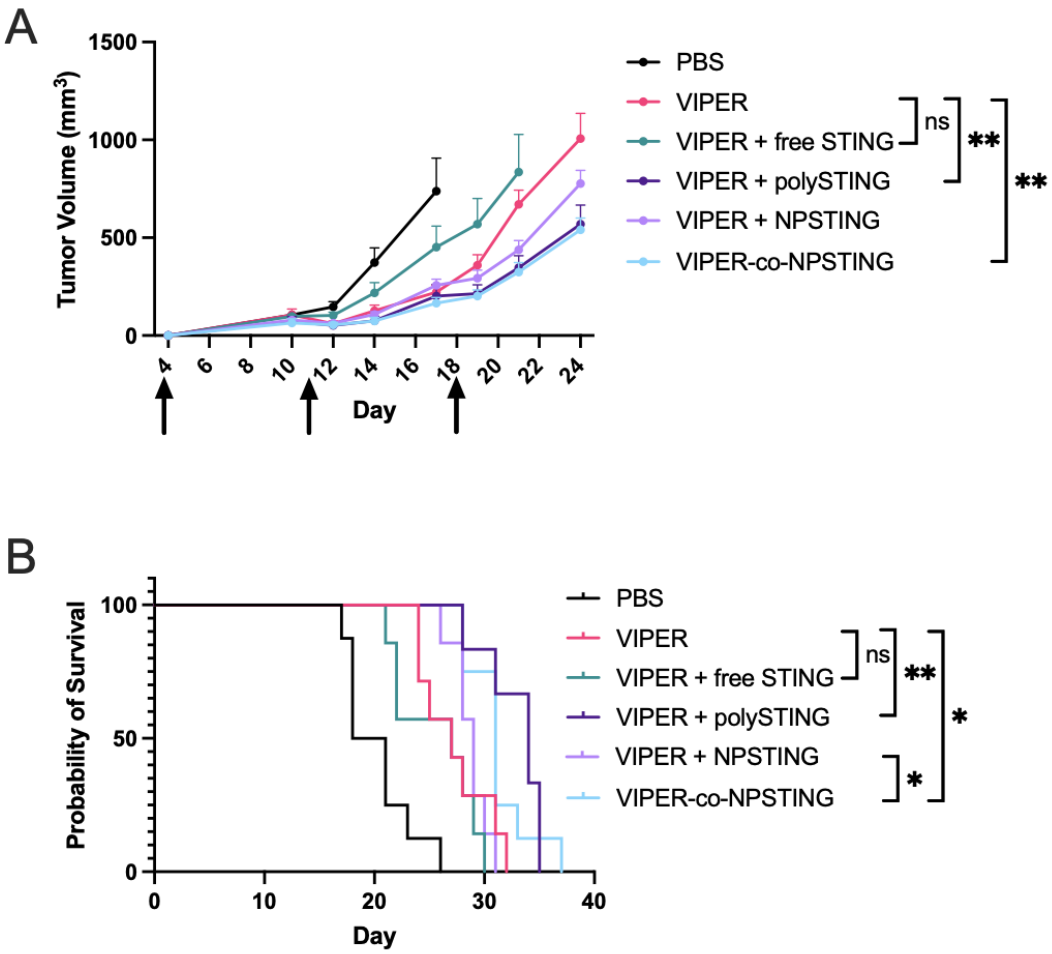

Figure S13. B16-OVA tumor reduction study with admixed and co-micellized NP-STING

(A) Tumor growth curve. Mice were inoculated with B16-OVA cells on day 0 and immunized on days 4, 11 and 18. Statistical analysis was performed using two-way ANOVA with Tukey's multiple comparisons test (**p ≤ 0.01, ns: not significant). (B) Kaplan–Meier survival curve (N = 6-8). Survival analysis was performed using the log-rank test (*p ≤ 0.05, **p ≤ 0.01, ns: not significant).

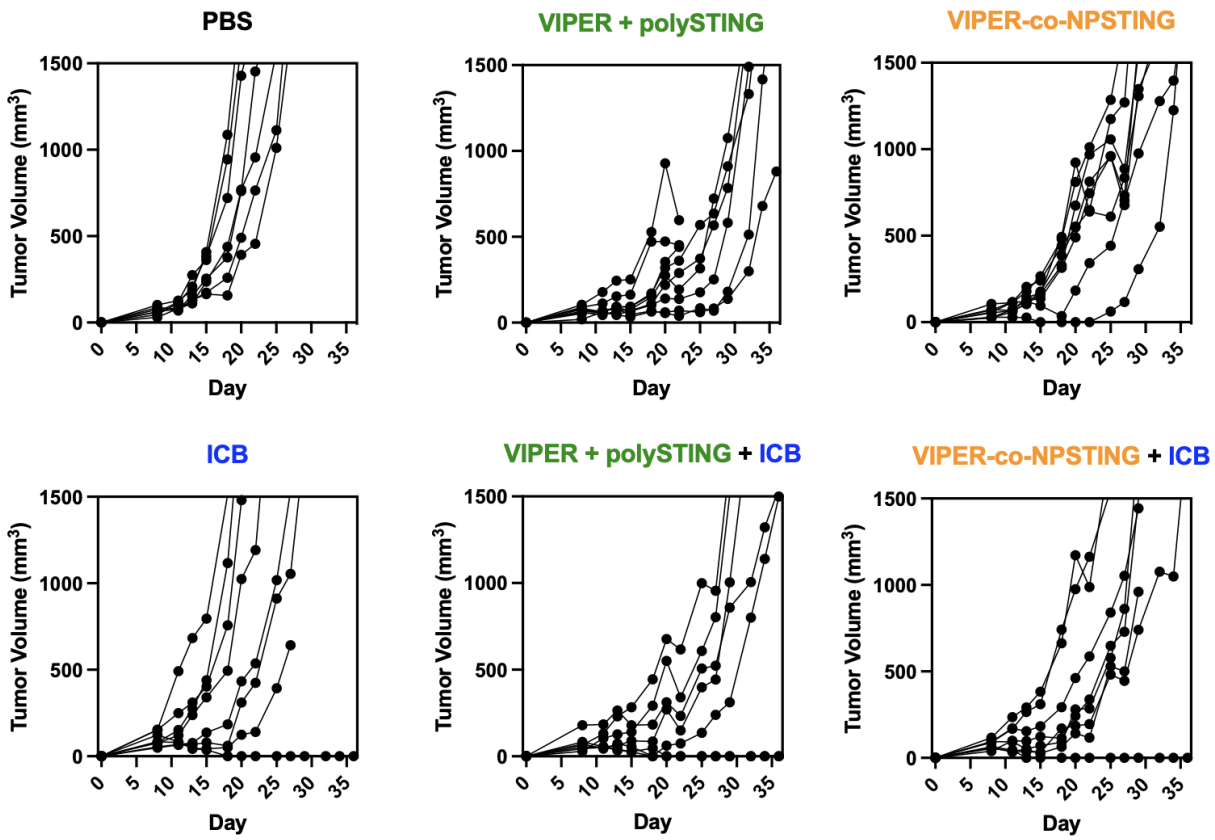

Figure S14. Individual MC38 tumor growth curves

Chapter 5. Cationic Bottlebrush Polymers Functionalized with Phenylboronic Acid for T-Cell Transfection

*Yonghui Wang, **Dinh Chuong Nguyen**, Kefan Song, Makenna A. Carnahan, Alexander N. Prossnitz, Karthikeya S. Varma Gottimukkala, Patrick S. Stayton, Suzie H. Pun*

Synopsis

Chimeric antigen receptor T-cell (CAR-T cell) therapy has revolutionized cancer treatment, but its cost and manufacturing complexity hinders its clinical impact. T-cell transfection is part of this complexity, relying on lentiviral transduction methods that incur bioprocess and regulatory challenges. Nonviral transfection methods are inefficient despite current advances, likely due to differences in T-cell biology in cargo uptake and processing. We previously synthesized cationic bottlebrush polymers capable of transfecting human T-cells, but its utility is limited by low uptake. Here, we incorporated phenylboronic acid (PBA) moieties into our cationic bottlebrush polymers that can engage surface glycoproteins on T-cells to induce internalization. We developed a RAFT polymerization-based bottlebrush synthesis method to facilitate PBA co-polymerization, and synthesized well-defined cationic and cationic-PBA bottlebrushes. Both polymers complexed with plasmid DNA at low N/P ratios, and the cationic-PBA bottlebrush exhibited higher transfection efficiency compared to cationic bottlebrush in Jurkat cells. This effect was not observed with HeLa cells, which have a different surface glycoproteome. Cationic-PBA bottlebrushes also mediate better transfection in Jurkat cells across a number of different nucleic acid cargoes (mRNA, circRNA), and both bottlebrush formulations can mediate endosomal disruption, which is crucial to transfection. Future work will compare the uptake of both polymers in different cell lines to validate the mechanism of action of cationic-PBA bottlebrushes, and utilize the platform for CAR transduction via encoding genes.

i. Introduction

Chimeric antigen receptor T-cell (CAR-T cell) therapy remains at the forefront of cancer treatment, and is under extensive clinical development for more advanced oncology indications and autoimmune diseases[1,2]. However, the cost and manufacturing complexity of CAR-T cell therapies is a major barrier to expanding its clinical impact. The multistep process covering leukapheresis, T-cell separation, activation, transduction and expansion each presents unique challenges that are under active investigation respectively[3]. This work addresses the step of T-cell transduction via gene transfer, which is traditionally achieved via lentiviruses. While effective, lentiviral transduction suffers from limited genetic cargo size, risk of insertion mutagenesis, and process variability. Lentivirus production is also costly and necessitates additional bioprocess regulatory controls, further complicating this step in CAR-T cell manufacturing[4]. Non-viral transfection methods (e.g. lipoplexes, polyplexes) can circumvent these limitations, but suffer from orders of magnitude lower transfection efficiencies than lentiviruses[5]. One potential factor is significant differences in the endolysosomal processing pathway in T-cells compared to others with which these nonviral platforms were developed[6].

We previously developed cationic bottlebrush polymers capable of moderate transfection in human T-cells[7]. Of a panel of gene transfer polymers with various compositions, topologies and mechanisms, a bottlebrush formulation consisting of 25 N,N-dimethylamino ethyl methacrylate (DMAEMA) homopolymer arms mediated efficient (up to 50%) transfection in the Jurkat (human immortalized T-lymphocyte) cell line without significant cation-mediated cytotoxicity. Further translation was impeded by lower transfection efficiencies in primary donor T-cells that were only marginally improved with transfection protocol optimization. This is in part due to low cell uptake of the bottlebrush polyplexes, as T-cells have diminished endocytic capacity compared to other cell lines[8].

In this section, we developed phenylboronic acid (PBA)-functionalized DMAEMA cationic bottlebrush polymers to increase T-cell uptake and improve transfection. PBA can reversibly form covalent bonds with vicinal diols, which is often leveraged for controlled drug delivery purposes[9]. Interestingly, this behavior can also be leveraged to target PBA-functionalized drug delivery platforms to cells via cell-surface sialic acid and/or glycoproteins[10]. As T-cells have been shown to express these moieties[11], we hypothesize that a PBA-DMAEMA bottlebrush formulation could mediate efficient transfection of primary human T-cells. Our preliminary results indicate that PBA enhances T-cell transfection with a variety of different genetic cargoes (pDNA, mRNA…), and this enhancement is specific to T-cells. We discuss these results and outline future work to understand, validate, and further translate this platform.

ii. Materials and Methods

Materials

4,4'-azobis(4-cyanovaleric acid) (ABCVA) Chemicals and 3-Aminophenylboronic acid pinacol ester (3-APBA-Pin), diethyl ether, acetone and ethyl acetate were purchased from Fisher Scientific. 2,2'-Azobis[2-methyl-N-(2-hydroxyethyl)propionamide] (V-85) was purchased from Fujifilm Wako. RAFT chain transfer agent 4-Cyano-4-[[(ethylthio)thioxomethyl]thio]pentanoic Acid (ECT) were purchased from Ambeed. RAFT agent 2-cyano-2-propyl dodecyl trithiocarbonate (CPDT), 2-mercaptoethanol, isoquinoline and Di-tert-butyl dicarbonate (Boc anhydride) were purchased from Oakwood Chemicals. mono-2-(Methacryloyloxy)ethyl succinate (SMA) and sodium periodate was purchased from Sigma. All were used as received. N-Dimethylamino ethyl methacrylate (DMAEMA) was purchased from Sigma. 1,4-Dioxane and hydroxyethyl methacrylate (HEMA) were purchased from Tokyo Chemical Industries. Both were passed

through a basic alumina column to remove any existing inhibitor prior to polymerization. Dimethyl sulfoxide (DMSO) was purchased from Sigma and stored with molecular sieves until use.

Synthesis of initial test polymers

The polymers DD10B10 and CP-25-16 were synthesized as previously described[7,9].

Synthesis of 1-tert-butoxy-2-tert-butoxycarbonyl-1,2-dihydroisoquinoline (BBDI)

BBDI was synthesized from previously published procedures[12]. Briefly, Boc anhydride (19.91 g, 91.2 mmol) was dissolved in 75 mL of hexane. Isoquinoline (3.87 g, 75.8 mmol) was added, and the solution was allowed to react at room temperature overnight. A white precipitate may form in the reaction process. The reaction mixture was then rotary evaporated to dryness to obtain an off white-purplish solid. The solid was added to 30 mL of boiling diethyl ether on a hotplate set to low heat, and diethyl ether (10-20 mL) was slowly added while maintaining a boil until all solids have been fully dissolved. Hexane (5-10 mL) was then added until small flakes appear in solution. The solution was then chilled overnight at -20C to crystallize BBDI in the form of small white prisms. The crystals were filtered off cold, recrystallized once more, dried in a vacuum chamber overnight, and stored closed at room temperature before being used without further purification.

Synthesis of protected phenylboronic acid monomer (SMA-PBA-Pin)

SMA (5.84 g, 25.4 mmol) and BBDI (9.616 g, 31.7 mmol) were added to 22.8 mL of ethyl acetate and allowed to stir for 30 minutes before the addition of 3-APBA-Pin (5 g, 22.8 mmol). The mixture was allowed to react overnight, and extracted with 0.1M HCl (3x100 mL), water (100 mL), saturated sodium bicarbonate (3 x 100 mL) and brine (100 mL). The crude was concentrated via rotary evaporation, purified via column chromatography (5% methanol/chloroform, Rf = 0.5 or 30% ethyl acetate/dichloromethane, Rf = 0.4) and dried in vacuo to obtain SMA-PBA-Pin in the form of a thick brown gel.

Synthesis of polymeric CTA (polyCTA)

HEMA (500 mg, 3.8 mmol) was added to a 10 mL round-bottom flask containing 2.541 mL of DMSO, to which was added CPDT (41.4 mg, 0.12 mmol) and AIBN (0.5 mg in 34.6 uL DMSO, 0.0031 mmol). The flask was sealed with a septum and purged with argon for 20 minutes. The mixture was then allowed to polymerize at 70 C for 18 hours (~95% conversion), then precipitated in 50:50 (v/v) diethyl ether:acetone three times, dissolving in 2-5 mL DMSO in-between. The solid polymer pellet was subject to high vacuum for 30 minutes and then dissolved in 10 mL DMSO, to which was added AIBN (5 mg, 0.03 mmol). The flask was sealed with a septum, and subject to house vacuum via a syringe needle for 5 minutes. The mixture was then allowed to end-cap at 70C overnight, then precipitated and sonicated in 50:50 (v/v) diethyl ether acetone:three times, dissolving in 2-5 mL methanol in-between. The solids were then dried under house vacuum overnight to yield an off-white powder (polyHEMA).

ECT (1.05g, 3.9 mmol) and BBDI (1.15g, 3.9 mmol) was added to 14 mL of 1,4-dioxane, and allowed to stir for 30 minutes. The solution color turned a darker orange during this period. The mixture was then added to a flask containing solid polyHEMA (415 mg, 3.19 mmol OH equivalent), rinsing with 2 mL of dioxane. The polyHEMA initially remained as a

solid. The solution was allowed to stir overnight, during which all polyHEMA was solubilized as it reacts with BBDI-activated ECT. Afterwards, the solution was concentrated to 2-3 mL by rotary evaporation at elevated temperature (40C), and precipitated into cold methanol three times, redissolving in acetone in-between. The solids were then dried under house vacuum overnight to yield the polyCTA as a yellow powder.

Synthesis of DMAEMA-PBA bottlebrush

To a 10 mL round-bottom flask with a stir-bar was added DMAEMA (400 mg, 2.54 mmol), SMA-PBA-Pin (217 mg, 0.51 mmol), polyCTA (23.88 mg in 0.955 mL of dioxane, 0.0014 mmol), V-85 (0.37 mg in 36.6 uL of DMF, 0.000076 mmol), and 4.09 mL of dioxane. The flask was sealed with a septum, purged with argon for 20 minutes, and allowed to react at 85C for 17 hours. The reaction mixture was then precipitated into pentane five times, redissolving in acetone in-between. The solid pellet was then dried under house vacuum to yield the protected DMAEMA-PBA bottlebrush.

The protected DMAEMA-PBA bottlebrush was deprotected with sodium periodate in accordance with previously published procedures with minor alterations. Briefly, the bottlebrush was treated with twice its mass of sodium periodate in deionized water, and allowed to react overnight. The mixture was dialyzed against deionized water for 3 days, changing solvent once per day. The mixture was then transferred to a new dialysis membrane, and dialyzed against 1 mM HCl overnight. The mixture was then desalted with a PD-10 column (Cytiva Biosciences) to remove excess HCl, and lyophilized for 3 days to yield the DMAEMA-PBA bottlebrush as a fluffy, off-white solid.

Synthesis of DMAEMA bottlebrush

To a 10 mL round-bottom flask with a stir-bar was added DMAEMA (400 mg, 2.54 mmol), polyCTA (23.88 mg in 0.955 mL of dioxane, 0.0014 mmol), V-85 (0.37 mg in 36.6 uL of DMF, 0.000076 mmol), and 4.09 mL of dioxane. The flask was sealed with a septum, purged with argon for 20 minutes, and allowed to react at 85C for 17 hours. The reaction mixture was then precipitated into pentane five times, redissolving in acetone in-between. The solid pellet was then dried under house vacuum to yield the DMAEMA bottlebrush. The DMAEMA bottlebrush was also subject to the same deprotection and dialysis process as the DMAEMA-PBA bottlebrush described above to account for any biophysical changes that may alter the activity of the DMAEMA-PBA formulation.

Polymer Characterization

All ^{1}H NMR spectra were recorded on a Bruker AV 300 (Bruker Corporation, Billerica, MA) nuclear magnetic resonance (NMR) instrument in deuterated DMSO (DMSO-d6). Polymer molecular weights (Mw, Mn) and polydispersity index (Đ = Mw/Mn) were determined by gel permeation chromatography (GPC). The system consisted of an Agilent 1260 HPLC stack running heated LiBr-supplemented (0.1% w/v) DMF mobile phase at a flow rate of 1 mL min^{-1} through a semi-prep three-column setup (Phenogel-TSKgel). Samples (5 mg/mL) were filtered through a 0.2 μm PTFE filter before analysis. Only protected PBA polymers were analyzed, as PBA can reversibly bind to GPC column packing and distort results. The size distribution profiles of micelles were recorded on a dynamic light scattering (DLS) system (Malvern Zetasizer, Malvern) at a micelle concentration of 1 mg/mL.

RNA, antibodies and plasmids

mRNA and circular RNA were purchased from Hongene biotech. Efluor450 anti-human CD3(clone: OKT3), APC anti-human CD8 (clone: RPA-T8), and Zombie NIR fixable live-dead stain were purchased from Biolegend . The PmaxGFP plasmid (Lonza) were transformed into XL10 Gold ultracompetent cells (Stratagene) and single colonies were grown in an overnight culture. Plasmids were purified using a NucleoBond Xtra Maxi Endotoxin Free kit (MachereyNagel); purity and concentration were quantified by using Nanodrop and a diagnostic gel.

Cell culture

Jurkat (clone E6-1) cell lines used were purchased from ATCC. Human peripheral blood mononuclear cells (PBMCs) were isolated from Leukocyte Reduction System cones (Bloodworks Northwest) using Ficoll-Paque density gradient centrifugation (GE). Human PBMC and Jurkat cells were cultured in RPMI-1640 supplemented with 10% fetal bovine serum (v/ v). HeLa cells were maintained in DMEM media supplemented with 10% fetal bovine serum. Frozen PBMC were thawed overnight and stimulated by the anit-CD3e (clone OKT3) and anti-CD28 (clone CD28.2) antibodies for two days before transfections. Hela and Jurkat cells were used in transfection studies 18–24 h after passaging. All cells were maintained in a 37 °C and 5% CO2 humidified incubator.

Polymer preparation and polyplex formulation

Polymers were dissolved in sterile filtered 25 mM acetic acid to 10 mg/mL and stored at -20 °C and diluted with the same acidic solution to desired amine concentration according to target amine-to-phosphate (N/P) ratios right before transfection studies . Polyplexes were formed immediately before transfection experiments. Plasmid DNA or RNA (0.2 mg/mL) was diluted in a sterile filtered 25 mM sodium acetate solution (pH = 4) after which the equal volume of diluted cationic polymers were added to a final volume of 10-30 μL. This mixture was pipette mixed and incubated at room temperature for 5–10 min before diluting ten times into OptiMEM.

Transfection

The same transfection protocol was used for Jurkat cells, hela cells and human PBMCs with cell density adjustment. Cells were washed once in phosphate buffered saline (PBS) via centrifugation at 300 ×g for 5 min and resuspended in transfection medium 30 min-1h prior to transfection. OptiMEM (Gibco), Jurkat culture medium were all used as transfection media in various experiments. Cells were plated at various concentrations in 250 μL transfection medium in a 24-well or 48-well or 96-well TC treated plate and stored in a 37°C and 5% CO2 humidified incubator until transfection. The Hela cells were seeded at 30 000 cells in 500 μL of OptiMEM in a 24 well plate 18–24 hours prior to transfection. The Jurkat cells were seeded 30000 cells in 250uL of OptiMEM in a 48 well plate (or 100000 cells per 500 uL OptiMEM seeding density in a 24 well plate) 0.5-1 hours prior to transfection. The stimulated PBMCs were collected and washed with 1x DPBS without magnesium and calcium ions, then resuspended in the OptiMEM at a seeding density of 50000 cells per well in a 96-well plate.1 μg of nucleic acid was used per 100k cells in Jurkat and Hela transfections, and 1 μg per 50k cells in primary PBMCs.

Polyplexes diluted in OptiMEM were added to designated wells dropwise. Plates were returned immediately to the 37 °C and 5% CO2 humidified incubator. For PBMCs transfection, the 96 well plate were centrifuged at 1000 tmp for 50 mins at 37°C after adding polyplexes. After transfecting 4 hours, the one third volume of media containing polyplexes was carefully aspirated without disturbing the cells and replaced with serum containing culturing media. Cells were cultured for 48 h prior to flow cytometry analysis.

Flow cytometry

Cells were transferred to a U-bottom 96-well plate by successive centrifugation and aspiration steps. Cells were washed once with PBS via centrifugation at 300 ×g for 5 min before being resuspended in 100 μL of a 1:500 dilution of Zombie NIR dye in PBS. Cells were incubated in the live/dead stain for 10–15 min at room temperature in the dark and subsequently washed twice with PBS with 1% BSA (PBSA from diluted 10% BSA stock, Miltenyi). If antibody staining was used in the experiment, cells were incubated in 100 μL of the diluted antibody cocktail for 20 min at room temperature, and washed twice with 1% PBSA. Cells were resuspended in 200 μL of 1% PBSA, and immediately analyzed on a MacsQuant Analyzer flow cytometer (Miltenyi) where at least 10,000 events in the "Live Cells" gate were collected. Data analysis was performed using FlowJo software (FlowJo, LLC), with serial gating (as following for pHEMA-g-pDMAEMA/mRNA polyplex at N/P 15) . Transfection efficiency was measured as the percentage of live cells expressing GFP fluorescence.

Statistical analysis

Statistical analysis was performed using the Graphpad Prism software. One-way ANOVA with post-hoc Tukey HSD test was used to compare more than two groups.

Synthesis of core-degradable polymeric CTA

Pyridyl disulfide ethyl methacrylate (PDSEMA) was synthesized as previously described[13]. PDSEMA (600 mg, 2.35 mmol) was added to a 5 mL round-bottom flask containing 1.5 mL of DMF, to which was added CPDT (26.1 mg, 0.076 mmol) and AIBN (1.24 mg in 49.61 uL DMF, 0.0076 mmol). The flask was sealed with a septum and purged with argon for 20 minutes. The mixture was then allowed to polymerize at 70C for 30 hours (~90% conversion). 2 mL of 2-mercaptoethanol was then added to the reaction mixture and reacted overnight to exchange pyridyl groups with ethanol. It is then precipitated in diethyl ether three times, dissolving in 2-5 mL DMF in-between. The solid polymer pellet was subject to high vacuum for 30 minutes and then dissolved in 10 mL DMSO, to which was added AIBN (5 mg, 0.03 mmol). The flask was sealed with a septum, and subject to house vacuum via a syringe needle for 5 minutes. The mixture was then allowed to end-cap at 70C overnight, then precipitated and sonicated in diethyl ether three times, dissolving in 2-5 mL methanol in-between. The solids were then dried under house vacuum overnight to yield a pure white solid.

ECT (170 mg, 0.67 mmol) and BBDI (244.8 mg, 0.81 mmol) was added to 1.5 mL of 1,4-dioxane, and allowed to stir for 30 minutes. The solution color turned a darker orange during this period. The mixture was then added to a flask containing solid polyPDSEMA (114.8 mg, 0.54 mmol OH equivalent), rinsing with 2 mL of dioxane. The polyHEMA initially remained as a solid. The solution was allowed to stir overnight, during which all polyHEMA was solubilized as it reacts with BBDI-activated ECT. Afterwards, the solution was concentrated to 2-3 mL by rotary evaporation at elevated temperature (40C),

and precipitated into cold methanol three times, redissolving in acetone in-between. The solids were then dried under house vacuum overnight to yield the core-degradable polymeric CTA as a yellow powder.

iii. Results and Discussion

Bottlebrush formulations transfect T-cells efficiently, while linear PBA formulations are uptaken efficiently

We synthesized the linear polymer DD10B10 consisting of N,N-dimethylamino ethyl acrylamide, 3-PBA acrylamide, and . rhodamine, and tested it for pDNA delivery efficiency and uptake in Jurkat cells. We compared DD10B10 with our previously-published DMAEMA bottlebrush formulation CP-25-16[7] (structure in **Figure 1a-b**). While DD10B10 mediated negligible transfection compared to CP-25-16, it achieved significantly higher uptake when measured by flow cytometry. A mixture of DD10B10 and CP-25-16 induced uptake, but did not improve transfection compared to CP-25-16 (**Figure 1c-d**). These results motivate the development of DMAEMA bottlebrushes incorporating PBA moieties for T-cell transfection.

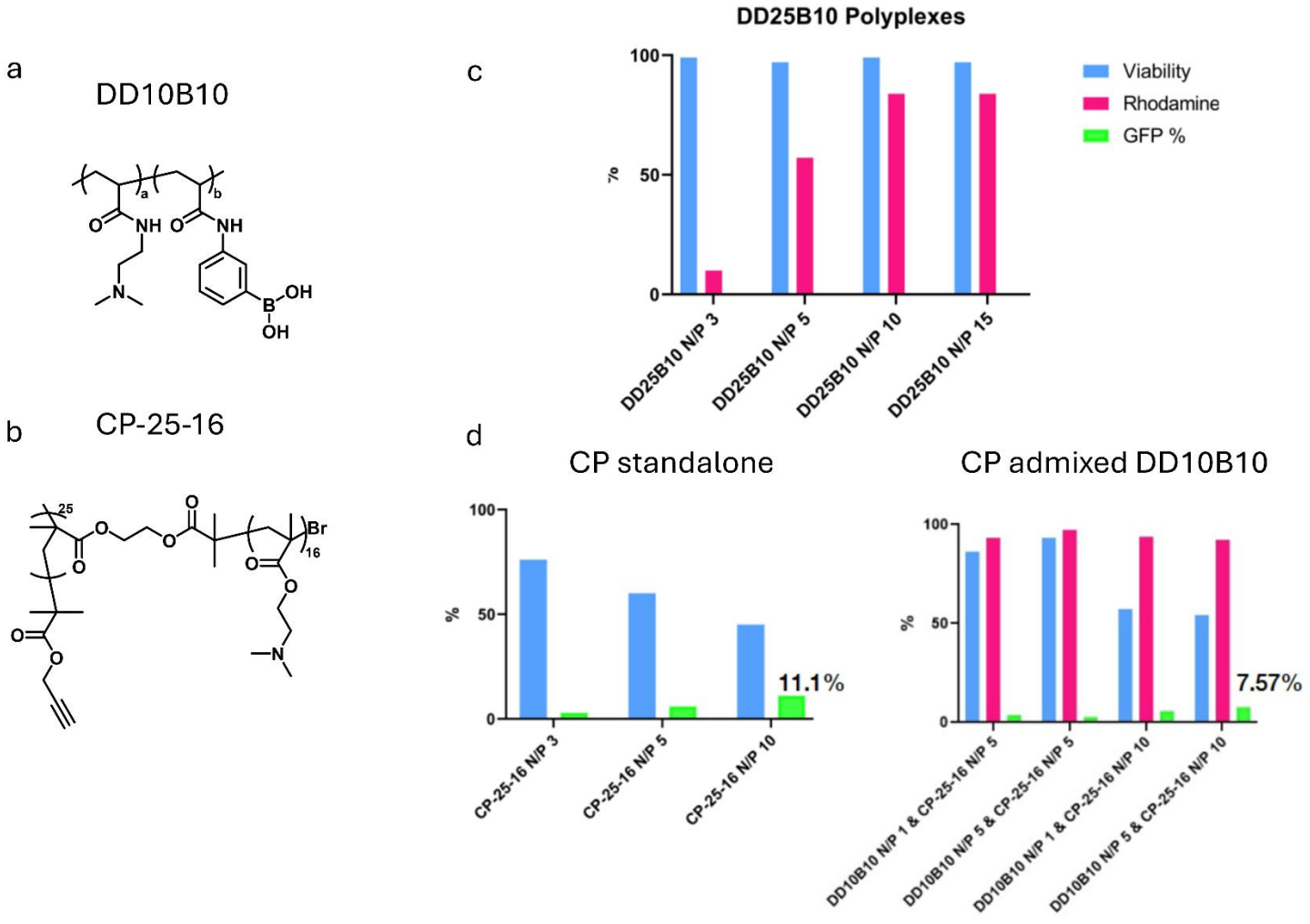

Figure 1. Preliminary examination of cationic brush polymer and linear PBA polymers. a) Chemical structure of linear PBA polymer. b) Chemical structure of DMAEMA bottlebrush polymer. c) Transfection efficiency and uptake of linear PBA

polymers. d) Transfection efficiency and uptake of DMAEMA bottlebrush polymer as a standalone, or admixed formulation with linear PBA polymers

Development of a fully RAFT-based method for bottlebrush synthesis

While ATRP is a well-developed method for bottlebrush polymer synthesis, there are several limitations that mediate further development of an alternative polymer synthesis protocol for this work[14]. Firstly, ATRP operates under copper ion catalysis, which poses cytotoxicity concerns if not properly purified. ATRP is also incompatible with PBAs – its acidic nature can degrade the Cu(I) complex necessary to ATRP, necessitating complex multistep synthesis. Finally, the synthesis of bottlebrush ATRP initiators require hazardous acyl halide chemistry that complicates process scale-up. Reversible addition-fragmentation chain transfer (RAFT) polymerization is another well-known controlled radical polymerization process with reported application in bottlebrush polymer synthesis[14]. Briefly, RAFT "chain-transfer agents" (CTAs) may be covalently attached to side chains of a polymer template with mild chemistry (e.g. click chemistry, esterification…) to yield functional side chains that can mediate polymer chain growth in a subsequent RAFT polymerization. Either the thiocarbonylthio moiety (also known as the 'Z-end') or the radical-forming moiety (also known as the 'R-end') may be grafted onto the polymer template to yield polymeric CTAs that can grow bottlebrushes via distinct mechanisms. We chose to graft the CTA via the 'R-end' in accordance with the "grafting-from" approach as it mechanistically ensures every CTA-functionalized side chain will result in a polymer at the end of the polymerization[15].

Analogous to our previous ATRP-based approach[7], we chose to functionalize a well-defined 28-armed poly(hydroxyethyl methacrylate) (polyHEMA) backbone with the common CTA 4-Cyano-4-[[(ethylthio)thioxomethyl]thio]pentanoic Acid (ECT). ECT possesses a carboxylic acid on its 'R-end' that can esterify with hydroxyls on polyHEMA, similar to previously reported approaches. We evaluated a number of esterification reactions, and chose 1-tert-butoxy-2-tert-butoxycarbonyl-1,2-dihydroisoquinoline (BBDI)-catalyzed esterification in 1,4-dioxane as it was able to fully functionalize all polyHEMA hydroxyls with mild reaction conditions. The ECT-functionalized polyHEMA (polyCTA) was able to form DMAEMA bottlebrushes upon RAFT polymerization with the common initiator 4,4'-azobis(4-cyanovaleric acid) (scheme in **Figure 2a**), albeit with moderate dispersity at relatively low conversions (D = 1.3, 60% conversion) (**Figure 2b**). This is a known drawback of RAFT "grafting-from" polymerization, as steric hindrance from growing bottlebrush side chains prevents efficient RAFT 'Z-end' interchain transfer crucial to maintaining polymerization control.

We explored two different approaches to address this issue. A "CTA-shuttled" approach exists whereby small-molecule CTAs are added to mediate this 'Z-end' transfer, restoring optimal RAFT equilibrium and thus polymerization control[15]. Encouragingly, free ECT addition decreased dispersity at 60% DMAEMA conversion in a dose-dependent manner (**Figure 2b**). However, the "CTA-shuttled" approach generates free linear polymer chains that may impact transfection efficiency and toxicity, necessitating complicated yield-lowering purification methods. As an alternative, we hypothesized that polymerization at higher temperatures will increase growing chain and 'Z-end' mobility in solution, alleviating interchain transfer hindrance. Polymerization at a higher temperature (85C from 70C) with a high-temperature initiator (2,2'-Azobis[2-methyl-N-(2-hydroxyethyl)propionamide] or V-85) that matches ABCVA's radical half-life at 70C also resulted in lowered dispersity (D = 1.2, 60% conversion), albeit higher than the "CTA-shuttled" approach (**Figure 2c**). Considering all factors, we opted for a polymerization protocol utilizing V-85 and targeting 50% conversion, as this yields a well-defined DMAEMA bottlebrush with comparatively diminished risk of linear polymer contamination.

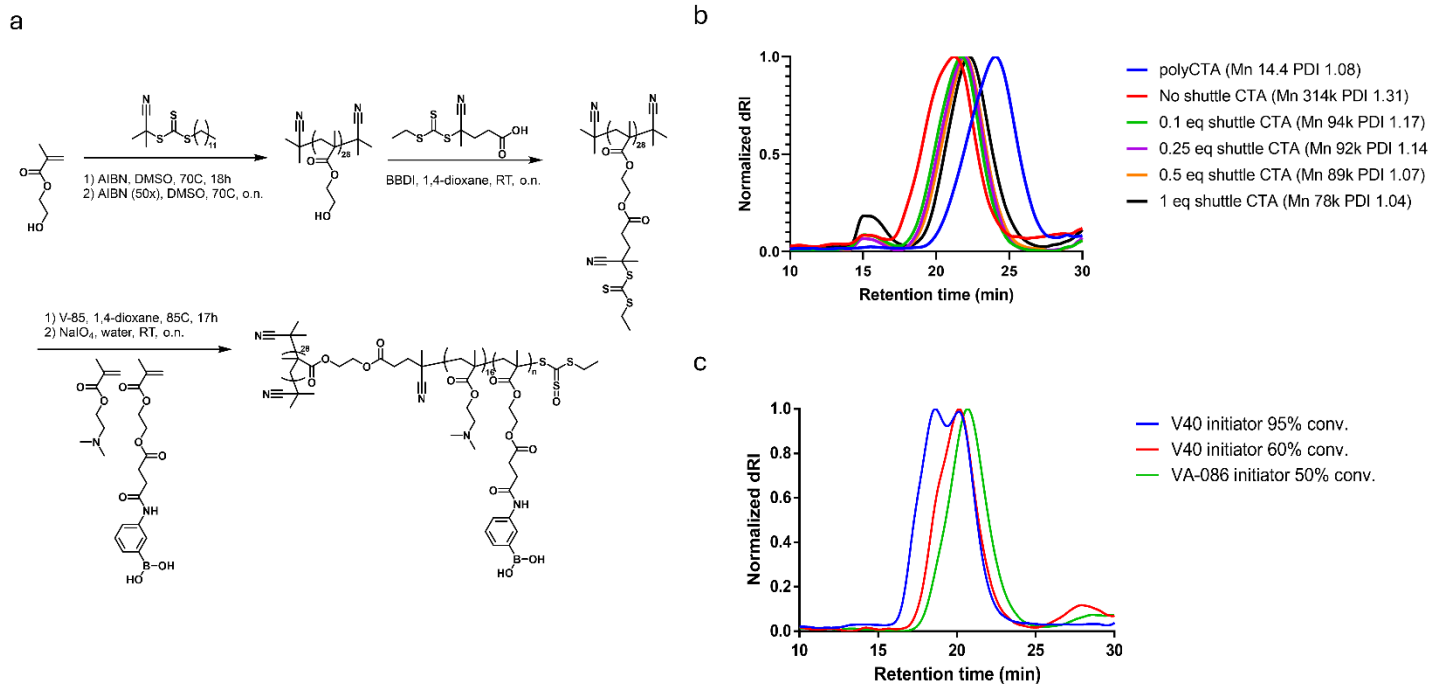

Figure 2. Development of RAFT bottlebrush synthesis method. a) RAFT-based synthesis scheme for DMAEMA-PBA bottlebrush polymers. b) GPC chromatogram of polyCTA and bottlebrush polymer synthesized with various additions of 'shuttle CTA'. c) GPC chromatogram of bottlebrush polymers synthesized with high-temperature initiators.

Synthesis and gene condensation evaluation of DMAEMA-PBA bottlebrushes

We next synthesized DMAEMA and DMAEMA-PBA bottlebrushes with our optimized synthetic protocol. To incorporate PBA moieties, we synthesized a methacrylic monomer of pinacol-protected PBA for co-polymerization with PBA. Pinacol protection of PBA is crucial to monomer purification via silica gel chromatography and polymer characterization with gel-permeation chromatography (GPC). The synthesized DMAEMA bottlebrush (pHEMA-g-pDMAEMA) contains 28 arms, each with 16 DMAEMA units. The DMAEMA-PBA bottlebrush (pHEMA-g-pDMAEMA-pBA) additionally contains 4 PBA units per arm. Both polymers exhibit unimodal distribution upon GPC analysis (**Figure 3a**), and both were subjected to sodium periodate PBA deprotection to normalize any factors in the deprotection process that may interfere with transfection. Both polymers complex with green fluorescent protein (GFP)-encoding plasmid DNA (pDNA) at N/P ratios above 1 in acetate buffer, forming well-defined polyplexes with sizes between 110-160 nm and polydispersity around 0.2 via dynamic light scattering (**Figure 3b**). These results showcase the bottlebrush polymers' crucial ability to condense nucleic acids.

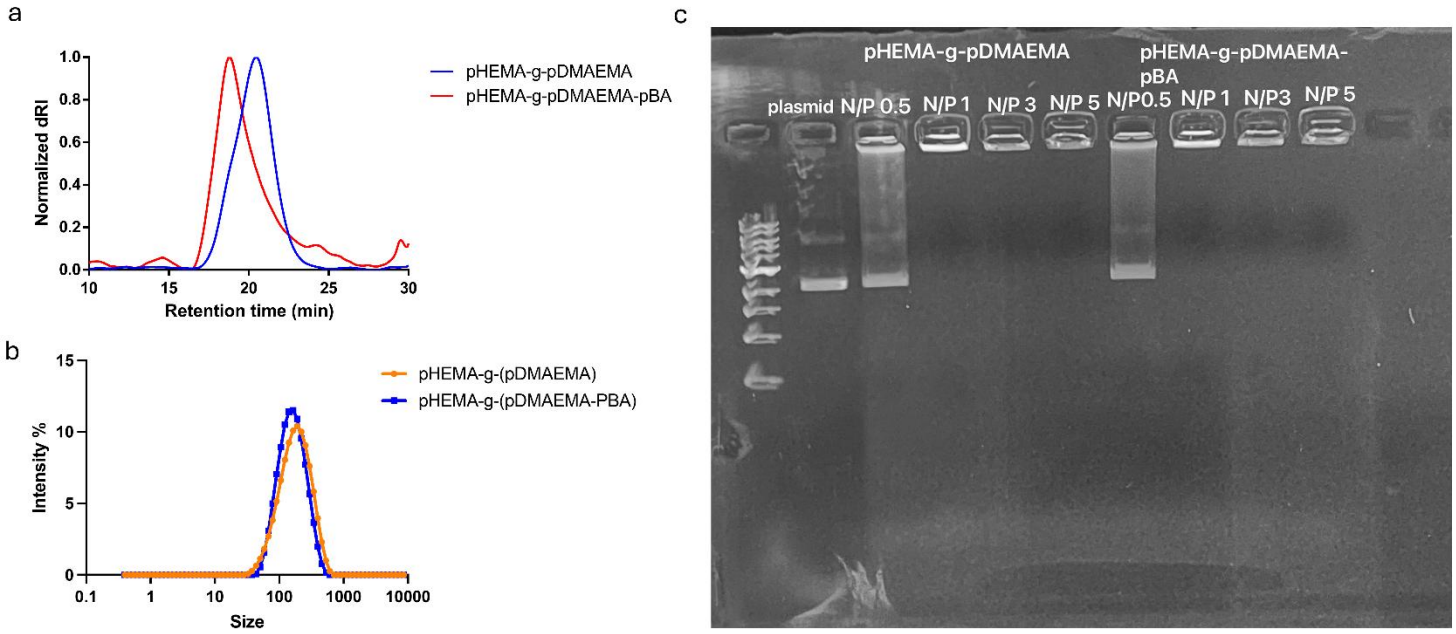

Figure 3. Synthesis and complexation of test bottlebrush polymers. a) GPC chromatogram of bottlebrush polymers tested in subsequent experiments. b) Dynamic light scattering of bottlebrush polyplexes. c) Gel electrophoresis of polyplex formulations at different N/P ratios.

PBA improves pDNA transfection of Jurkat cells in serum-free medium

We next evaluated the capability of both polymers to transfect Jurkat cells, an immortalized human T-cell line, with pDNA in serum-free conditions. We also compared both polymers to an optimized lipoplex formulation (LIPOLTX) that showed efficient transfection in DC 2.4s and Macrophages (internal privileged data, not shown). At N/P = 5 up to N/P = 15, pHEMA-g-pDMAEMA-pBA mediated higher transfection efficiency than pHEMA-g-pDMAEMA, while at N/P = 5 both polymer treatments did not significantly impact viability. At N/P over 5, pHEMA-g-pDMAEMA-pBA exhibited higher cytotoxicity than pHEMA-g-pDMAEMA, and at N/P over 15 both polymers mediate similar transfection efficiencies. In this experiment, LIPOLTX failed to transfect Jurkat cells with pDNA **(Figure 4a-b**).

We had hypothesized that PBAs mediate efficient transfection through uptake via cell-surface glycoproteins[10]. To investigate this in part, we also evaluated both polymers' ability to transfect HeLa cells, which have lower expression of surface glycoproteins. At N/P = 10, there was no difference in transfection efficiency between the two polymers. We also tested N/P = 20 and found significant cytotoxicity in pHEMA-g-pDMAEMA-pBA polymers, which diminished its transfection readout compared to the better-tolerated pHEMA-g-pDMAEMA **(Figure 4c-d**). This may be due to PBA polymers' reported ability to mediate lysosomal escape, which can induce cell death via caspase activation by lysosomal enzymes. Regardless, this lack of PBA-mediated transfection enhancement in HeLa cells indicate its specificity to T-cells. Further work will evaluate the uptake of labeled PBA bottlebrushes to determine the role of cell surface PBA-interacting moieties in T-cell transfection efficiencies. It should be noted that the transfection efficiency of bottlebrushes in HeLa cells is lower than previously reported[7], and further work will determine whether this is an issue with plasmid quality.

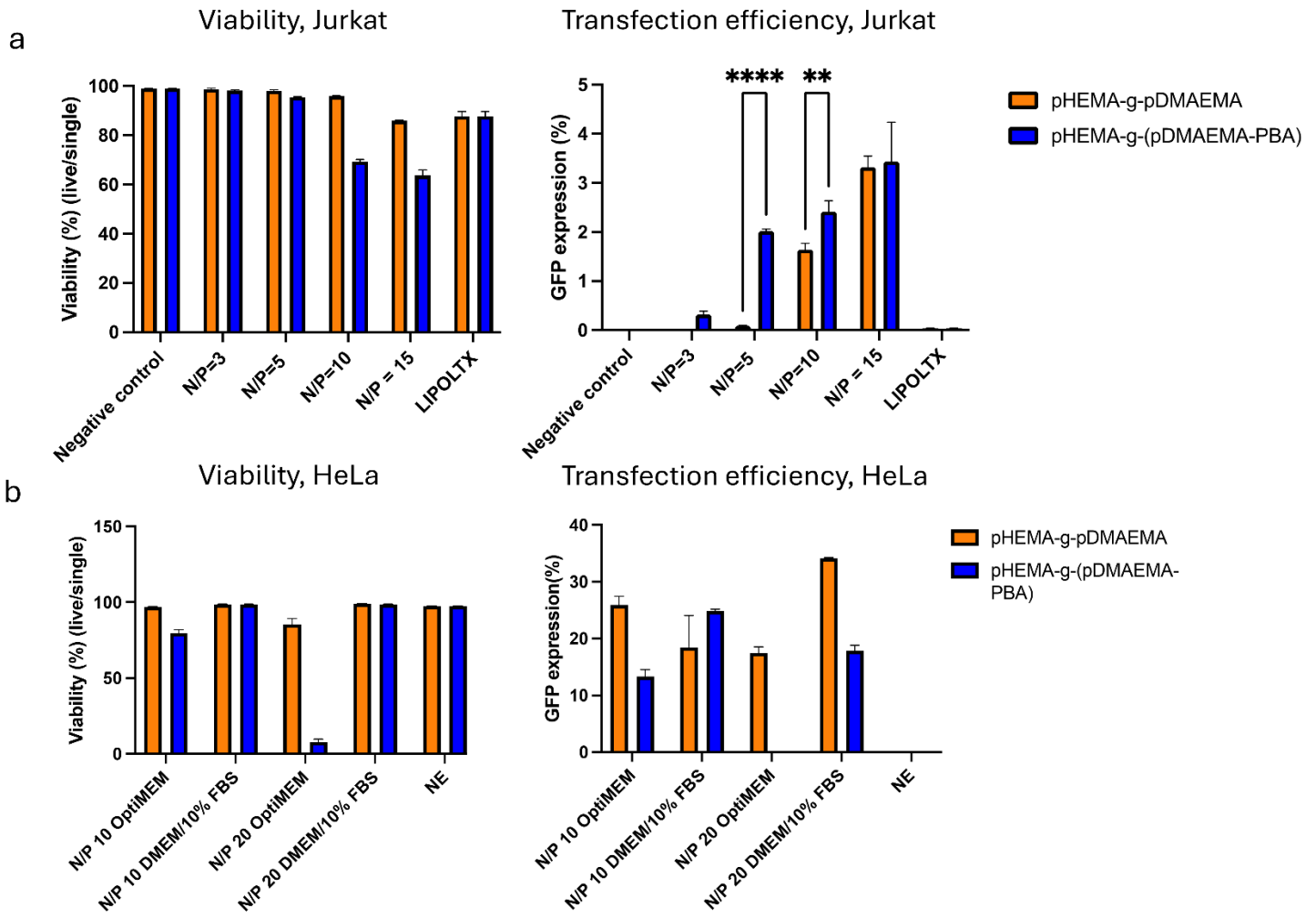

Figure 4. PBA enhances transfection efficiency in T-cells, in a manner specific to T-cells. a) Viability in Jurkat cells treated with bottlebrush polyplexes. b) Transfection efficiency in Jurkat cells. c) Viability in HeLa cells treated with bottlebrush polymers. d) Transfection efficiency in HeLa cells.

PBA also improves Jurkat cell transfection with other nucleic acid types

We also evaluated whether pHEMA-g-pDMAEMA-pBA polymers enhance T-cell transfection with other classes of nucleic acids. We transfect Jurkat cells with both polyplexes with messenger RNA (mRNA), pseudouridine-modified mRNA (PseudoU mRNA) and circular RNA (circRNA). PseudoU mRNA is used in mRNA vaccines for its lack of adverse immunogenicity, while circRNA is under active investigation as a next-generation nucleic acid therapeutic[16]. At N/P = 15, both polymers mediate efficient Jurkat cell transfection (efficiency >60%) with high cell viability across all RNA cargoes. Similar to pDNA, pHEMA-g-pDMAEMA-pBA polymers significantly outperformed its non-PBA variant (**Figure 5a**). These results highlight the utility of pHEMA-g-pDMAEMA-pBA polymers in a wide variety of T-cell transfection applications.

DMAEMA bottlebrushes mediate endosomolysis in serum-free conditions

Endosomal release of nucleic acids is a critical step in transfection, and is a mechanism with which cationic polymers enhance gene delivery[17]. We evaluated the capability of both polymers to induce endosome lysis via the Galectin-8-GFP assay in DC 2.4 cells. Briefly, cytosolic galectins are recruited to damaged endosomal membranes as an intracellular immune response mechanism[18]. Labeled galectins will form dense "punctae" from its diffuse state upon endosomolysis that quantifiable by confocal microscopy to provide a measure of endosomal escape[19]. DC 2.4-Gal8 cells treated with both polymers show visible punctae under confocal microscopy, albeit with no difference between the two. This showcases the DMAEMA bottlebrushes' ability to mediate endosomal escape and deliver genetic cargo to the cytosol for transfection. However, both bottlebrushes display diminished endosomolysis in serum-containing conditions, with slightly more punctae visible in pHEMA-g-pDMAEMA-p-BA polymers compared to pHEMA-g-pDMAEMA (**Figure 5b**)

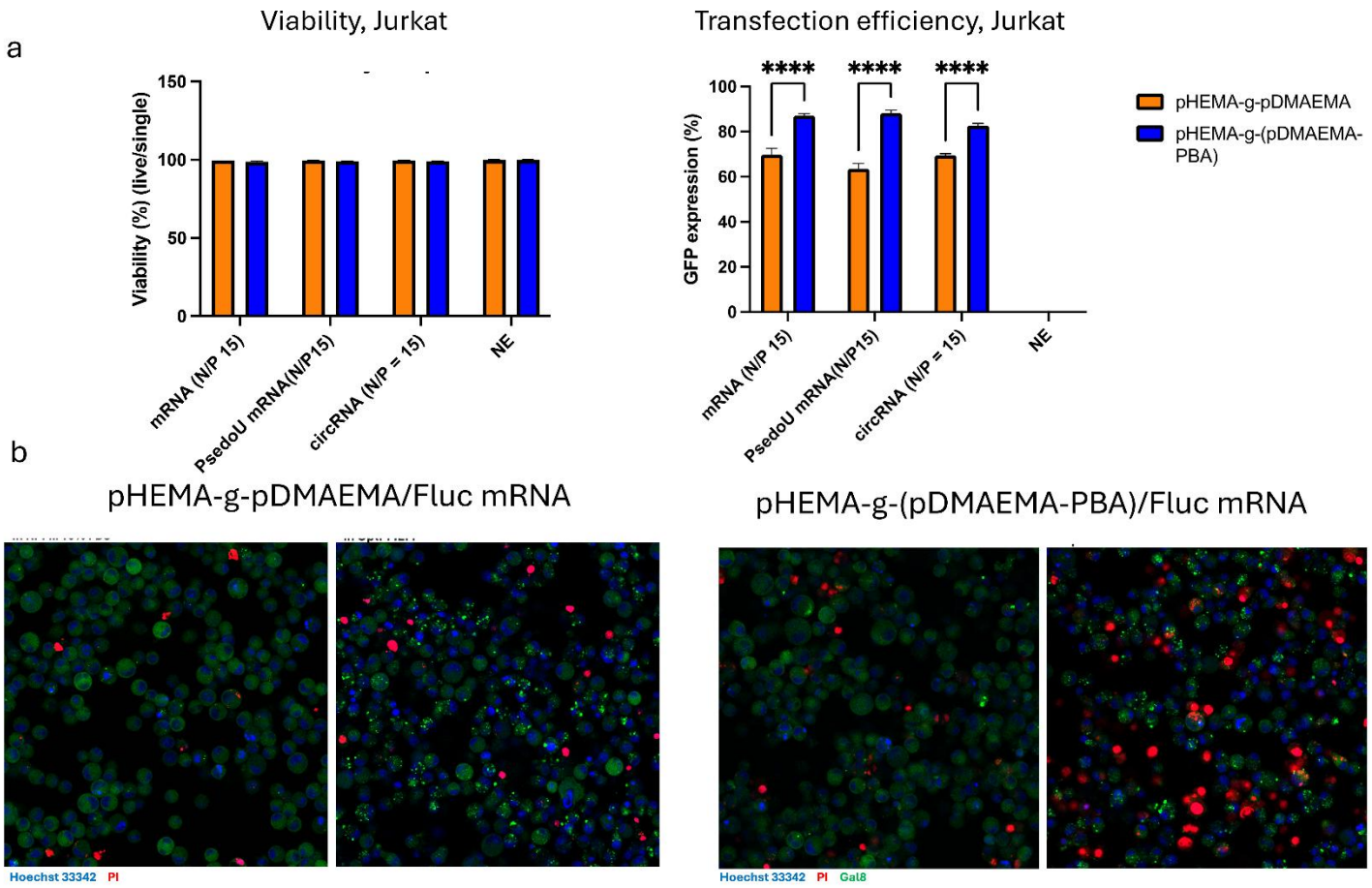

Figure 5. PBA bottlebrushes also enhance Jurkat cell transfection of other nucleic acid types, and mediates endosomal escape. a) Viability and transfection efficiency of Jurkat cells treated with bottlebrush polyplexes of various nucleic acid types. b) Representative confocal microscopy images of bottlebrush-treated DC 2.4-Gal8 cells in serum-containing (left panel of both polymers) and serum-free media (right panel).

iv. Current conclusion, ongoing and future work

We demonstrated that PBA-containing cationic bottlebrush polymers exhibit higher transfection efficiency specific to the Jurkat model human T-cell line. This effect is maintained across a variety of nucleic acids, and may present further design opportunities in CAR-T cell engineering. mRNA transfection in T-cells has been shown to result in efficacious CAR-T cell formulations in a shorter manufacturing timespan[20], and transient CAR expression and/or cytokine induction may result in

superior *in vivo* responses[21]. However, the purported mechanism by which DMAEMA-PBA bottlebrushes exhibit superior transfection to DMAEMA bottlebrushes remain unproven. Future work will compare the uptake of rhodamine-labeled versions of these bottlebrushes in serum-free, serum-containing and glycoprotein-rich media, the latter being expected to diminish uptake of PBA-containing formulations via competition with surface glycoproteins. Additionally, the uptake and transfection efficiency of these bottlebrushes will be evaluated in a wider variety of different cells with different degrees of surface sialylation and distinct endolysosomal processing pathways, such as immature and mature DCs. This platform will need to be validated in its intended application by transfecting T-cells with CAR-encoding nucleic acids, and possibly evaluating resultant production CAR-T cells in a preclinical tumor model utilizing published approaches[22].

Further structural and functional optimization of these cationic bottlebrushes is also warranted. The heightened toxicity of DMAEMA-PBA bottlebrushes may be addressed by introducing biodegradability[23], as the cytotoxicity of cationic polymers can be size-dependent[24]. The application of thiol-pyridyl disulfide chemistry to introduce polymer biodegradability has been previously reported[25] and may be introduced to this platform by a slight modification to the synthesis of the backbone (**Figure 6a-b**). We have been able to progress in this pathway up to the degradable polymeric CTA. Additionally, the application of these polymers to *in vivo* gene delivery is highly desirable[26]. Preliminary work has failed to establish *in vivo* transfection of fluorescent protein-encoding genes in tumor-bearing mice via intratumoral administration, which may be due to serum destabilization of bottlebrush polyplexes reflected by lower *in vitro* transfection efficiency with serum observed before in this work. Fluoropolymers have been reported to mediate efficient *in vivo* gene delivery, possibly due to their reduced serum protein adsorption and increased endosomal escape[27]. Fluorinated moieties may be introduced to the current design by co-polymerizing with commercially available fluorinated methacrylate monomers, such as trifluoroethyl methacrylate (**Figure 6c**).

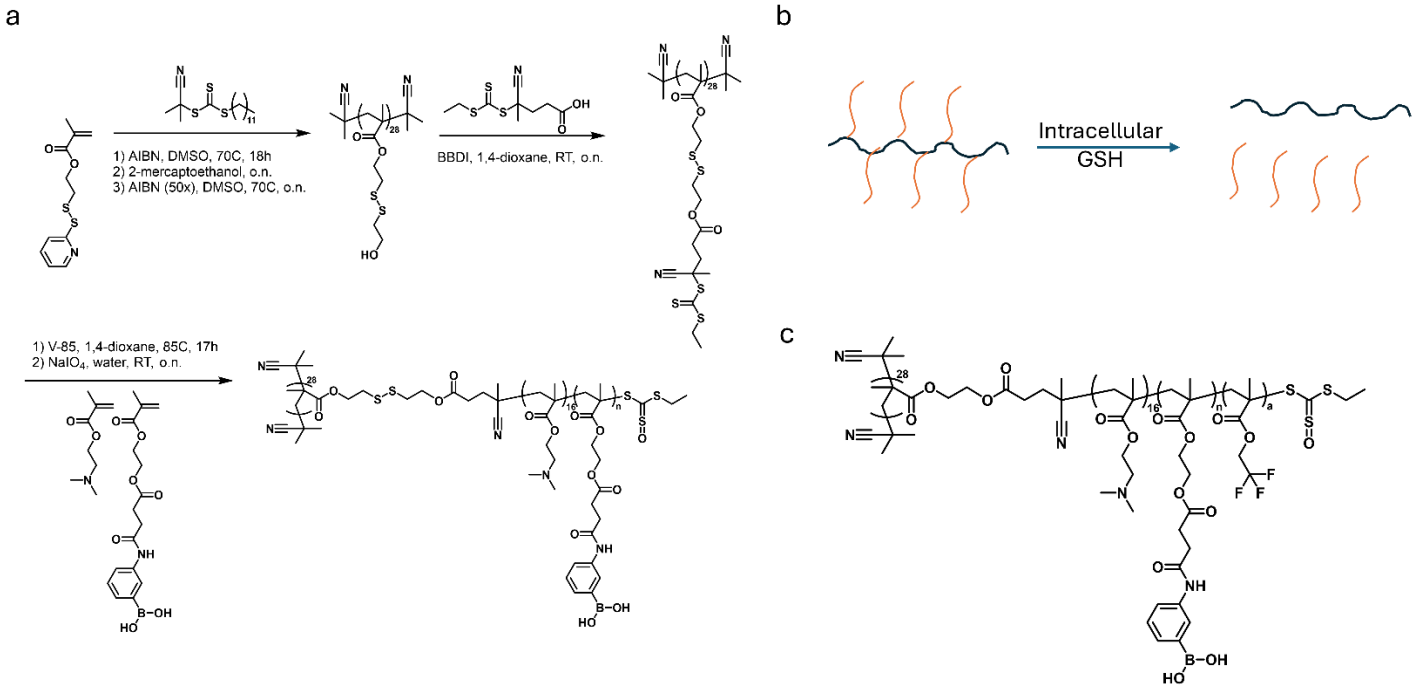

Figure 6. Proposed future polymer designs. a) Synthesis scheme of biodegradable DMAEMA-PBA bottlebrushes. b) Proposed degradation mechanism of biodegradable bottlebrushes. c) Proposed structure for DMAEMA-PBA bottlebrushes for *in vivo* gene delivery.

v. References

(1) Hao, Y.; Hsu, W.-C.; Parzynski, C. S.; Degtyarev, E.; Hampson, L. V.; Masood, A.; Wu, W.-H. Effectiveness of Tisagenlecleucel versus Real-World Standard of Care in Relapsed/Refractory Follicular Lymphoma. *J. Comp. Eff. Res.* **2023**, *12* (7), e220173. https://doi.org/10.57264/cer-2022-0173.

(2) Müller, F.; Taubmann, J.; Bucci, L.; Wilhelm, A.; Bergmann, C.; Völkl, S.; Aigner, M.; Rothe, T.; Minopoulou, I.; Tur, C.; et al. CD19 CAR T-Cell Therapy in Autoimmune Disease — A Case Series with Follow-Up. *N. Engl. J. Med.* **2024**, *390* (8), 687–700. https://doi.org/10.1056/NEJMoa2308917.

(3) Vormittag, P.; Gunn, R.; Ghorashian, S.; Veraitch, F. S. A Guide to Manufacturing CAR T Cell Therapies. *Curr. Opin. Biotechnol.* **2018**, *53*, 164–181. https://doi.org/10.1016/j.copbio.2018.01.025.

(4) Okuma, A. Generation of CAR-T Cells by Lentiviral Transduction. In *Mammalian Cell Engineering*; Humana, New York, NY, 2021; pp 3–14. https://doi.org/10.1007/978-1-0716-1441-9_1.

(5) Raes, L.; De Smedt, S. C.; Raemdonck, K.; Braeckmans, K. Non-Viral Transfection Technologies for next-Generation Therapeutic T Cell Engineering. *Biotechnol. Adv.* **2021**, *49*, 107760. https://doi.org/10.1016/j.biotechadv.2021.107760.

(6) Watts, C. The Endosome–Lysosome Pathway and Information Generation in the Immune System. *Biochim. Biophys. Acta BBA - Proteins Proteomics* **2012**, *1824* (1), 14–21. https://doi.org/10.1016/j.bbapap.2011.07.006.

(7) Olden, B. R.; Cheng, Y.; Yu, J. L.; Pun, S. H. Cationic Polymers for Non-Viral Gene Delivery to Human T Cells. *J. Controlled Release* **2018**, *282*, 140–147. https://doi.org/10.1016/j.jconrel.2018.02.043.

(8) Charpentier, J. C.; King, P. D. Mechanisms and Functions of Endocytosis in T Cells. *Cell Commun. Signal.* **2021**, *19* (1), 92. https://doi.org/10.1186/s12964-021-00766-3.

(9) Prossnitz, A. N.; Pun, S. H. Modulating Boronic Ester Stability in Block Copolymer Micelles via the Neighbor Effect of Copolymerized Tertiary Amines for Controlled Release of Polyphenolic Drugs. *ACS Macro Lett.* **2022**, *11* (3), 276–283. https://doi.org/10.1021/acsmacrolett.1c00751.

(10) Ji, M.; Li, P.; Sheng, N.; Liu, L.; Pan, H.; Wang, C.; Cai, L.; Ma, Y. Sialic Acid-Targeted Nanovectors with Phenylboronic Acid-Grafted Polyethylenimine Robustly Enhance siRNA-Based Cancer Therapy. *ACS Appl. Mater. Interfaces* **2016**, *8* (15), 9565–9576. https://doi.org/10.1021/acsami.5b11866.

(11) Bi, S.; Baum, L. G. Sialic Acids in T Cell Development and Function. *Biochim. Biophys. Acta BBA - Gen. Subj.* **2009**, *1790* (12), 1599–1610. https://doi.org/10.1016/j.bbagen.2009.07.027.

(12) Ouchi, H.; Saito, Y.; Yamamoto, Y.; Takahata, H. 1-Tert-Butoxy-2-Tert-Butoxycarbonyl- 1,2-Dihydroisoquinoline: A Novel and Chemoselective Tert-Butoxycarbonylation Reagent. *Org. Lett.* **2002**, *4* (4), 585–587. https://doi.org/10.1021/ol017183u.

(13) Wilson, J. T.; Keller, S.; Manganiello, M. J.; Cheng, C.; Lee, C.-C.; Opara, C.; Convertine, A.; Stayton, P. S. pH-Responsive Nanoparticle Vaccines for Dual-Delivery of Antigens and Immunostimulatory Oligonucleotides. *ACS Nano* **2013**, *7* (5), 3912–3925. https://doi.org/10.1021/nn305466z.

(14) Truong, N. P.; Jones, G. R.; Bradford, K. G. E.; Konkolewicz, D.; Anastasaki, A. A Comparison of RAFT and ATRP Methods for Controlled Radical Polymerization. *Nat. Rev. Chem.* **2021**, *5* (12), 859–869. https://doi.org/10.1038/s41570-021-00328-8.

(15) Zheng, Z.; Ling, J.; Müller, A. H. E. Revival of the R-Group Approach: A "CTA-Shuttled" Grafting from Approach for Well-Defined Cylindrical Polymer Brushes via RAFT Polymerization. *Macromol. Rapid Commun.* **2014**, *35* (2), 234–241. https://doi.org/10.1002/marc.201300578.

(16) Kim, Y.-K. RNA Therapy: Rich History, Various Applications and Unlimited Future Prospects. *Exp. Mol. Med.* **2022**, *54* (4), 455–465. https://doi.org/10.1038/s12276-022-00757-5.

(17) Chang, K.-L.; Higuchi, Y.; Kawakami, S.; Yamashita, F.; Hashida, M. Efficient Gene Transfection by Histidine-Modified Chitosan through Enhancement of Endosomal Escape. *Bioconjug. Chem.* **2010**, *21* (6), 1087–1095. https://doi.org/10.1021/bc1000609.

(18) Thurston, T. L. M.; Wandel, M. P.; von Muhlinen, N.; Foeglein, Á.; Randow, F. Galectin 8 Targets Damaged Vesicles for Autophagy to Defend Cells against Bacterial Invasion. *Nature* **2012**, *482* (7385), 414–418. https://doi.org/10.1038/nature10744.

(19) Munson, M. J.; O'Driscoll, G.; Silva, A. M.; Lázaro-Ibáñez, E.; Gallud, A.; Wilson, J. T.; Collén, A.; Esbjörner, E. K.; Sabirsh, A. A High-Throughput Galectin-9 Imaging Assay for Quantifying Nanoparticle Uptake, Endosomal Escape and Functional RNA Delivery. *Commun. Biol.* **2021**, *4* (1), 1–14. https://doi.org/10.1038/s42003-021-01728-8.

(20) Rabinovich, P. M.; Komarovskaya, M. E.; Wrzesinski, S. H.; Alderman, J. L.; Budak-Alpdogan, T.; Karpikov, A.; Guo, H.; Flavell, R. A.; Cheung, N.-K.; Weissman, S. M.; et al. Chimeric Receptor mRNA Transfection as a Tool to Generate Antineoplastic Lymphocytes. *Hum. Gene Ther.* **2009**, *20* (1), 51–61. https://doi.org/10.1089/hum.2008.068.

(21) Parayath, N. N.; Stephan, S. B.; Koehne, A. L.; Nelson, P. S.; Stephan, M. T. In Vitro-Transcribed Antigen Receptor mRNA Nanocarriers for Transient Expression in Circulating T Cells in Vivo. *Nat. Commun.* **2020**, *11* (1), 6080. https://doi.org/10.1038/s41467-020-19486-2.

(22) Cardle, I. I.; Scherer, D. R.; Jensen, M. C.; Pun, S. H.; Sellers, D. L. In Situ Bioconjugation of Synthetic Peptides onto Universal Chimeric Antigen Receptor T Cells for Targeted Cancer Immunotherapies. *ACS Nano* **2025**. https://doi.org/10.1021/acsnano.4c16824.

(23) Blakney, A. K.; Zhu, Y.; McKay, P. F.; Bouton, C. R.; Yeow, J.; Tang, J.; Hu, K.; Samnuan, K.; Grigsby, C. L.; Shattock, R. J.; et al. Big Is Beautiful: Enhanced saRNA Delivery and Immunogenicity by a Higher Molecular Weight, Bioreducible, Cationic Polymer. *ACS Nano* **2020**, *14* (5), 5711–5727. https://doi.org/10.1021/acsnano.0c00326.

(24) Werth, S.; Urban-Klein, B.; Dai, L.; Höbel, S.; Grzelinski, M.; Bakowsky, U.; Czubayko, F.; Aigner, A. A Low Molecular Weight Fraction of Polyethylenimine (PEI) Displays Increased Transfection Efficiency of DNA and siRNA in Fresh or Lyophilized Complexes. *J. Controlled Release* **2006**, *112* (2), 257–270. https://doi.org/10.1016/j.jconrel.2006.02.009.

(25) Phillips, D. J.; Gibson, M. I. Biodegradable Poly(Disulfide)s Derived from RAFT Polymerization: Monomer Scope, Glutathione Degradation, and Tunable Thermal Responses. *Biomacromolecules* **2012**, *13* (10), 3200–3208. https://doi.org/10.1021/bm300989s.

(26) Cheng, Y.; Yumul, R. C.; Pun, S. H. Virus-Inspired Polymer for Efficient In Vitro and In Vivo Gene Delivery. *Angew. Chem. Int. Ed.* **2016**, *55* (39), 12013–12017. https://doi.org/10.1002/anie.201605958.

(27) Song, T.; Gao, Y.; Song, M.; Qian, J.; Zhang, H.; Zhou, J.; Ding, Y. Fluoropolymers-Mediated Efficient Biomacromolecule Drug Delivery. *Med. Drug Discov.* **2022**, *14*, 100123. https://doi.org/10.1016/j.medidd.2022.100123.

Chapter 6. Proposed future directions

Dinh Chuong Nguyen, *Patrick S. Stayton, Suzie H. Pun*

Synopsis

Here, we propose future directions based on the work outlined in this thesis.

i. Incorporating splenic vaccination strategies into VIPER-STING cancer vaccination

Recent reviews have highlighted the spleen as an attractive target for immunotherapy[1]. Briefly, the spleen is the largest secondary lymphoid organ in the body, with a high density of antigen-presenting cells (APCs), T and B cells that overall can mobilize a vaccine response. Splenic APCs can be targeted by intravenous administration, and successful priming of splenic T-cells has been shown to result in meaningful antitumor responses. Work from Robert Seder's group on has shown that splenic vaccine responses from intravenous administration are faster than subcutaneous (days vs. weeks), both resulting in high lymphocyte activation[2]. Splenic targeting via intravenous administration naturally encounters hepatic uptake as an obstacle in combination with systemic toxicity, especially for mannosylated systems as in VIPER and STING drugamers[3,4]. Strategies such as blank nanoparticle pre-treatment may be assessed to overcome this challenge[5].

Splenic immune stimulation may yield two practical benefits. Firstly, some reports implicate the spleen in tumor antigen tolerance. Exposure to systemic circulation exposes the spleen to tumor antigens, often in tolerogenic context[6]. Thus, introducing tumor antigens in an inflammatory context may address this issue. In addition, the kinetic distinction of splenic responses compared to that of lymph nodes[2] may provide a dynamic multiphase vaccine response that can address tumor immunotherapy resistance. For instance, different tumor antigens can be targeted to the spleen and lymph node. The fast splenic response can temporarily provide a halt to resistance-conferring tumorigenesis and an inflammatory tumor microenvironment. The slower lymphoid response can subsequently mobilize towards a different antigen, reducing the likelihood of antigenic escape[7]. As the current generation of VIPER-STING vaccine described in Chapter 5 already elicited partial tumor remission, this strategy could invoke more complete responses while offering potential for vaccine design innovation via tailoring vaccine formulation (e.g. antigen dose and identity, adjuvant dose and identity) for each lymphoid and splenic targeting.

ii. Combining polymeric tumor-lytic therapies with polymeric immunotherapies

Combining adjuvant immunotherapy with first-line therapies, such as chemotherapy and radiotherapy, are viable tumor therapies with promising preclinical results[8,9]. We restrict discussion here to chemotherapy, as radiotherapy experiments require substantial changes to our institutional Biological Use Authorization but are available and under investigation at collaborating groups. Preliminary work explored the combinatorial use of polySTING intravenous immunotherapy (in the manner discussed in Chapter 4) and the common chemotherapy doxorubicin. While the combination therapy regimen better suppressed tumor growth than monotherapy of each kind, this avenue was not pursued further due to observed unrecovered weight loss from this regimen, indicating significant toxicity. The type and dosing of chemotherapy could be optimized, for instance by moving to cisplatin and chemotherapy in a pre-treatment context, and can yield findings of therapeutic interest.

A further avenue of engineering interest can be to combine our current polymeric immunotherapies (e.g. polySTING) with our previously-reported polymeric tumor-lytic therapies. Lv and Sylvestre et al reported that intravenous administration of PEG-(DIPAMA-D-melittin) micelles (DMM) is tolerable and results in immunogenic cell death that restrains tumor growth[10]. DMM was also shown to synergize with immune checkpoint blockade therapy (anti-PD-1 and anti-CTLA-4), demonstrating potential for therapeutic synergy with polySTING that maintains tolerability. Both Pun and Stayton Labs have reported polymer conjugates with tumor-targeting ligands (e.g. aptamers[11], antibodies[12]) that may be utilized to further increase selectivity and reduce off-target toxicity[13]. The Stayton Lab has previously reported prodrug monomers of chemotherapeutics[14,15] that may be redesigned and incorporated into tumor-targeting formulations for selective prodrug cleavage within tumor cells, further achieving therapeutic design goals.

iii. Immunosuppressive drugamers for tumor therapy

Drugamers for immune suppression is a natural progression from drugamers for immune stimulation, with multiple therapeutic avenues for application. Multiple immunosuppressive small molecules are amenable to drugamer functionalization, and have seen use in other drug delivery platforms for immune modulation[16]. However, an interesting application exists in oncology for the use of tumor-targeted immunosuppressive therapeutics – sensitizing tumors to first-line therapy. Immune activation in pro-tumor components of the tumor microenvironment may confer tumorigenesis and treatment resistance[17]. For instance, cGAS-STING activation in cancer-associated fibroblasts has been shown to induce resistance to platinum-based chemotherapies in breast cancer. Pharmacological abrogation of STING with a small-molecule STING inhibitor H-151 results in superior tumor suppression upon cisplatin treatment in a murine preclinical breast cancer model[18]. Thus, tumor-targeted immunosuppressive drugamers may provide an innovative alternative approach to tumor therapy. Immune activation is also associated with toxicity in other chemotherapies (e.g. cGAS-STING in doxorubicin-mediated cardiotoxicity[19]), and thus immune modulation may enhance the therapeutic window of such first-line therapies.

iv. Small-molecule checkpoint inhibitor drugamers, and tumor-associated macrophages

Aside from purely immunological hurdles, immune checkpoint blockade (ICB) therapy also encounters traditional drug delivery challenges. Hemodilution and systemic clearance necessitate high and/or repeat dosing, increasing risk of off-target toxicity via systemic immune activation. Local ICB delivery has been identified as a promising therapeutic avenue[20], and it may be possible to achieve this by leveraging cells within the tumor microenvironment (e.g. tumor-associated macrophages/TAMs) as drug depots[21]. Recently, small-molecule ICBs have been reported with demonstrable antitumor activity and functional groups amenable to drugamer functionalization[22]. The drugamer platform has been previously utilized to maintain high local concentrations of therapeutics (e.g. antibiotics, antimalarial drugs…) through intracellular prodrug cleavage within local macrophages[4,23]. A similar application could be conceived whereby TAM-targeted ICB prodrugs with an appropriate linker are utilized to maintain an intracellular 'depot' of small-molecule ICBs in the tumor microenvironment. In this application, small-molecule ICBs may be superior to their traditional protein counterparts as intracellular cleavage conditions may degrade secondary structures in a manner that negatively impacts protein ICB activity[24]. This application could be evaluated standalone or in conjunction with our reported immunotherapy (i.e. polySTING) or vaccine (i.e. VIPER-STING) treatment regimen. It should be noted that the requirements on the small-molecule ICB candidate for drugamer application are rather stringent for this application. The lipophilicity of the candidate must be high enough to allow for membrane diffusion of cleaved drug into the extracellular space, and the antagonism of the ICB candidate must be validated to be preserved across preclinical and clinical models[25]. It is therefore conceivable that current small-molecule ICBs as of this writing may not yet be suitable, but the promise of this approach warrants investigation should a suitable candidate arise.

v. Polymeric peptide delivery platforms for tolerogenic therapy

Antigen presentation without inflammatory context is often cited as a mechanism of tolerance, and can be leveraged to address allergy and/or autoimmune disease[26]. Recently, the Hubbell group reported on a polymeric mannose-antigen conjugate that prevented anaphylaxis against cow's milk antigen in a dysbiotic murine model through both intravenous and subcutaneous administration[27]. Such an application may be envisioned with the mannosylated VIPER platform, which may bring additional benefits such as facile antigen incorporation (Hubbell utilized a protracted bioconjugation approach),

protection of antigens from systemic degradation in nanoparticulate form, and potential tunability towards MHC-II or cross-presentation via melittin dose modulation[28]. As melittin and cationic comonomers may be inflammatory[29,30], anti-inflammatory drugamers (e.g. dexamethasone[31]) may be co-delivered to achieve tolerogenic context.

Additionally, the ability of VIPER and related polymers to deliver MHC-II antigens with drugamer-mediated inflammatory context may be exploited to generate regulatory cellular immunity. Recently, MHC-II neoantigens have been shown to induce type-I cytotoxic regulatory T-cells (Tr1 cells), which can be detrimental in the context of antitumor immunity by lysing antigen-presenting pro-inflammatory DCs in the tumor microenvironment[32]. However, Tr1 cells can also address autoimmune conditions (e.g. autoimmune diabetes[33]) and may represent an innovative application and mechanism of action of biomaterials in autoimmune management, distinct from the common approach of delivering or inducing tolerogenic cytokines[34].

vi. Investigating vaccine-mediated CD4 response, and exploring B-cell responses

VIPER formulations, adjuvanted and unadjuvanted, induce significantly stronger CD4+ T-cell responses as measured by intracellular cytokine staining (IL-2, IFN-y), compared to antigen and antigen-only polymers[28]. Further characterization of CD4 responses had not been explored in this work due to practical technical constraints, such as the intracellular localization of tolerogenic CD4 markers (e.g. FoxP3)[35]. However, characterization of CD4+ T-cell response profiles (e.g. Th1/Th2, Th1/Th17…) is important to understanding the big picture of vaccine responses, especially for applications beyond oncology (e.g. infectious diseases)[36]. Within VIPER cancer vaccines, the Th1/Th2 ratio is a common inquiry after conference presentations. Therefore, it is important for future work for our groups to develop expertise in characterizing CD4+ T-cells, or initiate collaborations with such experience.

Both the Pun and Stayton Labs are at a position to consider characterizing and exploring modulation of B-cell responses for future work. B-cell-derived antibody responses play a major role in antitumor and antiviral/antibacterial immunity[37], both being therapeutic focus areas for both groups. It is conceivable that our formulations generate a B-cell response given their lymph node-homing nature and the presence of adjuvants that can bias antibody responses[38]. Straightforward experiments such as characterizing antibody class-switching in response to our formulations may highlight unexplored therapeutic avenues that benefit from such B-cell response profiles. Additionally, characterizing antibody responses may provide insight into potential toxicity mechanisms of our polymeric therapeutics, as demonstrated by Sylvestre et al's work on PEGylated melittin polymers[39].

vii. References

(1) He, X.; Wang, J.; Tang, Y.; Chiang, S. T.; Han, T.; Chen, Q.; Qian, C.; Shen, X.; Li, R.; Ai, X. Recent Advances of Emerging Spleen-Targeting Nanovaccines for Immunotherapy. *Adv. Healthc. Mater.* **2023**, *12* (23), 2300351. https://doi.org/10.1002/adhm.202300351.

(2) Baharom, F.; Ramirez-Valdez, R. A.; Tobin, K. K. S.; Yamane, H.; Dutertre, C.-A.; Khalilnezhad, A.; Reynoso, G. V.; Coble, V. L.; Lynn, G. M.; Mulè, M. P.; et al. Intravenous Nanoparticle Vaccination Generates Stem-like TCF1+ Neoantigen-Specific CD8+ T Cells. *Nat. Immunol.* **2021**, *22* (1), 41–52. https://doi.org/10.1038/s41590-020-00810-3.

(3) Nguyen, D. C.; Song, K.; Jokonya, S.; Yazdani, O.; Sellers, D. L.; Wang, Y.; Zakaria, A.; Pun, S. H.; Stayton, P. S. Mannosylated STING Agonist Drugamers for Dendritic Cell-Mediated Cancer Immunotherapy. *ACS Cent. Sci.* **2024**. https://doi.org/10.1021/acscentsci.3c01310.

(4) Srinivasan, S.; Roy, D.; Chavas, T. E. J.; Vlaskin, V.; Ho, D.-K.; Pottenger, A.; LeGuyader, C. L. M.; Maktabi, M.; Strauch, P.; Jackson, C.; et al. Liver-Targeted Polymeric Prodrugs of 8-Aminoquinolines for Malaria Radical Cure. *J. Controlled Release* **2021**, *331*, 213–227. https://doi.org/10.1016/j.jconrel.2020.12.046.

(5) Ouyang, B.; Poon, W.; Zhang, Y.-N.; Lin, Z. P.; Kingston, B. R.; Tavares, A. J.; Zhang, Y.; Chen, J.; Valic, M. S.; Syed, A. M.; et al. The Dose Threshold for Nanoparticle Tumour Delivery. *Nat. Mater.* **2020**, *19* (12), 1362–1371. https://doi.org/10.1038/s41563-020-0755-z.

(6) Ugel, S.; Peranzoni, E.; Desantis, G.; Chioda, M.; Walter, S.; Weinschenk, T.; Ochando, J. C.; Cabrelle, A.; Mandruzzato, S.; Bronte, V. Immune Tolerance to Tumor Antigens Occurs in a Specialized Environment of the Spleen. *Cell Rep.* **2012**, *2* (3), 628–639. https://doi.org/10.1016/j.celrep.2012.08.006.

(7) Lin, H.; Yang, X.; Ye, S.; Huang, L.; Mu, W. Antigen Escape in CAR-T Cell Therapy: Mechanisms and Overcoming Strategies. *Biomed. Pharmacother.* **2024**, *178*, 117252. https://doi.org/10.1016/j.biopha.2024.117252.

(8) Salas-Benito, D.; Pérez-Gracia, J. L.; Ponz-Sarvisé, M.; Rodriguez-Ruiz, M. E.; Martínez-Forero, I.; Castañón, E.; López-Picazo, J. M.; Sanmamed, M. F.; Melero, I. Paradigms on Immunotherapy Combinations with Chemotherapy. *Cancer Discov.* **2021**, *11* (6), 1353–1367. https://doi.org/10.1158/2159-8290.CD-20-1312.

(9) Zhang, Z.; Liu, X.; Chen, D.; Yu, J. Radiotherapy Combined with Immunotherapy: The Dawn of Cancer Treatment. *Signal Transduct. Target. Ther.* **2022**, *7* (1), 1–34. https://doi.org/10.1038/s41392-022-01102-y.

(10) Lv, S.; Sylvestre, M.; Song, K.; Pun, S. H. Development of D-Melittin Polymeric Nanoparticles for Anti-Cancer Treatment. *Biomaterials* **2021**, *277*, 121076. https://doi.org/10.1016/j.biomaterials.2021.121076.

(11) Cardle, I. I.; Raman, J.; Nguyen, D. C.; Wang, T.; Wu, A. Y.; Sellers, D. L.; Pichon, T. J.; Cheng, E. L.; Kacherovsky, N.; Salipante, S. J.; et al. DNA Aptamer-Polymer Conjugates for Selective Targeting of Integrin A4β1+ T-Lineage Cancers. *ACS Appl. Mater. Interfaces* **2025**. https://doi.org/10.1021/acsami.4c17788.

(12) Berguig, G. Y.; Convertine, A. J.; Shi, J.; Palanca-Wessels, M. C.; Duvall, C. L.; Pun, S. H.; Press, O. W.; Stayton, P. S. Intracellular Delivery and Trafficking Dynamics of a Lymphoma-Targeting Antibody–Polymer Conjugate. *Mol. Pharm.* **2012**, *9* (12), 3506–3514. https://doi.org/10.1021/mp300338s.

(13) Lammers, T.; Kiessling, F.; Hennink, W. E.; Storm, G. Drug Targeting to Tumors: Principles, Pitfalls and (Pre-) Clinical Progress. *J. Controlled Release* **2012**, *161* (2), 175–187. https://doi.org/10.1016/j.jconrel.2011.09.063.

(14) Das, D.; Srinivasan, S.; M. Kelly, A.; Y. Chiu, D.; K. Daugherty, B.; M. Ratner, D.; S. Stayton, P.; J. Convertine, A. RAFT Polymerization of Ciprofloxacin Prodrug Monomers for the Controlled Intracellular Delivery of Antibiotics. *Polym. Chem.* **2016**, *7* (4), 826–837. https://doi.org/10.1039/C5PY01704A.

(15) N. Son, H.; Srinivasan, S.; Y. Yhee, J.; Das, D.; K. Daugherty, B.; Y. Berguig, G.; G. Oehle, V.; H. Kim, S.; Kim, K.; C. Kwon, I.; et al. Chemotherapeutic Copolymers Prepared via the RAFT Polymerization of Prodrug Monomers. *Polym. Chem.* **2016**, *7* (27), 4494–4505. https://doi.org/10.1039/C6PY00756B.

(16) Pastora, L. E.; Namburu, N. S.; Arora, K.; Christov, P. P.; Wilson, J. T. STING-Pathway Inhibiting Nanoparticles (SPINs) as a Platform for Treatment of Inflammatory Diseases. *ACS Appl. Bio Mater.* **2024**, *7* (8), 4867–4878. https://doi.org/10.1021/acsabm.3c01305.

(17) He, L.; Xiao, X.; Yang, X.; Zhang, Z.; Wu, L.; Liu, Z. STING Signaling in Tumorigenesis and Cancer Therapy: A Friend or Foe? *Cancer Lett.* **2017**, *402*, 203–212. https://doi.org/10.1016/j.canlet.2017.05.026.

(18) Liu, J.; Liu, C.; Ma, Y.; Pan, X.; Chu, R.; Yao, S.; Chen, J.; Liu, C.; Chen, Z.; Sheng, C.; et al. STING Inhibitors Sensitize Platinum Chemotherapy in Ovarian Cancer by Inhibiting the CGAS-STING Pathway in Cancer-Associated Fibroblasts (CAFs). *Cancer Lett.* **2024**, *588*, 216700. https://doi.org/10.1016/j.canlet.2024.216700.

(19) Luo, W.; Zou, X.; Wang, Y.; Dong, Z.; Weng, X.; Pei, Z.; Song, S.; Zhao, Y.; Wei, Z.; Gao, R.; et al. Critical Role of the cGAS-STING Pathway in Doxorubicin-Induced Cardiotoxicity. *Circ. Res.* **2023**, *132* (11), e223–e242. https://doi.org/10.1161/CIRCRESAHA.122.321587.

(20) Chen, X.; Ding, W.; Jiang, Y.; Shi, W.; Qiu, Y.; Zhao, H.; Luo, X. Emerging Strategies for Local Delivery of Immune Checkpoint Inhibitors to Potentiate Cancer Immunotherapy: Current Status and Future Prospects. *ACS Appl. Mater. Interfaces* **2024**, *16* (44), 59682–59696. https://doi.org/10.1021/acsami.4c12603.

(21) Miller, M. A.; Zheng, Y.-R.; Gadde, S.; Pfirschke, C.; Zope, H.; Engblom, C.; Kohler, R. H.; Iwamoto, Y.; Yang, K. S.; Askevold, B.; et al. Tumour-Associated Macrophages Act as a Slow-Release Reservoir of Nano-Therapeutic Pt(IV) pro-Drug. *Nat. Commun.* **2015**, *6* (1), 8692. https://doi.org/10.1038/ncomms9692.

(22) Sun, C.; Cheng, Y.; Dong, J.; Hu, L.; Zhang, Y.; Shen, H.; Zhang, G.; Jiang, B.; Adam Youssouf, S.; Min, W.; et al. Novel PD-L1/VISTA Dual Inhibitor as Potential Immunotherapy Agents. *J. Med. Chem.* **2025**, *68* (1), 156–173. https://doi.org/10.1021/acs.jmedchem.4c01640.

(23) Su, F.-Y.; Srinivasan, S.; Lee, B.; Chen, J.; Convertine, A. J.; West, T. E.; Ratner, D. M.; Skerrett, S. J.; Stayton, P. S. Macrophage-Targeted Drugamers with Enzyme-Cleavable Linkers Deliver High Intracellular Drug Dosing and Sustained Drug Pharmacokinetics against Alveolar Pulmonary Infections. *J. Controlled Release* **2018**, *287*, 1–11. https://doi.org/10.1016/j.jconrel.2018.08.014.

(24) Press, O. W.; Farr, A. G.; Borroz, K. I.; Anderson, S. K.; Martin, P. J. Endocytosis and Degradation of Monoclonal Antibodies Targeting Human B-Cell Malignancies1. *Cancer Res.* **1989**, *49* (17), 4906–4912.

(25) Masubuchi, T.; Chen, L.; Marcel, N.; Wen, G. A.; Caron, C.; Zhang, J.; Zhao, Y.; Morris, G. P.; Chen, X.; Hedrick, S. M.; et al. Functional Differences between Rodent and Human PD-1 Linked to Evolutionary Divergence. *Sci. Immunol.* **2025**, *10* (103), eads6295. https://doi.org/10.1126/sciimmunol.ads6295.

(26) Klein, L.; Petrozziello, E. Antigen Presentation for Central Tolerance Induction. *Nat. Rev. Immunol.* **2025**, *25* (1), 57–72. https://doi.org/10.1038/s41577-024-01076-8.

(27) Cao, S.; Maulloo, C. D.; Raczy, M. M.; Sabados, M.; Slezak, A. J.; Nguyen, M.; Solanki, A.; Wallace, R. P.; Shim, H.-N.; Wilson, D. S.; et al. Glycosylation-Modified Antigens as a Tolerance-Inducing Vaccine Platform Prevent Anaphylaxis in a Pre-Clinical Model of Food Allergy. *Cell Rep. Med.* **2024**, *5* (1). https://doi.org/10.1016/j.xcrm.2023.101346.

(28) Song, K.; Nguyen, D. C.; Luu, T.; Yazdani, O.; Roy, D.; Stayton, P. S.; Pun, S. H. A Mannosylated Polymer with Endosomal Release Properties for Peptide Antigen Delivery. *J. Controlled Release* **2023**, *356*, 232–241. https://doi.org/10.1016/j.jconrel.2023.03.004.

(29) Dezfuli, H. T.; Shahbazzadeh, D.; Eidi, A.; Bagheri, K. P.; Pakravan, N.; Amini, S.; Aghasadeghi, M. R.; Mahdavi, M. Induction of IFN-γ Cytokine Response against Hepatitis B Surface Antigen Using Melittin. *Gastroenterol. Hepatol. Bed Bench* **2014**, *7* (2), 108–117.

(30) Huang, Z.; Yang, Y.; Jiang, Y.; Shao, J.; Sun, X.; Chen, J.; Dong, L.; Zhang, J. Anti-Tumor Immune Responses of Tumor-Associated Macrophages via Toll-like Receptor 4 Triggered by Cationic Polymers. *Biomaterials* **2013**, *34* (3), 746–755. https://doi.org/10.1016/j.biomaterials.2012.09.062.

(31) Falcón-Beas, C.; Tittarelli, A.; Mora-Bau, G.; Tempio, F.; Pérez, C.; Hevia, D.; Behrens, C.; Flores, I.; Falcón-Beas, F.; Garrido, P.; et al. Dexamethasone Turns Tumor Antigen-Presenting Cells into Tolerogenic Dendritic Cells with T Cell Inhibitory Functions. *Immunobiology* **2019**, *224* (5), 697–705. https://doi.org/10.1016/j.imbio.2019.05.011.

(32) Sultan, H.; Takeuchi, Y.; Ward, J. P.; Sharma, N.; Liu, T.-T.; Sukhov, V.; Firulyova, M.; Song, Y.; Ameh, S.; Brioschi, S.; et al. Neoantigen-Specific Cytotoxic Tr1 CD4 T Cells Suppress Cancer Immunotherapy. *Nature* **2024**, *632* (8023), 182–191. https://doi.org/10.1038/s41586-024-07752-y.

(33) Chen, C.; Lee, W.-H.; Yun, P.; Snow, P.; Liu, C.-P. Induction of Autoantigen-Specific Th2 and Tr1 Regulatory T Cells and Modulation of Autoimmune Diabetes1. *J. Immunol.* **2003**, *171* (2), 733–744. https://doi.org/10.4049/jimmunol.171.2.733.

(34) Shodeinde, A. B.; Murphy, A. C.; Oldenkamp, H. F.; Potdar, A. S.; Ludolph, C. M.; Peppas, N. A. Recent Advances in Smart Biomaterials for the Detection and Treatment of Autoimmune Diseases. *Adv. Funct. Mater.* **2020**, *30* (37), 1909556. https://doi.org/10.1002/adfm.201909556.

(35) Li, F.; Yang, M.; Wang, L.; Williamson, I.; Tian, F.; Qin, M.; Shah, P. K.; Sharifi, B. G. Autofluorescence Contributes to False-Positive Intracellular Foxp3 Staining in Macrophages: A Lesson Learned from Flow Cytometry. *J. Immunol. Methods* **2012**, *386* (1), 101–107. https://doi.org/10.1016/j.jim.2012.08.014.

(36) Weaver, J. M.; Sant, A. J. Understanding the Focused CD4 T Cell Response to Antigen and Pathogenic Organisms. *Immunol. Res.* **2009**, *45* (2), 123–143. https://doi.org/10.1007/s12026-009-8095-8.

(37) Bachmann, M. F.; Zinkernagel, R. M. NEUTRALIZING ANTIVIRAL B CELL RESPONSES. *Annu. Rev. Immunol.* **1997**, *15* (Volume 15, 1997), 235–270. https://doi.org/10.1146/annurev.immunol.15.1.235.

(38) Darling, R. J.; Senapati, S.; Kelly, S. M.; Kohut, M. L.; Narasimhan, B.; Wannemuehler, M. J. STING Pathway Stimulation Results in a Differentially Activated Innate Immune Phenotype Associated with Low Nitric Oxide and Enhanced Antibody Titers in Young and Aged Mice. *Vaccine* **2019**, *37* (20), 2721–2730. https://doi.org/10.1016/j.vaccine.2019.04.004.

(39) Sylvestre, M.; Lv, S.; Yang, L. F.; Luera, N.; Peeler, D. J.; Chen, B.-M.; Roffler, S. R.; Pun, S. H. Replacement of L-Amino Acid Peptides with D-Amino Acid Peptides Mitigates Anti-PEG Antibody Generation against Polymer-Peptide Conjugates in Mice. *J. Controlled Release* **2021**, *331*, 142–153. https://doi.org/10.1016/j.jconrel.2021.01.015.